Investigating circadian disruption in mouse models of neurological and metabolic disorders

DPhil Thesis

Achilleas Livieratos

Wolfson College

University of Oxford

Michaelmas 2013



Abstract

Sleep and circadian rhythm disturbance has been widely observed in neurological disorders although the mechanistic basis for this association remains unknown. In order to understand this association further, a combination of rest/activity and molecular profiling was carried out on mouse models of Parkinson's Disease (PD), Lysosomal Storage Disorders (LSDs) and schizophrenia.

Data from rest/activity behavioural screening of new BAC (Bacterial Artificial Chromosome) transgenic PD models displayed scotophase hyperactivity and decreased fragmentation patterns. Interestingly, rest/activity profiles of LSD models displayed possible core clock defects under constant conditions (*Hexb*$^{-/-}$) and potential re-entrainment deficits following a 6hr phase advance (*Npc1*$^{-/-}$). Together these data suggest new associations between disruptions in rest/activity cycles and neurodegeneration.

The blind-drunk (*Bdr*) mutant is a mouse model of synaptosomal-associated protein *(Snap)-25* exocytotic disruption that displays schizophrenic endophenotypes and phase advanced rest/activity cycles. Despite identification of phase advanced expression of signalling neuropeptides (e.g. arginine vasopressin) in the *Bdr* suprachiasmatic nucleus (SCN), the underlying mechanisms regulating circadian disruption in this model remain elusive; therefore, label-free shotgun proteomics was carried out over 24 hours to elucidate potential post-transcriptional pathways. A number of novel circadian patterns of protein expression were identified including myristoylated alanine-rich C-kinase substrate (MARCKS) which exhibited a robust phase advanced expression profile. This study has identified novel SCN post-transcriptional mechanisms that may link schizoaffective disorder biomarkers to dysfunctional rest/activity cycles.

Table of contents

Abstract 2

1 General introduction 10

1.1 The mammalian circadian axis 10

1.2 Homeostatic and circadian regulation of sleep 14

1.3 TTFL, Non-transcriptional oscillation and SCN Neuropeptides 17

1.4 Bad clocks: Neuropathology linked to circadian pathology 21

1.5 Schizophrenia 23

1.5.1 Circadian Disruption in Schizophrenia 24

1.5.2 Circadian Disruption in Schizophrenia: Historical Background 26

1.5.3 Circadian Disruption in Schizophrenia: Pharmacological Background 26

1.5.4 Circadian Disruption in Schizophrenia: Genetic Background 27

1.5.5 Circadian Disruption in Schizophrenia: Functional Background 28

1.5.6 Circadian Disruption in Schizophrenia: Endophenotype 29

1.5.7 Circadian Disruption in Schizophrenia: Evidence from Mouse Models 30

1.6 Parkinson's Disease 39

1.6.1 Circadian and Sleep Disruption in PD 43

1.6.2 Circadian and Sleep Disruption in PD: Evidence from Mouse Models 45

1.7 Metabolic Disorders: Lysosomal Storage Disorders 47

1.7.1 Metabolism and Circadian Disruption: Core Clock Genes 49

1.7.2 LSD: Sandhoff Disease and Niemann-Pick type C 51

1.8 Aims 54

1.9 Hypotheses 55

2 Methods 56

2.1 Animals 56

2.1.1 The blind-drunk mutant mouse 56

2.1.2 BAC PD mouse models 57

2.1.3 *Parkin*, *Hexb* and *Npc1* knockout mice 58

2.2 Motor and non-motor phenotype monitoring 59

2.2.1 Circadian running-wheel screening 59

2.2.2 Type II phase delay 60

2.2.3 Nonparametric activity and sleep analysis 60

2.2.4 Light 61

2.3 ‘‘Molecular’’ Methodologies 63

2.3.1 Tissue collection 64

2.3.2 Acute light-induced SCN IEGs profiling 65

2.3.3 RNA extraction/quantification/reverse transcription and primers 66

2.3.4 qRT-PCR analysis 67

2.3.5 Cloning and *in situ* hybridisation 69

2.3.6 Proteomic 24h circadian molecular profiling 71

2.3.7 BCA Protein Assay 71

2.3.8 Protein Extraction-Fractionation/Mass Spectrometry 71

2.3.9 Below 10kDa targets 73

2.3.10 Above 10kDa targets 74

2.3.11 Proteomic Data Analysis 75

2.3.12 Immunohistochemistry 76

2.3.13 Western Blot 78

2.3.14 Enzyme-linked immunosorbent assay 79

2.4 Statistics 80

3 Results I: Circadian screening of PD mouse models 81

3.1 Non-motor symptoms of PD 81

3.2 BAC SNCA mouse models 82

3.3 MAPT mouse models 84

3.4 *Parkin* KO mouse models 86

3.5 Objectives 89

3.6 Materials and Methods 90

3.6.1 Clocklab/Matlab 90

3.6.2 Nonparametric activity and sleep analysis software 90

3.6.3 Circadian Screen 90

3.7 Circadian data of BAC a-synucleinopathic models 91

3.8 Circadian data of BAC tauopathic models 103

3.9 Circadian data of *Parkin* KO mouse model 115

3.10 Discussion on PD/FTDP-17 mouse models 125

3.10.1 BAC SNCA Overview 125

3.10.2 BAC OVX versus ASO 127

3.10.3 BAC MAPT Overview 129

3.10.4 MAPT mutants 131

3.10.5 *Parkin* KO Overview 133

4 Results II: Circadian screening of *Npc* and *Hexb* KO mice 136

4.1 NPC and neurodegeneration 136

4.2 HEXA/B and neurodegeneration 138

4.3 *Npc1* KO mouse model 139

4.3 Tay-Sachs and Sandhoff KO mouse models 141

4.5 Objectives 143

4.6 Materials and Methods 144

4.6.1 Clocklab/Matlab 144

4.6.2 Circadian Screen 144

4.7 Circadian data of *Npc1* KO mouse model 146

4.8 Circadian data of *Hexb* KO mouse model 156

4.9 Discussion on *Npc1* KO 166

4.10 Discussion on *Hexb* KO 168

5 Results III: Proteomic profiling of the *Bdr* SCN 171

5.1 *Snap-25* and the *Bdr* 171

5.2 Objectives 176

5.3 Materials and Methods 177

5.3.1 Acute light-induced SCN IEGs profiling/qRT-PCR/ISH 177

5.3.2 SCN proteomics-MS optimisation/quantitation/validation 177

5.4 Results 178

5.4.1 Acute light-induced SCN IEGs 178

5.4.2 SCN proteomics--MS optimisation 181

5.4.3 SCN proteomics-MS data 186

5.4.4 SCN proteomics-MS analysis 187

5.4.5 SCN proteomics-IHC/WB/ELISA validation 205

5.5 Discussion 212

6 Main Discussion 225

6.1 Overview 225

6.2 The *Bdr* model: Circadiomics 227

6.3 LSDs: Circadian Disruption and Metabolism 230

6.4 BAC models of PD and Circadian Disruption 234

6.5 Summary 236

6.6 Future Efforts 237

6.6.1 LSDs (Sandhoff and NPC) 237

6.6.2 PD mouse models 239

6.6.3 The schizophrenic *Bdr* model 241

6.7 Beyond this Project 243

7 Acknowledgements 244

8 Appendix 244

8.1 Abbreviations 244

8.2 Tables 251

8.3 Figures 252

8.4 Mouse models 256

9 References 257

1 General Introduction

1.1 The mammalian circadian axis

Life, at its fundamental level, is governed by rhythmic molecular, network and behavioural oscillations that approximate the daily sunrise and sunset periods (Levi and Schibler, 2007). These rhythmic oscillations are identified by their period length (τ) with circadian (*lat: circa diem*, around a day) rhythms showing approximately a 24h period (Albrecht *et al*., 2005). Circadian rhythms have evolved to adapt to the Earth's daily rotation (Albrecht *et al*., 2005). Absence of external synchronizers (Zeitgebers) does not impede the rhythmic oscillations of this system (Albrecht *et al*., 2005).

Circadian rhythms ensure an organism's life-sustaining activities such as feeding and sleeping continue. Functional sleep/wake cycles are critical for maintaining cognitive, physiological and emotional fitness while disruption of the circadian system can impede the metabolic, cardiovascular, cognitive as well as immunological system (Carskadon, 2004; Karatsoreos *et al*., 2011; Colwell *et al*., 2011).

The circadian axis (Figure 1.1) possesses both an input and an output component (Liu *et al*., 2007). Light-dependent input pathways involve a non-visual retinal photopigment, melanopsin, which detects light intensity changes (Hattar *et al*., 2003). In addition, classical visual photoreceptors also participate in photic entrainment of the core clock to daily light variations (Mrosovsky, 2003). Light cues can propagate via neuronal retino-hypothalamic projections to the master circadian pacemaker, the suprachiasmatic nucleus (SCN) (Donaldson and Stephan, 1982; Irwin and Allen, 2007). Light dependent or independent cues, such as food cues, exert temporal and spatial neuropeptide secretions that impose robust

network oscillations on the 20,000 neurons of the bilateral SCN (Yamaguchi *et al*., 2003; Aton *et al*., 2005; Maywood *et al*., 2006; Maywood *et al*., 2010).

Output components of the circadian axis allow central and peripheral nervous system synchronisation via neuronal and paracrine signals (Panda and Hogenesch, 2004; Kalsbeek et al., 2006; Kohsaka and Bass, 2007). This includes the rhythmic regulation of hormonal, behavioural and temperature oscillations (Liu *et al*., 2007). Temperature rhythms are SCN driven and are not dependent on a sleep-active state (Scheer et al., 2005). Body temperature changes can entrain peripheral clocks while the SCN exhibits temperature compensation to maintain its phase (Abraham *et al*., 2010). Hormonally, glucocorticoids have a diurnal release pattern and are able to entrain peripheral tissues via the pituitary-adrenocortical axis (Balsalobre *et al*., 2000). Additionally, melatonin secretion is implicated in the regulation of sleep (Dubocovich *et al*., 2003). An important behavioural output of the circadian axis is structured sleep/wake cycles (Sujino *et al*., 2003; Hastings and Herzog, 2004; Webb *et al*., 2010). Robust free-running periods (non-entrained circadian rhythms) are maintained in the absence of external synchronizers (Mohawk *et al*., 2012). The reticular activating system, cerebral cortex, basal forebrain, thalamus and hypothalamus all participate in sleep/wake cycles (Steriade *et al*., 1993; McCormick and Bal, 1997; Saper *et al*., 2001; McGinty and Szymusiak, 2003).

Figure 1.1: The circadian axis

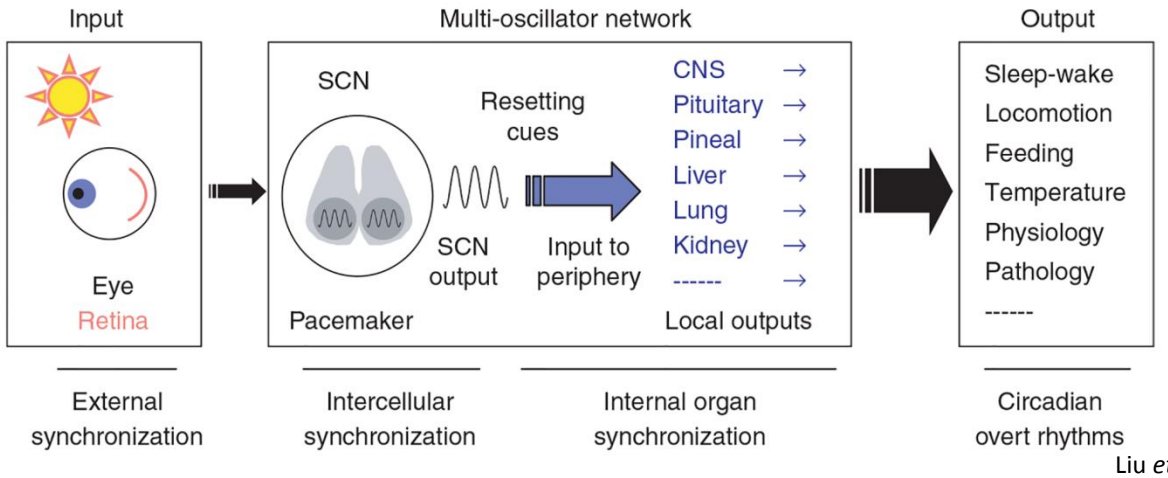

Liu *et al*., 2007

Figure 1.1: The circadian axis is composed of the input, the oscillator and output components. Light represents the primary input to the SCN and firing rate rhythm an output. The SCN maintains control over peripheral oscillators and therefore SCN outputs regulate local outputs.

Hypothalamic areas are integration sites of sleep/wake dynamics with lateral hypothalamic (LH) hypocretin neurons, ventrolateral pre-optic nucleus (VLPO), median pre-optic area (MPO) and tuberomamillary nucleus (TMN) in receipt of dorsal subparaventricular zone (dSPZ) and dorsomedial hypothalamic (DMH) projections (Figure 1.2) in order to organise sleep architecture and maintain appropriate sleep/wake cycles (Saper *et al*., 2001; Saper, 2006; Nishino, 2007). Peripheral cortical clocks are synchronised by sub-cortical projections providing a link between thalamic and cortical synchronisation (Pace-Schott and Hobson, 2002; Lu *et al*., 2006; Fuller *et al*., 2007).

The SCN consists of a heterogeneous neuronal population, that activate in a temporally dependent manner, projecting to both sleep-promoting and wake-promoting regions (van den Pol, 1993; O'Hara *et al*., 1995; Hermes *et al*., 1996; Belenky *et al*., 2008). SCN neurons fire in a 24h cycle that is driven by a transcriptional-translational loop (TTFL) (Saper *et al*., 2005). Hence, circadian clocks are vital in regulating an organism's sleep/wake

cycles. Sleep deprivation activates sleep-promoting homeostats that interplay with the circadian clock of what is now known as the two-process model (Borbely, 1982; Daan *et al*., 1984; McGinty and Szymusiak, 2000). This complex integration between the circadian and sleep/arousal neuroanatomy as well as the interconnectivity involved suggests potential sleep/wake disruptions to be associated with circadian anomalies which in turn may underlie broader cognitive and behavioural deficits.

Figure 1.2: SCN sleep/wake connectivity

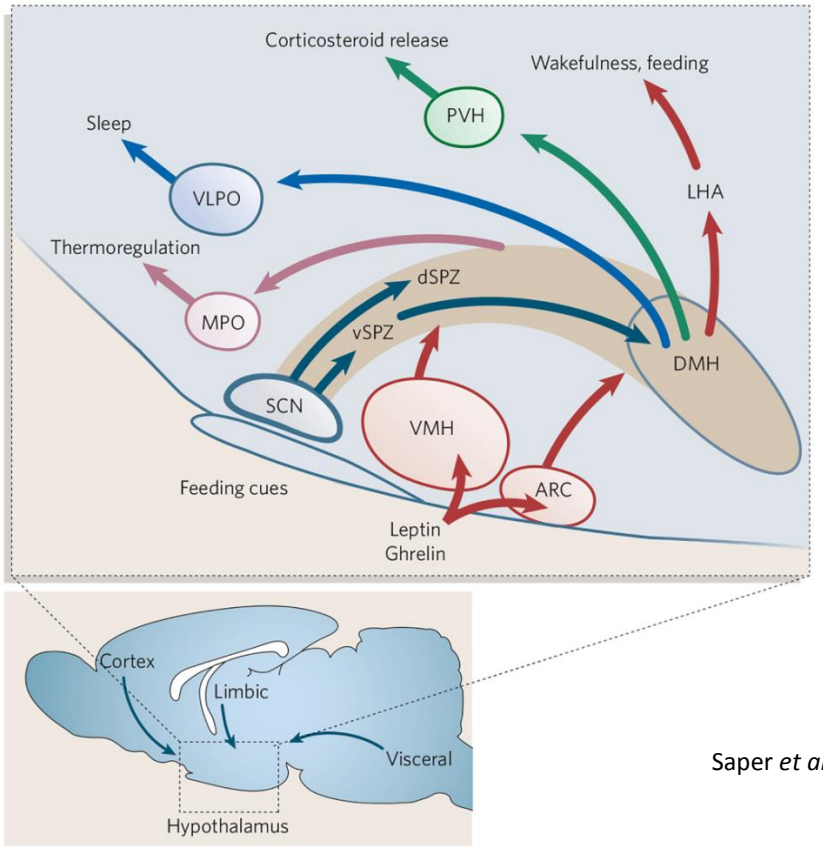

Saper *et al*., 2005

Figure 1.2: SCN projections are designated by dark blue arrows, wake promoting areas are in red, sleep promoting areas are light blue, corticosteroid regulation in green and thermoregulation in pink. The major output of the SCN is received through the d/vSPVZ and the DMH. The hypothalamic areas project to the brainstem, VLPO, MPO, TMN, LH and PVH. The LHA contains the arousal driving orexin neurons which share reciprocal connections with the SCN. Major sleep-promoting areas include the VLPO and MPO. Non-photic information is conveyed to the SCN by several areas including the raphe nucleus, VMH nuclei, ARC nuclei and IGL where the DMH is suspected to be important in the food entrainable oscillator. Additionally, visceral stimuli, emotional limbic inputs and cortical cognitive inputs participate in the circadian synchronization to external influences. Further abbreviations-ARC: Arcuate nuclei, d/vSPVZ: Dorsal/ventral subparaventricular zone of the hypothalamus, DMH: Dorsomedial hypothalamus, VMH: Ventromedial nuclei, VLPO: Ventrolateral preoptic area, MPO: Medial preoptic area, TMN: Tuberomamillary nucleus, PVH: Paraventricular nucleus, PH: Posterior Hypothalamus, LH: Lateral Hypothalamus, IGL: Intergeniculate Leaflet.

1.2 Homeostatic and circadian regulation of sleep

Borbely originally described the two-process model which postulates that the homeostatic and circadian processes interact to regulate sleep/wake cycles (Borbely, 1982). Specifically, the homeostatic process controls the exponentially increasing need to sleep during prolonged wakefulness (Figure 1.3A). Sleep onset is triggered when the homeostatic process reaches an upper threshold; awakening when the same process approaches a lower threshold (Figure 1.3A). Importantly, it has been shown to be functionally different from the circadian system as SCN lesioned rodents display elevated sleep requirements following prolonged wake periods (Tobler *et al*., 1983). Similarly, VLPO lesioned animals display abnormal fragmentation, characteristic of irregular sleep/wake patterns during their sleep cycle (Lu *et al*., 2000; Saper *et al*., 2005). These animals show significant increase of sleep episodes and decreased sleep durations per episode, leading to chronic fatigue (Lu *et al*., 2000). Nevertheless, the homeostatic and circadian processes are indeed interacting as the sleep/wake homeostatic thresholds show a circadian rhythm (Daan *et al*., 1984) (Figure 1.3A). The circadian control of sleep was evident when rhythmic sleep/wake cycles persisted in free-running conditions (Czeisler *et al*., 1980). The circadian process controls the phase of high and low sleep propensity across a 24h period independent of previous wake episodes (Figure 1.3A).

Hypothalamic centres of sleep regulation include the sleep-promoting neurons of the VLPO and MPO (Gong *et al*., 2004). Despite the lack of an activity increase in the VLPO during sleep deprivation, the firing rate doubles during the sleep/wake transition following restricted sleep periods (Sherin *et al*., 1996; Lu *et al*., 2002). Adenosine, a product of ATP catabolism, is up-regulated during sleep deprivation as a result of glycogen metabolism in the

brain (Strecker *et al*., 2000; Kong *et al*., 2002). Interestingly, an injection of adenosine A2a receptor agonist near the VLPO of rats induces sleep and also up-regulates expression of Fos, a marker of neuronal activity (Scammell *et al*., 2001). Additionally, serotonin, noradrenaline and other neurotransmitters can suppress the VLPO (Gallopin *et al*., 2000; Chou *et al.*, 2002). One such example is orexin, which forms the basis of the flip-flop switch model (Saper *et al*., 2001). The orexin system is active during wakefulness and contains ascending projections to the cerebral cortex while it also innervates all monoaminergic and cholinergic neurons involved in arousal (Chemelli *et al*., 1999; Peyron *et al*., 2000). Mutual projections between the VLPO neurons and the orexin neurons exist, although the VLPO lack any orexin receptors (Sakurai *et al*., 2005). Therefore, orexin neurons participate in the arousal process but do not directly regulate VLPO processes. This asymmetric regulation of sleep may help generate consolidated sleep periods following prolonged wakefulness (Figure 1.3B). Narcoleptic people appear to lack this flip-flop switch as sleep duration is relatively stable when compared to healthy individuals. Instead, destabilisation of the flip-flop mechanism in such individuals leads to an increase of sleep episodes (Sakurai *et al*., 2005).

Recently cortical neuronal populations have also been associated with the homeostatic regulation of sleep (Vyazovskiy *et al*., 2011; Nobili *et al*., 2012). The best marker of the homeostatic driver is the EEG (electroencephalography) slow-wave activity (low frequency, high-amplitude waves) during non-rapid eye movement sleep (NREM), which increases with prolonged wakefulness and decreases across sleep epochs (Borbely *et al*., 1981; Lancel *et al*., 1991). It was shown that cortical neuronal subpopulations enter in slow oscillation during sleep deprivation, a mechanism that may partially explain the reduction of cognitive performance during prolonged wakefulness (Vyazovskiy *et al*., 2011; Nobili *et al*., 2012).

Figure 1.3: Homeostatic and circadian regulation of sleep/wake cycles

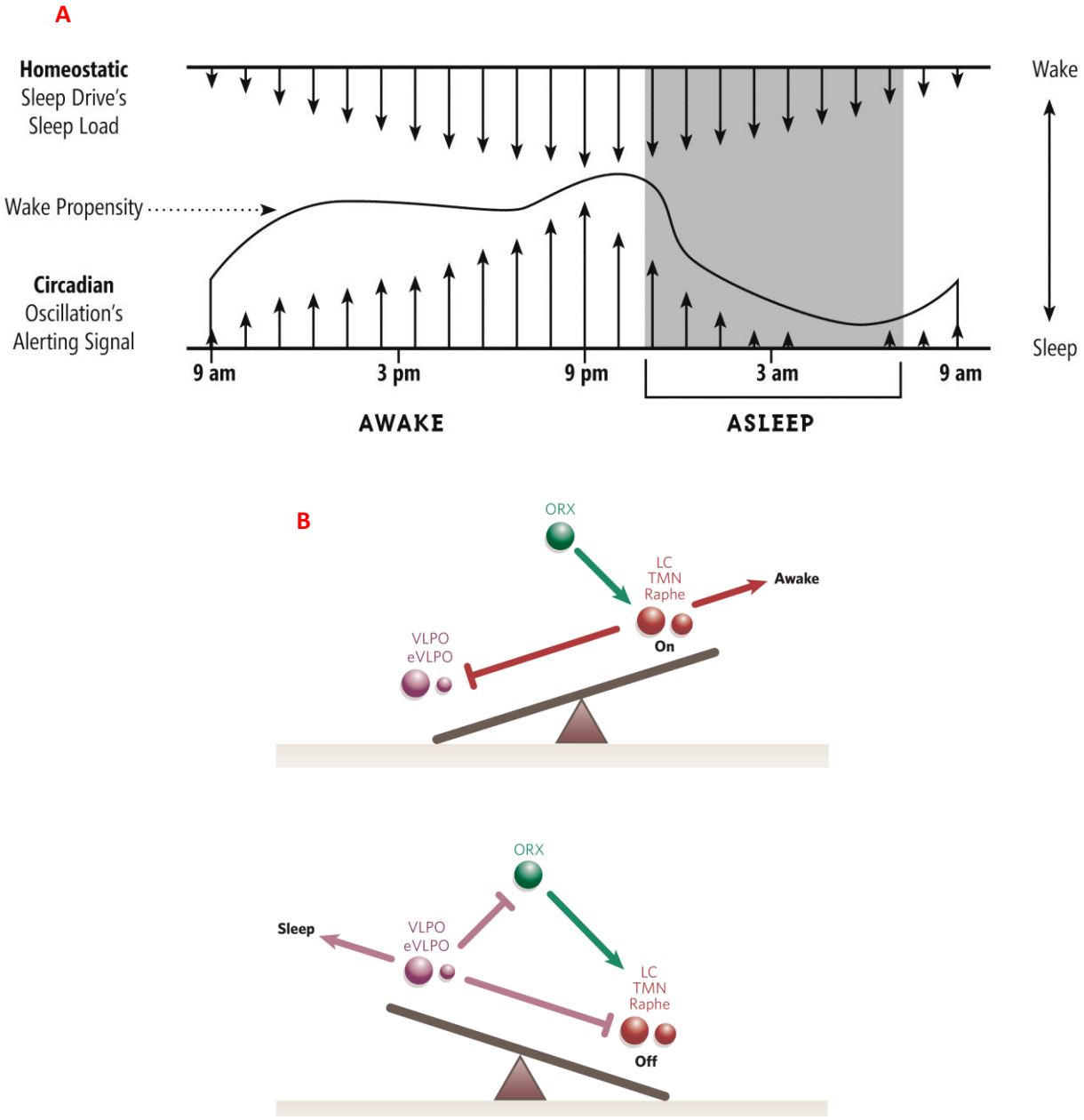

Based on Dijk and Edgar, 1999

Figure 1.3: (**A**) Graphic illustration of the two-process model of sleep regulation. The contribution of the homeostatic and circadian process in structured sleep/wake cycles is represented. The homeostatic process has an increase in the accumulating sleep load during wakefulness and this load is alleviated during sleep. The different, yet interacting, circadian process of sleep regulation facilitates the rhythmic cycle of sleep and is reinforced by the light input to the retina during the day and the release of melatonin from the pineal gland during the night (**B**) Diagram demonstrating the interaction of hypothalamic centres participating in the homeostatic regulation of sleep. During wakefulness, the monoaminergic nuclei (in red) inhibit the ventrolateral preoptic nucleus (VLPO; in purple), while the orexin (ORX) neurons (in green) reinforce the activity of these arousal promoting centres. During sleep, the VLPO firing neurons inhibit both the monoaminergic and orexin centres preventing any arousal to occur. This interacting mechanism between sleep- and wake-promoting hypothalamic centres forms the basis of the flip-flop switch during sleep/wake transitions. Further abbreviations-eVLPO: Extended ventrolateral preoptic nucleus, LC: Locus coeruleus, TMN: Tuberomammillary nucleus.

1.3 TTFL, Non-transcriptional oscillation and SCN Neuropeptides

The suprachiasmatic nucleus (SCN) is believed to be the dominant circadian pacemaker driving behavioural rhythms (Stephan and Zucker, 1972; Moore *et al*., 1983; Ralph *et al*., 1990). When examined independently, neuronal cells from the SCN region behave autonomously and are able to regulate neuronal firing in a rhythmic way (Green and Gillete, 1982; Welsh *et al*., 1995; Yamazaki et al., 1998; Gachon *et al*., 2004). Interconnectivity in the SCN is complementary to the cellular autonomy exhibited by the SCN neurons when dissociated in cell culture (Low-Zeddies and Takahashi, 2001; Reppert and Weaver, 2002; Panda *et al*., 2002; Liu *et al*., 2007b; Hastings *et al*., 2008). This interconnectivity promotes phase plasticity of output signals to peripheral tissues (Tousson and Meissl, 2004; Gachon *et al*., 2004; Herzog *et al*., 2004; Kalsbeek *et al*., 2006; Liu *et al*., 2007b).

The suprachiasmatic nucleus regulates the circadian synchronisation of numerous peripheral organs such as the liver and the heart (Pando *et al*., 2002; Reppert and Weaver, 2002). It generates circadian rhythms independently but is also able to entrain in response to light stimulation (Shigeyoshi *et al*., 1997; Lucas *et al*., 2001; Wright *et al*., 2002). At the circadian cellular level a core transcriptional feedback mechanism by Circadian locomotor output kaput/Brain and muscle ARNTL1 (CLOCK/BMAL1) heterodimers is chiefly responsible in regulating a negative loop (Herzog *et al*., 1998; Gekakis *et al*., 1998; Lee *et al*., 2001; Maywood *et al*., 2003; Sato *et al*., 2006). This particular basic helix-loop-helix transcription factor binds to E-box promoter regions acting as an enhancer on a family of Period (*Per1* to *Per3*) and Cryptochrome (*Cry1* and *2*) genes; thus increasing their protein expression (Kume *et al*., 1999; Vitaterna *et al*., 1999; Shearman *et al*., 2000; Travnickova-Bendova *et al*., 2002).

Post-transcriptional and post-translational processes including PER/CRY dimerisation and delay of nuclear entry generate a time lag in negatively inhibiting the transcription process of their own genes (Lee *et al*., 2001; Eide *et al*., 2002; Akashi *et al*., 2002). Finally, ubiquitin ligase modifications on CRY and PER induce decreasing levels by F-box/LRR-repeat protein 3 (FBXL3) and Beta-transducin repeat containing E3 ubiquitin protein ligase (β-TrCP1) complexes that aid the resetting of rhythmic oscillations (Lee *et al*., 2001; Yagita *et al*., 2002; Siepka *et al*., 2007; Reischl *et al*., 2007). In addition to the above feedback mechanism, an additional loop is present whereby nuclear receptor subfamily 1, group D, member 1 (REV-ERBa) binds at RAR-related orphan receptor (ROR) elements in order to reduce the mRNA levels of *Bmal1*, further contributing to the robustness of the system (Shearman *et al*., 2000; Ueda *et al*., 2002; Preitner *et al*., 2002). Therefore, intracellular transcriptional/translational feedback loop (TTFL) mechanisms dictate a rhythmic daily cycle governed by a network of genetic factors establishing parallel positive and negative feedback loops in an attempt to regulate precisely the expression of the core clock genes (Shearman *et al*., 2000; Panda *et al*., 2002).

Emerging evidence suggests the existence of a non-transcriptional oscillation (NTO) mechanism (Tomita *et al*., 2005; O'Neil *et al*., 2011; van Ooijen and Millar, 2012). Cyanobacteria could have their molecular clock reconstituted with 3 proteins and ATP (Nakajima *et al*., 2005; van Ooijen and Millar, 2012). Additionally, NTOs were subsequently shown to rhythmically regulate transcriptional and cell division events (Dong *et al*., 2010; Hosokawa *et al*., 2011; van Ooijen and Millar, 2012). Importantly, peroxiredoxin modifications in human red blood cells exhibited rhythmic oscillations without a rhythmic RNA counterpart (O'Neil *et al*., 2011). This peroxiredoxin NTO mechanism appears to be

shared across all species tested, suggesting a universal mechanism to timekeeping (Edgar *et al*., 2012; van Ooijen and Millar, 2012).

Variations in daily photoperiods influence circadian expression patterns (Ciarleglio *et al*., 2011; Zantke *et al*., 2013). Photic stimulation induces the expression of immediate early genes (Figure 1.4) such as *c-fos* (FBJ mouse osteosarcoma viral oncogene homolog), *jun-B* as well as *Per1* and *Per2* to generate a new feedback cycle (Saffen *et al*., 1988; Rusak *et al*., 1990; Kornhauser *et al*., 1990; Shigeyoshi *et al*., 1997). Glutamatergic as well as pituitary adenylate cyclase activating polypeptide (PACAP) signalling transmit electrical pulses due to photic activation in parallel to neuropeptide Y (NPY) via the intergeniculate leaflet (IGL) (van den Pol, 1991; Hamada *et al*., 1999; Chen *et al*., 1999). Intercellular SCN synchronisation relies heavily on G-Protein-coupled receptor and neuropeptide synchronisers such as vasoactive intestinal polypeptide (VIP) and gastrin-releasing peptide (GRP) in the core with arginine vasopressin (AVP) in the shell (Samson *et al*., 1979; Honma *et al*., 1998; Murakami *et al*., 1991; Aton *et al*., 2005). Non-photic synchronisation via 5-hydroxytryptamine (5-HT) from the raphe nucleus, NPY via the IGL as well from the dorsomedial hypothalamus (DMH) is vital in maintaining a balanced circadian rhythm (Maywood *et al*., 1997; Ehlen et al., 2001; Glass et al., 2003; Challet and Pevet, 2003). Calcium (Ca^{2+}) and cyclic adenosine monophosphate (cAMP) response-elements are vital in regulating period gene expression, a process enabled via signalling cascades along the cAMP response-element binding protein pathway (phospho-CREB) (von Gall *et al*., 1998; Tischkau *et al*., 2000; Travnickova-Bendova *et al*., 2002; Oster *el al*., 2003; Tischkau *et al*., 2003). Gamma-amino butyric acid (GABA) and glutamatergic output signalling are vital in regulating a coherent peripheral synchrony and work in concert with AVP and prokineticin 2 (PK2) (Robinson *et al*., 1988; Okamura *et al*., 1989; Cheng *et al*., 2002; Albus *et al*., 2005).

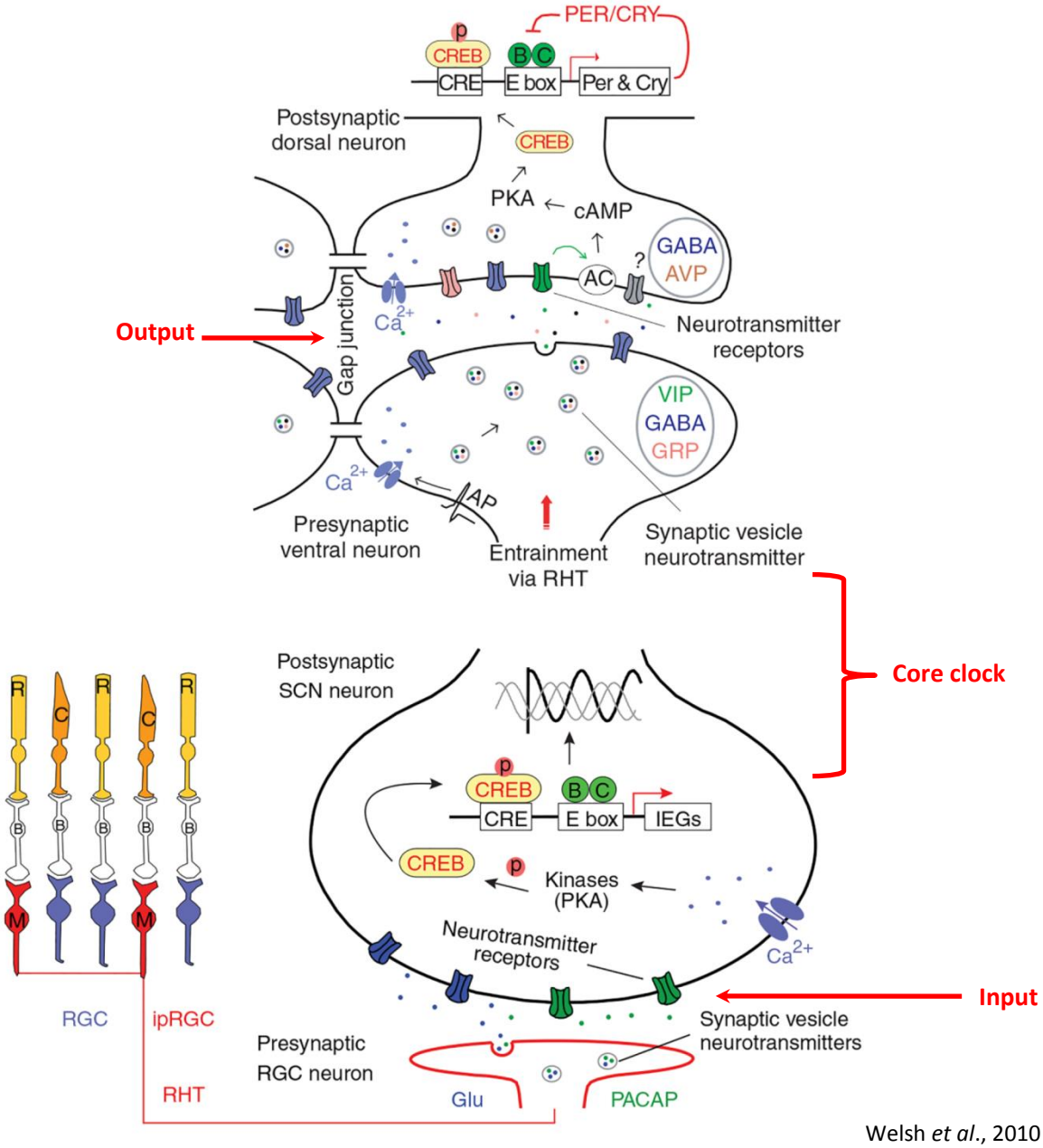

Welsh *et al*., 2010

Figure 1.4: Signalling in the circadian axis

Rods (R) and Cones (C) of the retina recognise light and via Bipolar cells (B) communicate to the Melanopsin-containing intrinsically photosensitive retinal ganglion cells (ipRGC) whose axonal projections form the Retinohypothalamic Tract (RHT). RHT-mediated electrical stimulation is succeeded by neurotransmitter release between the presynaptic and postsynaptic cleft (Input stage). Glutamate and PACAP are primary neurochemicals relaying the input information. The acute signalling cascade leads to PKA phosphorylating CREB and subsequent immediate early gene expression. Entrainment of a new circadian cycle has commenced and is followed by the spread of the generated Action Potential (AP) to the rest of the SCN and eventually peripheral organs (Output stage). Ca^{2+} influx in pre- and post-synaptic terminals as well as cAMP levels in association with neurotransmitter release (such as VIP and AVP) in the synapse are fundamental for interneuronal communication.

1.4 Bad clocks: Neuropathology linked to circadian pathology

Numerous neuropathological CNS (central nervous system) disorders such as Alzheimer's and Parkinson's disease show considerable circadian disruption (Barnard and Nolan, 2008). In neurodegenerative diseases and ageing, disruptions in sleep-related mechanisms and the circadian axis are common secondary features to the deterioration associated in the brain network (Ferreira *et al*., 2006; Landolt *et al*., 1996; Morton *et al*., 2005; Van Someren, 2000; Volicer *et al*., 2001; Dijk *et al*., 2000).

Age-associated circadian malfunction includes increased variability in activity onset, considerable lengthening of the period, circadian amplitude reduction and abnormal electrophysiology in rodents (Valentinuzzi *et al*., 1997; Nygard *et al*., 2005). Recent work has illustrated how circadian misalignment can contribute to altered emotional wellbeing (Easton *et al*., 2003; Roybal *et al*., 2007). Loss or mutations in any of the clock genes (*Bmal*1, *Clock/Npas2*, *Per1* and *Per2*) generate cognitive phenotypes (e.g. defective long-term potentiation), altered emotional states with deficits in fear-conditioning paradigms as well as motor defects (Garcia *et al*., 2000; Sakai *et al*., 2004; Zueger *et al*., 2006; Easton *et al*., 2003; Roybal *et al*., 2007). Similarly, defects in SCN-expressed neuropeptides such as NPY or VIP generate increased emotional instability in rodents such as anxiety and aggression (Karl *et al*., 2006; Wersinger *et al*., 2007). The correlation between circadian anomalies and cognitive perturbation has been extensively documented. In addition, pharmacological treatments with mood-stabilising agents (e.g. lithium) are able to rescue behavioural disturbances in *Clock*Δ19 mutants possibly via a glycogen synthase kinase 3β (GSK3β) circadian dependent mechanism (GSK3β controls PER2 and REV-ERBa clock protein stabilty) (Roybal *et al*., 2007; Iitaka *et al*., 2005; Yin *et al*., 2006).

Although the exact mechanisms linking circadian rhythm disruption and neuropathology remain largely unexplored, considerable efforts to document the precise circadian phenotype for each neurodegenerative and neuropsychiatric disorder have been undertaken (Table 1.1). Sleep disturbances in two of these disorders (PD and schizophrenia) are investigated in this thesis by evaluating circadian rhythm abnormalities in animal models.

Table 1.1: Human neurological diseases and sleep endophenotypes

Human Disease	Disturbed Sleep/Wake Rhythms
Familial advanced sleep phase syndrome (FASP)	Shorter circadian rhythms (Jones *et al*., 1999)
Delayed sleep phase syndrome (DSPS)	Delayed activity phase, core body temperature, sleep and melatonin cycles (Okawa *et al*., 2007)
Mood disorders (unipolar and depression) and psychoses (schizophrenia, bipolar)	Depression: Increased sleep latency, impaired sleep continuity, phase advance in endogenous circadian schedule, phase advance in growth hormone/plasma melatonin and increased plasma cortisol during night Psychoses: Major phase disturbances in sleep-activity cycles, hormonal and temperature levels (Boivin, 2000; Mc Clung, 2007; Wirz-Justice, 2006)
Parkinson's Disease (PD)	Sleep fragmentation, sleep apnoea, REM sleep disorder and excessive daytime sleepiness (Ferreira *et al*., 2006)
Huntington's disease (HD)	Nocturnal awakening and progressive loss of daily activity rhythms (Morton *et al*., 2005)
Alzheimer's disease (AD)	Sleep fragmentation, increased nocturnal activity and reduced daytime activity (Volicer *et al*., 2001)
Ageing	Sleep disturbances due to shorter sleep epochs. Attributed to age-related circadian amplitude inhibition and rhythm advance (Van Someren, 2000; Dijk *et al*., 2000)

Based on Barnard and Nolan, 2008

Table 1.1: Human CNS Disease and corresponding sleep perturbations.

1.5 Schizophrenia

Schizophrenia is a neurodevelopmental disorder with a high genetic penetrance between monozygotic twins (85% heritability) (Cannon *et al*., 1998; Cardno *et al*., 1999; Cardno *et al*., 2000; Cardno *et al*., 2002, Rijsdijk *et al*., 2005; Corradini *et al*., 2009). Incidence rates are roughly 1% of global population arising in a post-adolescent context through possible genetic predispositions interplaying with environmental insults (Corradini *et al*., 2009; Ayalew *et al*., 2012).

Clinically, schizophrenia is characterised by 'positive' and 'negative' symptoms that possibly arise from dysfunctional neurotransmitter circuitry (Corradini *et al*., 2009). 'Positive' symptoms include hallucinations and emotional instability while 'negative' symptoms such as cognitive decline and delusions are also present (Corradini *et al*., 2009). Alterations in early brain circuitry in the dopaminergic as well as glutamatergic systems have been indicated as potential neurodevelopmental mechanisms (Rehn and Rees, 2005; Lang *et al*., 2007; Walsh *et al*., 2008; Corradini *et al*., 2009).

Numerous GWAS (Genome-Wide Association Study) and meta-analyses have reported a dozen promising candidate genes (Gogos and Gerber, 2006; Johnson *et al*., 2008; Ayalew *et al*., 2012; Ginsberg *et al*., 2012). Candidate proteins appear to cluster around the synaptic area and include chromosomal region 22q11, proline dehydrogenase (Karayiorgou *et al*., 1995; Johnson *et al*., 2008; Sleiman *et al*., 2013). Dysbindin in chromosomal region 6p, neuregulin 1 on chromosome 8p and catechol-O-methyltransferase on 22q11 have been strongly implicated as candidate risk genes (Straub *et al*., 2002; Stefansson *et al*., 2002; Shifman *et al*., 2004; Johnson *et al*., 2008; Ayalew *et al*., 2012). Additionally, SNARE (Soluble

N-ethylmaleimide sensitive factor (NSF) Attachment Receptor proteins) have been linked to schizophrenia with SNPs in syntaxin 1 and alterations in complexin, synaptotagmin XI and SNAP-25 (Synaptosomal-associated protein 25) (Wong *et al*., 2004; Tachikawa *et al*., 2001; Muller *et al*., 2005; Lee *et al*., 2005; Inoue *et al*., 2007; Johnson *et al*., 2008; Ayalew *et al*. 2012; Sleiman *et al*., 2013). Cytoskeletal scaffolds such as DISC1 (disrupted-in-schizophrenia-1) and metabotropic glutamate receptors such as GRM3 have also been associated with this disorder underscoring the relevance of synaptic dis-connectivity (Kirov *et al*., 2005; Corradini *et al*., 2009; Ayalew *et al*., 2012; Costas *et al*., 2013).

1.5.1 Circadian Disruption in Schizophrenia

Circadian rhythm disruption in schizophrenic patients has been well observed and characterised (Figure 1.5) (Martin *et al*., 2001; Poulin *et al*., 2003; Chouinard *et al.*, 2004; Martin *et al*., 2005; Wulff *et al*., 2006; Benson, 2006; Mattai *et al*., 2006; Forest *et al*., 2007; Krystal *et al*.,2008; Wulff *et al*., 2012). Circadian abnormalities are highly penetrant among schizophrenic patients (up to 80% of patients) (Tan and Ang, 2001; Monti and Monti, 2005; Wulff *et al*., 2012). Furthermore, circadian deficits associated with schizophrenic genetic predisposition increases the risk for developing a schizophrenic phenotype (Ruhrmann *et al*., 2010).

Schizophrenic endophenotypes include longer sleep latency and greater sleep fragmentation, severe circadian biomarker phase misalignments including perturbed sleep/wake cycles (Figure 1.5), temperature and hormonal rhythms (Boivin, 2000; Mc Clung, 2007; Wirz-Justice, 2006; Barnard and Nolan, 2008). Particularly, sleep latency and sleep periods are significantly longer in the schizophrenic group suggesting inconsistent sleep/wake epochs (Figure 1.5) (Wulff *et al*., 2012). Interestingly, 50% of schizophrenic participants

exhibit an irregular melatonin rhythm (Figure 1.5), while the rest exhibit normal melatonin rhythms despite irregular and fragmented sleep patterns (Wulff *et al*., 2012). Indeed, disruption of melatonin rhythms has been associated with non-24h sleep patterns (Figure 1.5) (Pandi-Perumal *et al*., 2008; Jan *et al*., 2009; Wulff *et al.*, 2009). Altered REM (Rapid eye movement) sleep activity and slow-wave sleep deficits are also present with the condition (Hudson *et al*., 1993; Hoder *et al*., 2004; Keshavan *et al*., 1998). These findings suggest potential circadian disturbances in schizophrenia and are independent of antipsychotic treatment (Wulff *et al*., 2012; Pritchett *et al*., 2012).

Figure 1.5: Representative control versus schizophrenic actograms

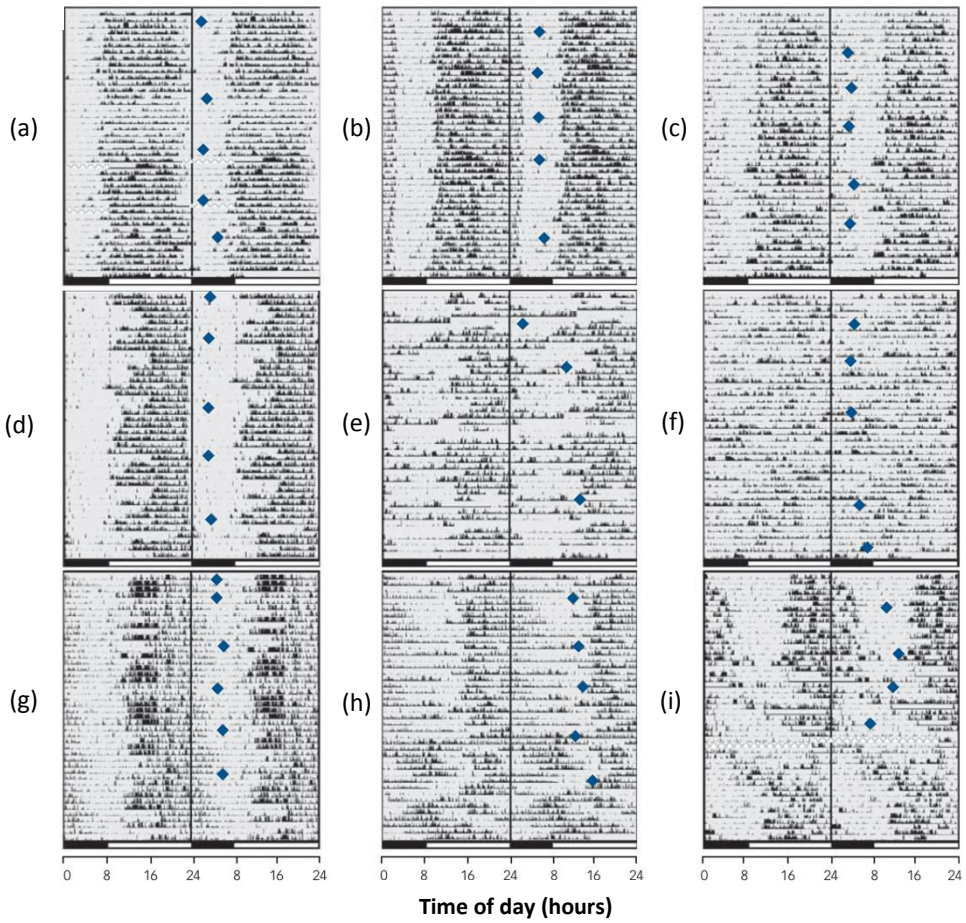

Wulff *et al.,* 2012

Figure 1.5: Representative (**a-c**) control actograms showing entrainment, schizophrenic (**d**) actogram showing entrainment with variable sleep periods, schizophrenic (**e**) actogram showing disrupted rest/activity cycles, schizophrenic (**f**) actogram showing irregular cycles, schizophrenic (**g**) actogram showing phase delayed rest/activty cycles, schizophrenic (**h**) actogram showing reversed rest/activity cycles alternating with free-running periods and schizophrenic (**i**) actogram showing delayed rest/activity cycles alternating with free-running periods. Blue diamonds correspond to peaks of melatonin rhythms, an indicator of circadian phase. Interestingly, some actograms (**f**) from schizophrenic patients display disrupted rest/activity cycles despite normal melatonin peak times.

1.5.2 Circadian Disruption in Schizophrenia: Historical Background

Circadian abnormalities in schizophrenia have been partially documented since the early 20th century, an era predating the discovery and widespread distribution of antipsychotics in the mid-1950s (Ewen, 1934). Early investigations recorded fragmented sleep/wake cycles; compromised interdaily stability, enhanced intradaily variability as well as circadian phase alterations (Ohta and Endo, 1985; Martin *et al*., 2005).

1.5.3 Circadian Disruption in Schizophrenia: Pharmacological Background

Historically, physicians reported sleep disturbances in schizophrenia to be associated with side-effects of antipsychotic medication (Miller, 2004). Many typical antipsychotics do carry a sedative side-effect at higher doses but sleep deficits are also present in medication-free schizophrenic subgroups (Miller, 2004; Krystal *et al*., 2008; Wulff *et al*., 2010). Importantly, sleep disruption constitutes a crucial prodromal symptom prior to the first psychotic schizophrenic episode, occurring during a medication-free period (Wulff *et al*., 2010). In fact, emerging data point out that administration of antipsychotics improves sleep/wake cycles in patients (Cohrs, 2008; Krystal *et al*., 2008). Diminished sleep fragmentation and improved sleep quality are exhibited in antipsychotic-treated schizophrenics (Cohrs, 2008). Additionally, numerous animal models of schizophrenia demonstrate alleviation of schizophrenic endophenotypes during antipsychotic treatments, and mood-stabilisers (e.g. Lithium) appear to at least partly exert their therapeutic effect via the circadian axis (Sorge *et al*., 2004; Tada *et al*., 2004; Nilsson *et al*., 2006; Su *et al*., 2007; Roybal *et al*., 2007). Thus, emerging evidence in both animal and patient investigations appear to positively correlate antipsychotic treatment with structured sleep/wake cycles. Since many schizophrenic patients display abnormal rest/activity cycles it may be

hypothesised that circadian disruption may partly contribute to this phenotype (Wulff *et al*., 2012).

1.5.4 Circadian Disruption in Schizophrenia: Genetic Background

Animal studies have correlated core clock genes with mood disorders such as schizophrenia and bipolar disorder. *Clock*, *Per1*, *Per3*, *Bmal1* and *Cry1* have all been identified as potential candidate genes participating partly in the neurodevelopment of schizophrenic endophenotypes in subgroups of patients (Mansour *et al*., 2006; Peng *et al*., 2007; Takao *et al*., 2007). Moreover, schizophrenic candidate genomic regions (Figure 1.6), flagged by GWAS and linkage studies, suggest synaptic communication is potentially compromised in the disorder (Craddock *et al*., 2005). Candidate genes like *Disc1*, *Nrg1*, *Comt*, *Dao, Dysbindin* and *Snap-25* have been strongly implicated in the pathogenesis of the disorder (Johnson *et al*., 2008; Corradini *et al*., 2009).

Figure 1.6: Chromosomal map of genetic anomalies associated with schizophrenia and bipolar disorder

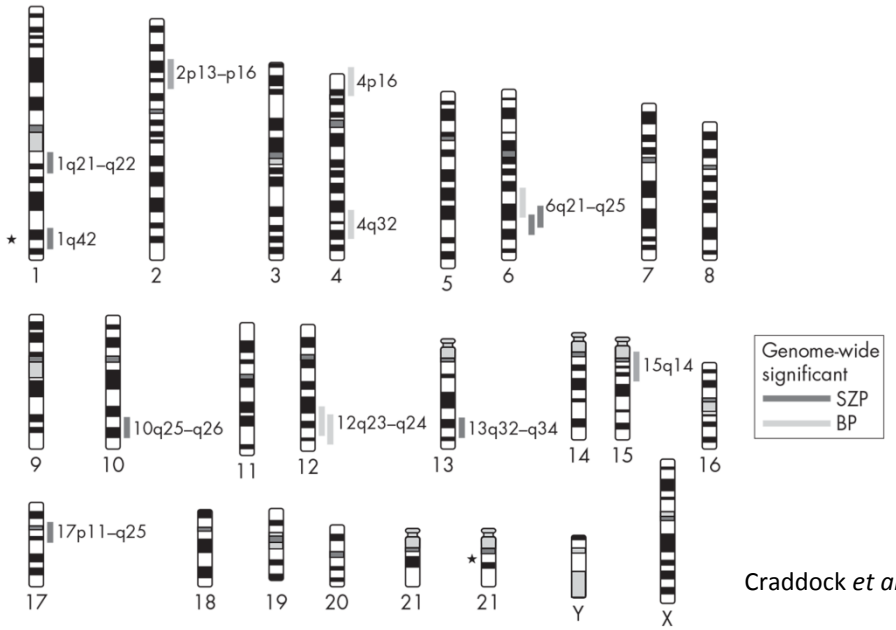

Craddock *et al.,* 2005

Figure 1.6: Chromosomal aberrations overlap between neuropsychiatric conditions. Asterisks denote schizophrenic only defects.

1.5.5 Circadian Disruption in Schizophrenia: Functional Background

Malfunctions of thalamic and hypothalamic circuitry are a hallmark symptom of schizophrenic patients (Goldstein *et al*., 2007; Koolschijn *et al*., 2008). Sleep/wake centres are irregularly operating due to compromised neuronal circuitry as measured by abnormal glutamate signalling in the schizophrenic thalamus (Meador-Woodruff *et al*., 2003; Crespo-Facorro *et al*., 2007; Harms *et al*., 2007; Watis *et al*., 2008). Sub-cortical hypothalamic structures principally participating in sleep/wake mechanisms are also impaired, compromising hypothalamic-cortical connectivity (Lambe *et al*., 2007). This was determined by a reduction of excitatory postsynaptic currents in the prefrontal cortex from rat brain slices (Lambe *et al*., 2007). Moreover, partial cognitive decline coupled to cognitive arousal is strongly associated with sub-cortical and pre-frontal cortex regions, networks interacting directly or indirectly with the circadian system of an individual (Chen and Faraone, 2000; Cornblatt and Malhotra, 2001; Nieuwenstein *et al*., 2001).

Emerging evidence suggests widespread compromise of the circadian axis in multiple psychiatric disorders including schizophrenia, bipolar disorder, attention deficit hyperactivity disorder (ADHD), Parkinson's and Alzheimer's diseases (Berrettini and Berrettini, 2000; Sachs, 2000; Maziade, 2001; Becker, 2004; Banaschewski, 2005). Particularly, neuropsychiatric conditions that share common genetic mechanisms like schizophrenia and bipolar disorder may also share overlapping circadian deficits (Freinberg and Campbell, 2010). The significance of functional sleep/wake cycles in cognitive fitness and neuropsychiatric conditions is well established and it is therefore critical to characterise the circadian deficits of such neurological disorders with standardised methodologies.

1.5.6 Circadian Disruption in Schizophrenia: Endophenotype

Identifying robust endophenotypes in complex neuropsychiatric disorders is critical (Braff, 2008). Disrupted sleep/wake cycles in neuropsychiatry are increasingly emerging as robust translational endophenotypes (Yang and Winkelman, 2006; Chen *et al*., 2006; Cryan and Slattery, 2007). Given the extensive interconnectivity between cognitive fitness and circadian endophenotypes circadian disruption has been proposed as a potential endophenotype in a clinical setting (Ferrarelli *et al*., 2007; Gottesmann and Gottesman, 2007). The genetic heritability of sleep is complex and potential co-segregation with schizophrenic risk genes may identify endophenotypes associated with circadian irregularities (Mackiewicz and Pack, 2003; Hamet and Tremblay, 2006; Ebisawa, 2007). Interactions between circadian pathology and schizophrenia have broader consequences for the well-being of a patient (Table 1.2). Demotivation, anti-social behaviour and progressive cognitive decline are established symptoms of schizophrenics in a clinical setting.

Table 1.2: Disrupted sleep/wake cycles and associated systemic impact

Emotional impact	Cognitive impact	Somatic impact
Mood alterations (Banks and Dinges, 2007; Oginaska and Pokorski, 2006; Scott *et al*., 2006; Selvi *et al*., 2007)	Cognitive deficits and multi-tasking impairment (Dinges *et al*., 1997; Lamond *et al*., 2007; Pilcher and Huffcutt, 1996)	Micro-sleeps and excessive sleepiness (Philip and Akerstedt, 2006; Pilcher *et al*., 2000; Scott *et al*., 2007)
Depression and psychosis (Johnson *et al*., 2006; Kahn-Greene *et al*., 2007; Riemann and Voderholzer, 2003; Sharma and Mazmanian, 2003)	Memory and attention deficits (Chee and Chuah 2008; Dworak *et al*.,2007; Goder *et al*., 2007; Oken *et al*., 2006)	High cancer risk (Davis and Mirick, 2006; Hansen, 2006)
Irritability, impulsivity and frustration (Dahl and Lewin, 2002; Kelman, 1999; Muecke 2005)	Communication deficits and poor decision making (Baranski *et al*., 2007; Harrison and Home 2000; Lucidi *et al*., 2000; Killgore *et al*., 2007).	Metabolic defects, diabetes and cardiovascular disease (Gangwisch *et al*., 2005; Knutson *et al*., 2007; Laposky *et al*., 2008; Maemura *et al*., 2007; Yang and Winkelman 2006; Young and Bray, 2007)
Risk-taking (Acheson *et al*., 2007; McKenna *et al*.,2007; O'Brien and Mindell, 2005; Venkatraman *et al*., 2007)	Impaired creativity and motor performance (Jones and Harrison 2001; Killgore *et al*., 2008; Randazzo *et al*., 1998; Kahol *et al*., 2008)	Impaired immunity to infections (Irwin 2002; Lorton *et al*., 2006) Deregulated hypothalamic-pituitary-adrenal (HPA) axis (Meerlo *et al*., 2008)

Table 1.2: Emotional, cognitive and somatic effects of disrupted sleep/wake cycles.

Based on Pritchett *et al.,* 2012

1.5.7 Circadian Disruption in Schizophrenia: Evidence from Mouse Models

Interspecies variability of endophenotypes constitutes a major challenge in translational studies of human neurological diseases (Chen *et al*., 2006; O'Tuathaigh *et al*., 2007). Animal models are assessed on their overall face and predictive validity (Amann *et al*., 2010). These factors account for the genetic pathophysiological aetiology equivalent to

human disease, the overlap in symptoms between animal models and their human counterparts and the pharmacological response to the diseased state (Lu, 2009).

Duplications within the *Vipr2* (VIP-receptor) gene generate elevated risks for developing schizophrenic-like behaviours (Vacic *et al*., 2011; Pritchett *et al*., 2012). Importantly, VIP and *Vipr2* synchronise the rhythmic SCN oscillations and are vital for inter-neuronal synchronisation (Maywood et al., 2006). A subset of *Vipr2*$^{-/-}$ mice displayed circadian abnormalities including a shorter free-running period of roughly 22 hours (Hughes and Piggins, 2008). Another subset of Vipr2$^{-/-}$ mice displayed arrhythmia, suggesting a continuum of behavioural phenotypes (Hughes and Piggins, 2008). Responses to nocturnal light pulses appeared normal in a subset of mice when compared to wild-type (WT) phase-response curve (PRC) (Hughes and Piggins, 2008). However, aberrant gating of photic input was recorded in Vipr2$^{-/-}$ as measured by immediate early gene (IEG; e.g. c-fos) immunohistochemistry (Hughes *et al*., 2004).

Neuregulin 1 is a growth protein participating in synaptic plasticity and dendritic arborisation and was identified recently as a schizophrenic candidate gene (Harrison and Law, 2006; Mei and Xiong, 2008). Schizophrenics exhibit altered CNS Nrg1 expression while *Nrg1*$^{+/-}$ mice have disrupted rest/activity rhythms (Johnson *et al*., 2002). Neuregulin is also present in both retinal ganglion cells and hypothalamic cells further confirming possible circadian involvement (Snodgrass-Belt *et al*., 2005; Bernstein *et al*., 2006; Sharif *et al*., 2009).

Cckar (Cholecystokinin A receptor) is a metabotropic receptor that exhibits altered expression levels in the CNS of schizophrenics (Bachus *et al*., 1997; Zachrisson *et al*., 1999; Noble *et al*., 1999). In addition, correlations between *Cckar* have been proposed particularly due to the dopaminergic involvement in *Cckar*-mediated production of catecholamines in the

mesolimbic system (Tachikawa *et al*., 2000; Toirac *et al*., 2007; Koefoed *et al*., 2009). Intraperitoneal administration of CCK induces circadian alterations including slow-wave sleep induction and locomotor activity suppression (Kapas *et al*., 1988). The arousal-promoting neurotransmitter orexin is stimulated by CCK, while its emerging role in photosensitivity and phase shifts suggests strong functional links to the circadian axis (Tsujino *et al*., 2005; Shimazoe *et al*., 2008).

Circadian Disruption and *Snap-25*

Part of the work in this project revolved around comprehending the mechanistic links between circadian rhythm disruption and synaptic dysfunction in the *Bdr* (blind-drunk) mouse model of schizophrenia that harbours a dominant gain-of-function mis-sense mutation in *Snap-25* (Synaptosomal-associated protein, 25kDa).

***Snap-25* and the synapse**

SNARE (Soluble NSF attachment protein receptor) factors are a group of functionally interacting binding partners vital in vesicle-trafficking and recycling (Figure 1.7) (Johnson *et al*., 2008). All SNARE factors share a homologous 60—70 amino acid long motif vital in synaptic vesicle-trafficking events (Johnson *et al*., 2008). SNAP-25 (synaptosomal-associated protein of 25 kDa), syntaxin-1A and VAMP-2 (vesicle-associated membrane protein/synaptobrevin) formulate a stable four-helix bundle termed the trans-SNARE complex (Sollner *et al*., 1993; Johnson *et al*., 2008).

Clostridial toxin experiments that fragment *Snap-25* demonstrated the obligatory nature of such a factor in facilitating vesicle-trafficking (Schiavo *et al*., 2000; Jahn *et al*., 2003; Jahn and Scheller, 2006; Corradini *et al*., 2009). *Snap-25*$^{-/-}$ and *Vamp2*$^{-/-}$ mice are postnatally lethal (Schoch *et al*., 2001; Washbourne *et al*., 2002). *Snap-25*$^{-/-}$ mice can be distinguished

from heterozygous viable embryos from excessive inactivity and locked posture (Johnson *et al*., 2008). Respiratory failure in the *Snap-25*$^{-/-}$ mice leads to death despite functional heart muscle contraction (Molnar *et al*., 2002; Johnson *et al*., 2008; Bark, 2009). On the other hand, syntaxin 1a$^{-/-}$ mice are viable with moderate spatial memory impairments probably due to compensatory effects of the syntaxin 1b isoform (Fujiwara *et al*., 2006).

Figure 1.7: SNAREs facilitate fusion of synaptic vesicles to the membrane

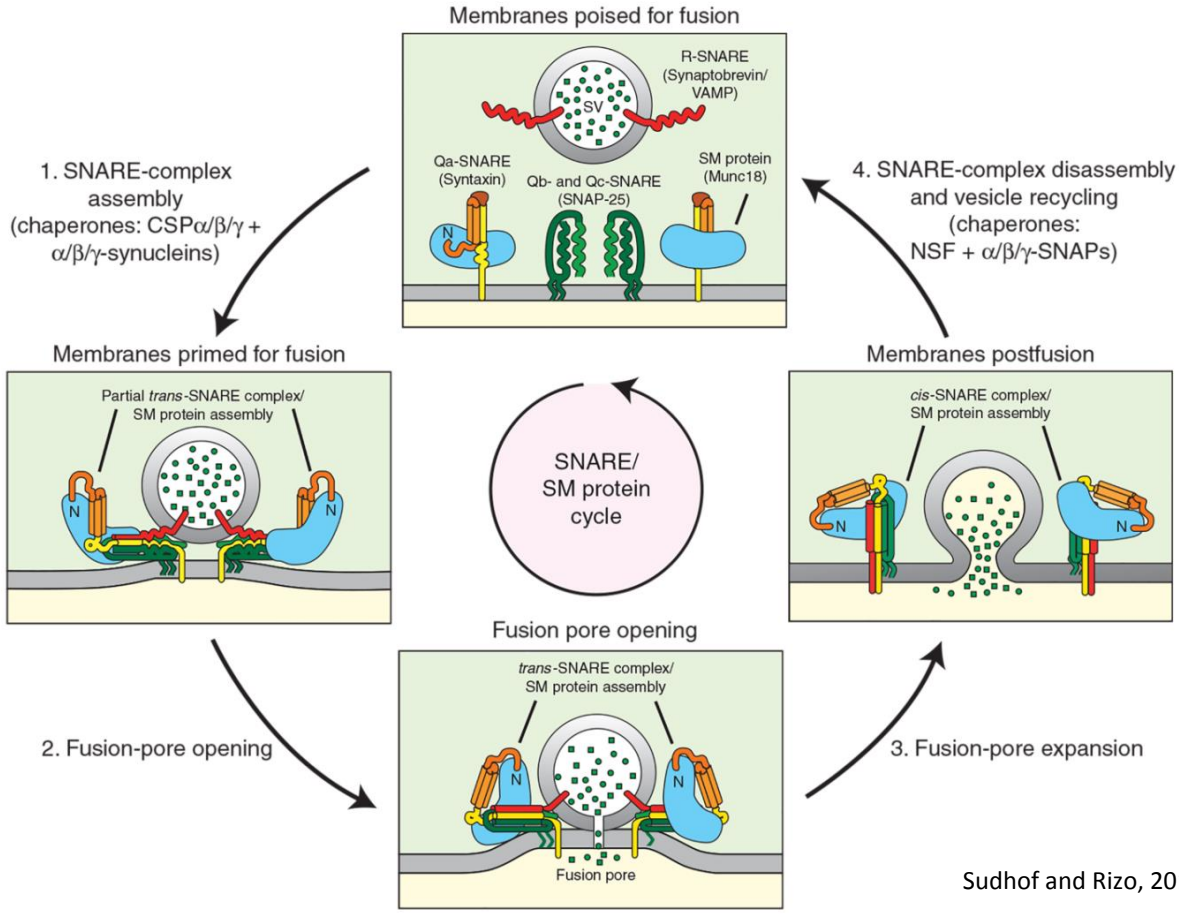

Sudhof and Rizo, 2011

Figure 1.7: The SNARE/SM (Sec1/Munc18-like) protein cycle. The diagram on top illustrates the SNARE/SM proteins prior to a fusion event. The fusion apparatus is either natively unfolded (e.g. R-SNARE) or folded in complexes (e.g. Synatixin/Munc18 binding). Next, the trans-SNARE complex begins assembling and zipping up (left diagram). Once the full-SNARE complex is assembled the fusion pore is generated, which expands so that the vesicle membrane collapses into the target membrane (bottom diagram). Finally, conversion to a cis-SNARE complex follows and subsequent dissociation by chaperones (e.g. NSF) occurs (right diagram).

Due to the fundamental role of SNAP-25 in vesicle-trafficking and neurotransmitter release (Figure 1.7), mutations that have an impact on this genomic locus or its regulatory elements can potentially generate disrupted sleep-activity rhythms (Stephan *et al*., 2006; Rockstroh *et al*., 2007). Candidate risk genes for schizophrenia associated with the synaptic machinery could provide insights into the mechanistic networks underlying schizophrenia and circadian disruption (Pritchett *et al*., 2012). Linkage and GWAS studies have implicated SNAP-25 in the pathogenesis of schizophrenia and mutant mouse models of the gene demonstrate schizophrenic endophenotypes (Lewis *et al*., 2003; Jeans *et al*., 2007; Oliver and Davies, 2009; Fanous *et al*., 2010; Oliver *et al*., 2012). Meta-analyses have associated the SNAP-25 chromosomal area (20p12.2) among the strongest 12 candidate risk regions (Moises *et al*., 1995; Lewis *et al*., 2003; Arinami *et al*., 2005; Gogos and Berber, 2006; Johnson *et al*., 2008).

Given its essential role in synaptic trafficking and evoked neurotransmission, the SNAP-25 candidate gene could represent a unique opportunity in comprehending any potential schizophrenic circadian disruption (Blasi *et al*., 1993; Sollner *et al*., 1993; Pozzi *et al*., 2008; Tafoya *et al*., 2008). Its ubiquitous expression across the CNS and the developmentally regulated levels of the embryonic/post-natal Snap-25a isoform and adult Snap-25b isoform demonstrate the spatial and temporal heterogeneity of the synaptic machinery (Tafoya *et al*., 2006; Garbelli *et al*., 2008; Matteoli *et al*., 2008). SNAP-25 protein de-regulation in schizophrenia has been documented in the cortex, hippocampus as well as cerebellum (Young *et al*., 1998; Karson *et al*., 1999; Fatemi *et al*., 2001; Honer *et al*., 2002; Mukaetova-Ladinska *et al*., 2002; Thompson *et al*., 2003; Knable *et al*., 2004). Additionally, pharmacological interventions potentially alter SNAP-25 levels and have an impact on cognitive abilities (Muller *et al*., 2005; Barr *et al*., 2006; Gosso *et al*., 2008; Spellman *et al*., 2008). Dysbindin and *Disc1* candidate genes also generate disrupted SNAP-25 pathways

revealing the mechanistic overlap of identified predisposing schizophrenic markers (Pletnikov *et al*., 2008; Ghiani *et al*., 2009). Abnormal synaptic interactions in the SNARE trafficking machinery in patients versus controls have been identified in the basal ganglia (Barakauskas *et al*., 2010).

Snap-25 is expressed in rodent SCN and is therefore useful for investigating circadian disruption in schizophrenia (Deery *et al*., 2009). Functional network oscillations and daily rhythms are vital in regulating SCN core clock and output factors (Webb *et al*., 2009). Diurnal sleep/wake cycles rely on regional hypothalamic vesicle-trafficking and disruptions to that system may result in circadian abnormalities (Hastings and Herzog, 2004; Welsh *et al*., 2010; Wulff *et al*., 2010; Wulff *et al*., 2012). SNAP-25-dependent NMDAR receptor trafficking is vital in regulating post-synaptic synchrony particularly at retinal input regions (Pennartz *et al*., 2001). Deficits in this system are manifesting as re-entrainment alterations to shifted LD cycles or abnormal photic sensitivities to variable illumination (Moldavan and Allen, 2010). Additionally, SNAP-25 is involved in GABAergic signalling transduction crucial in retinal homeostasis (Alix *et al*., 2008). Given the implicated role of SNAP-25 in schizophrenia and its suspected involvement in diurnal sleep/wake rhythms, systematic behavioural and molecular investigations were undertaken in a mutant mouse model, the *Bdr*.

The blind-drunk (Bdr) mouse model of schizophrenia

Random ENU mutagenesis programs have successfully generated a number of useful mouse models for a variety of mood-related behavioural disorders (Godinho and Nolan, 2006; Vitaterna *et al*., 2006; Oliver, 2011). The *Bdr* mice exhibit a slow ataxic gait as a result of a point mutation in the adult-expressed isoform *Snap-25b* (Oliver, 2011). The resulting mis-

sense point mutation transforms an isoleucine residue to a threonine residue at position 67 of exon 5b of *Snap-25b* (Figure1.8) (Jeans *et al*., 2007; Oliver *et al*., 2012).

Figure 1.8: Mouse protein *Snap-25b* sequence versus orthologous and paralogous targets



Jeans *et al*., 2007

Figure 1.8: Snap-25b amino acid sequences in different organisms and paralogous sequences demonstrating conservation of isoleucine at position 67 as indicated by the black arrow. Notice the *Bdr* mis-sense mutation to threonine at the same position.

The *Bdr* I67T dominant gain-of-function mis-sense mutation impairs the exocytotic vesicle recycling rates leading to cortical glutamatergic deficits (Jeans *et al*., 2007; Oliver, 2011). Experiments reported an inability to mobilise the reserve pool (RP) vesicles for replenishment of the readily releasable pool (RRP) due to an increasing binding affinity of the SNARE complex during vesicle-trafficking (Jeans *et al*., 2007; Oliver *et al*., 2011). Gross brain morphology appears unaltered up to a year of age while ataxia onset begins around 2 months of age (Jeans *et al*., 2007; Oliver and Davies, 2009). Behaviourally, the Bdr mice exhibit impaired sensorimotor gating as assessed by defective pre-pulse inhibition (PPI) (Oliver and Davies, 2009). In addition, pre-natal environmental stressors (PNS) enhance the PPI deficit, identifying a specific genetic x environment interaction (Oliver and Davies, 2009). This finding supports the genetic x environment interplay, contributing to the onset of neuropsychiatric conditions like schizophrenia and bipolar disorder in humans (Mirsky and Duncan, 1986; Harrison and Weinberger, 2005; Oliver, 2011). Importantly, PPI is a recognised schizophrenic

endophenotype that is rescued in the *Bdr* through the administration of antipsychotic drugs supporting the predictive validity of the model (Oliver and Davies, 2009; Oliver, 2011).

Initial circadian behavioural analysis of *Bdr* mice showed phase advance under LD (light-dark) cycles (24 hour period; divided between 12hr light and 12hr dark) with a fragmented rhythm (running activity in mutant mice began up to 6hr earlier than wild-type mice when adjusted for variability among mice examined) (Figure 1.9A). Response to a 6hr phase shift showed no significant difference between the wild type and mutant mice in terms of entrainment to the new Light-Dark cycle (Figure 1.9B). Moreover, free-running period assessment under constant DD (dark-dark) conditions was carried out to investigate the endogenous clock in both wild-type and mutant mice. Results illustrated no significant differences in period between the two groups with the exception of a less stable free-running onset in *Bdr* mice (Figure 1.9C). Finally, activity repression during a scotophase light pulse (negative masking-Figure 1.9D) and pupillometry data (not shown) reported no significant differences between genoypes. Taken together, these data suggest possible circadian defects in the *Bdr* mutant mice.

Figure 1.9: Circadian wheel-running data on *Bdr* mice

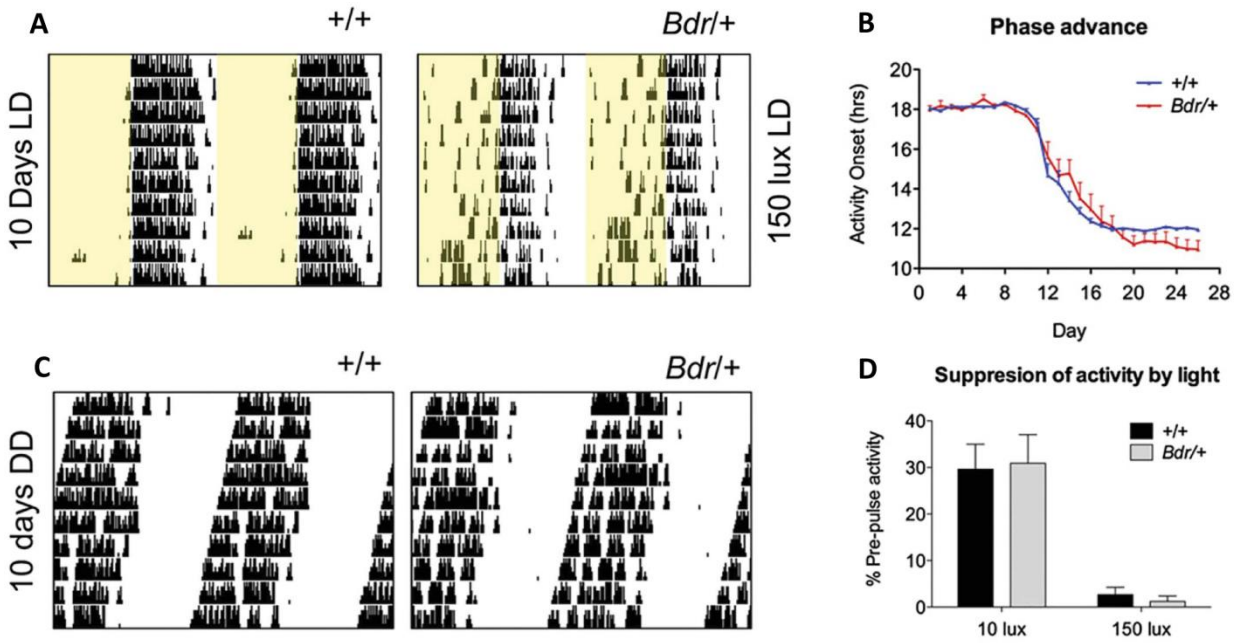

Oliver *et al*., 2012

Figure 1.9: (**A**) *Bdr* mice show phase advance of 6 hours and increased fragmentation under 12:12hr Light-Dark 150 lux conditions (**B**) 6hr phase advance curve illustrating no significant difference between genotypes (**C**) Dark-Dark period illustrates no significant difference between genotypes (**D**) illustrates cessation of running activity following administration of photic stimulus during dark phase in both genotypes.

Importantly, the *Bdr* LD actograms display considerable heterogeinity (Oliver *et al*., 2012). Although the WT actograms demonstrate clear entrainment to an LD cycle, *Bdr* actograms span from robustly rhythmic to highly irregular (Oliver *et al.*, 2012). Activity fragmentation is increased in the *Bdr* mice under an LD, DD and LL paradigm (Oliver *et al*., 2012). However, the ataxic phenotype of the *Bdr* could potentially contribute to this finding (Jeans *et al*., 2007). Circadian behavioural data suggested that the light input pathway via the RHT is likely unaffected (Figures 1.9B & 1.9D) but the 6hr phase advance under LD conditions (Figure 1.9A) in *Bdr* required further investigation. The endogenous core clock appears unaffected (Figure 1.9C) pointing to the direction of output neuronal communication factors affected in *Bdr*.

1.6 Parkinson's Disease

Parkinson's disease (PD) is a progressive neurodegenerative disease with a high penetrance among the elderly population (1% of individuals above the age of 60) (Venda *et al*. 2010). Motor symptoms including resting tremor and postural instability are primarily induced by loss of midbrain dopamine neurons (Olanow and Tatton, 1999; Dauer and Przedborski, 2003; Taylor *et al*., 2014). Nigrostriatal dopaminergic degeneration is prominent alongside intracellular proteinaceous inclusions containing α-synuclein, termed Lewy bodies (Dawson *et al*., 2010). Disease progression is often preceded by prodromal non-motor manifestations including sleep disruption and gastrointestinal defects (Braak *et al*., 2003; Langston, 2006; Taylor *et al*., 2014).

Roughly 10% of PD patients are familial cases linked to α-synuclein (SNCA) point mutations on chromosome 4 (Polymeropoulos *et al*., 1997; Kruger *et al*., 2001; Zarranz *et al*., 2004; Taylor *et al*., 2014). Point mutations such as A53T, E46K and A30P in SNCA generate a distinct neuropathological profile in post-mortem analyses from PD patients (Dawson *et al*., 2010). Overlapping mechanisms in pathological neurophysiology between familial and sporadic PD cases confirm the relevance of SNCA in PD (Table 1.3) (Seidel *et al*., 2010).

Parkin gene defects also appear to be a relevant genetic factor for familial PD (Table 1.3) (Bertoli-Avella *et al*., 2004; Lu, 2009). Parkin loss of function mutations impair proteasomal clearance pathways (Hattori and Mizuno, 2004; Imai and Takahashi, 2004; Lu, 2009). Imaging studies from PD patients carrying heterozygous parkin mutations illustrate dopaminergic deficits (Hilker *et al*., 2001; Varrone *et al*., 2004; Lu, 2009). Overall, parkin mutations possibly lead to earlier onset of PD symptoms (Sun *et al*., 2006; Lu, 2009).

Table 1.3: Risk genes in familial PD

Gene	Inheritance	Function
a-synuclein	Autosomal dominant	Synaptic vesicle formation
Parkin	Autosomal recessive	Ubiquitin ligase
UCHL1	Autosomal dominant	Ubiquitin hydrolase
PINK1	Autosomal recessive	Mitochondrial kinase
DJ1	Autosomal recessive	Oxidative stress response
Dardarin	Autosomal dominant	Kinase

Table 1.3: Table illustrates candidate PD genes, their inheritance pattern and functional role.

Dementia linked to parkinsonism is associated with protein tau mutations (MAPT) (Caffrey and Wade-Martins, 2012). FTDP-17 (Frontotemporal dementia with parkinsonism linked to chromosome 17) is characterised by a variety of neuropsychiatric symptoms including hallucinations and sleep disturbances (Wong and Wallhagen, 2012). A defective isoform ratio between tau products is considered a major cause of FTDP-17 and associated tauopathies (Table 1.5) (Wade-Martins, 2012). Tau is a major cytoskeletal structural component participating in microtubule stabilisation while tau phosphorylation and aggregation induces cellular defects (Denk and Wade-Martins, 2009).

The work in this project revolves around comprehending the circadian non-motor prodromal phenotypes of a variety of PD models including *Snca*, *Parkin* and *Tau* mouse mutants. Given the limited progress in comprehending non-motor manifestations in traditional mouse models (Tables 1.4-1.5) of PD, bacterial artificial chromosomes (BAC) were utilised to replicate the endogenous pattern of neuronal over-expression of PD risk genes (Chesselet, 2008; Taylor *et al*., 2014).

Table 1.4: Summary of α-synuclein transgenic mouse models

Human α-syn	Promoter	Genetic background	Expression levels	Neuropathology	Motor phenotype
wt	PDGF – β	C57BL/6 X DBA/2	10-80-fold of non Tg levels	↓striatal Tyrosine Hydroxylase (TH) (levels, activity) ↓DA levels; ↓TH fibers; glia+, ubiquitin+	middle age onset, mild↓ rotarod
A53T	mu Thy-1	C57BL/6	2.5-fold end α.syn	motor neurons degeneration; I: T, B, C, SC, ubiquitin+	early onset, severe (rotarod)
wt, A30P	mu Thy-1	C57BL/6	2-fold end. α-syn	I: SN, STR, H, Cx, B, Th	none
wt, A30P, A53T	rat TH	Swiss Webster x C57blk6/DBA	1.8-fold end. α-syn	Ubiquitin-	NA
wt, A53T	mouse prion	C57BL/C3H	2.5- to 30-fold end. α-syn	I: SC, B, C, Th, STR	middle age onset, hunched back, freezing, paralysis (fatal)
wt, A30P, A53T	mouse prion	C3H/HeJ x C57BL/6J	4-15 times > non-Tg	I: M, C, B, SC; ubiquitin+	late onset, ataxia dystonia (fatal)
wt, A30P + A53T	rat TH	C57BL/6	0.3- to 0.5-fold of mouse α-syn	↓DAT density	middle age onset, mild; ↓locomotor activity and coordination
wt, A30P	mu Thy-1	C57BL/6 x DBA/2	10-fold end. α-syn	I: SN, STR,H, Cx, B, Th	NA
wt, A53T	mouse prion	FVB/N	5- to 20-fold end. α-syn	altered neuronal morphology, diffuse accumulation of α-syn	↓ stride length, grip strength; ↓vertical activity; ↓ rotarod

I indicates inclusions; B, brainstem; C, cerebellum; Cx, cortex; H, hippocampus; M, midbrain; SC, spinal cord; SN, substantia nigra; STR, striatum; T, telencephalon; Th, thalamus; end.α-syn, endogenous levels of α-synuclein.

Table 1.4: Table illustrates transgenic a-synuclein models. Transgenic nature on the first column followed by the promoter utilised, mouse genetic background, expression levels of transgene, neuropathology and finally motor phenotype observed.

Based on Fernagut and Chesselet, 2004

Table 1.5: Summary of MAPT transgenic mouse models

Mutation Models	Line	Transgene	Neuropathology	Phenotype	Reference
Exon 9 G272V	PrP-TA mice	Mouse prion promoter	Hyperphosphorylated tau in neurons	Not reported	Gotz *et al*., 2001
G272V/P301L/R406W	VWL	4R/2N; mouse Thy1 promoter	Hyperphosphorylated tau; tau Filaments	Not reported	Lim *et al*., 2001
Exon 10 P301L	pR5	4R/2N; mouse Thy1.2 promoter	NFTs in cortex, spinal cord; mitochondrial dysfunction	Small increase in exploratory behaviour; accelerated extinction; weight loss;	Pennanen *et al*., 2004, 2006; David *et al*., 2005
Exon 10 P301L	PL-T34	4R/1N; mouse CNP promoter	Tau inclusions in oligodendrocytes only; impaired axonal transport; altered myelin	Progressive weight loss and muscle weakness	Higuchi *et al*., 2005
Exon 10 P301L	Tg tau (P301L) 23027	4R/2N; hamster prion promoter	Progressive neurofibrillary tangle pathology; independent development of glial pathology (glial plaques); brain atrophy in temporal lobe	Deficits on Morris water maze; conditioned taste aversion task	Murakami *et al*., 2006
Exon 10 P301L	Tau-4R-P301L	4R/2N; Thy1 gene promoter	Increased tau expression and changed phosphorylation patterns, but no aggregates	Motor defect (beam walking, rotarod); improved memory recall in young mice	Terwel *et al*., 2005
Exon 10 P301L	Tg4510	4R/0N; CaMKII promoter under the control of the tet-operon response element	Pretangles and NFTs, progressing with age; progressive neuronal loss; suppression of transgene by doxycycline led to reduction in neuronal loss, but continuing increase in NFTs	Hunched posture and hind limb dysfunction at old age; increasing impairment on Morris water maze starting at 2.5 months; reduction in deficit if transgene suppressed at 5.5 months despite unchanged NFT load	Ramsden *et al*., 2005; Santacruz *et al*., 2005; Spires *et al*., 2006
Exon 10 P301L	TAPP	JNPL3×Tg 2576 mice	NFTs and amyloid plaques affect tangles, but not the reverse	Not reported	Lewis *et al*., 2001
Genomic models	htau	Genomic *MAPT* PAC of the H1 haplotype on a *Mapt*−/- background	All six human tau isoforms expressed; hyperphosphorylated tau; neurofibrillary tangles; cell loss in spatiotemporal distribution similar to AD	Not reported	Duff *et al*., 2000; Andorfer *et al*., 2003, 2005

Table 1.5: Table illustrates transgenic MAPT models. Mutation model on the first column followed by the line, transgene, neuropathology and phenotype observed.

Based on Denk and Wade-Martins, 2009

1.6.1 Circadian and Sleep Disruption in PD

Sleep deficits are apparent in aged individuals particularly when in the context of a complex neurodegenerative disorder like PD (Larsen and Tandberg, 2001). PD patients experience extensive non-motor disturbances including autonomic, neuropsychiatric and sleep abnormalities such as decreased sleep, excessive daytime sleepiness, increased REM and sleep/arousal bouts which can affect up to 90% of PD patients (Park and Stacy, 2009; Rodrigues-Oroz *et al*., 2009; Chaudhuri *et al*., 2006; Dauvilliers, 2007; Menza *et al*., 2010; Larsen and Tandberg, 2001). 'Sleep benefit' episodes in PD patients arise from temporary motor improvement possibly due to restored dopamine levels during rest cycles (Tandberg *et al*., 1999). Melatonin, a hormone involved in circadian entrainment, is believed to induce motor decline in patients (Willis *et al*., 2012). Comorbidity with depression is apparent and has an impact on the quality of life for 50% of PD patients (Aarsland *et al*., 2012).

Melanopsin-containing retinal ganglion cells appear to be modulated by dopaminergic signalling in terms of circadian photic entrainment (Sakamoto *et al*., 2005). Dopamine depletion is associated with circadian rhythm de-synchronisation in PD patients (Imbesi *et al.,* 2009; Hampp *et al*., 2008; Hood *et al*., 2010). *Per2* gene expression appears to have a direct impact on dopaminergic circuitry by participating in striatal metabolic processes (Hampp *et al*., 2008). In addition, agonists of dopamine receptors have an impact on striatal core clock period gene expression (Imbesi *et al*., 2009). Nigro-striatal neurotransmitters (e.g. dopamine, acetylcholine) have an impact on REM and NREM sleep (Askenasy, 2003). Increased cholinergic receptor activity and decreased dopaminergic activity correspond to REM sleep (Askenasy, 2003). Suppression of REM sleep inhibits the cholinergic system and reverses PD motor pathology (Askenasy, 2003).

Defects in the input to the SCN lead to alterations of circadian oscillations (Tabandeh *et al*., 1998; Leger *et al*., 1999; Sakamoto *et al*., 2005; Turner and Mainster, 2008). Elderly individuals display reduced photic sensitivity (van Someren, 2000). Pupillary miosis and decreased transmission of short-wavelength light are especially evident (Turner and Mainster, 2008). This leads to light deprivation of the SCN and pineal gland (Turner and Mainster, 2008). PD and ageing promote motor disabilities that lead to longer time indoors. As a result, light-stimulated SCN gene expression is further reduced (van Someren, 2000). Taken together, these reductions of circadian rhythm amplitude may result in altered daily cortisol and melatonin rhythms which would further contribute to pathology in PD and elderly patients (Bordet *et al*., 2003; Devos *et al*., 2003).

Sleep disruption can occur due to motor (rigidity or restless limb syndrome) and non-motor (nocturia) manifestations (Park and Stacy, 2009; Adler and Thorpy, 2005). Neuropsychiatric manifestations of PD such as hallucinations and psychotic episodes can also perturb sleep/wake cycles (Larsen and Tandberg, 2001). Co-morbid depression enhances sleep disruption, leading to potential sleep fragmentation (Aarsland *et al*., 2012). Neurodegeneration of neurons in the dopaminergic system impairs the functional links between homeostatic and circadian drivers and may therefore alter structured sleep/wake cycles (Baglioni *et al*., 2010).

Administration of dopaminergic drugs in PD patients further imbalances the circadian axis (Figure 1.10) (Rutten *et al*., 2012). Levodopa (dopamine precursor) alters sleep quality by prolonging sleep latency and decreasing REM sleep epochs (Bruguerolle and Simon, 2002; Deschenes and McCurry, 2009). In addition, studies have reported that Levodopa-treated PD

patients exhibit markedly phase-advanced rhythms (Fertl *et al*., 1991; Fertl *et al*., 1993; Bordet *et al*., 2003).

Figure 1.10: Potential PD impacts on the circadian axis

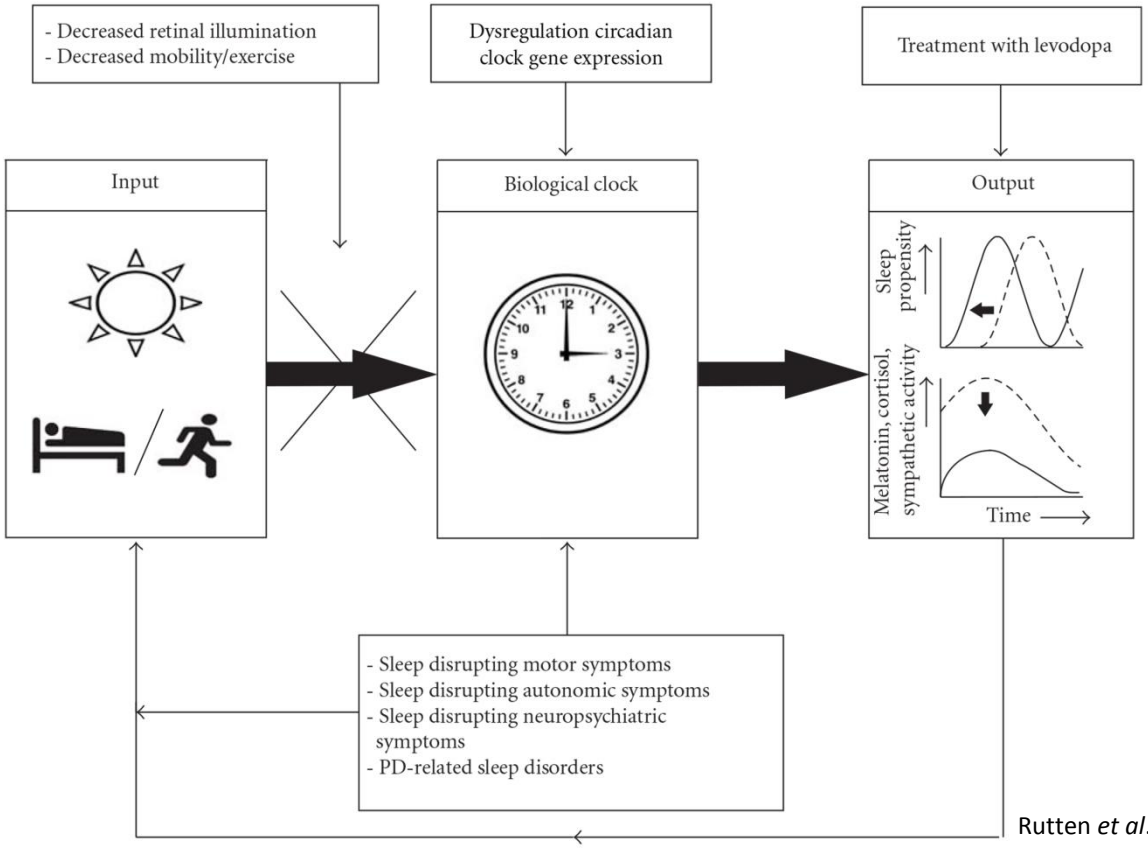

Rutten *et al*., 2012

Figure 1.10: Impact of motor and non-motor manifestations of PD on the circadian axis. Defective input pathways lead to a de-regulated core clock and variations in output cortisol, melatonin and sleep factors. Ageing, pathology and dopaminergic drugs (Levodopa) further aggravate potential circadian disruption in PD.

1.6.2 Circadian and Sleep Disruption in PD: Evidence from Mouse Models

Circadian disruption is a potential endophenotype in the diagnosis of complex neurodegenerative disorders such as PD. Preliminary behavioural experiments on mouse models of PD for prodromal non-motor manifestations suggest a potentially perturbed circadian axis and homeostatic sleep physiology.

Dopamine β-hydroxylase (*Dbh*)$^{-/-}$ mice exhibit catecholamine deficiency as they lack post-natal noradrenaline, leading to earlier sleep onset than their heterozygous counterparts which have normal neurotransmitter levels (Hunsley and Palmiter, 2003; Hunsley and Palmiter, 2004; Michell *et al*., 2008; Taylor *et al*., 2010). Modafinil (wake-inducing agent) treatment resulted in wakefulness in WT and heterozygous mice while *Dbh*$^{-/-}$ exhibited a hypersensitive response to the chemical arousal (Mitchell *et al*., 2008; Taylor *et al*., 2010).

Vesicular monoamine transporter 2 (VMAT-2)-deficient mice exhibit impaired oxidative stress response mechanisms as well as progressive dopaminergic neuronal loss in the substantia nigra pars compacta and aggregation of α-synuclein (Caudle *et al*., 2007; Taylor *et al*., 2009; Taylor *et al*., 2011). Moreover, progressive olfactory, gastric and sleep deficits are reported as well as an age-dependent depressive phenotype (Taylor *et al*., 2009). A shorter sleep latency phenotype in the *Vmat*$^{-/-}$ mouse and circadian activity deficits suggest prodromal non-motor sleep disturbances in the knockout animals reminiscent of older normal mice (Taylor *et al*., 2011).

Transgenic mice over-expressing human α-synuclein (ASO) under the Thy-1 driver exhibited progressive motor and non-motor abnormalities (Fleming and Chesselete, 2009; Kudo *et al*., 2011). Prodromal olfactory, cognitive and circadian rhythm deficits all progressively worsened in an age-dependent fashion (Fleming *et al*., 2004; Fleming *et al*., 2006; Fleming *et al*., 2008; Kudo *et al*., 2011). Circadian locomotor activity was compromised in the ASO line with increased rhythm fragmentation and a hypoactive phenotype (Table 1.5) (Kudo *et al*., 2011). Although period clock gene expression in the SCN was normally phased, electrophysiological SCN recordings reported reduced daytime firing rates (Kudo *et al*., 2011;

Willison *et al*., 2013). The reduction of output electrical SCN impulses is likely having an impact on cognitive and autonomic processes (Kudo *et al*., 2011).

Table 1.6: Circadian deficits in the ASO line

Aging (>12 mo)	PD
↓ activity rhythms: amplitude, coherence, precision	✓
↓ physiological outputs: heart rate, body temperature	?
↓ SCN neural activity	✓
≈ clock gene expression (Per 2)	✓

Willison *et al*., 2013

Table 1.6: 12 month WT mice exhibit reduced behavioural and physiological outputs (Nakamura *et al*., 2011). This circadian phenotype matches 3 month old ASO mice and it is also encountered in PD patients.

1.7 Metabolic Disorders: Lysosomal Storage Disorders

Metabolic genetic perturbations lead to dysfunctional lysosomal compartments (Platt and Walkley, 2004; Fuller *et al*., 2006; Ballabio and Gieselmann, 2009; Platt *et al*., 2012). Penetrance rates of lysosomal storage disorders (LSDs) reach 1 in 5,000 births although misdiagnosis of these inherited disorders could underestimate the numbers (Fuller *et al*., 2006; Platt *et al*., 2012). Common mechanisms underlie most LSDs including macromolecular accumulation of metabolites in endosomal compartments such as the lysosomes (Platt *et al*., 2012). Biochemical testing reported defective autophagic lysosomal pathways in LSDs, either in the form of abnormal enzymatic processing (Sandhoff disease/SD) or transporting non-enzymatic deficiencies (Niemann-Pick type C/NPC) (Table 1.7) (Hers, 1963; Winchester, 2004; Saftig and Klumperman, 2009; Platt *et al*., 2012). Therefore, LSDs allow investigation of

separate genetic perturbations that occupy overlapping biochemical mechanisms and pathophysiology (Platt *et al*., 2012).

Early infantile NPC in humans is characterised by motor abnormalities by 1 year of age (Vanier *et al*., 2010). Brain imaging studies reveal cerebral atrophy and death by 5 years of age (Iturriaga *et al*., 2006; Vanier *et al*., 2010). In the late infantile form hearing loss, gait deficits and seizures are evident in the majority of patients (Vanier *et al*., 2010). In the adult form, psychosis, auditory and visual hallucinations as well as depressive/aggressive traits and anti-social tendencies are symptoms exhibited by patients (Vanier *et al*., 2010). CNS deficits are therefore highly prevalent in LSDs.

Most LSDs involve CNS pathology with multiple brain regions affected including the thalamus, cortex and cerebellum (Wraith, 2004; Platt *et al*., 2012). LSD neuropathology involves neurodegeneration and inflammation that arises from heterogeneous neuronal susceptibility to accumulating macromolecular aggregates (e.g. Purkinje cell loss in LSDs leading to cerebellar ataxia) (Platt *et al*., 2012). Moreover, innate immune response stimulation during these disorders enhances the CNS pathology detected (Vitner *et al*., 2010; Platt *et al*., 2012). Astrogliosis contributes to an inflammatory response whereby glial scarring damages peripheral neuronal populations (Jesionek-Kupnicka *et al*., 1997; Vitner *et al*., 2010). Numerous transgenic animal models have empirically demonstrated the negative effects of astrogliosis on neuronal populations in LSDs (Farfel-Becker *et al*., 2011; Pressey *et al*., 2012).

Table 1.7: LSDs genetic perturbations and phenotype observed

LSD mechanism	Disease	Defect	Accumulating substrate	Systemic involvement	CNS deficits
Enzymatic defect	GM1-gangliosidosis	β-Galactosidase	GM1-ganglioside	Skeleton, Heart	+
Enzymatic defect	Sandhoff	β-hexosaminidase A and B	GM2-ganglioside	Eye	+
Soluble non-enzymatic defects	Niemann-Pick disease type C2	NPC2 (soluble cholesterol binding protein)	Cholesterol and sphingolipids	Liver	+
Transmembrane lysosomal defects	Mucolipidosis IV	Mucolipin-I	Mucopolysaccharides and lipids	Eye	+
Transmembrane lysosomal defects	Niemann-Pick disease type C1	NPC1 (membrane protein involved in lipid trafficking)	Cholesterol and sphingolipids	Liver	+

Platt *et al*., 2012

Table 1.7: Table listing LSD mechanism, disease example, gene defect, aggregating substrate, peripheral organs affected and neuropathology reported in patients. Animal models of LSDs in red were investigated.

1.7.1 Metabolism and Circadian Disruption: Core Clock Genes

The circadian axis is vital for proper metabolic regulation. Core clock genetic perturbations have been associated with decreased physical fitness and metabolic diseases (Circadian Disruption and Metabolic Disorders-Kramer and Merrow, 2013). Emerging evidence is underscoring the fundamental link between circadian-regulated metabolic pathways and how reciprocal cross-talk dictates SCN rhythmic oscillations (Circadian Disruption and Metabolic Disorders-Kramer and Merrow, 2013). *Bmal1* core clock gene

deficits have been implicated in defective pancreatic beta islets of Langerhans associated with diabetes mellitus (Marcheva *et al*., 2010). Moreover, clock gene perturbations in *Clock/Npas2*, *Per2* and *Rev-Erba* have been associated with cancer and various metabolic syndromes (Sahar and Sassone-Corsi, 2012).

Activity during nocturnal periods in shift workers has been suggested to have an impact on metabolic pathways and lead to cardiovascular stress (De Bacquer *et al*., 2009; Karlsson *et al*., 2001; Marcheva *et al*., 2013). Evidence from nocturnal rodents suggested that light-stimulation during dark epochs was associated with obesity, increased light phase food consumption and glucose intolerance (Fonken *et al*., 2010). The phenotype was rescued via restricted feeding during the dark phase (Fonken *et al*., 2010). Photophase-fed high-fat diets promoted weight gain in rodents underscoring circadian control over metabolic processing of food intake (Arble *et al*., 2009).

Circadian timing of food intake alongside quality of diet appears to regulate circadian rhythms (Circadian Disruption and Metabolic Disorders-Kramer and Merrow, 2013). High-fat diets in rodents altered circadian oscillations and ‘‘impacted’ on the free-running periods of the SCN (Kohsaka *et al*., 2007). Core clock gene expression was altered in mice fed a high-fat diet that consumed food mostly during the light epochs (Kohsaka *et al*., 2007). *Clock*Δ19 mutant mice are arrhythmic in constant darkness and display obesity developing metabolic disorder phenotypes including fat enriched hepatocytes and hyperglycaemia (Turek *et al*., 2005). *Clock*Δ19 mutant mice also display de-regulated rhythms of orexin and ghrelin neuropeptides which are vital in the neuroendocrine control of food consumption (Saper *et al*., 2002; Adamantidis and de Lecea, 2009). Finally, cardiovascular abnormalities are present in *Clock*$^{-/-}$ mutant mice including decreased arterial blood pressure (Zuber *et al*., 2009).

1.7.2 LSD: Sandhoff Disease and Niemann-Pick type C

Nieman-Pick type C is a genetic, lipid storage disorder associated with mutations in the *Npc1* and *Npc2* genes. Sandhoff disease is an inherited, lysosomal storage disorder caused by a deficiency to express functional beta-hexosaminidases A and B (*Hexb* gene). Both of these disorders exhibit accumulation of macromolecular glycosphingolipid aggregates in endolysosomal compartments, a progressive neurodegenerative phenotype, systemic involvement of accumulating lipid metabolic products, associated dysfunctions of mitochondrial and innate immune responses, ROS (Reactive oxygen species) generation and SNCA/Huntingtin secondary build-up (Vanier *et al*., 2010). CNS involvement in LSDs is frequent and neuronal loss occurs in multiple areas (hypothalamus, cortex, and cerebellum) (Platt *et al*., 2012). Storage lesions are ubiquitous throughout the CNS in LSDs and certain neuronal subpopulations (e.g. GABAergic neurons) exhibit extensive neuronal dystrophy (Parente *et al*., 2012).

However, the master pacemaker (SCN) has intra- and inter-cellular network properties able to resist genetic, environmental and chemical perturbations (Level of Abstraction-Kramer and Merrow, 2013). The most prominent network property of the SCN is the strong coupling of its cellular oscillators (Welsh *et al*., 2010). This coupling supports a coherent circadian period and phase within the SCN tissue (Liu *et al*., 2007). Evidence of this property has been reported by the *Clock*Δ19 mutant SCN neurons which showed less prevalent cellular rhythmicity in dispersed cultures than in slices, due to the loss of coupling of the SCN network (Nakamura *et al*., 2002). Similar findings were reported by knockout mice lacking *Cry1* and *Per1* genes (Liu *et al*., 2007b). Furthermore, chimeric *Clock*Δ19 mice exhibited behavioural rhythms with intermediate circadian periods, despite a long period *in vitro* (Low-Zeddies and Takahashi, 2001). Therefore, SCN neurons of different periods couple

together to establish a compromised circadian period thereby resisting genetic perturbation. In addition, coherent cellular rhythmicity of the SCN is reinforced by a rhythmic input signal that entrains the network (Welsh *et al*., 2010). It is possible, despite extensive CNS pathology, that the hypothalamic oscillatory network is able to maintain its rhythmic properties and exhibit only minor defects in these disorders.

Hexb (β-hexosaminidase B) and *Npc1* genes display dissimilar cellular localisation and have different roles in sphingolipid catabolism. *Hexb* is a lysosomal enzyme catalysing the degradation of GM2 gangliosides (Platt *et al*., 2012). *Hexb*$^{-/-}$ mice exhibit progressive motor deterioration, reduced lifespan, extensive neuropathology (spinal cord axonal loss) and behavioural impairments, including impaired memory consolidation (Phaneuf *et al*., 1996; Gullinelo *et al*., 2008). *Npc1* is a transmembrane cholesterol-binding glycoprotein responsible for transporting cholesterol to the extracellular space (Schulze and Sandhoff, 2011). *Npc1*$^{-/-}$ mice exhibit progressive neurodegeneration, reduced lifespan, sphingomyelin deposition as well as motor and cognitive defects (Voikar *et al*., 2002; Walkley and Suzuki, 2004; Platt *et al*., 2012). Although the underlying defects in these two LSD disorders vary, this difference would provide some insight as to the cross-talk (Figure 1.11) between the circadian axis and different metabolic syndromes. The link between potential core clock deficits and metabolic pathology would be closely monitored. Additionally, the light input pathways would be investigated as previously identified retinal pathology in *Hexb*$^{-/-}$ mice may become evident in this investigation (Sango *et al*., 2008). Therefore, the effects of glycolipid accumulation and CNS neurodegeneration on circadian axis functionality would be examined.

Figure 1.11: Circadian and metabolic factors cooperate

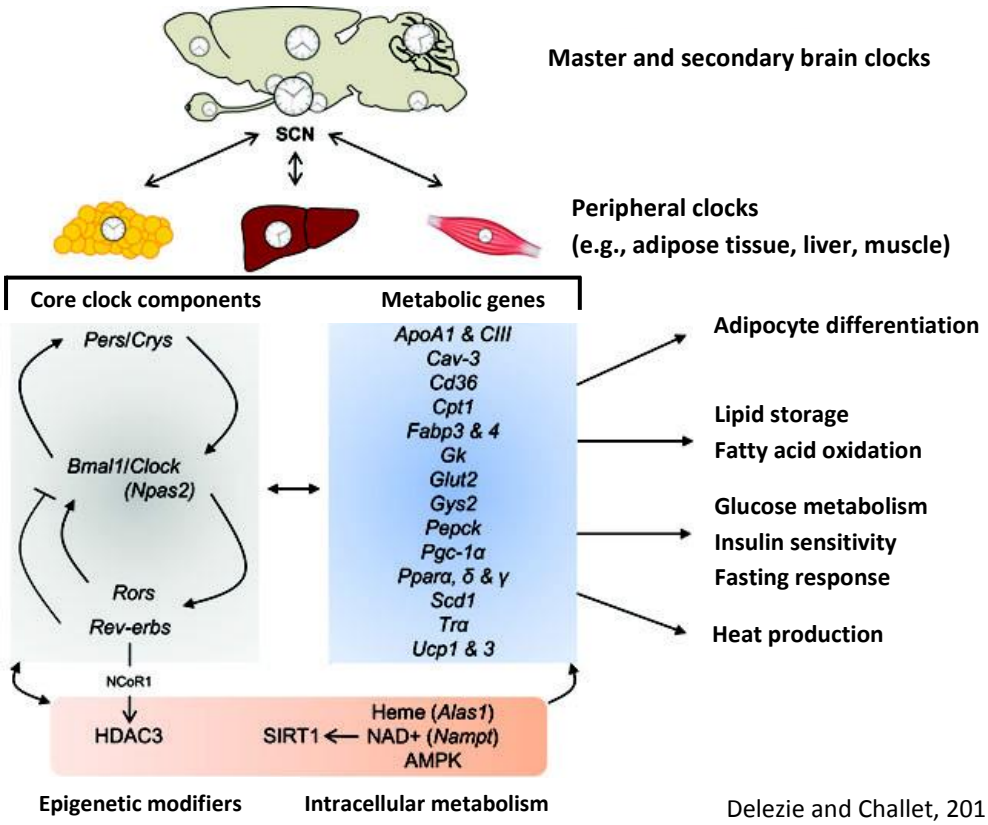

Delezie and Challet, 2011

Figure 1.11: The crosstalk between master and peripheral circadian organs (liver, muscle, adipose tissue) is illustrated. Core clock genes regulate epigenetic modifiers (HDAC3) and metabolic enzymes (NAD+) alter metabolic gene expression. Similarly, metabolic gene pathology may alter epigenetic regulators of core clock genes such as Rev-Erba and thereby modulate circadian rhythms.

1.8 Aims

This project deploys a variety of behavioural and molecular methodologies in addressing circadian disruption in animal models of metabolic, neurodegenerative and neuropsychiatric disorders. Abnormal circadian regulation of sleep can reflect sleep disturbances according to the two-process model of sleep regulation (Borbely, 1982, Tobler *et al*., 1983). Numerous human and animal studies have demonstrated the apparent links between neuropathology and circadian deficits. However, a mechanistic association between circadian disruption and neuropathology has been largely elusive. Therefore, the main objectives of this study are:

1. Identify whether circadian rhythm disruption occurs in animal models of metabolic and neurological disorders in order to:
    - Ascertain the circadian role of pathology-risk genes in different disorders.
    - Comprehend the impact of circadian disruption on different disorders and its role in the disease process.
    - Utilise these findings from animal models to evaluate the translational potential of circadian disruption in future human studies.

2. Identify the mechanistic association between circadian disruption and synaptic dysfunction in a model of schizophrenia, the *blind-drunk* mutant mouse.
    - Investigate light-mediated retinal input pathways to the SCN.
    - Proteomic investigation of the SCN in wild-type and mutant animals by employing mass spectrometry.
    - Utilise this dataset to identify potential signalling pathways that link circadian disruption to schizophrenia.

1.9 Hypotheses

Parkinson's Disease

Sleep disruption has been well documented as an early symptom in a variety of neurodegenerative disorders such as Parkinson's disease (Schenck *et al*., 2013; McCarter *et al*., 2013). More specifically, sleep abnormalities (sleep fragmentation and excessive daytime sleepiness (EDS)) could arise due to defective circadian processes in PD patients (Jankovic, 2007). Therefore, mouse models of PD investigated were predicted to display possible circadian (fragmentation differences) rhythm abnormalities in activity reminiscent of PD pathology in patients.

Lysosomal Storage Disorders

Lysosomal Storage Disorders in patients (LSD) exhibit progressive neurodegeneration and sleep/wake abnormalities (Alonso and Sheldon, 2010; Platt *et al*., 2012). Additionally, core clock deficits have been associated with metabolic abnormalities and neurodegeneration (Turek *et al*., 2005; Musiek *et al*., 2013). Therefore, mouse models of LSDs investigated were predicted to exhibit potential core clock defects.

The *Bdr* model of schizophrenia

The blind-drunk (*Bdr*) mutant is a mouse model of exocytotic disruption that displays schizophrenic endophenotypes and phase advanced rest/activity cycles. The *Bdr* also display phase-advanced up-regulation of output SCN neuropeptides reflecting the circadian phenotype (Oliver *et al*., 2012). Importantly, post-transcriptional processes are critical in maintaining functional rhythmic cycles (Deery *et al*., 2009; McGlincy *et al*., 2012; Robles *et al*., 2014; Mauvoisin *et al*., 2014). Therefore, proteomic analysis of the *Bdr* SCN was predicted to identify perturbed synaptic trafficking mechanisms significant for diurnal cycles.

2 Methods

This chapter outlines the methodological approaches used in addressing the aims of this project. Methodological variations between experiments are addressed in individual chapters and this section reports the general approach undertaken.

2.1 Animals

2.1.1 The blind-drunk mutant mouse

ENU mutagenesis screens conducted at the Mammalian Genetics Unit, MRC- Harwell (UK) initially detected the *blind-drunk* mutant mice exhibiting a mild ataxic phenotype at one month of age. Continuous backcrossing of heterozygous mutant males to wild-type C3H/HeH mice has been maintained in order to compare all the studies together.

Polymorphic microsatellite genomic regions neighbouring the *Snap-25* gene were utilised for genotype screening (Jeans *et al*., 2007). Polymorphic genomic loci arise from the mouse strain variations between the originally injected BALB/c mouse and the wild-type C3H strains used for breeding. The original mis-sense mutation involved conversion of an Isoleucine residue to threonine at exon 5b, position 67 of the *Snap-25* gene. This dominant gain-of-function mutation generates increasing binding affinity within the SNARE fusion complex, during synaptic trafficking, thereby reducing cortical glutamatergic transmission (Jeans *et al*., 2007). Despite normal neuroanatomy, vesicle recycling pathways appear retarded generating impaired sensorimotor gating deficits in the form of abnormal PPI (Pre-pulse inhibition) as well as an increased apathetic phenotype (Oliver and Davies, 2009). Importantly, the schizophrenic PPI deficit was rescued following antipsychotic treatment giving face and predictive validity to the model (Oliver and Davies, 2009).

Experiments conducted utilised congenic wild-type controls and all mice were kindly supplied by Dr Peter Oliver and Prof. Dame Kay Davies (Biomedical Sciences Building, University of Oxford, UK).

2.1.2 BAC PD mouse models

SNCA and MAPT knockout mice were acquired from established homozygous colonies (Department of Preclinical Veterinary Sciences and Fujisawa Institute of Neuroscience, University of Edinburgh, Edinburgh, UK) (Abeliovich *et al*., 2000; Robertson *et al*., 2004). Bacterial artificial chromosomes including the MAPT and SNCA transgenes containing the wild-type human SNCA/MAPT locus or SNCA A30P mutation, N296H MAPT mutation or multiplications of the SNCA locus (OVX) were engineered utilizing a BAC recombineering microinjection into C57BL/6 mouse pronuclei (Peruzzi *et al*., 2009; Taylor *et al*., 2014, Janezic *et al*., 2013). BAC engineering occurred on a SNCA and MAPT knockout background to prevent the endogenous expression of the gene of interest. F0 generation chimeric mice were subsequently backcrossed to their respective knockout line and PCR-screened to establish the presence of the different transgenes. Generation of the A30P SNCA, OVX SNCA and N51 MAPT lines and corresponding wild-types controls in a hemizygous state was further pursued.

Due to the limited construct and predictive validity of traditional mouse models of PD, the development of BAC transgenics has been greatly anticipated. Despite progressive motor deterioration exhibited by traditional mouse models, the lack of major dopaminergic abnormalities suggests unfaithful reproduction of endogenous spatio-temporal expression of the SNCA or MAPT loci (Chesselet, 2008). Theoretically, BAC technologies utilise most regulatory genomic elements associated with the coding sequence and therefore more accurately reflect the genetic neurophysiology of this complex disease.

Experiments were conducted utilising their corresponding initial knockout line during the BAC recombineering procedure as well as the human wild-type versus the mutated/ over-expressed transgene. All mice were kindly supplied by Dr Richard Wade-Martins (Biomedical Sciences Building, University of Oxford, UK).

2.1.3 *Parkin, Hexb* and *Npc1* knockout mice

The *Parkin*$^{-/-}$ was generated by exon 3 deletion leading to an exon 4 premature stop codon preventing expression of a functional parkin product (Goldberg *et al*., 2004). RT-PCR screening for the missing gene product allowed generation of knockout colonies. All mice were kindly supplied by Dr Peter Oliver and Prof. Dame Kay Davies (Biomedical Sciences Building, University of Oxford, UK).

The *Npc1*$^{-/-}$ was generated by retroposon insertion of 1100bp of DNA simultaneously deleting 800bp of the gene of interest (Loftus *et al*., 1997; Maue *et al*., 2012). The resulting frame shift leads to the presence of a minimally truncated Npc1 RNA product (Hsu *et al*., 2000; Maue *et al*., 2012). However, complete absence of the protein product is reported in the homozygous animals (Elrick *et al*., 2010; Maue *et al*., 2012).

The *Hexb*$^{-/-}$ was generated when a neomycin-resistant vector disrupting exon 2 of the gene of interest was microinjected into C57BL/6 blastocysts (Phaneuf *et al*, 1996). Backcrossing of chimeric mice generated heterozygous normal *Hexb*$^{+/-}$ mice (Phaneuf *et al*., 1996). Heterozygous inbreeding eventually generated H*exb*$^{-/-}$ colonies.

The *Npc1* and *Hexb*$^{-/-}$ mice exhibit rapid onset of metabolic disease, progressive motor and cognitive pathology and markedly reduced lifespans. As a result, modified, shorter versions of circadian screens were undertaken in order to examine prodromal non-motor and

motor pathology in these two mouse models. The *Npc1*$^{-/-}$ and *Hexb*$^{-/-}$ mice were kindly supplied by Prof. Fran Platt (Biomedical Sciences Building, University of Oxford, UK).

2.2 Motor and non-motor phenotype monitoring

Numerous mouse models were subjected to running-wheel screening in order to ascertain circadian disruption in a variety of disorders. Investigation of the daily rest/activity cycles was undertaken under stable and acute photic paradigms.

2.2.1 Circadian running-wheel screening

Running-wheels are able to register locomotor activity of mice (Careau *et al*., 2012). Mouse models of PD undertook a similarly designed circadian protocol (Figure 2.1), while mouse models of metabolic disorders had a modified, shorter version due to their limited lifespan (Figure 2.2).

A behavioural circadian screen adapted from previous work on the *Bdr* mice covering the most commonly employed circadian paradigms was utilised. Age-matched females/males were individually housed in large cages (44x26x12cm) with running-wheels. Due to limited resources, the BAC SNCA and MAPT screens utilised female mice (2 per mouse line). Illuminated coffins with 7 running cages in each were light-controlled while mice were placed in alternating genotype order. Temperature and humidity levels were kept constant; coffins were well ventilated with *ad libitum* food and water while intensity of LED lighting was assessed at 150lux by a light meter. Each running-wheel was connected to a central computer supporting the Actimetrics Clocklab software package and activity levels (wheel revolutions/minute) were recorded. Data were analysed using Actimetrics Clocklab toolbox

for Matlab and statistically interpreted utilising ANOVA/Student's t-test in Excel (Microsoft) or Graphpad Prism 5.0.

2.2.2 Type II phase delay

One hour of light pulsing during the dark phase (ZT14) induces a phase delay in accordance with the phase response curve (PRC). A ZT14 light pulse induces up-regulation of the *Per2* gene vital for PRC phase delays (Albrecht *et al*., 2001). PRC changes in disease models can be partly monitored via their ability to up-regulate *Per2* and exhibit a phase delay following a ZT14 light pulse (Albrecht *et al*., 2001). Photic stimulation prior to release into constant darkness is performed in order to investigate the PRC. Type II phase delay was preferred versus a Type I protocol due to the unnecessary handling involved in the latter. Previous transgenic animal circadian work incorporating a Type II protocol determined the degree of the phase shift by incorporating a weeks LD (Light-Dark) onset regression line, while subtracting it from an equivalent free-running activity onset regression line (in DD: Dark-Dark) following the light pulse (Albrecht *et al*., 2001). Immediate transitory effects following the phase shift were ignored and not included in the calculation process. The impact of the phase shift was calculated on the day of the pulse via the Actimetrics Clocklab software and was statistically assessed by two-tailed unpaired Student t-tests or one-way ANOVA.

2.2.3 Nonparametric activity and sleep analysis

Nonparametric rhythm recording assesses intradaily stability and interdaily variability as additional parameters to the Actimetrics Clocklab measurements when investigating circadian rhythmicity (Van Someren *et al*., 1999; Pallier *et al*., 2007). The Actiwatch Sleep analysis package by Cambridge Neurotechnology is particularly useful for assessing

rest/activity fragmentation patterns that might exhibit stable or variable rhythms (Pallier *et al*., 2007).

2.2.4 Light

A light metre was utilised for regulating the light intensity in the illuminated coffins at a stable 150 lux at cage level. Light was supplied by an adjustable LED lighting strip with diffuser whose intensity was externally controlled by a manual switch for each coffin.

Figure 2.1: Circadian screening protocol illustration of PD mouse models

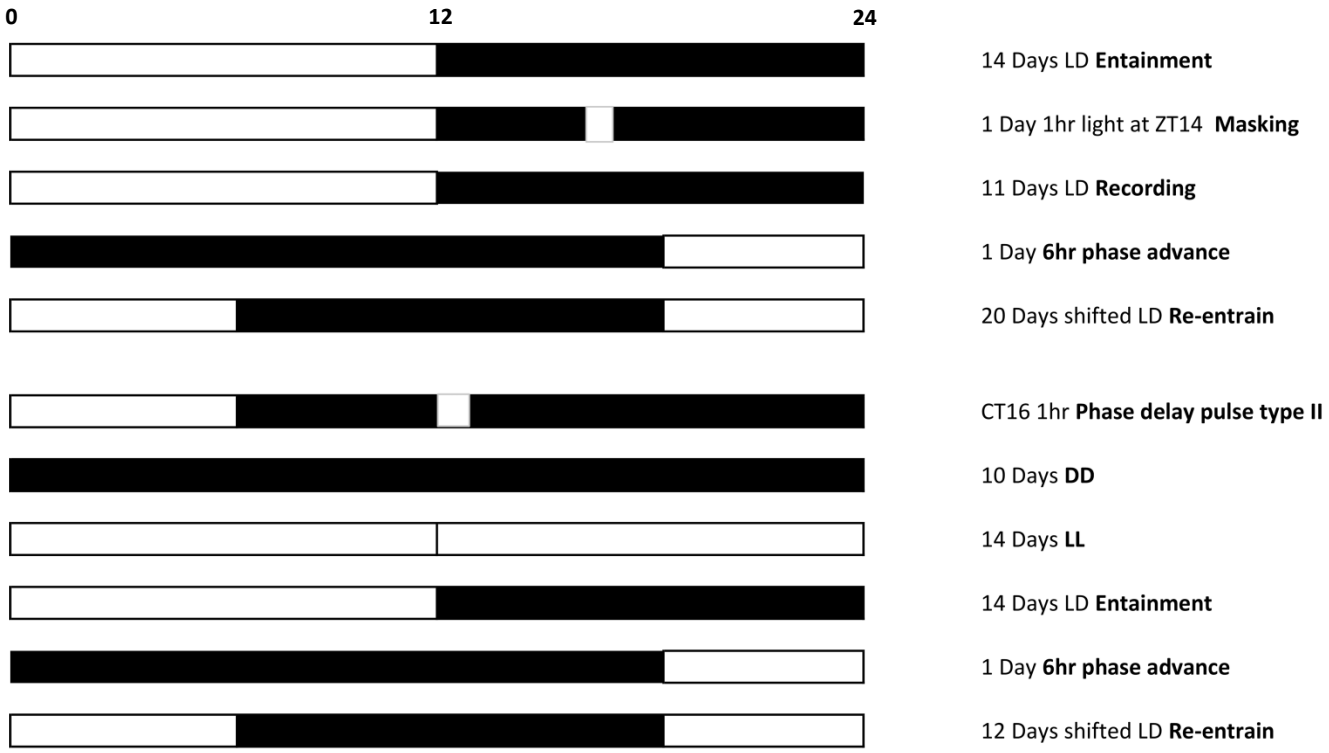

Figure 2.1: The numbers along the top denote Zeitgeber Time (ZT) under the initial 12:12hr Light-Dark (LD) cycle. All environmental lighting changes are stated in the brief description of a given paradigm (right). The black (dark) and white (light) bars graphically represent the changing photic conditions as the screen progresses. Lighting was set at an intensity of 150lux. Further abbreviations–DD: 24 hour Dark, CT: Circadian Time and LL: 24 hour Light.

Note: This specimen protocol represents the extended version and minor variations among PD screens are indicated in each chapter. Only the BAC SNCA/MAPT screens used both male and female mice.

Figure 2.2: Circadian screening protocol illustration of LSD mouse models

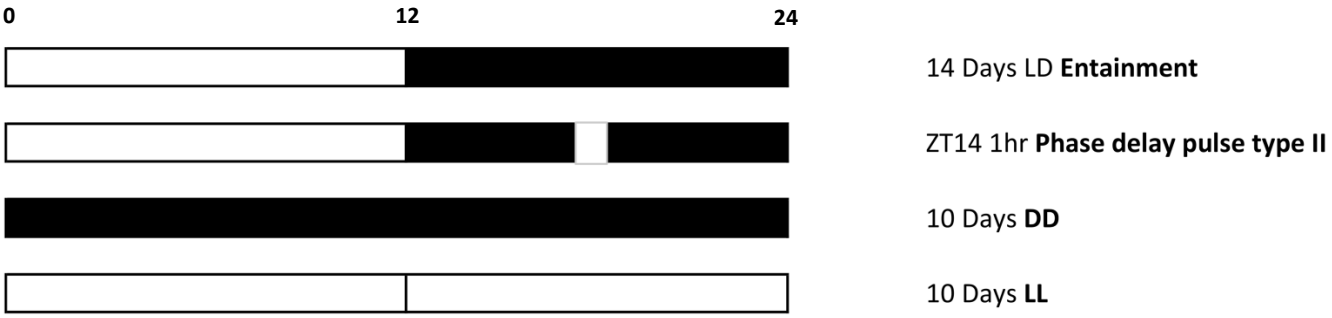

Figure 2.2: The numbers along the top denote Zeitgeber Time (ZT) under the initial 12:12hr Light-Dark (LD) cycle. All environmental lighting changes are stated in the brief description of a given paradigm (right). The black (dark) and white (light) bars graphically represent the changing photic conditions as the screen progresses. Lighting was set at an intensity of 150lux. Further abbreviations–DD: 24 hour Dark and LL: 24 hour Light.

Note: This specimen protocol represents the extended version and minor variations among LSD screens are indicated in each chapter. Limited lifespans of LSD mouse models demanded shorter circadian protocols.

Figure 2.3: Representative circadian running-wheel set-up



LeGates and Altimus, 2011

Figure 2.3: Running-wheels integrated in each cage during circadian screening

Table 2.1: Circadian parameters investigated during screening of transgenic mouse models

Circadian Parameter	Units	Description
Tau	Hrs	*The circadian period (tau) assigned by the activity onset*
Tau Onset Error	Hrs	*The error associated with the onset tau assigned by the activity onset variation*
Tau Offset	Hrs	*The circadian period (tau) assigned by the activity offset*
Tau Offset Error	Hrs	*The error associated with the onset tau assigned by the activity offset variation*
Mean Activity Onset	Hrs	*Average activity onset utilised for phase angle of entrainment calculation if subtracted from ZT when lights off*
Mean Activity Offset	Hrs	*Average activity offset*
Alpha	Hrs	*Length of the active phase*
Rho	Hrs	*Length of the rest phase*
Periodogram Tau	Hrs	*Chi-squared periodogram method for rhythm determination (Sokolove and Bushell, 1978)*
Periodogram Amplitude	AU	*Indicator of rhythm stability and consistency, the zenith of a periodogram curve.*
Total Activity	Total Counts	*Daily Average counts*
Light Activity	Total Light Counts	*Light phase Average counts*
% Light Activity	%	*The percentage of light phase average counts from the total daily average counts*
Dark Activity	Total Dark counts	*Dark phase Average counts*
Total Bouts	Bouts/day	*Activity-rest fragmentation epochs identified by a minimum of 10 minutes per state*
Intradaily variability (IV)	AU	*Daily activity-rest fragmentation pattern magnitude*
Interdaily stability (IS)	AU	*Degree of resemblance between activity patterns on individual days*
Activity profile or Activity plot	Counts/min in 10min bins	*Mean activity-rest patterns over several days*
Phase Advance Activity Onsets	Hrs	*Mean Activity Onsets during a 6hr phase advance paradigm illustrating the rate of re-entrainment to the new LD cycle*
Type II Phase Delay Phase Shift	Hrs	*The degree of phase shift on the light pulsed day calculated by the numerical difference of LD activity onsets minus DD activity onsets*

2.3 ‘‘Molecular’’ Methodologies

A variety of ‘‘molecular’’ techniques were undertaken in the *Bdr* mouse. This includes label-free MS (mass spectrometry-QExactive) quantitation, immunohistochemistry (IHC), western blot (WB), *in situ* hybridisation (ISH), quantitative reverse transcriptase polymerase

chain reaction (qRT-PCR), enzyme-linked immunosorbent assay (ELISA) and Bicinchoninic acid (BCA) protein assay.

2.3.1 Tissue collection

Depending on the aim of each experiment different numbers of mutant and wild-type animals were required. However, in each case the suprachiasmatic nucleus (SCN), paraventricular (PVH) nucleus of the hypothalamus and cerebral cortex (CTX) were usually collected from sectioned mouse brains.

Age- (12 weeks) and sex-matched (5 males and 5 females per genotype per ZT) mice were culled by cervical dislocation following 10 days of entrainment to a 12:12hr LD cycle. Whole brains were sectioned on a steel matrix and anatomical regions of interest were sectioned at 1mm and tissue-punched using a 1mm diameter sample corer (Figure 2.4). Collected brain tissues were individually snap-frozen on dry ice and subsequently stored in -80°C.

Figure 2.4: Anatomical mouse brain areas of SCN, PVH and CTX collected

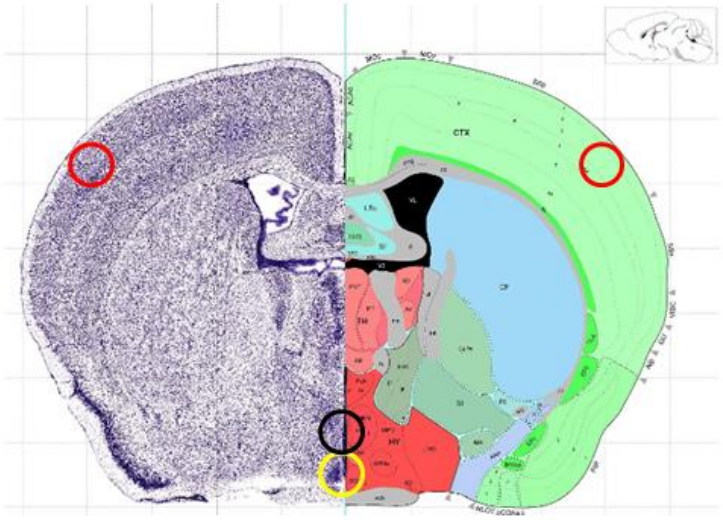

Figure 2.4: 1mm diameter tissue punches (not to scale) were collected from the SCN (yellow circle), PVH (black circle) and CTX (red circles) areas for molecular analysis.

Note: Tissue punches collected varied among experiments but the SCN was constantly collected across all ‘‘molecular’’ work.

2.3.2 Acute light-induced SCN IEGs profiling

Three month old age-matched *Bdr* and wild-type mice (n= 4 per genotype) were individually housed in large cages (44x26x12 cm) for at least 10 days in a LD cycle. Brains were dissected at ZT 16 +/- 30 minutes light stimulation on day 11 of the experiment (Figure 2.5). Collected 1mm diameter brain tissue punches were individually snap-frozen on dry ice and subsequently stored in -80°C.

Figure 2.5: Abrupt 30 minute photic stimulation experiment investigating retinal input pathways to the SCN

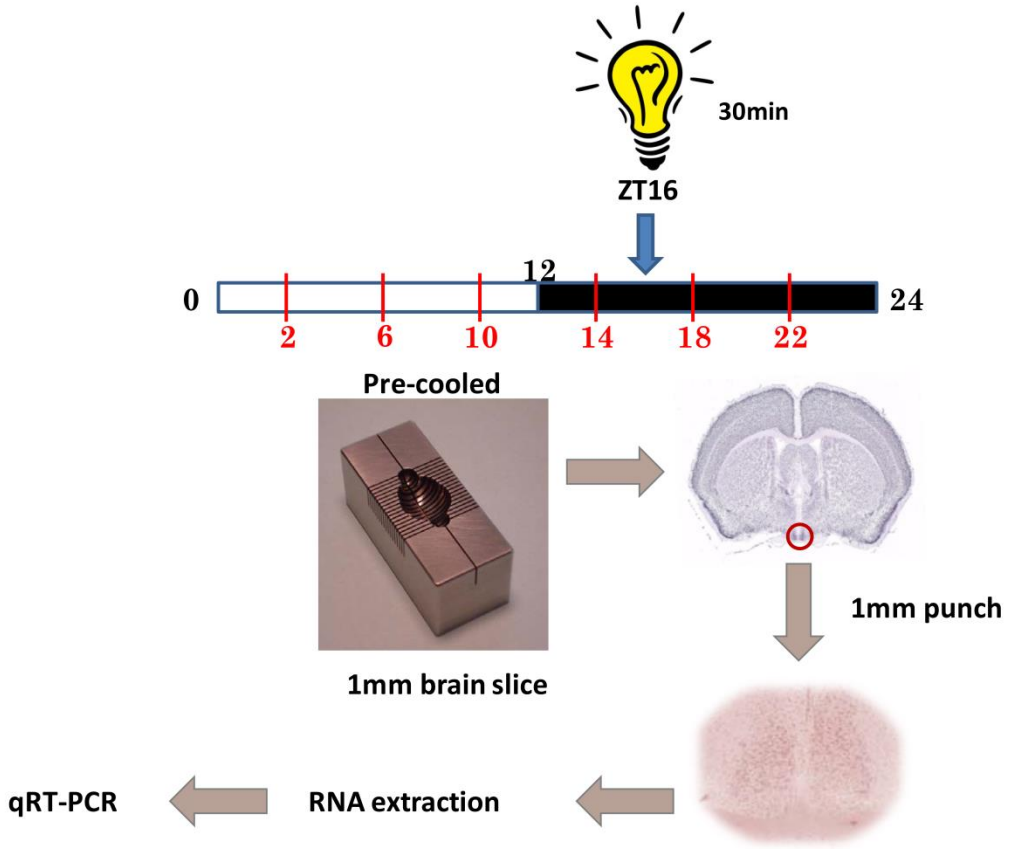

Figure 2.5: Protocol undertaken during 30 minute light pulse at ZT16. Figure includes a picture of the pre-cooled steel matrix utilised for positioning mouse brains for 1mm thick sectioning, an illustration of the SCN anatomical area collected and downstream molecular steps followed.

2.3.3 RNA extraction/quantification/reverse transcription and primers

Total RNA extraction was accomplished using RNeasy Micro Kit (Qiagen) as per manufacturer's recommendations. Total RNA was extracted from both genotypes and total RNA was then quantified using a Thermo Scientific Nanodrop 1000. The measurements were used to calculate the volume of total RNA required for cDNA synthesis. 100ng of extracted RNA was used for poly(A) tail Reverse Transcription using the SuperScript(R) III First-Strand Synthesis System (Invitrogen) according to manufacturer's recommendations. Quantitative PCR (qPCR) was performed on StepOnePlus Real time PCR system (Applied Biosystems) using 1:10 diluted cDNA. Final volume of reaction mixture was 20 µl with optimised forward and reverse primer concentration, 10ng of cDNA and 1x SYBR Green PCR Master Mix (Applied Biosystems). Triplicate reactions of each sample were undertaken and the table below summarises the primers utilised (Table 2.2). Glyceraldehyde 3-phosphate dehydrogenase (GAPDH) is a housekeeping gene and was therefore selected as a reference for expression normalisation due to its constitutive high expression.

Primers were designed with standard requirements of 20 base pairs (bp), 50% GC content, product size of 50-150 bp and a melting temperature of 60°C. All primers were tested for specificity using a qPCR melt curve and acrylamide gel analysis and for amplification efficiency using cDNA standard concentration curves. All primer pairs were tested using mouse whole brain cDNA or SCN cDNA via a qPCR melt curve to test the quality of the primer product (multiple products or noisy melt curves were discarded) and the ideal $T^{o}C$ for the experiment. All products deemed satisfactory were subsequently run on a gel to confirm the expected size of product. Sample DNA was then put through the same process.

2.3.4 qRT-PCR analysis

Ct (critical threshold) value reflects a fluorescent limit recorded for a given mRNA amount. Averaging replica Ct values, transformation to 2^{-Ct} and normalisation of each gene to the housekeeping gene (GAPDH) allows relative variation of expression levels to be quantified. Data were statistically interpreted utilising ANOVA/Student's t-test in Excel (Microsoft) or Graphpad Prism 5.0.

Table 2.2: qRT-PCR targets investigated and primers utilized

Gene	Gene Description	Forward primer sequence	Reverse primer sequence
Fos	*ENSMUST00000021674* FBJ osteosarcoma oncogene Light induction in SCN, immediate early gene (IEG), marker of neuronal excitation	GAAGACCGTGTCAGGAGGCAGA	CAGACCTCCAGTCAAATCCAG
JUNB	*ENSMUSG00000052837* Transcription factor jun-B, Light induction in SCN, immediate early gene	CAGACACAGGCGCATCTCTGAA	GAGGCGGCTCCGGACCAGCATA
Per1	*ENSMUST00000021271* Period homolog 1 Light induction in SCN, core clock gene	CCAGGATGTGGGTGTCTTCT	GAGACCTGAACCTGCAGAGG
Per2	*ENSMUST00000069620* Period homolog 2 Light induction in SCN, core clock gene	GGGGTGAGATTCGTCATTGAACTTG	AGGACATTGGCACACTGGAAAGAG
Six-6	*ENSMUST00000021519* Sine oculis-related homeobox 6 homolog Gene Transcription factor, SCN Validation	AGAGTGGTACCTTCAGGACCCATA	AGAACCTGCTGCTGGAGTCTGTTT
VIP	*ENSMUSG00000019772* Vasoactive intestinal peptide precursor SCN neuropeptide and synchronisation factor	TTTCACCAGCGATTACAGCAG	GCTGATTCGTTTGCCAATGAG
GAPDH	*ENSMUSG00000097148* Glyceraldehyde 3-phosphate dehydrogenase Housekeeping gene	TGTGTCCGTCGTGGATCTGA	CCTGCTTCACCACCTTCTTGA

Table 2.2: qRT-PCR gene column investigated in acute light induction experiment, gene description and ensembl transcript code columns identify the sequence utilised for forward and reverse primer manufacturing.

2.3.5 Cloning and *in situ* hybridisation

Gene targets (Table 2.3) were amplified in a temperature gradient-driven PCR reaction (50°C-65°C) from total brain cDNA. A 1% agarose gel was loaded with the completed PCR reactions and efficiently amplified products were cloned in pCR4-TOPO (Invitrogen) vectors (TOPO TA Cloning Kit for Sequencing). TOP10 cells (Invitrogen) were transformed as per manufacturer's recommendations. Warm lysogeny broth (LB) agar (Invitrogen) enriched in 50 µg/ul Kanamycin (Sigma) was used for plating out transformed cells, incubating them overnight at 37°C. DNA was then extracted from transformed cells using the Qiagen Spin Miniprep Kit. 500 ng/µl of DNA was digested, incubated for 90 minutes at 37°C, run on 1% agarose gel, extracted using the QIAquick Gel Extraction Kit (Qiagen) and sent for sequencing. Correct insert orientation products had an additional digestion step for 2-3 hours at 37°C and digested samples were run on a 1% agarose gel. Linearised single band plasmids were gel-purified using QIAquick Gel Extraction Kit (Qiagen) and used to make digoxigenin-labelled (Roche) riboprobes as previously described (Jeans *et al*., 2007). Products were purified on QuickSpin RNA column (Roche) and run on gel to ensure RNA *in vitro* transcription had occurred prior to use.

Table 2.3: *In situ* genes investigated and corresponding primer sequence

Gene	GenBank accession numbers	Forward primer sequence	Reverse primer sequence
Fos FBJ osteosarcoma oncogene	NM_010234.2	AGAATCCGAAGGGAACGG	GGAGGCCAGATGTGGATG
JUNB Transcription factor jun-B	NM_008416.3	ACCTGCACAAGATGAACCAC	CGTTCTCAGCCTTGAGTGTC
VIP Vasoactive intestinal peptide precursor	NM_011702	CGTTTGAAGGAGCAGGTGAC	AGCCCCAGATTGGACGATC

Three month old age-matched *Bdr* and wild-type mice (n= 4 per genotype) were individually housed in large cages (44x26x12 cm) for at least 10 days in LD cycle. Brains were removed at ZT 16 +/- 30 minutes light stimulation on day 11 of the experiment.

Freshly killed mice had their brains removed and frozen in a foil cup filled with OCT (VWR) on dry ice. The equipment utilised throughout the protocol was RNaseZAPed (Ambion) prior to use and all solutions included DEPC treated water. 13 µM sections were cut on a cryostat and slides were fixed in 4% PFA PBS at room temperate as previously described (Nieto *et al*., 1996; Jeans *et al*., 2007). 80 ng of probe was added to hybridisation solution and 200 µl was added to drained slides and subsequently covered in parafilm and incubated at 60°C overnight.

Slides were washed in 5 X SSC before 500 µl blocking solution (50 ml B1-30 ml 5M NaCl, 100 ml 1M Tris-HCl pH=7.6 to 1 L of H2O and 0.5 g of blocking solution in DIG detection kit (Roche)) was added per slide and left for 1 hour at room temperature (Jeans et al., 2007). Slides were then drained and 500 µl anti-DIG antibody (Roche) in blocking reagent (1:5000) was added per slide and incubated at 4°C overnight (Jeans *et al*., 2007).

Finally, 500 µl detection NBT/BCIP mix (Roche) was added per slide and incubated in the dark room at room temperature for 6 to 8 hours (Jeans *et al*., 2007). Slides were mounted in a few drops of 90% glycerol with a glass coverslip, photographed at low/high magnification using the Axiovision 4.6 (Axiovision) and visualised via Image J software (NIH).

2.3.6 Proteomic 24hr circadian molecular profiling

Previous SCN molecular experiments reported the significance of NTO in circadian homeostasis (Deery *et al*., 2009; Tian *et al*., 2011; McGlincy *et al*., 2012; Lee *et al*., 2013). Additionally, a microarray conducted at ZT6, ZT11 and ZT13 on the *Bdr* SCN only recorded AVP (Arginine Vasopressin) and NT (Neurotensin) as de-regulated factors (Oliver *et al*., 2012). Therefore, an expanded proteomic SCN investigation (6 time points) was vital to comprehend the underlying mechanisms linking circadian disruption and schizophrenic endophenotypes.

2.3.7 BCA Protein Assay

1mm and 2mm SCN slices were tissue-punched and peptide/protein extracted under alternative reagents (CHAPS, Lauryl Maltoside, Invitrosol, Urea) at different concentrations (1%, 2% and 4%). Protein concentration was quantified after diluted albumin (BSA) standards were generated with maximum concentration of 2,000 µg/ml and a minimum 0 µg/ml (Blank). BCA Working Reagent (WR) was generated by 50:1 ratio of BCA Reagent A to BCA Reagent B. The absorbance of SCN samples was measured at 562nm and was correlated to the BSA standard curve as per manufacturer's recommendations (Pierce BCA Protein Assay Kit-Thermo Scientific).

2.3.8 Protein Extraction-Fractionation/Mass Spectrometry

Alternative methodologies and reagents were tested adopting Bora *et al's* and Lee *et al*'s methodology and hybrid approaches for optimisation of data generation (Bora *et al*., 2008; Lee *et al*., 2010; Lee *et al*., 2013). Most optimised methodology included ten age-matched (12 week) wild-type and *Bdr* animals (n= 10 per ZT), entrained in LD for ten days. On day 11 mice had their brains, after cervical dislocation, sectioned on a steel matrix so that SCN tissue punches were collected using a 1 mm sample corer (FST Ltd.) and subsequently

snap-frozen. A minimum of ten frozen pooled SCN punches were protein-extracted using 450 µl 8M Urea chaotropic agent; buffer also included 50mM TEAB (Sigma), 150mM NaCl and 1% v/v Protease Inhibitors (Sigma). Samples were sonicated for 5X5sec (10 amplitude microns) and incubated for 45 minutes on ice. Each sample was then centrifuged for 20min, 12,500 rpm at 4°C. The supernatant was subsequently collected and fractionated (between below and above 10kDa) in 10kDa Amicon Ultra 0.5 mL centrifugal filters before passing it through a C18 tip. A C18 (silica stationary phase column) tip can be manufactured by punching a small diameter plug of C18 material from a disk of Empore Octadecyl C18 47mm diameter Extraction disk (SIGMA part number 66883-U) and packing the small disk into a P10 pipette tip.

Figure 2.6: Methodology for quantifying SCN peptidome and proteome

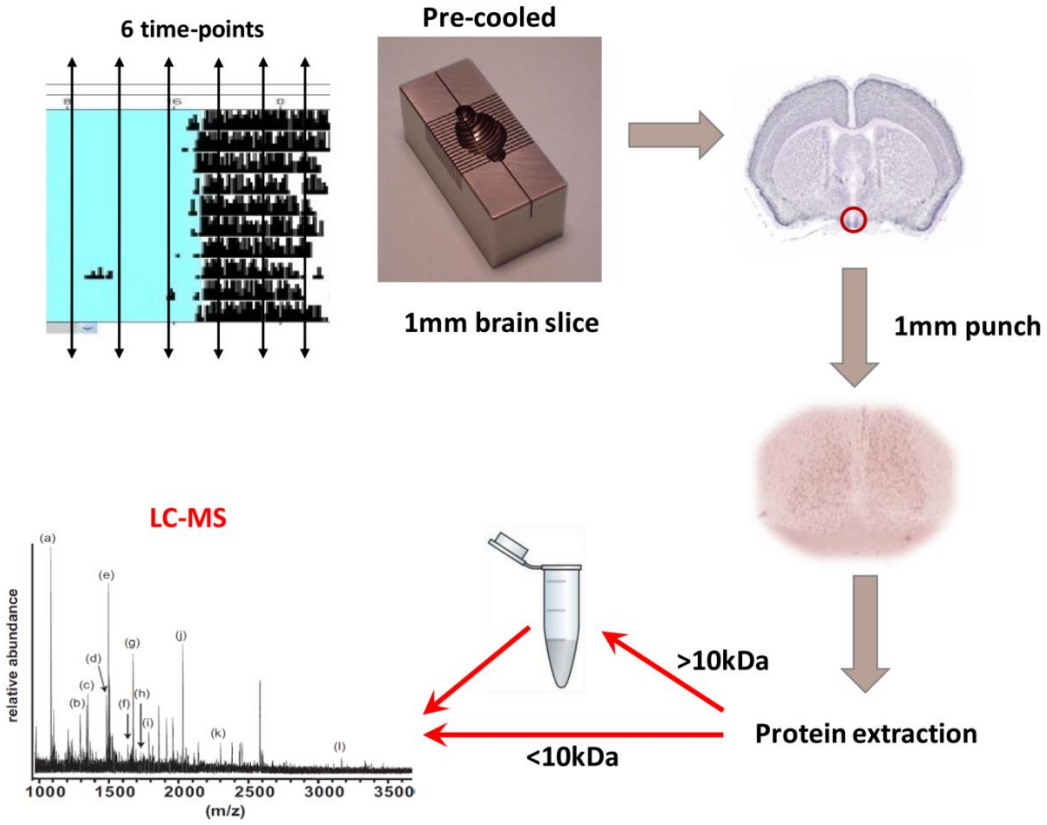

Figure 2.6: Flowchart represents the experimental steps undertaken for 24h SCN proteomic investigation.

2.3.9 Below 10kDa targets

C18 tips were prepared by loading 100ul of wetting buffer into the top of the C18 tip. Wetting buffer (0.1% formic acid in acetonitrile-ACN) could be pushed through the C18 material by using a large plastic syringe (e.g. 10mL plastic disposable syringe) or a vacuum manifold. The C18 column was equilibrated by loading 100 µl of equilibration buffer (0.1% formic acid in water) onto the C18 tip and pushing the buffer through. The device was then ready to bind peptides. The peptide sample was equilibrated in acidified aqueous buffer (typically 0.1% formic acid in water) and could now be loaded onto the C18 tip. The sample solution was loaded onto the C18 tip and slowly pushed over the C18 phase or sucked through slowly on a vacuum manifold. The flow-through was collected in a clean Eppendorf tube (and passed a second time over the C18 column). If the peptides failed to bind to the C18 tip, this would contain the peptides. Capture efficiency could be improved by passing the flow-through over the C18 tip again – this could lead to a more efficient binding of the peptides to the C18 tip. The peptides were de-salted by loading 100 µl of wash buffer onto the C18 tip (0.1% aqueous formic acid). The washes were collected in a clean Eppendorf tube. The de-salted peptides were eluted by loading 30 µl of elution buffer (step-wise elution→10 µl 30%ACN, 10 µl 50% ACN to 10 µl 100% ACN) onto the C18 tip. The sample was concentrated to dryness/near dryness in a SpeedVac and flash frozen and stored at -20°C or -80°C prior to mass spec analysis.

Samples were analysed on a Q Exactive (Thermo, Hemel Hempstead) mass spectrometer coupled to an Ultimate 3000 RSLCnano HPLC (Dionex, Camberley, UK). Samples were resolved on a 25 cm long by 75 µm internal diameter home-packed nano HPLC column (Thermo, Hemel Hempstead) at a flow rate of 300 nL min^{-1} using a 120 min gradient. The mass spectrometer was operated in a “top 10” data-dependent mode with +1 precursors

excluded. Dynamic exclusion was enabled and set at 30 s. HCD (High–energy Collisional Dissociation) was used to fragment precursors with normalised collision energy of 28%. Label-free quantitation was performed via Progenesis LC-MS v4.0 (Non-linear Dynamics, Newcastle) and Mascot (Matrixscience, London).

2.3.10 Above 10kDa targets

In-solution trypsin digestion and C18 de-salting of proteins was undertaken as recommended by the Central Proteomics Facility in the Sir William Dunn School of Pathology. Briefly, samples stored at -20°C or -80°C were initially defrosted in sonication for 10min. An aliquot of 100µl was transferred to a new tube and 100µl of 25mM ammonium bicarbonate was added to each sample, vortexed and incubated for 20min at room temperature. 5µl of 80mM DTT was added (2mM final concentration DTT) to each sample, vortexed, centrifuged and incubated for 30min at room temperature. 5µl of 400mM of iodoacetamide was added to each sample (10mM final concentration iodoacetamide), vortexed, centrifuged and incubated in the dark for 60min at room temperature. Samples were diluted from 4M Urea to 1M Urea with 25mM ammonium bicarbonate. A 1:100 trypsin-to-protein ratio (Promega) was used and incubated overnight at room temperature. 2µl of acetic acid was added to each sample, vortexed and centrifuged. The C18 protocol utilised for the below 10kDa fraction was repeated at this stage for the removal of salts, DTT, iodoacetamide and urea prior to mass spec analysis. Samples were analysed on a Q Exactive (Thermo, Hemel Hempstead) mass spectrometer as stated above.

2.3.11 Proteomic Data Analysis

Samples were randomised and analysed in duplicates (for the above 10kDa) while a single run was performed on the below 10kDa fraction. Resulting LC-MS/MS files (*raw) were analysed using Progenesis LC-MS v4.0. Alignment across Retention Time (RT) and m/z axis of generated 2D ion intensity maps per sample was performed against two different internal controls for increased confidence, and overlapping data followed-up. Peptides were detected and quantified with Progenesis LC-MS software (version 4.0) using default settings (no de-convolution/de-isotoping). A merged peaklist generated by Progenesis LC-MS was searched against the UniProtCP_mouse database using Mascot version 2.4. Database search was performed with the following parameters: carbamidomethyl (C) was set as a fixed modification whereas oxidation (M) was set as a variable modification. Peptide tolerance was set at ± 20ppm of the theoretical mass while MS/MS tolerance at ±0.02Da. Mascot cutoff score was set to 30. The number of allowed missed cleavages was set to 2 (0 cleavages and no trypsin set for the below 10kDa fraction) and the significance threshold set to 0.05 ($p<0.05$). Identified proteins had at least two unique peptides and presence in 2 technical replicas. For label-free protein quantitation Mascot results were imported into Progenesis LC-MS. Similar proteins were grouped and only non-conflicting features were used for quantitation. Finally, both raw/normalised protein abundances alongside raw spectral counts were utilised for increased confidence of follow-up targets (Figure 2.7).

Figure 2.7: Experimental and data analysis flowchart pursued for the 24hr (6 time points) SCN WT versus *Bdr* proteomic investigation

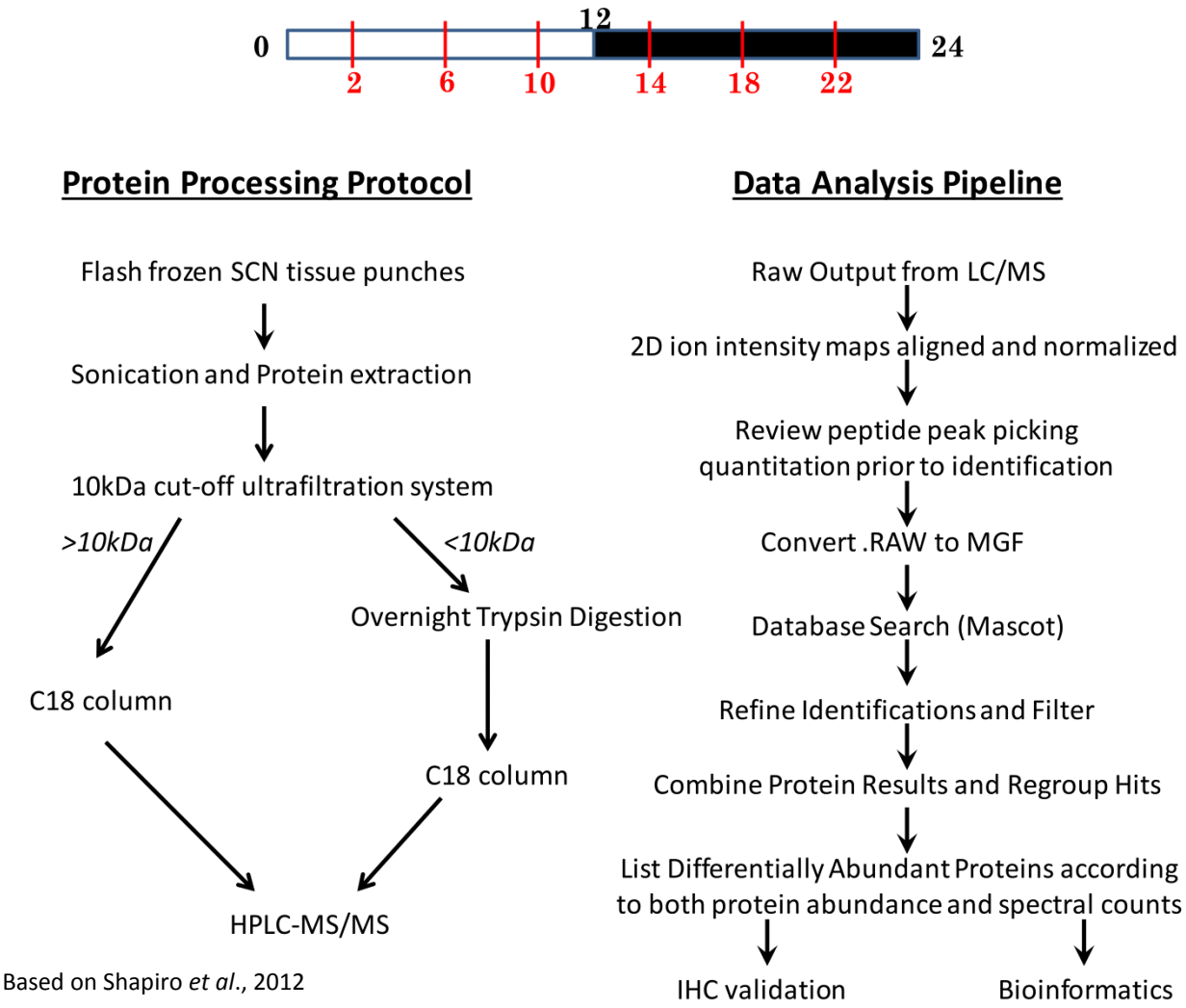

Figure 2.7: Graph reflects the proteomics methodology utilised for the pooled 10 SCN tissue punches per genotype (WT and *Bdr*) per time point for 6 time points (ZT2, ZT6, ZT10, ZT14, ZT18, ZT22).

2.3.12 Immunohistochemistry

The aim of the immunohistochemisty (IHC) experiments was to confirm proteomic findings from the 24hr MS screen. An independent cohort of age-matched (12 week) male *Bdr* and WT animals (n= 6 x 3) was entrained to a 12:12 LD cycle at 150 lux for 10 days prior to the day of tissue collection at ZT2, 6, 10, 14, 18 and 22. On day 11 animals were perfused with 4% PFA, brains dissected and stored overnight in 4°C. Days 2 and 3 involved incubating

the fixed brains in increasing sucrose (Fisher) concentrations (20% and 30%). Cryostat sectioning followed at 11µM.

After washes in phosphate buffered saline (PBS), sections were incubated in sodium citrate and microwaved for antigen retrieval to occur. Sections were subsequently blocked in 5% normal goat serum with 0.5% Tween-20, followed by incubation with primary rabbit antibodies (antisera) in the same solution. Biotinylated secondary antibody (2 hr, room temperature) and avidin-biotin complex (ABC) (1 hr, room temperature) treatment followed using Vectastain ABC immunohistochemistry method (Vectorlabs). Staining was visualised using diaminobenzidine (DAB) as the substrate for 2 min. Sections were dehydrated and mounted using Histomount (National Diagnostics). For each animal two sections representing the SCN were examined bilaterally. Sections were analysed using Axiovision 4.6 (Axiovision) and Image J software (NIH).

Table 2.4: SCN proteomic targets investigated by IHC

Protein Target	Antibody Supplier	Dilution Factor
Calbindin	Swant	1:10,000
GAP-43 (Growth Associated Protein 43)	Sigma	1:4,000
MARCKS (Myristoylated alanine-rich C-kinase substrate)	Abcam	1:6,000
pMARCKS (Ser152/156)	Millipore	1:8,000
Secretogranin II	Abcam	1:8,000
Substance P	Millipore	1:10,000

Table 2.4: Table summarizes the targets examined via IHC, the antibody supplier and the dilution factor.

2.3.13 Western Blot

The aim of the western blot (WB) experiments was to confirm proteomic findings from the 24hr MS screen. Independent cohorts of age-matched (12 week) male *Bdr* and WT animals (n= 2 x 4) were entrained to a 12:12 LD cycle at 150 lux for 10 days prior to the day of SCN tissue collection at ZT10 and ZT14. On day 11, after cervical dislocation, animals had their brains sectioned on a steel matrix and SCN tissue punches were collected using a 1 mm sample corer (FST Ltd.) and were subsequently snap-frozen. Protein extraction of the SCN followed as described in the MS section (above 10kDA fraction was investigated via WB).

25 µg of protein extracted from WT and *Bdr* SCN was prepared for 1D SDS gel electrophoresis. The samples were denatured in lysis buffer (8M Urea chaotropic agent, 50mM TEAB (Sigma), 150mM NaCl and 1% v/v Protease Inhibitors (Sigma)) and boiled at 100°C for 5 minutes. Samples were run on 8% SDS-PAGE resolving gel. The gel was then transferred to a nitrocellulose membrane (Millipore). Subsequent 1 hour blocking of the membrane occurred in 5% skimmed-milk in TBST (Tris-buffered Saline Tween-20). Primary antibody serum incubation occurred overnight at 4°C in 5% Milk-TBST. Blots were developed through a horse peroxidase reaction (HPR) on a conjugated secondary antibody serum (1:10,000, GE healthcare) and ECL (enhanced chemiluminescence) (Amersham). Bands were visualised and quantified using Image J software (NIH).

Primary antibodies utilised for SCN samples were rabbit anti-GAP43 (Chemicon, 1:1,000), rabbit anti-Calbindin (Swant, 1:1,000) and rabbit beta-tubulin (Abcam, 1:500).

2.3.14 Enzyme-linked immunosorbent assay

The aim of the enzyme-linked immunosorbent assay (ELISA) was to investigate the potential involvement of PKC activity in the circadian pathology of *Bdr* mice. An independent cohort of age-matched (12 week) male *Bdr* and WT animals (n= 2 x 4) was entrained to a 12:12 LD cycle at 150 lux for 10 days prior to the day of tissue collection at ZT2 and ZT6. On day 11 animals, after cervical dislocation, had their brains sectioned on a steel matrix and SCN tissue punches were collected using a 1 mm sample corer (FST Ltd.) and subsequently snap-frozen. Protein extraction of the SCN followed as described in the MS section (no ultrafiltration was undertaken to prevent potential loss of protein kinase C enzymes).

Protein kinase C (PKC) activity was detected using an ELISA kit (Enzo Life Sciences International). Briefly, micro-plates were pre-coated with PKC substrate. After 10 min of pre-soaking per well, the dilution buffer was aspirated and followed by the addition of 30µl of brain supernatant per well. The reaction was initiated by the addition of 10µl ATP per well and incubation for 90 minutes at 30°C. Each well was aspirated and followed by primary phospho-peptide antibody incubation for 1 hr. Following primary antibody incubation, 4 washes were undertaken and then a 30 minute incubation with a peroxidase-conjugated secondary antibody. The mean absorbance (x10^{3}) reading at 450nm was recorded and divided by the total protein amount per assay (Ji *et al*., 2012).

2.4 Statistics

Statistical analysis was undertaken in Excel (Microsoft) or Graphpad Prism 5.0. Two-tailed unpaired Student t-tests were used for direct comparison across one categorical variable with no more than two groups, and one dependent measurement. ANOVAs investigated one categorical variable with more than two groups, or multiple categorical variables and one or more dependent measurements, when repeated measures ANOVA was not relevant. Repeated measures ANOVAs (rANOVA) were utilised when the same subjects recorded for the same parameters were consistently altering one categorical variable (e.g. time) between readings. To guard against Type I errors, Bonferroni post-hoc analysis was utilised in statistical testing and significance assessment. Univariate or multivariate pair-wise comparisons were used in most instances to assess the source of the main effects.

The following p value thresholds were applied during statistical assessment

$P \leq 0.05$*	$P \leq 0.01$**	$P \leq 0.001$***	$P \leq 0.0001$****

3 Results I: Circadian screening of PD mouse models

3.1 Non-motor symptoms of PD

Sleep disruption has been well documented in a variety of neurodegenerative disorders and early non-motor endophenotypes of Parkinson's disease (PD) include circadian deficits whose onset precedes movement abnormalities (Table 3.1) (Kudo *et al*., 2011). More specifically, sleep fragmentation and excessive daytime sleepiness (EDS) underlie some early circadian non-motor symptoms in PD patients (Jankovic, 2007). Therefore, it is worthwhile to examine the correlation between circadian phenotype and PD models at a pre-symptomatic phase as a potential important early biomarker.

Table 3.1: Parkinson's disease motor and non-motor symptoms

Motor symptoms	Non-motor symptoms
Tremor, bradykinesia, rigidity, postural instability	Cognitive impairment
Dysarthria, dysphagia, sialorrhoea	Depression apathy, fatigue and psychiatric problems
Decreased arm swing, turning in bed	Sensory symptoms: anosmia, paresthesias
Micrographia, slow activities of daily living	Orthostatic hypotension, constipation, urinary dysfunction and abnormal sweating
Striatal deformity, scoliosis	Sleep disorders (REM disorder, daytime drowsiness, sleep fragmentation, restless legs syndrome)

Based on Jankovic, 2007

Table 3.1: Table illustrates PD symptoms. Sleep deficits in PD highlighted in red.

Recent focus in sleep disorders as an early premotor cognitive marker of PD has identified deleterious effects on rapid eye movement (REM) and NREM sleep (Fernandez *et*

al., 2012). Importantly, 81% of RBD (REM sleep behaviour disorder) sufferers go on to develop Parkinsonian disorders within a decade (Rothman and Mattson, 2012; Schenck *et al*., 2013). However, due to the complexity of the neurocircuits such as subtantia nigra, and pathology involved in PD-related sleep disorders, the direct mechanism between the two remains elusive (Fernandez *et al*., 2012). Emerging data suggest that PD-RBD may more readily involve cognitive pathology such as dementia (McCarter *et al*., 2013).

Mouse models of FTDP-17 and PD have been constructed in an effort to understand the complex neurological pathology involved. These involve traditional neuronal promoters (e.g. Prion promoter) expressing a particular cDNA isoform often in non-physiological spatio-temporal expression patterns (Tables 1.4-1.5). Recent efforts to mimic endogenous expression levels of risk genes have led to the generation of BAC SNCA/MAPT models of PD.

3.2 BAC SNCA mouse models

Mouse models generated to model PD display numerous neuropathological features ranging from severe early onset phenotypes to very mild late onset with no neurodegeneration (Table 1.4). A potentially more pathologically relevant method for modelling PD is the generation of human BAC transgenic mice (Lu, 2009). The fundamental advantages of utilising BAC transgenic animals are the inclusion of inherent regulatory domains that follow the genomic locus (most closely mimicking complex pathological states) aiming to generate physiologically relevant expression levels (Wade-Martins and Johnson, 2011). Moreover, *in vitro* studies showed that equimolar mouse and human α-synuclein partially decelerated the toxic conformation changes vital in Lewy pathology, further

underscoring the limited face validity generated by conventional over-expressing (OVX) transgenic mouse models of PD (Fernagut and Chesselet, 2004). The Wade-Martins group has therefore generated human BAC-based models of PD (Janezic *et al*., 2013; Taylor *et al*., 2014).

Copy number variations in SNCA have been strongly associated with PD pathology in GWAS studies (Singleton *et al*., 2003; Venda *et al*., 2010; Janezic *et al*., 2013). Mutant human BAC OVX transgenic mice on a null background (*Snca*$^{-/-}$) display roughly a 2-fold increase in human SNCA versus endogenous mouse levels, a spatio-temporal expression pattern closer resembling duplications of the SNCA locus in PD patients (Janezic *et al*., 2013). BAC OVX mice display dopaminergic deficits in the dorsal striatum prior to neuronal loss (Janezic *et al*., 2013). Preceding dopaminergic deficits are associated with altered vesicle dynamics in striatal axons (Janezic *et al*., 2013). BAC OVX mice display a marked reduction of spontaneous electrical firing from substantia nigra pars compacta neurons (Janezic *et al*., 2013). Non-motor pathology, including prodromal gastrointestinal dysfunction is observable in the OVX line as well as a late (18 months old) motor phenotype as assessed by rotarod. Importantly, the molecular pathology appears progressive and deteriorates with age only in the OVX mice versus WT/KO controls. Dopaminergic nigrostratial neuronal loss occurs in the OVX mice at 18 months of age and complements the observable motor phenotype (Janezic *et al*., 2013). However, no observable fibrillation of SNCA and Lewy pathology is noticeable even at 18 months of age in the OVX (Janezic *et al*., 2013).

Studies have implicated (chromosome 4) SNCA point mutations A30P, A53T and E46K with familial PD (Kruger *et al*., 2001; Taylor *et al*., 2014). BAC SNCA A30P mice also display preceding regional dopamine-specific deficits in the dorsal striatum (Taylor *et al*., 2014). Other catecholamine systems, including norepinephrine, appear unperturbed in the mutated

transgenic line or complementary controls (Taylor *et al*., 2014). BAC SNCA A30P and BAC SNCA WT controls display sensitivity to MPTP (1-methyl-4-phenyl-1,2,3,6-tetrahydropyridine) while *Snca*$^{-/-}$ appear unaffected (Taylor *et al*., 2014). Previous mouse work has demonstrated a lack of MPTP susceptibility in *Snca*$^{-/-}$ (Nemani *et al*., 2010; Taylor *et al*., 2014). However, no nigrostratial neuronal loss or Lewy body pathology is associated with the A30P mutant line (Taylor *et al*., 2014). Additionally, motor function tests such as accelerating rotarod and forepaw stride length did not record any overt phenotype (Taylor *et al*., 2014).

In summary, the OVX and A30P display preceding dopaminergic alterations in a regionally CNS specific manner. Deficits in dopaminergic neurocircuitry coupled to substantia nigra neuronal loss enhance the face validity of the BAC OVX when compared to conventional transgenic Thy-1 and prion promoter models. Moreover, deficits of the dopaminergic circuitry alone in a BAC context could potentially provide insights into its impact on the circadian axis. Prodromal non-motor and motor circadian assessment of the BAC SNCA mice is particularly relevant as dopamine depletion is associated with circadian rhythm de-synchronisation in PD patients (Hampp *et al*., 2008; Imbesi *et al.,* 2009; Hood *et al*., 2010).

3.3 MAPT mouse models

Over the years a number of MAPT transgenic mouse models have been generated in an attempt to comprehend the role of MAPT and the pathogenic neurodegeneration it promotes (Table 1.5). MAPT$^{-/-}$ mice do not present any overt phenotype or histological aberrations (Harada *et al*., 1994, Dawson *et al*., 2001). Open-field tests of MAPT$^{-/-}$ generated a hyperactive phenotype while muscle strength was significantly reduced as reported by the

rod-walking tests (Ikegami *et al*., 2000). No phenotype was detected on a Morris water maze for *Mapt*$^{-/-}$, a test that examines spatial working memory, and therefore MAPT is classified as a developmentally accessory protein with an axonal localisation (Denk and Wade-Martins, 2009). However, *Mapt*$^{-/-}$ mice do display some mild structural aberrations in hippocampal neurons, probably due to reduced microtubule number and density, which complements the existing mild behavioural phenotype (Harada *et al*., 1994). Mice generated to model FTDP-17 display numerous neuropathological features ranging from severe early onset phenotypes to very mild late onset with no neurodegeneration (Table 1.5). More recently, research has focused on over-expressing mutated copies of the MAPT gene discovered in FTDP-17. Most of these mutations localise at the microtubule binding region in exons 9 to 12. Given the significance of exon 10 most mouse work is now focused on replicating mutations localised at this particular exon (Denk and Wade-Martins, 2009).

cDNA transgenic mouse models with FTDP-17 mutations alone are sufficient for inducing tauopathic neurodegeneration (Table 1.5). The same does not apply to the over-expressing human wild-type tau equivalent. Andorfer and colleagues have now reported a htau (human tau) genomic transgenic mouse model to support the differential splicing hypothesis of the MAPT gene and the imbalance of isoform variants expressed in tauopathies (Duff *et al*., 2000; Andorfer *et al*., 2003, 2005). These models express physiological transgene levels throughout the CNS, an improvement over conventional mouse models (Table 1.5). The absence of the endogenous *Mapt* mouse copy by recombineering on a *Mapt*$^{-/-}$ background would allow the human mutant copy to be examined. Therefore, BAC MAPT transgenic hemizygous mutant mice on a MAPT$^{-/-}$ background were generated for the human WT copy (MAPT-WT$^{+/-}$) and the human mutation N296H (termed MAPT-N51$^{+/-}$). This particular

mutation lies in exon 10. Preliminary longitudinal phenotypic characterisation of the BAC MAPT N51 mice identified a non-motor depression phenotype at 6 months of age (increased immobility time at the tail suspension test). Therefore, this project investigated preliminary motor and non-motor circadian pathology via a circadian running screen on the BAC SNCA/MAPT mice.

3.4 *Parkin* KO mouse models

Approximately 8-10% of early onset PD cases are due to homozygous deletions of exons 3-7 of the Parkin (PARK2) gene (Kitada *et al*., 1998, Houlden and Singleton, 2012). In 2003, Goldberg *et al* reported the generation of a *Parkin*$^{-/-}$ mouse through deletion of exon 3 that resulted in a frameshift after amino acid 57 and a premature termination stop codon in exon 4 (Goldberg *et al*., 2003). These mice exhibited no overt changes in brain morphology when compared to wild-type, while striatal intracellular recordings demonstrated reduced synaptic excitability consistent with nigrostratial PD pathology (Goldberg *et al*., 2003, Zhu *et al*., 2007). Despite elevated extracellular dopamine levels, these mice did not recapitulate any of the dopaminergic neurodegeneration in the substantia nigra characteristic of PD patients (Goldberg *et al*., 2003). Parkin substrates such as a-synuclein and synphilin-1 appeared unaltered pointing only to a novel role of Parkin in dopamine release and a non-essential role in neuronal survival (Goldberg *et al*., 2003).

Behaviourally, exon 3 deleted *Parkin*$^{-/-}$ mice exhibit sensorimotor impairments, weight loss, impairments in mitochondrial function as well as reduced anti-oxidant mechanisms

leading to redox imbalances (Palacino *et al*., 2004). Other independently-generated exon 3 deleted *Parkin*$^{-/-}$ mice exhibit inhibited amphetamine-induced dopamine release as well as impairment of glutamatergic transmission in the hippocampus (Itier *et al*., 2003). Behaviourally, these mice exhibit cognitive deficits as well as locomotor hypoactivity (Itier *et al*., 2003).

Given the limited face and predictive validity of the exon 3 *Parkin*$^{-/-}$ PD mouse models, alternative mutant lines were constructed. Exon 7 deleted *Parkin*$^{-/-}$ mice demonstrate a different phenotype. Loss of *Parkin* in these mice leads to acoustic impairments and tyrosine hydroxylase positive neuronal loss in the locus coeruleus (Von Coelln *et al*., 2004). Furthermore, impaired noradrenaline levels were detected along the spinal cord and olfactory bulb of these mice (Von Coelln *et al*., 2004). No dopaminergic nigrostratial impairment was present, but nonetheless the mice exhibited PD-like neurodegeneration in the locus coeruleus (German *et al*., 1992).

Exon 2 deletions also generate a *Parkin*$^{-/-}$ mouse that shows no loss of nigrostratial dopamine neurons (Perez and Palmiter, 2005). Additionally, no locus coeruleus neurodegeneration was detected and no catecholine impairments were reported (Perez and Palmiter, 2005). Absence of any overt behavioural phenotype was also recorded (Perez and Palmiter, 2005).

Given the inconsistent phenotypes recorded in previously generated *Parkin*$^{-/-}$ mice, Zhu *et al* generated an independent exon 3 *Parkin*$^{-/-}$ mouse (Zhu *et al*., 2007). The mice reported abnormal anxiety phenotypes during light/dark exploration tests (Zhu *et al*., 2007). Additionally, impaired exploratory behaviours and thigmotaxis in the open field paradigm

were recorded (Zhu *et al*., 2007). Given the enhanced striatal dopamine metabolism in these *Parkin*$^{-/-}$ mice, they appear to exhibit non-motor manifestations consistent with the dopamine-induced cognitive decline also recorded in PD patients (Zhu *et al*., 2007). Therefore, this project investigated preliminary motor and non-motor circadian pathology via a circadian running screen on the *Parkin*$^{-/-}$ mice.

3.5 Objectives

PD diagnosis integrally relies on classical motor symptoms such as postural instability and resting tremor. FTDP-17 also relies on neuropsychiatric involvement with dementia and disturbed night-time behaviours. Increasingly, non-motor symptoms such as sleep disorders, constipation and olfactory impairments are recognised as critical for early diagnosis and therapeutic intervention, especially due to their extensive impact on PD patient morbidity. Based on the two-process model, the circadian regulation of sleep is distinct from the homeostatic drive (Borbely, 1982). By measuring circadian activity in animal models of PD one of the regulatory processes of sleep/wake cycles is investigated. Potential abnormalities in the circadian system may give rise to sleep disturbances.

BAC models generated by the Wade-Martins lab display subtle early onset non-motor pathology coupled to late onset motor pathology. Additionally, dopaminergic alterations in the dorsal striatum of the BAC OVX mice prior to neurodegeneration in the substantia nigra pars compacta (SNc) identify early neurotransmitter deficits. Physiological expression of risk genes enhances the construct validity of the BAC SNCA/MAPT transgenic mouse models in their ability to mimic complex pathological states. This screen would monitor the behavioural effects of SNCA/MAPT/*Parkin* on the circadian axis. Rest/activity cycles in BAC SNCA/MAPT and *Parkin*$^{-/-}$ mouse models would be investigated to possibly establish circadian non-motor/motor symptom progression in PD/FTDP-17. Therefore, the main objective of this work is to:

- Study circadian rest/activity behavioural phenotypes in the BAC SNCA/MAPT and *Parkin*$^{-/-}$ mouse models of PD and FTDP-17.

3.6 Materials and Methods

3.6.1 Clocklab/Matlab

A behavioural circadian screen adapted from previous work on the *Bdr* mice covering the most commonly employed circadian paradigms was utilised. 20 BAC SNCA (n= 5 per mouse line: BAC SNCA WT, BAC SNCA A30P, BAC SNCA OVX, SNCA KO) mice at 8 months of age, 18 BAC MAPT mice (n= 6 per mouse line: BAC MAPT WT, BAC MAPT N51, MAPT KO) at 10 months of age and 7 *Parkin*$^{-/-}$ mice (n= 4 KO and 3 WT; male mice only) at 10 months of age, age-matched females/males (n= 2 females per SNCA/MAPT mouse line, n= 3 males per SNCA mouse line and n= 4 males per MAPT mouse line) were individually housed in large cages (44x26x12cm) with running-wheels. Student's t-tests were used in cases of direct comparison across one categorical variable with no more than two groups, and one dependent measurement. ANOVAs were used in the case of one categorical variable with more than two groups where repeated-measures tests were not applicable.

3.6.2 Nonparametric activity and sleep analysis software

As previously stated (see page 60)

3.6.3 Circadian Screen

A number of circadian paradigms were completed including 12:12hr Light-Dark (LD) cycle, 1hr ZT14 light pulse (negative masking), phase shift (6 hours phase advance) Dark-Dark (constant dark conditions-DD), Light-Light (constant light conditions-LL) cycles, re-entrainment back to a 12:12hr LD cycle and an additional phase shift (6 hours phase advance). Light conditions were maintained at 150 lux.

3.7 Circadian data of BAC α-synucleinopathic models

BAC SNCA-WT, OVX and A30P and KO models were screened for rest/activity profiles from 8 months of age. Due to the length of the study, age-related effects on the behavioural circadian phenotype could be also assessed**.** Numerous circadian paradigms (Figure 3.1) were utilised for screening the BAC transgenic models of PD.

Figure 3.1: Representative double-plotted actograms of the screen for each line

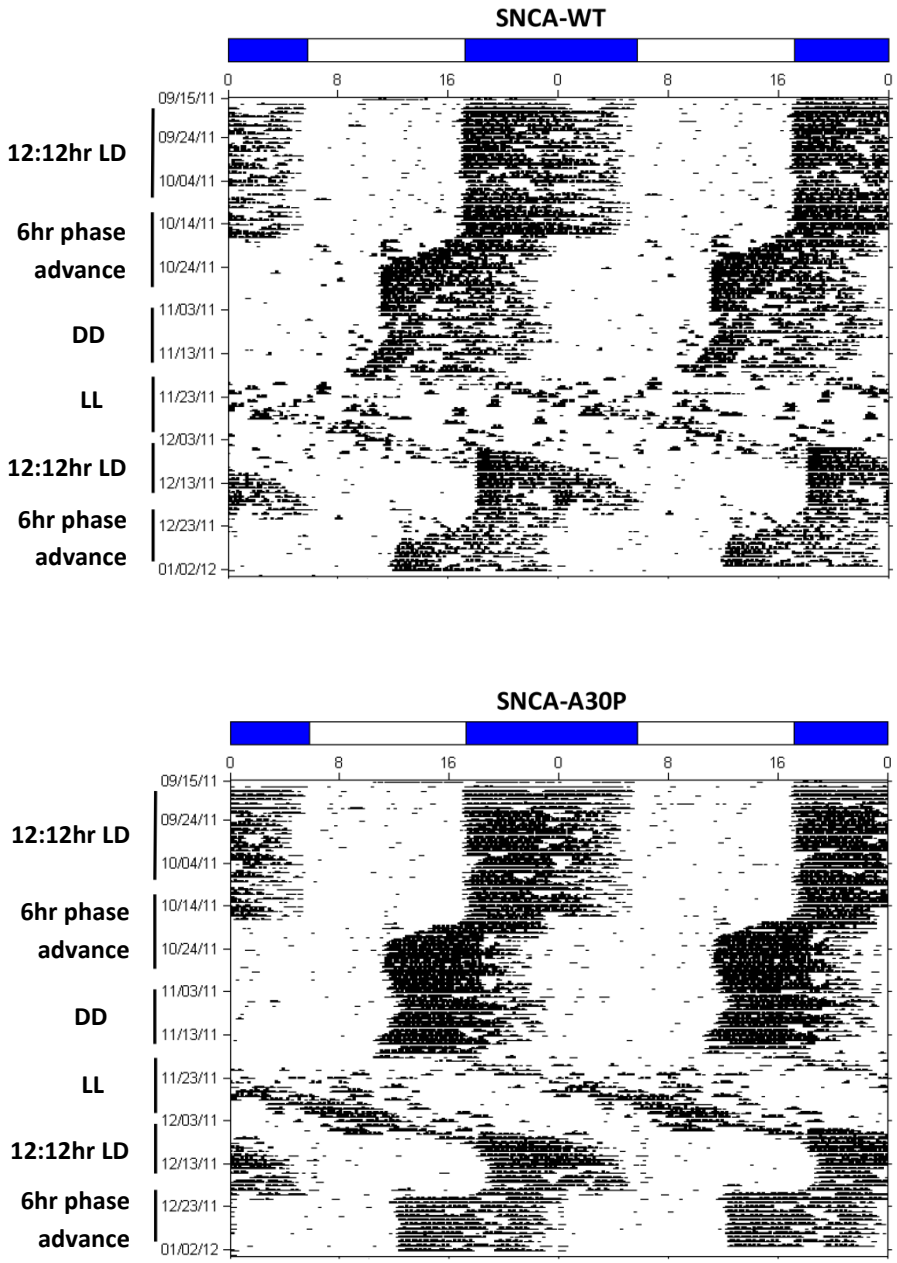

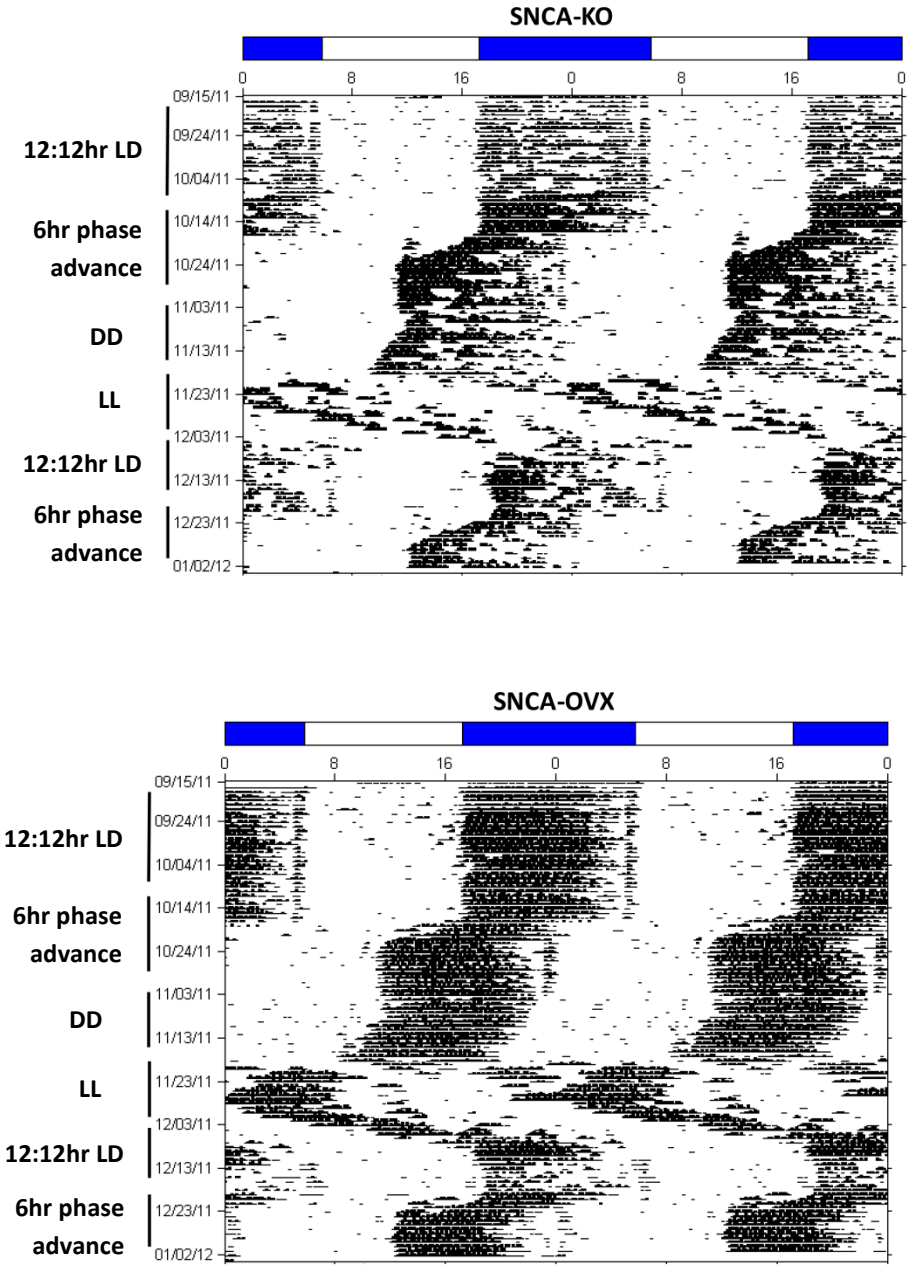

Figure 3.1: Blue bars indicate the dark phase and white bars the light phase (this reflects only the starting 12:12hr LD cycle and not 6hr phase advanced, DD or LL paradigms). Black spikes represent activity data recorded from each individual mouse and each line represents 48h with dates presented on the left hand side of each diagram. Alternative circadian paradigms and their respective duration are represented on the left hand side of actograms.

Entrainment to a 12:12hr Light-Dark cycle was observed in all lines (Figure 3.1). However, OVX and A30P lines exhibited scotophase hyperactivity as well as decreased

rhythm fragmentation (Figure 3.2). A *count by day* plot of the entire circadian screen illustrates the activity variation associated with each circadian paradigm (Figure 3.2).

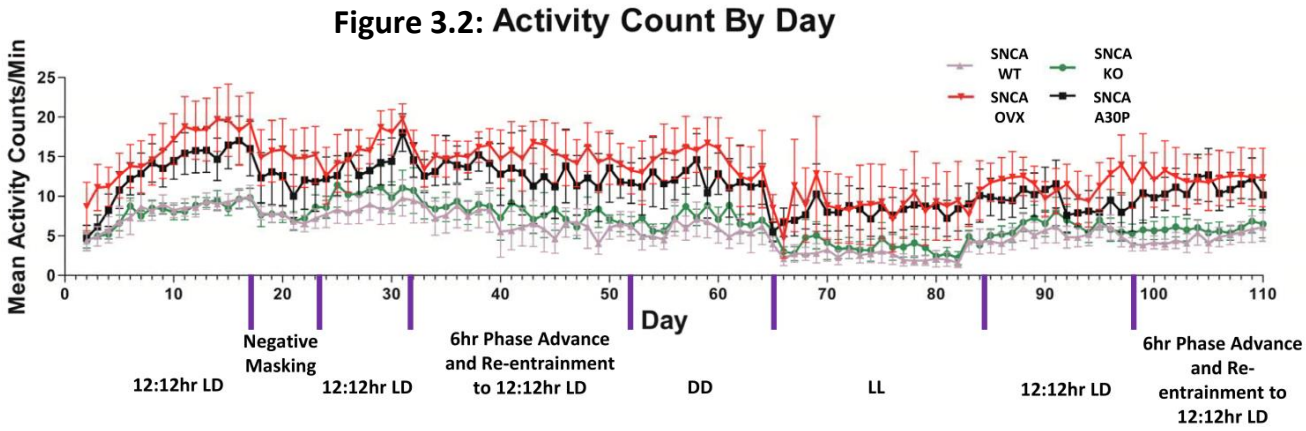

Figure 3.2: The graph illustrates mean activity counts per min for each day of the 110 days of PD circadian screen. X-axis represents each day clustered in circadian paradigms. Data presented as mean ± SEM (n= 5 per mouse line, SNCA-OVX n= 4 after day 25). The SNCA-OVX and SNCA-A30P lines exhibited hyperactivity versus SNCA-WT/KO controls. Appendix 8.4 contains further information regarding the mouse models.

Hyperactivity of OVX and A30P versus SNCA-WT and KO is shown throughout most of the circadian screen (Figure 3.2). Days 2 to 16 illustrate progressive increase in activity counts by day in all lines. This underscores the motivational reinforcement the wheel exercises on mouse behavioural activity patterns (Careau *et al*., 2012). Importantly, this effect is also observed after an LL paradigm (day 84 onwards). Possible age effects include lower activity counts but the preceding LL paradigm does represent a possible confounding variable.

All lines displayed suppression of activity under LL (LeGates and Altimus, 2011). Activity levels in all lines were restored when animals were returned to a 12:12hr LD cycle following an LL paradigm. LD activity plots display the activity variation exhibited among lines across a 24h period (Figure 3.3).

Figure 3.3: LD activity profiles over 7-14 days at different stages of the circadian screen

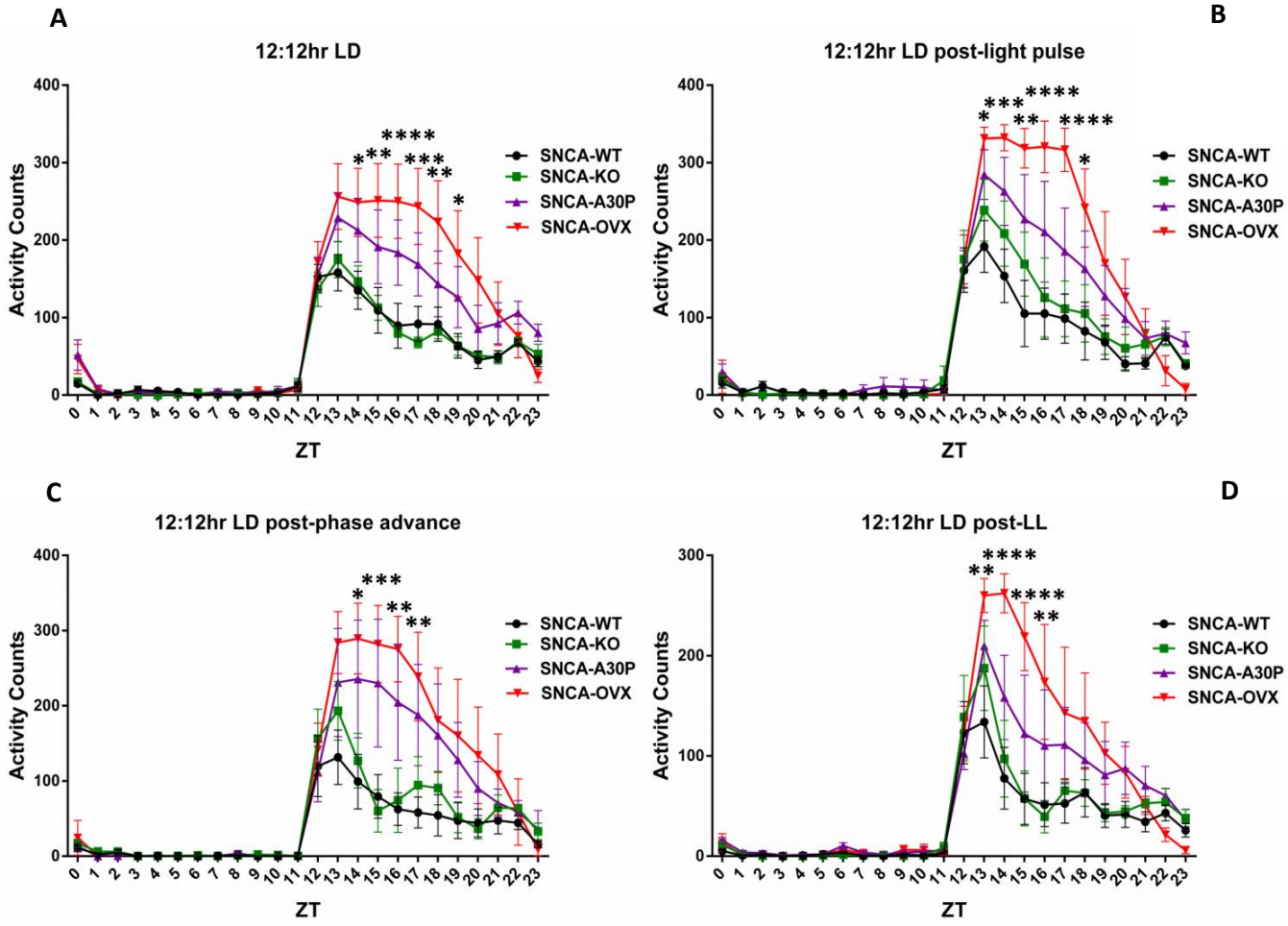

Figure 3.3: (**A**) Activity profile over 15 days during a 12:12hr LD paradigm (days 3 to 17-figure 3.3) (**B**) Activity profile over 8 days during a 12:12hr LD post-light pulse stage (days 24 to 31-figure 3.3) (**C**) Activity profile over 11 days during a 12:12hr LD post-6hr phase advance stage (days 42 to 52-figure 3.3) (**D**) Activity profile over 11 days during a 12:12hr LD post-LL stage (days 88 to 98-figure 3.3). Data presented as mean ± SEM (n= 5 per mouse line, SNCA-OVX n= 4 for graphs B, C and D, n= 2 females and n= 3 males per mouse line). The SNCA-OVX and SNCA-A30P lines exhibited hyperactivity versus SNCA-WT/KO controls.

Scotophase-specific OVX and A30P hyperactivity is shown versus WT/KO controls (Figure 3.3). No difference was detected during photophase epochs. Progressively the A30P line lost its mild hyperactive phenotype while hyperactivity persisted in the OVX line (Figure 3.3: A→D). Altered fragmentation bouts among lines were also recorded (Figure 3.4). Rhythm fragmentation measurements can be correlated to activity levels as it may indicate fatigue and/or motivational levels of each PD line for the circadian wheel.

Figure 3.4: Total activity bouts over 7-14 days at different stages of the circadian screen

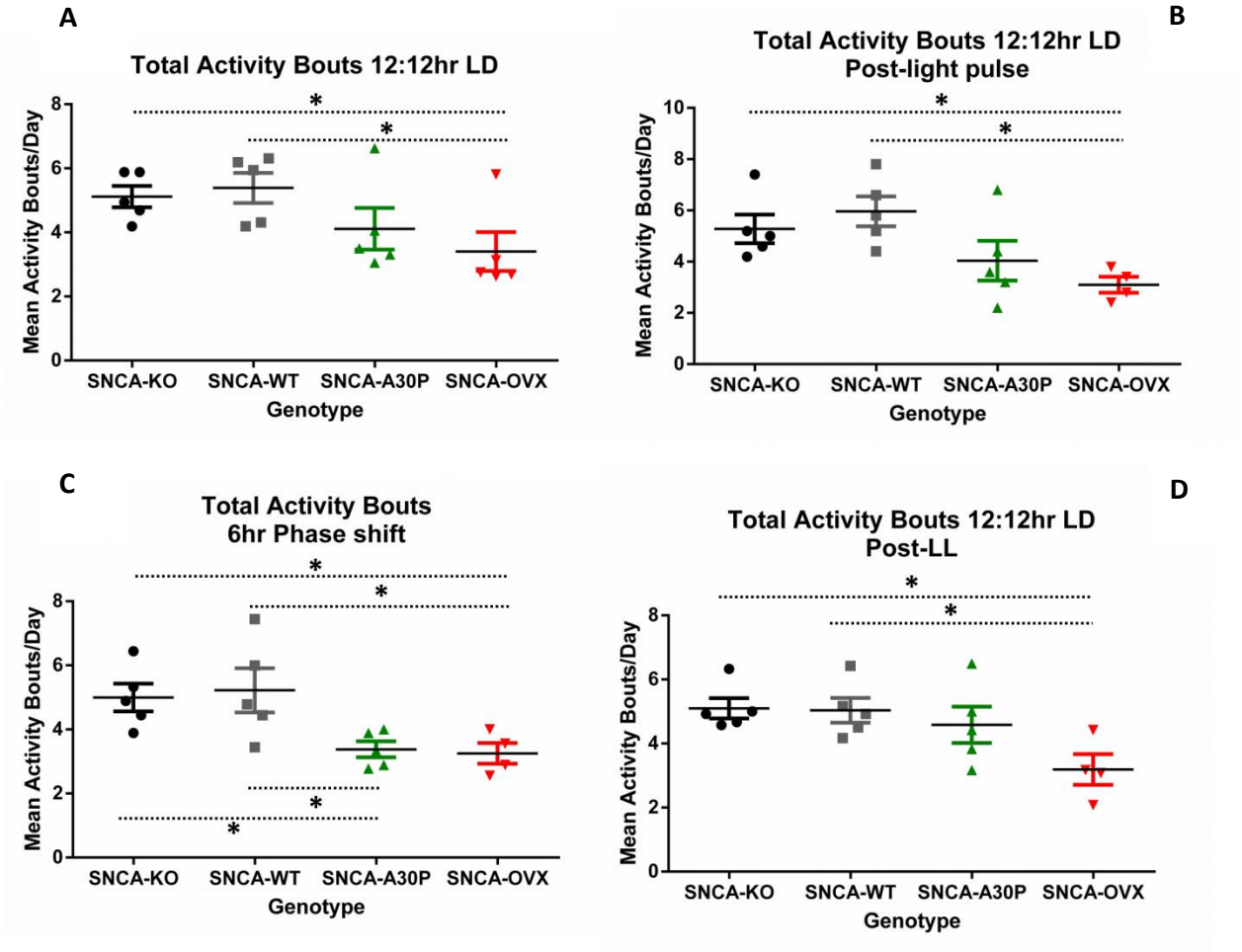

Figure 3.4: (**A**) Total activity bouts over 15 days during a 12:12hr LD paradigm (days 3 to 17-figure 3.3) ($F_{(2, 12)} = 4.96$, p= 0.027)(**B**) Total activity bouts over 8 days during a 12:12hr LD post-light pulse stage (days 24 to 31-figure 3.3) ($F_{(3, 15)} = 4.20$, p= 0.024) (**C**) Total activity bouts over 9 days during a 6hr phase shift (days 33 to 41-figure 3.3) ($F_{(3, 15)} = 4.85$, p= 0.015) (**D**) Total activity bouts over 11 days during a 12:12hr LD post-LL stage (days 88 to 98-figure 3.3) ($F_{(3, 15)} = 3.57$, p= 0.040). Data presented as mean ± SEM (n= 5 per mouse line, SNCA-OVX n= 4 for graphs B, C and D, n= 2 females and n= 3 males per mouse line). SNCA-OVX mice consistently display less fragmentation versus SNCA-WT/KO controls.

Throughout the screen the OVX mice recorded statistically fewer activity bouts versus SNCA-WT and/or KO (a measurement of reduced rhythm fragmentation) (Figure 3.4). Moreover, increase in variation on rhythm fragmentation during phase shifting is shown (Figure 3.4C).

Figure 3.5: IS and IV values among mouse lines in LD

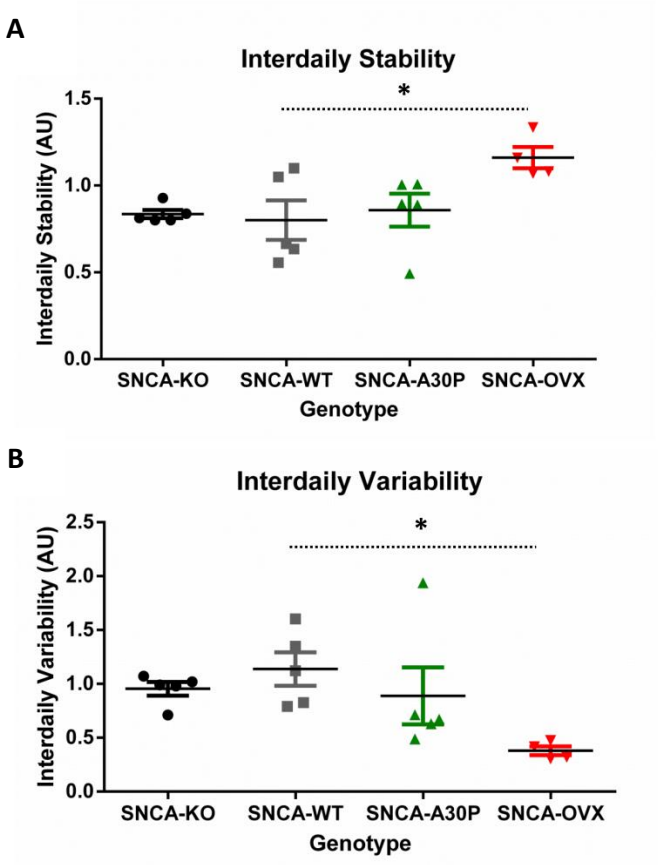

Figure 3.5: (**A**) Interdaily stability (IS) over 11 days during 12:12hr LD (Days 2-12: Figure 3.2) ($F_{(3, 15)}$ = 3.56, p= 0.040) and (**B)** Intradaily stability (IV) over 11 days during 12:12hr LD (Days 2-12: Figure 3.2) ($F_{(3, 15)}$ = 3.43, p= 0.045). Data presented as mean ± SEM (n= 5 per mouse line, SNCA-OVX n= 4). SNCA-OVX show significant difference in both IS and IV factors versus SNCA-WT control.

The OVX mice display more robust rest/activity bouts between days (IS, $F_{(3, 15)}$ = 3.56) and considerably less fragmentation on individual days (IV, $F_{(3, 15)}$ = 3.43) during LD (Figure 3.5). A numerical summary of the circadian parameters per paradigm illustrates any potential significance (Tables 3.2-3.4).

Table 3.2

12:12hr LD Cycle

Parameter	SNCA KO (mean/SEM)	SNCA OVX (mean/SEM)	SNCA A30P (mean/SEM)	SNCA WT (mean/SEM)	P-value
Tau	24.0/0.0	24.0/0.0	23.9/0.1	24.0/0.1	Non-sig
Tau Onset Error	0.5/0.2	0.3/0.1	1.0/0.7	0.4/0.2	Non-sig
Alpha	9.0/1.3	9.6/2.2	9.0/1.5	9.6/0.8	Non-sig
Rho	15.0/1.3	14.4/2.1	14.9/1.4	14.3/0.8	Non-sig
Total Activity	11328/1000	22591/4855	18746/3330	11486/1838	<0.05
Total Dark Activity	9494/667	20313/4499	16504/3243	9435/1741	<0.05
Total Light Activity	1835/392	2278/411	2242/183	2052/207	Non-sig
% Light Activity	15.6/2.1	11.5/2.0	13.7/3.0	19.1/2.4	<0.05
Chi-square Periodogram Peak (Hours)	23.9/0.0	23.9/0.0	23.9/0.0	24.0/0.0	Non-sig
Chi-square Periodogram Peak (Amplitude)	1646/83	2234/256	1798/237	1688/201	Non-sig
Phase of entrainment	-0.3/0.2	-0.3/0.0	0.0/0.3	-0.1/0.1	Non-sig
Total Activity Bouts	5.1/0.3	3.4/0.6	4.1/0.7	5.4/0.5	<0.05

Table 3.2: Circadian and locomotion parameters analysed for each line. Statistical differences illustrated in red. Table 3.2 corresponds to days 3 to 17 from figure 3.2. Mean ± SEM values for each circadian parameter of each line are also presented (n= 5 per mouse line).

Table 3.3

DD Period

Parameter	SNCA KO (mean/SEM)	SNCA OVX (mean/SEM)	SNCA A30P (mean/SEM)	SNCA WT (mean/SEM)	P-value
Tau	23.8/0.0	23.8/0.0	23.9/0.0	23.9/0.0	Non-sig
Tau Onset Error	1.4/0.2	1.3/0.4	3.1/1.2	2.2/0.8	Non-sig
Alpha	6.9/1.1	7.1/1.2	5.3/1.2	6.5/0.1	Non-sig
Rho	16.9/1.1	16.7/1.2	18.6/1.2	17.3/0.1	Non-sig
Total Activity	10257/1964	20891/5068	17313/4409	8363/2306	<0.05
Chi-square Periodogram Peak (Hours)	23.8/0.0	23.8/0.0	23.8/0.0	23.8/0.0	Non-sig
Chi-square Periodogram Peak (Amplitude)	1249/163	1939/335	1461/313	1099/214	Non-sig
Total Activity Bouts	5.8/0.5	2.7/0.4	3.3/0.3	5.4/0.9	<0.05

Table 3.3: Circadian and locomotion parameters analysed for each line. Statistical differences illustrated in red. Table 3.3 corresponds to days 54 to 63 from figure 3.2. Mean ± SEM values for each circadian parameter of each line are also presented (n= 5 per mouse line except n= 4 for SNCA-OVX).

Table 3.4

LL period

Parameter	SNCA KO (mean/SEM)	SNCA OVX (mean/SEM)	SNCA A30P (mean/SEM)	SNCA WT (mean/SEM)	P-value
Tau	25.2/0.2	25.4/0.2	25.3/0.2	25.3/0.2	Non-sig
Total Activity	4772/1691	12628/6478	11603/3433	3342/1321	Non-sig
Chi-square Periodogram Peak (Hours)	25.2/0.2	24.8/0.6	25.3/0.2	25.3/0.3	Non-sig
Chi-square Periodogram Peak (Amplitude)	686/110	747/158	937/78	483/23.8	<0.05
Total Activity Bouts	3.9/0.5	2.2/0.5	4.1/0.4	4.5/0.7	<0.05

Table 3.4: Circadian and locomotion parameters analysed for each line. Statistical differences illustrated in red. Table 3.4 corresponds to days 65 to 82 from figure 3.2. Mean ± SEM values for each circadian parameter of each line are also presented (n= 5 per mouse line except n= 4 for SNCA-OVX).

Significant variation in activity levels/bouts was observed in the OVX line (Tables 3.2-3.4). Non-motor circadian parameters such as tau remained largely unaltered. Despite the absence of significance in total activity levels in the A30P line, significant early scotophase hyperactivity is detected (Figure 3.3). Fragmentation bouts, IV, IS and periodogram peak values all suggest the OVX line displays greater rhythm stability throughout the circadian screen (Tables 3.2-3.4, Figures 3.4-3.5). Mild variations in % of light activity/total activity measurements partly reflect the variation in rhythm stability (Table 3.2).

Activity levels and fragmentation differences could be artifacts of the circadian running-wheel that were addressed via locomotor activity cages, particularly in the dark phase where most of the statistical differences appear to be localised. No significant locomotor differences were recorded when using beam-break cages (Taylor *et al*., 2014). Nevertheless, it is noteworthy to point out the consistency of OVX's significant hyperactivity and reduced rhythm fragmentation versus controls during most of the 110 days of circadian screening. Indeed, wheel-running generates motivational reinforcement on mouse behavioural activity patterns (Careau *et al*., 2012). Interestingly, dopamine deficits in PD have been implicated in reward-related impulsivity, and increased wheel-running in the BAC PD models could potentially reflect that phenotype (Aarts *et al*., 2012).

In addition to the circadian parameters presented (Tables 3.2-3.4), activity onset under different lighting conditions constitutes a fundamental circadian marker of the functionality of input, core clock and output signalling (LeGates and Altimus, 2011). Light is a prominent zeitgeber for suppressing activity in nocturnal rodents (Albrecht *et al*., 2005; LeGates and Altimus, 2011). Therefore, for examination of the short-term retinal input

signalling pathways of each PD model, a 1hr light pulse, 150lux at ZT14 (during the subjective night-active phase for nocturnal rodents) was administered (negative masking).

Figure 3.6: Negative masking effects of photic stimulation on day of pulse administration on each PD line

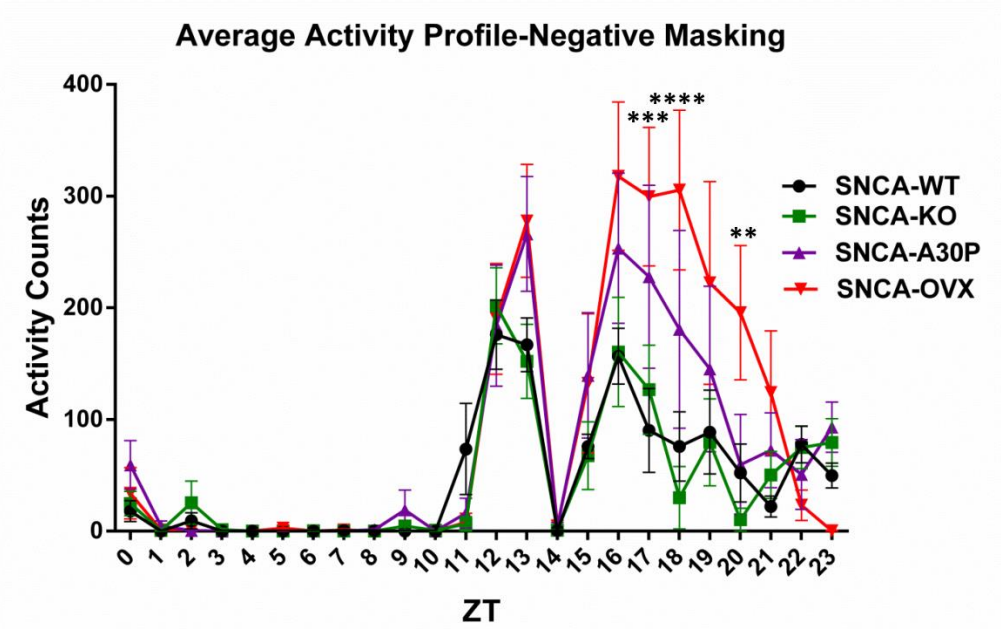

Figure 3.6: Average activity profiles for each line on day of 1hr 150 lux pulse administration at ZT14. All lines exhibit activity suppression upon nocturnal photic stimulation. Data presented as mean ± SEM (n= 5 per mouse line).

All lines responded to nocturnal photic stimulation by a negative masking (suppression of activity) effect, suggesting functional retinal input pathways (Figure 3.6). Similarly, phase shift curves were examined for each circadian paradigm (6hr phase advance, DD and LL) in order to establish the functionality of the endogenous core clock and the SCN output.

All PD lines exhibited similar phase advance curves, suggesting no circadian abnormalities during phase shifts (data not shown). Finally, DD and LL activity onsets were not different among genotypes in constant dark or light conditions (data not shown). Similar

DD and LL activity onsets among genotypes show no core clock abnormalities under constant lighting conditions. Increased variability of activity onset on alternate days of DD exhibited by A30P (Figure 3.7C) was the result of technical issues (partial rotation blockage of the circadian wheel due to excessive cage bedding) and an outlier (Figure 3.7B).

Figure 3.7: Representative SNCA-A30P double-plotted actograms of the DD paradigm

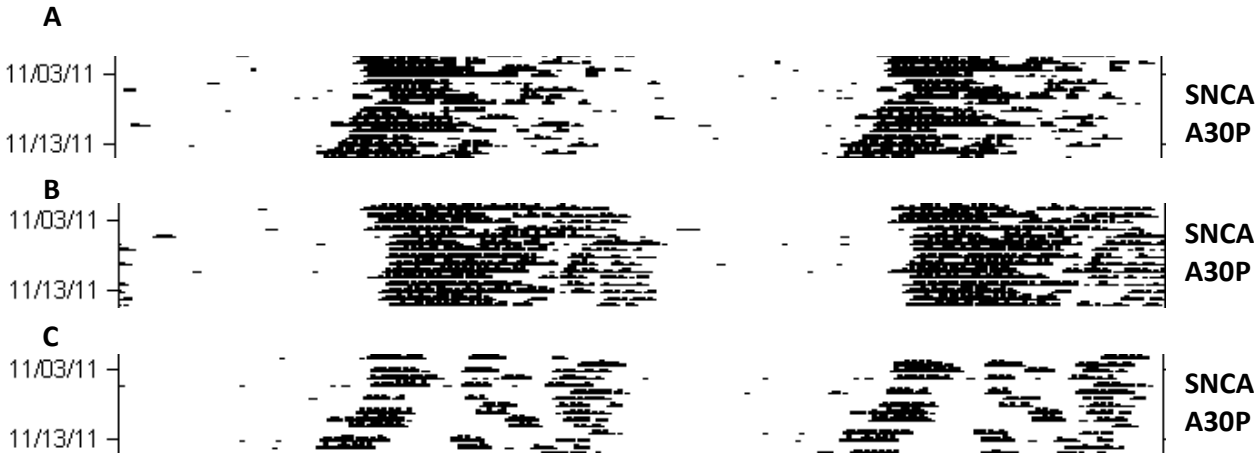

Figure 3.7: Double-plotted actograms of SNCA-A30P DD paradigm. Black spikes represent activity data recorded from each individual mouse and each line represents 48h with dates presented on the left hand side of each diagram. (**A**) illustrates the DD activity profile of a representative SNCA-A30P mouse (**B**) illustrates the DD activity profile of an outlier SNCA-A30P mouse (**C**) illustrates the DD activity profile of an SNCA-A30P mouse with technical issues (partial rotation blockage of the circadian wheel was due to excessive cage bedding).

A summary table of the BAC SNCA screen is presented.

Table 3.5: Summary table of screened BAC SNCA mice

Genotype	Activity Levels	Fragmentation Pattern	LD entrainment	Negative masking	Phase Advance	DD	LL
SNCA OVX	↑↑	↓↓	✓	✓	✓	✓	✓
SNCA A30P	↑	↓	✓	✓	✓	✓	✓
SNCA WT	-	-	✓	✓	✓	✓	✓
SNCA KO	-	-	✓	✓	✓	✓	✓

↑↑: Significant Up-regulation; ↑: Mild Up-regulation; ↓↓: Significant Down-regulation; ↓: Mild Down-regulation; ✓: Normal Response; - :Baseline Level

Table 3.5: Table summarises activity levels, fragmentation pattern and circadian response of each mouse line.

3.8 Circadian data of BAC tauopathic models

BAC MAPT-WT, N51 and KO models were screened for rest/activity profiles from 10 months of age (Figure 3.8).

Figure 3.8: Representative double-plotted actograms of the screen for each line

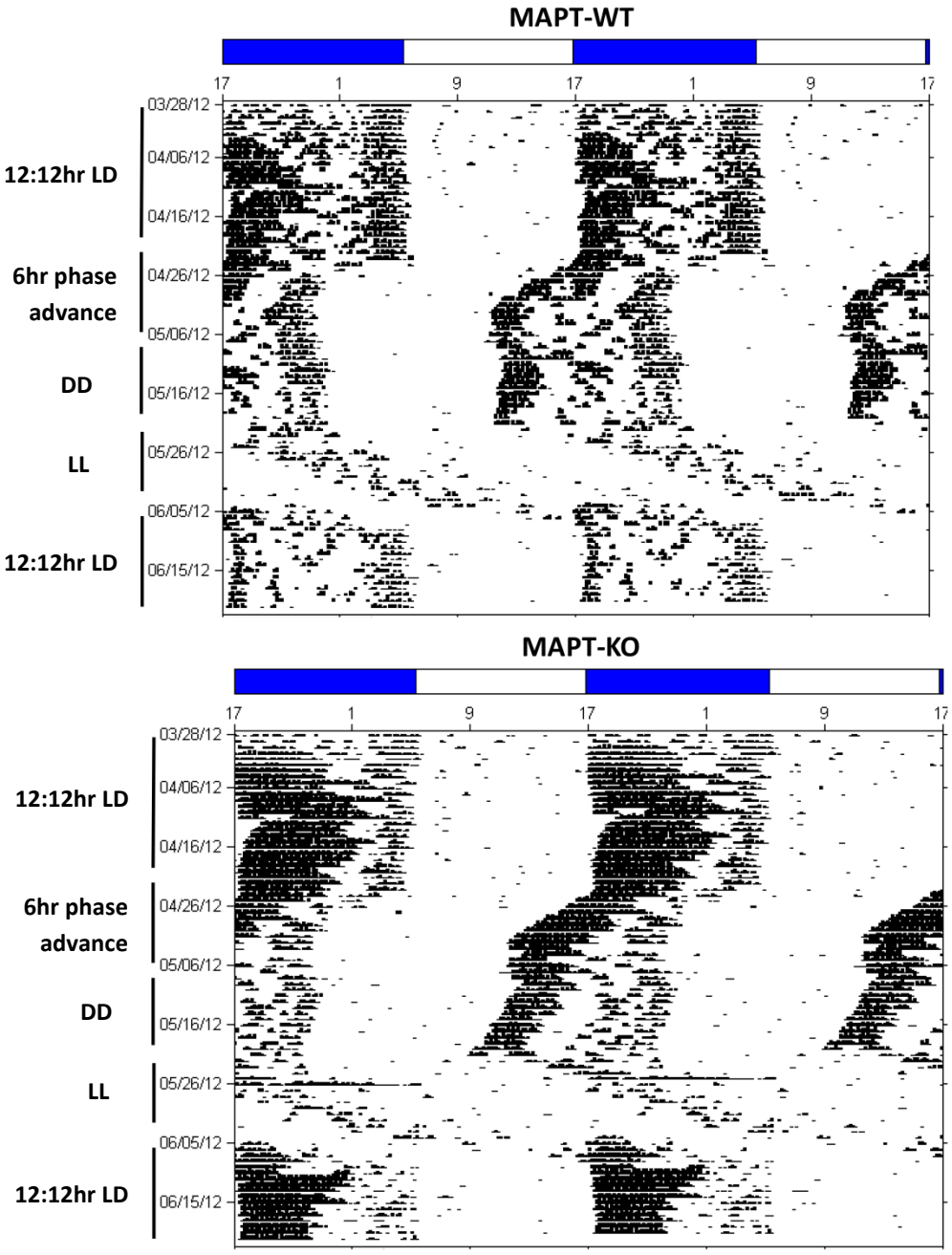

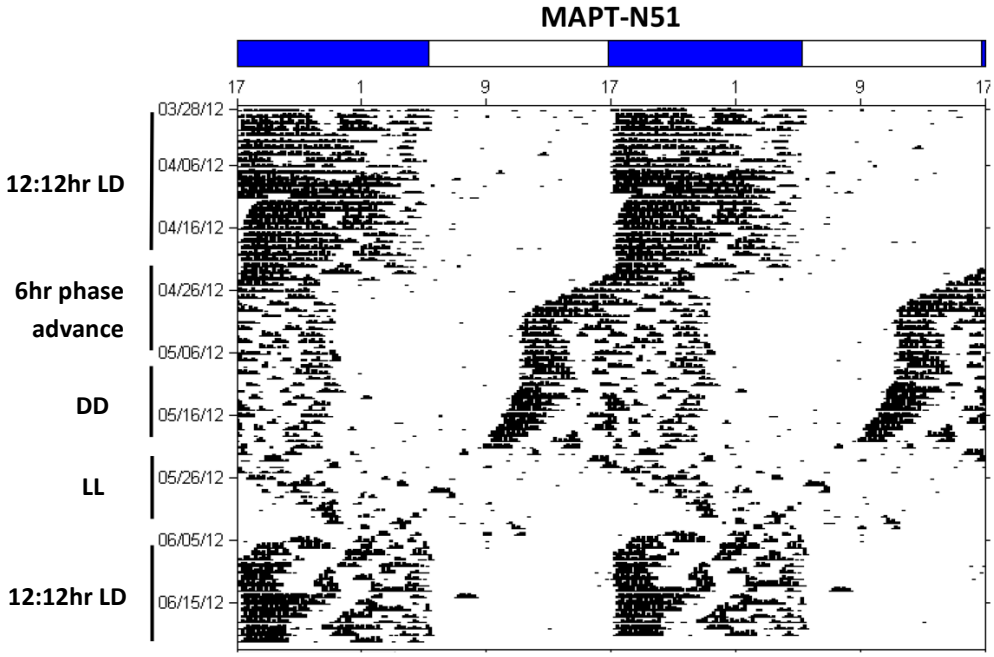

Figure 3.8: Blue bars indicate the dark phase and white bars the light phase (this reflects only the starting 12:12hr LD cycle and not 6hr phase advanced, DD or LL paradigms). Black spikes represent activity data recorded from each individual mouse and each line represents 48h with dates presented on the left hand side of each diagram. Alternative circadian paradigms and their respective duration are represented on the left hand side of actograms.

Entrainment to a 12:12hr Light-Dark cycle was observed in all lines (Figure 3.8). However, the mutant N51 line exhibited mild scotophase hyperactivity (Figure 3.8). A *count by day* plot of the entire circadian screen illustrates the activity variation associated with each circadian paradigm (Figure 3.9).

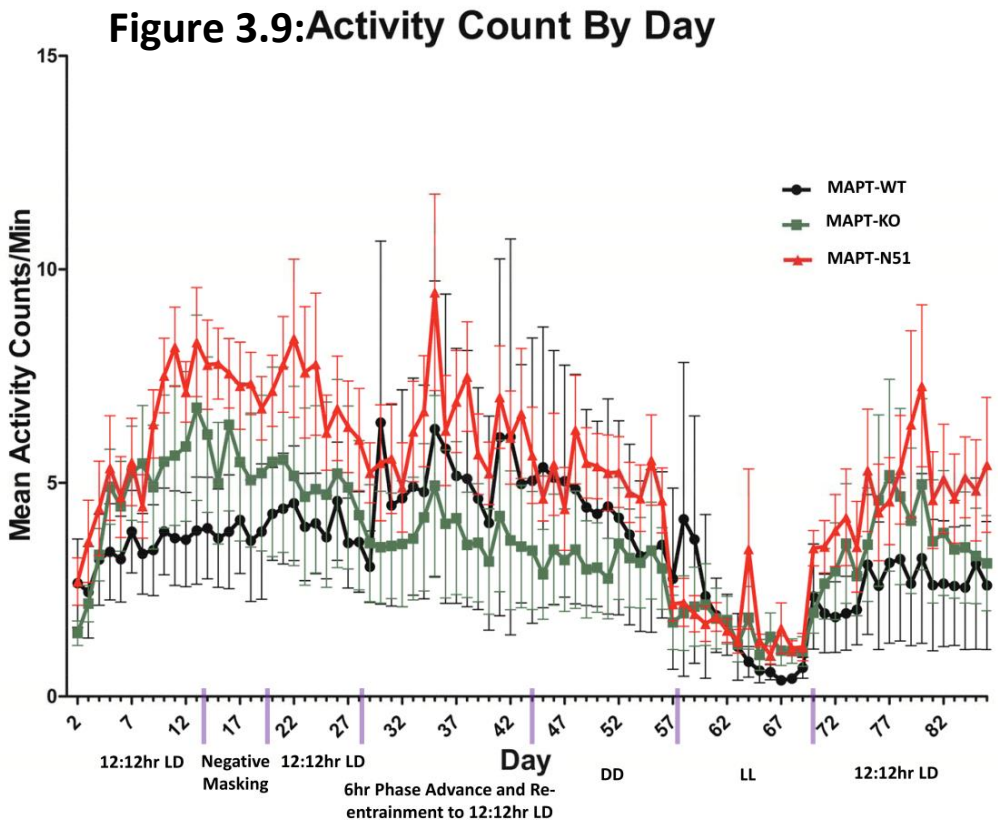

Figure 3.9: The graph illustrates mean activity counts per min for each day of the 86 days of PD circadian screen. X-axis represents each day clustered in circadian paradigms. Data presented as mean ± SEM (n= 6 per mouse line). Mild hyperactivity is recorded by the MAPT-N51 versus MAPT-WT/KO controls. Appendix 8.4 contains further information regarding the mouse models.

Mild hyperactivity of the N51 versus MAPT-WT and KO is shown throughout most of the circadian screen (Figure 3.9). Days 2 to 16 illustrate a progressive increase in activity counts by day in all lines.

All lines displayed suppression of activity under LL (LeGates and Altimus, 2011). Activity levels in all lines were restored when animals were returned to a 12:12hr LD cycle following an LL paradigm. LD activity plots display the activity variation exhibited among lines across a 24h period (Figure 3.10).

Figure 3.10: LD activity profiles over 7-14 days at different stages of the circadian screen

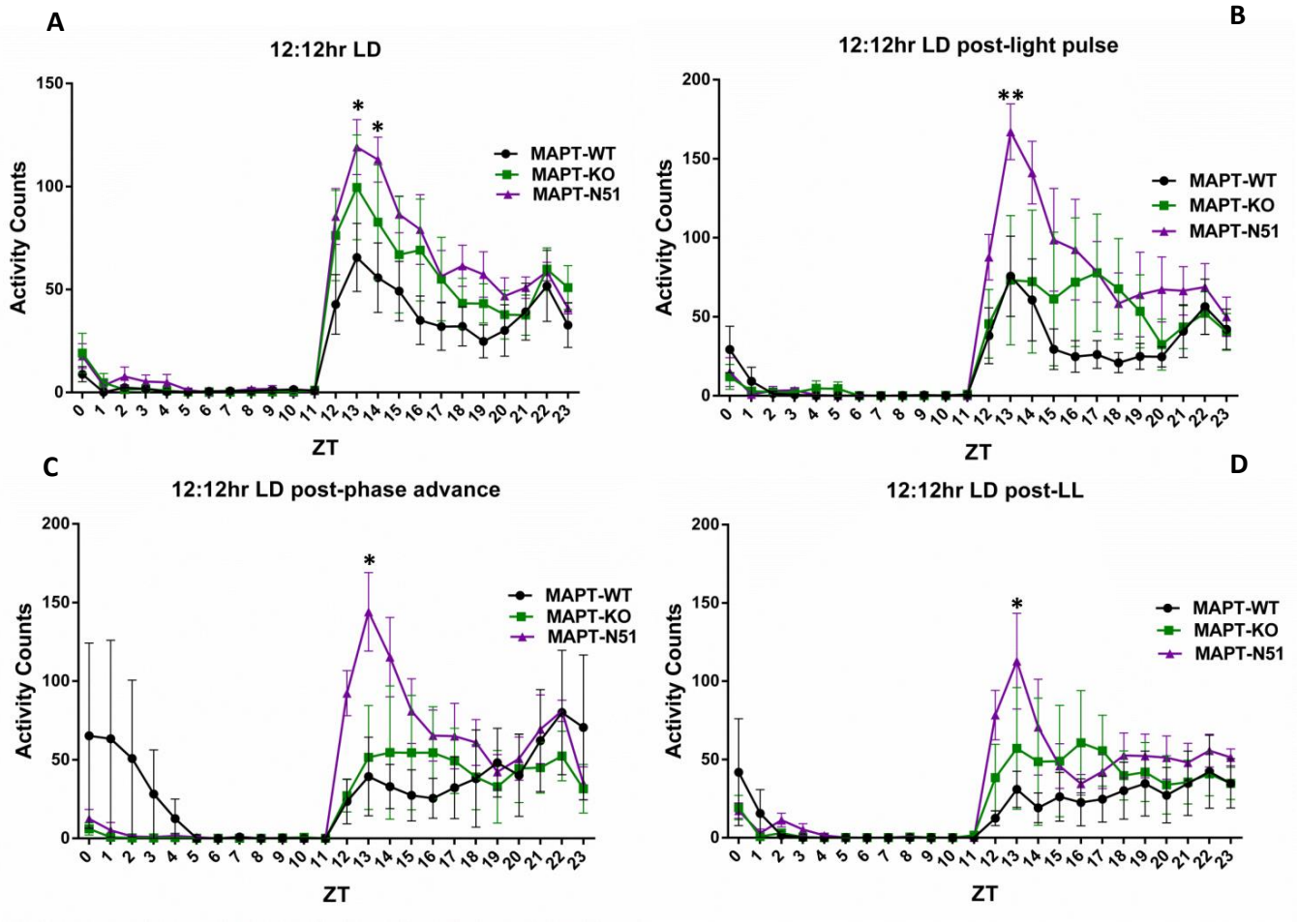

Figure 3.10: (**A**) Activity profile over 12 days during a 12:12hr LD paradigm (days 2 to 13-figure 3.9) (**B**) Activity profile over 8 days during a 12:12hr LD post-light pulse stage (days 20 to 27-figure 3.9) (**C**) Activity profile over 7 days during a 12:12hr LD post-6hr phase advance stage (days 37 to 43-figure 3.9) (**D**) Activity profile over 11 days during a 12:12hr LD post-LL stage (days 77 to 87-figure 3.9). Data presented as mean ± SEM (n= 6 per mouse line, n= 2 females and n= 4 males per mouse line). Mild hyperactivity is recorded by the MAPT-N51 versus MAPT-WT/KO controls.

Scotophase-specific N51 hyperactivity is shown versus WT/KO controls (Figure 3.10). No difference was detected during photophase epochs. The mild hyperactive phenotype persisted in the N51 line during the early scotophase throughout the screen (Figure 3.10: A→D). A numerical summary of the circadian parameters per paradigm illustrates any potential significance (Tables 3.6-3.8).

Table 3.6

12:12hr LD Cycle

Parameter	MAPT KO (mean/SEM)	MAPT WT (mean/SEM)	MAPT N51 (mean/SEM)	P-value
Tau	24.1/0.2	24.2/0.2	24.0/0.1	Non-sig
Alpha	9.5/1.0	9.1/1.8	10.6/1.0	Non-sig
Rho	14.6/1.0	15.1/1.9	13.3/1.0	Non-sig
Total Activity	6847/1705	4942/1433	8416/970	Non-sig
Total Dark Activity	6468/1683	4674/1392	7949/926	Non-sig
Total Light Activity	379/136	268/71	467/170	Non-sig
% Light Activity	6.4/2.2	7.8/2.6	5.5/1.6	Non-sig
Chi-square Periodogram Peak (Hours)	24.0/0.1	23.9/0.1	24.0/0.1	Non-sig
Chi-square Periodogram Peak (Amplitude)	732/80	604/91	776/109	Non-sig
Phase of entrainment	-0.2/0.2	-0.3/0.3	-0.2/0.2	Non-sig
Total Activity Bouts	5.1/0.8	5.2/0.7	4.4/0.3	Non-sig

Table 3.6: Circadian and locomotion parameters analysed for each line. Statistical differences illustrated in red. Table 3.6 corresponds to days 2 to 13 from figure 3.9. Mean ± SEM values for each circadian parameter of each line are also presented (n= 6 per mouse line).

Table 3.7

DD Period

Parameter	MAPT KO (mean/SEM)	MAPT WT (mean/SEM)	MAPT N51 (mean/SEM)	P-value
Tau	23.9/0.1	23.9/0.1	23.8/0.1	Non-sig
Tau Onset Error	2.0/0.6	1.2/0.4	0.9/0.5	Non-sig
Total Activity	4594/1640	6294/3502	7452/1234	Non-sig
Chi-square Periodogram Peak (Hours)	23.9/0.1	23.9/0.1	23.8/0.0	Non-sig
Chi-square Periodogram Peak (Amplitude)	662/130	677/140	716/89	Non-sig
Total Activity Bouts	4.9/1.0	4.8/0.7	5.2/0.8	Non-sig

Table 3.7: Circadian and locomotion parameters analysed for each line. Statistical differences illustrated in red. Table 3.7 corresponds to days 46 to 56 from figure 3.9. Mean ± SEM values for each circadian parameter of each line are also presented (n= 6 per mouse line).

Table 3.8

LL Period

Parameter	MAPT KO (mean/SEM)	MAPT WT (mean/SEM)	MAPT N51 (mean/SEM)	P-value
Tau	25.1/0.1	24.9/0.2	25.1/0.1	Non-sig
Total Activity	2114/749	2191/1400	2366/492	Non-sig
Chi-square Periodogram Peak (Hours)	25.1/0.1	25.1/0.1	25.6/0.1	Non-sig
Chi-square Periodogram Peak (Amplitude)	450/82	409/51	322/33	Non-sig
Total Activity Bouts	3.4/0.6	2.4/0.3	3.7/0.2	Non-sig

Table 3.8: Circadian and locomotion parameters analysed for each line. Statistical differences illustrated in red. Table 3.8 corresponds to days 58 to 69 from figure 3.9. Mean ± SEM values for each circadian parameter of each line are also presented (n= 6 per mouse line).

Mild variation in activity levels was observed in the N51line (Tables 3.6-3.8). Non-motor circadian parameters such as tau remained largely unaltered. Despite the lack of significance in total activity levels in the N51 line, significant early scotophase hyperactivity is detected (Tables 3.6-3.8, Figure 3.10). Fragmentation remained unchanged throughout the circadian screen (Tables 3.6-3.8). It is noteworthy to point out the consistency of N51's mild hyperactivity during most of the 87 days of screening.

For examination of the short-term retinal input signalling pathways of each PD model, a 1hr light pulse, 150lux at ZT14 (during the subjective night-active phase for nocturnal rodents) was administered (negative masking).

Figure 3.11: Negative masking effects of photic stimulation on day of pulse administration on each PD line

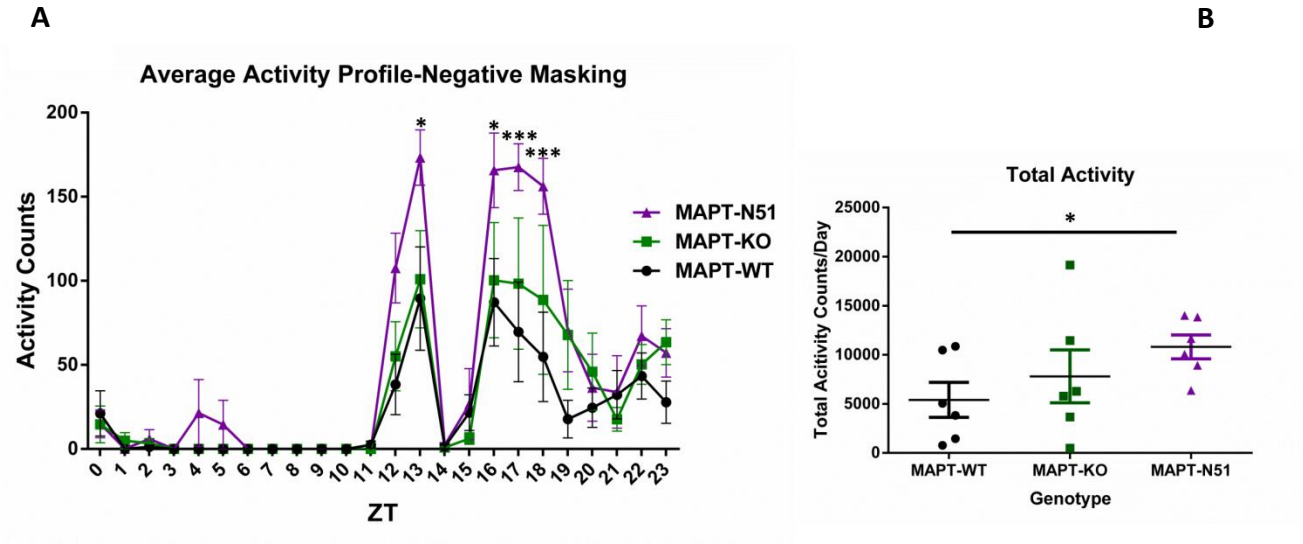

Figure 3.11: (**A**) Average activity profiles for each line on day of 1hr 150 lux pulse administration at ZT14. All lines exhibit activity suppression upon nocturnal photic stimulation (**B**) Mean activity counts per min scattergraph, illustrating activity variability between lines 5 days post pulse. MAPT-N51 exhibit significant activity increase versus MAPT-WT. Data presented as mean ± SEM (n= 6 per mouse line).

All lines responded to nocturnal photic stimulation by a negative masking (suppression of activity) effect suggesting functional retinal input pathways (Figure 3.11A). Total activity is significantly increased in N51 versus MAPT-WT 5 days following the light pulse (Figure 3.11B).

Figure 3.12: Phase advance observed in all lines during the 6hr phase shift

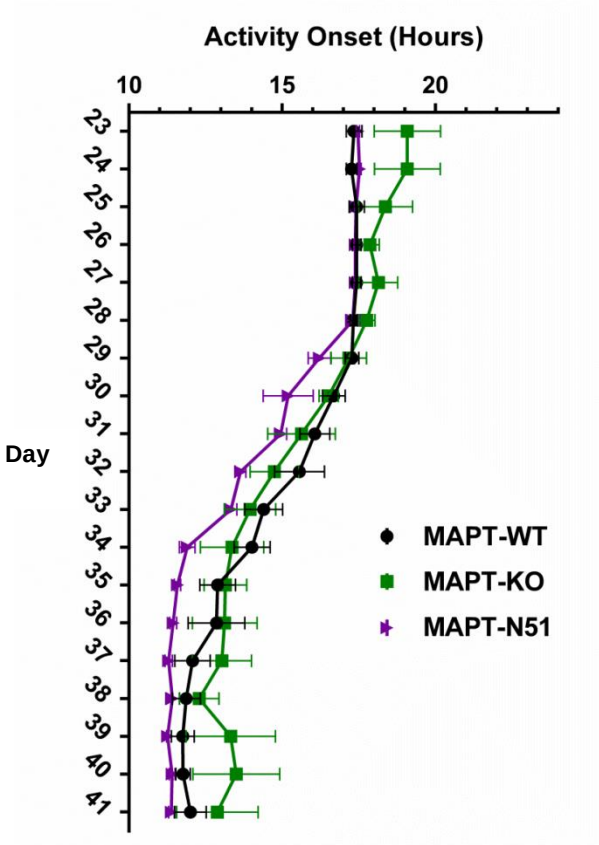

Figure 3.12: Illustrates the phase advance curve of MAPT-N51 versus MAPT-WT and MAPT-KO during a 6hr phase shift. Data presented as mean ± SEM (n= 6 per mouse line). No significant difference among lines was recorded.

All lines exhibited similar phase advance curves, suggesting no circadian abnormalities during phase shifts (Figure 3.12). Increased variability in the onset activity of KOs (Figure 3.12) resulted from the cessation of activity in a few mice as a result of technical issues (partial rotation blockage of the circadian wheel due to excessive cage bedding). Representative 6hr phase advance double-plotted actograms of each line are illustrated (Figure 3.13).

Figure 3.13: Representative double-plotted actograms of the 6hr phase shift

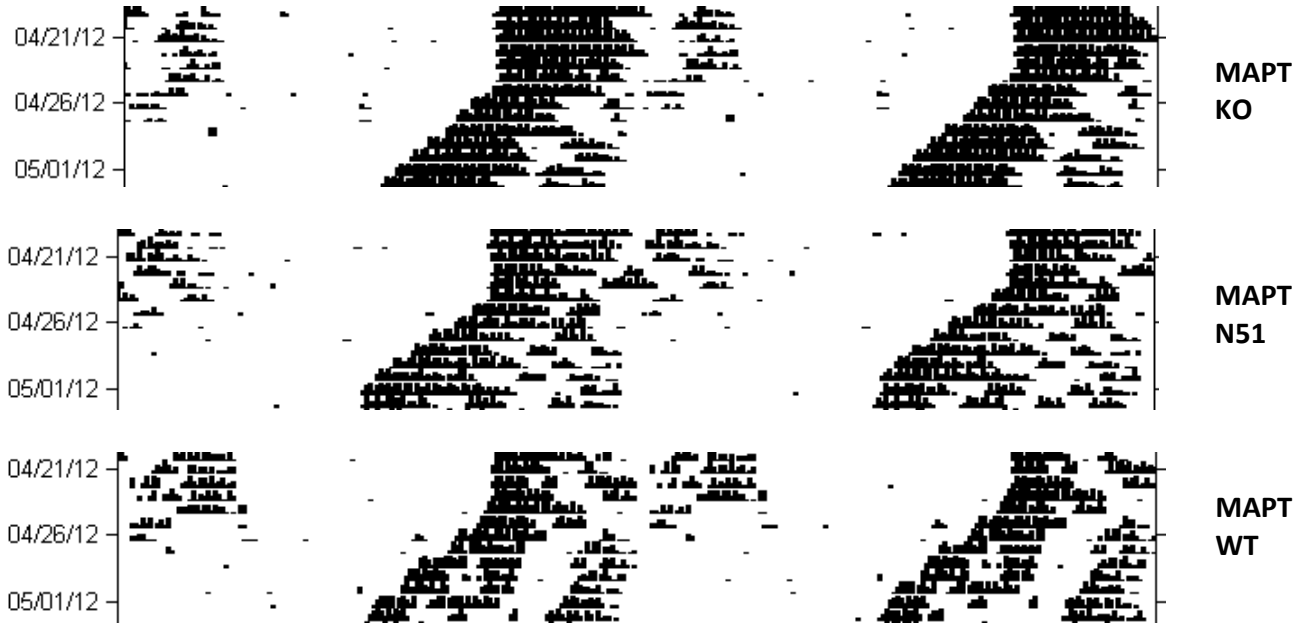

Figure 3.13: Double-plotted actograms of 6hr phase advance. Black spikes represent activity data recorded from each individual mouse and each line represents 48h with dates presented on the left hand side of each diagram.

A DD activity onset plot was also constructed in order to graphically illustrate the functionality of the SCN light-independent core clock (Figure 3.14).

Figure 3.15: DD phase onset plots

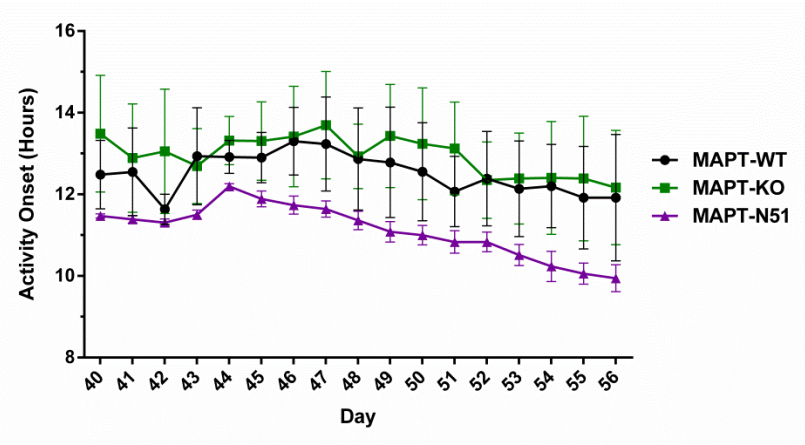

Figure 3.14: Illustrates the DD activity onset of MAPT-N51 versus MAPT-WT and MAPT-KO during constant darkness conditions. Data presented as mean ± SEM (n= 6 per mouse line). No significant difference among lines was recorded.

Similar DD activity onsets among lines suggest no core clock abnormalities under constant lighting conditions (Figures 3.14, 3.15, 3.16). Increased variability of activity onset under DD exhibited by KO mice (Figure 3.14) was the result of technical issues (partial rotation blockage of the circadian wheel due to excessive cage bedding).

Figure 3.15: Type II Phase Delay

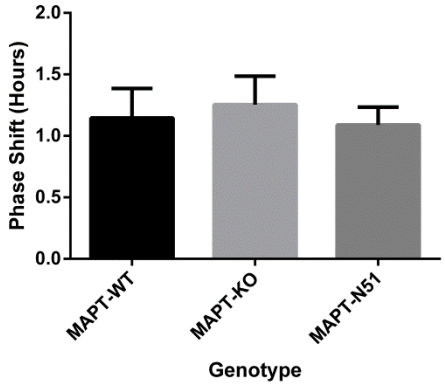

Figure 3.15: Type II Phase Delay graph of MAPT-N51 versus MAPT-WT and MAPT-KO. Graph illustrates the ability of each line to phase shift following an acute photic stimulus in the subjective night of the preceding day. No significant difference among lines was recorded. Data presented as mean ± SEM (n= 6 per mouse line).

Figure 3.16: Representative BAC MAPT double-plotted actograms of the DD paradigm

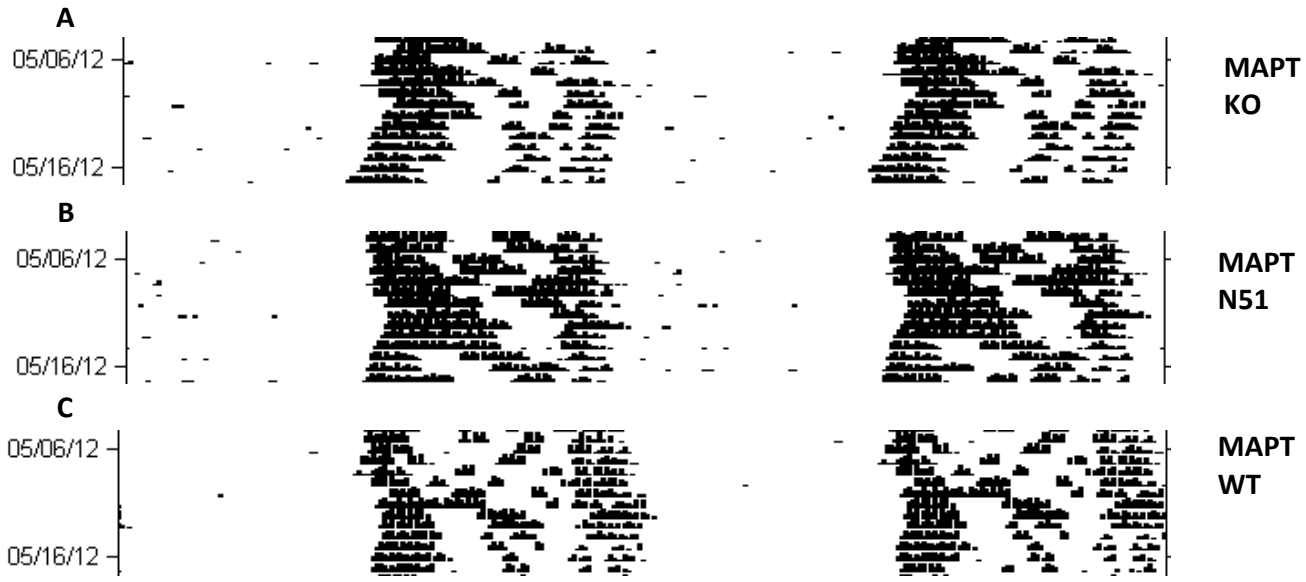

Figure 3.16: Double-plotted actograms of MAPT-KO vs MAPT-N51 vs MAPT-WT under DD paradigm. Black spikes represent activity data recorded from each individual mouse and each line represents 48h with dates presented on the left hand side of each diagram. (**A**) illustrates the DD activity profile of a representative MAPT-KO mouse (**B**) illustrates the DD activity profile of a representative MAPT-N51 mouse (**C**) illustrates the DD activity profile of a representative MAPT-WT mouse.

Finally, LL activity onset profiles were also constructed to report on clock functionality under constant 150lux lighting conditions (Figure 3.17).

Figure 3.17: LL phase onset plots

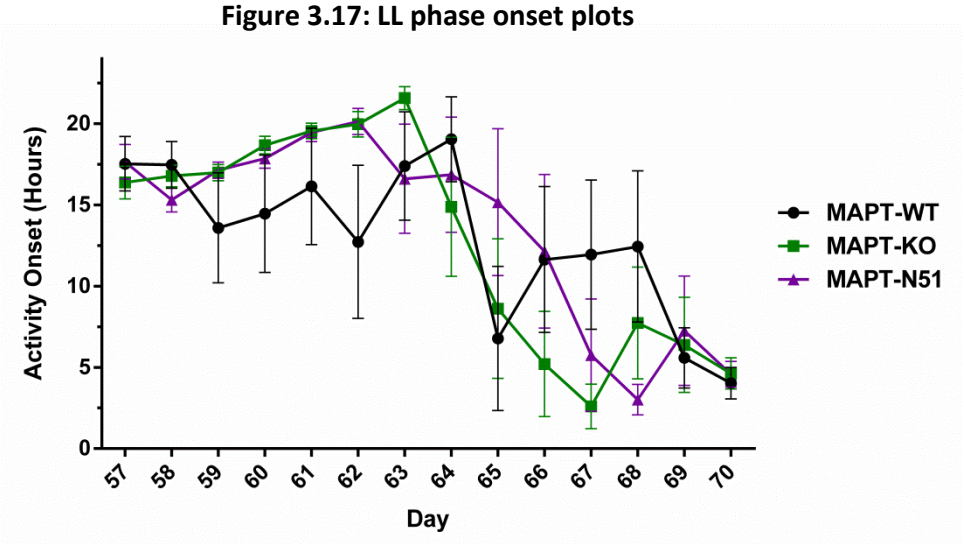

Figure 3.17: Illustrates the LL activity onset of MAPT-N51 versus MAPT-WT and MAPT-KO. Data presented as mean ± SEM (n= 6 per mouse line). No significant difference among lines was recorded.

Similar LL activity onsets among lines were recorded suggesting absence of clock abnormalities under constant lighting conditions (Figure 3.17). A summary table of the BAC MAPT screen is presented.

Table 3.9: Summary table of screened BAC MAPT mice

Genotype	Activity Levels	Fragmentation Pattern	LD entrainment	Negative masking	Phase Advance	DD	LL
MAPT N51	↑	-	✓	✓	✓	✓	✓
MAPT WT	-	-	✓	✓	✓	✓	✓
MAPT KO	-	-	✓	✓	✓	✓	✓

↑: Mild Up-regulation; ✓: Normal Response; - :Baseline Level

Table 3.9: Table summarises activity levels, fragmentation pattern and circadian response of each mouse line.

3.9 Circadian data of *Parkin* KO mouse model

Parkin$^{-/-}$ and WT (+/+) controls were screened for rest/activity profiles from 10 months of age (Figure 3.18).

Figure 3.18: Representative double-plotted actograms of the screen for each genotype

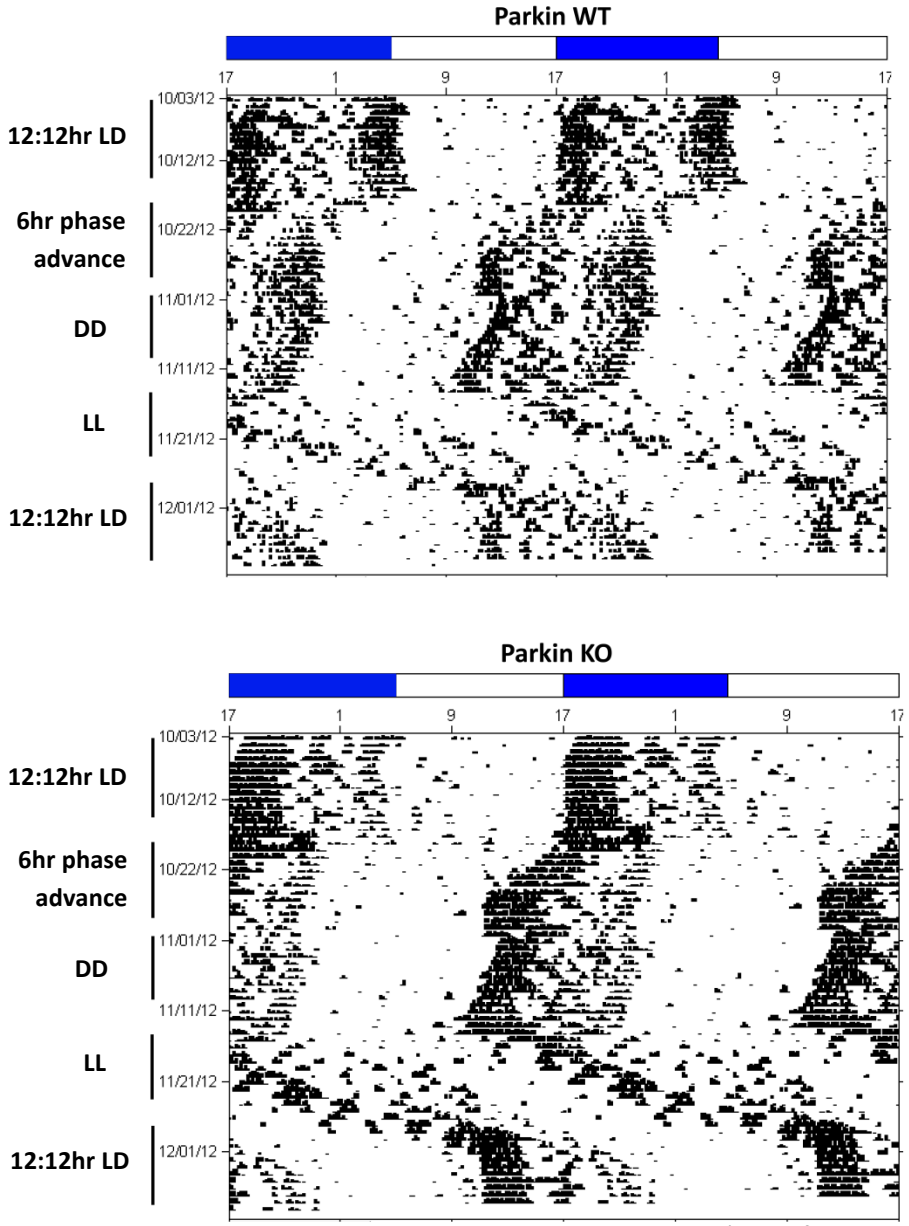

Figure 3.18: Blue bars indicate the dark phase and white bars the light phase (this reflects only the starting 12:12hr LD cycle and not 6hr phase advanced, DD or LL paradigms). Black spikes represent activity data recorded from each individual mouse and each line represents 48h with dates presented on the left hand side of each diagram. Alternative circadian paradigms and their respective duration are represented on the left hand side of actograms.

Entrainment to a 12:12hr Light-Dark cycle was observed in both genotypes (Figure 3.18). However, the *Parkin*$^{-/-}$ exhibited mild scotophase hyperactivity (Figure 3.19). A *count by day* plot of the entire circadian screen illustrates the activity variation associated with each circadian paradigm (Figure 3.19).

Figure 3.19:Activity Count By Day

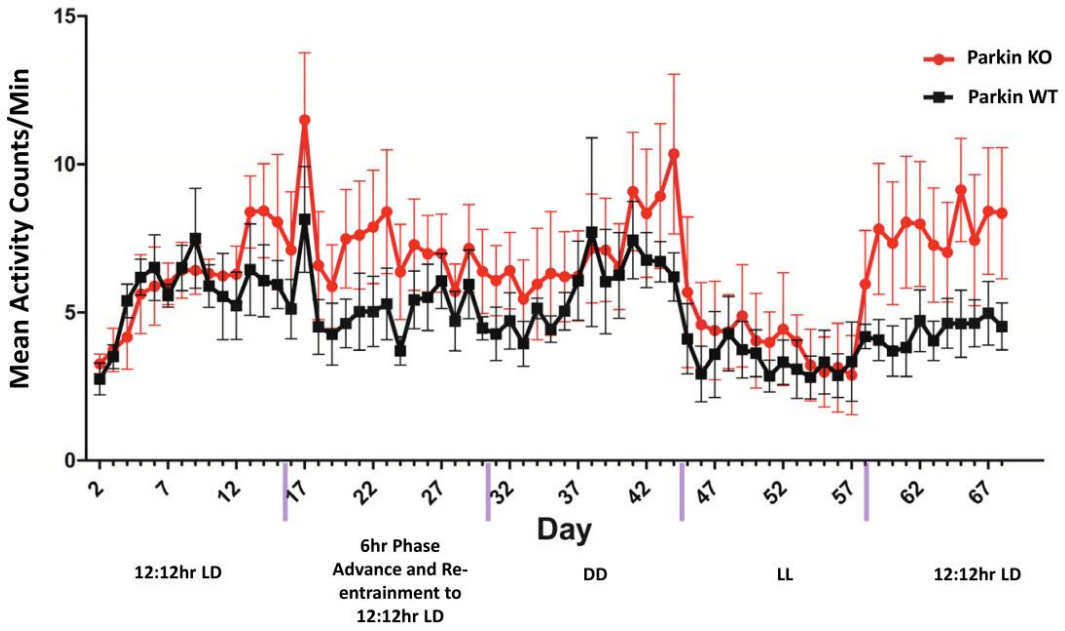

Figure 3.19: The graph illustrates mean activity counts per min for each day of the 68 days of PD circadian screen. X-axis represents each day clustered in circadian paradigms. Data presented as mean ± SEM (n= 4 KO, n= 3 WT). Mild hyperactivity is recorded by the Parkin KO versus the Parkin WT control. Appendix 8.4 contains further information regarding the mouse models.

Mild hyperactivity of the KO versus WT is shown throughout most of the circadian screen (Figure 3.19). Days 2 to 10 illustrate progressive increase in activity counts by day in both genotypes. Both genotypes displayed suppression of activity under LL (LeGates and Altimus, 2011). Activity levels in both genotypes were restored when animals were returned to a 12:12hr LD cycle following an LL paradigm. LD activity plots display the activity variation exhibited between genotypes across a 24h period (Figure 3.20).

Figure 3.20: LD activity profiles over 7-14 days at different stages of the circadian screen

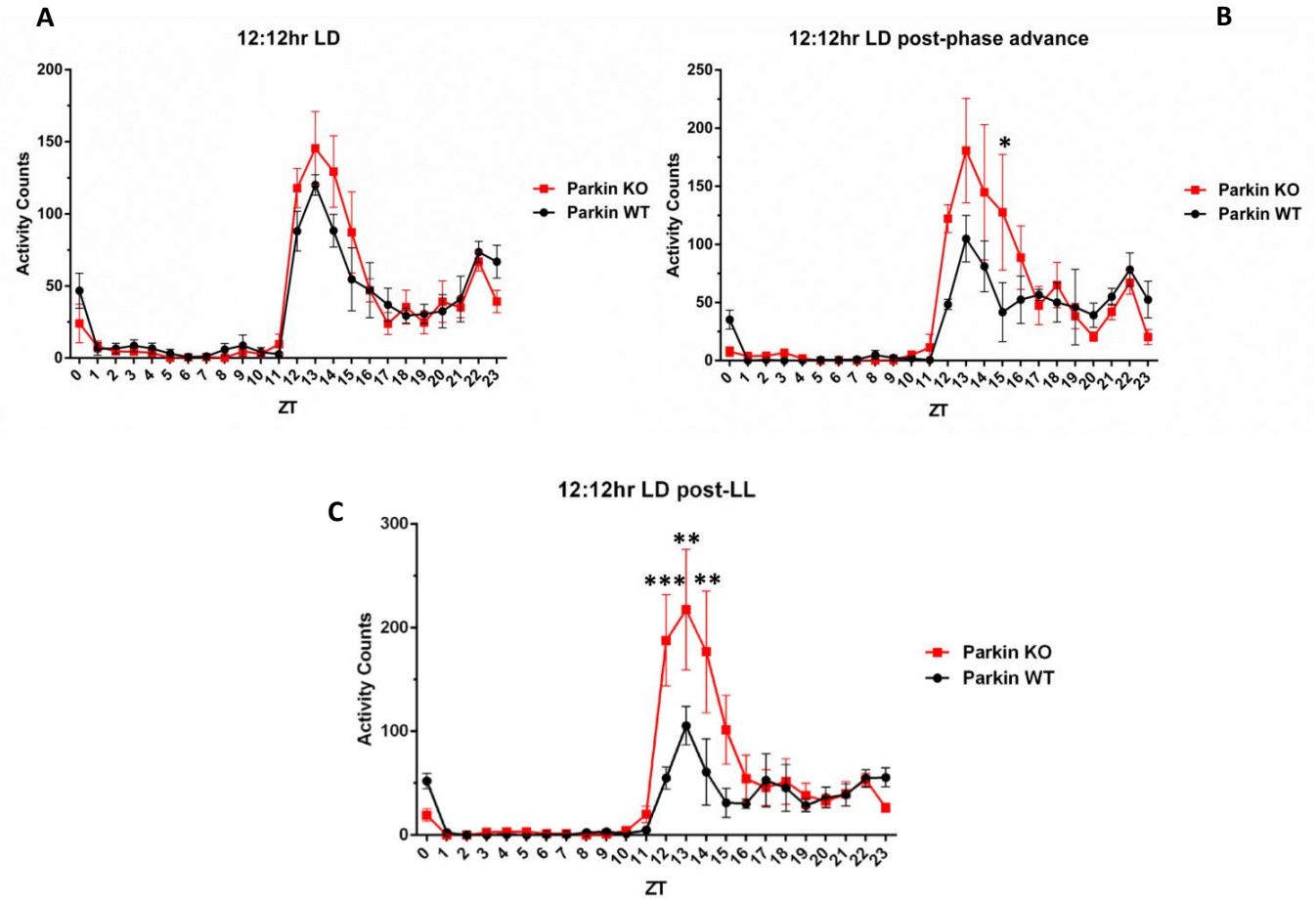

Figure 3.20: (**A**) Activity profile over 14 days during a 12:12hr LD paradigm (days 2 to 16-figure 3.19) (**B**) Activity profile over 7 days during a 12:12hr LD post-6hr phase advance stage (days 25 to 30-figure 3.19) (**C**) Activity profile over 10 days during a 12:12hr LD post-LL stage (days 59 to 68-figure 3.19). Data presented as mean ± SEM (n= 4 KO, n= 3 WT, male mice used only). Mild hyperactivity is recorded by the Parkin KO versus the Parkin WT control.

Scotophase-specific KO hyperactivity is shown versus WTs (Figure 3.20). No difference was detected during photophase epochs. The hyperactive phenotype increased in the KO during the early scotophase as the screen progressed (Figure 3.20: A→C). A numerical summary of the circadian parameters per paradigm illustrates any potential significance (Tables 3.10-3.12).

Table 3.10

12:12hr LD Cycle

Parameter	Parkin KO (mean/SEM)	Parkin WT (mean/SEM)	P-value
Tau	23.9/0.1	23.9/0.1	Non-sig
Tau Onset Error	0.5/0.1	1.9/1.0	Non-sig
Alpha	6.0/1.5	8.8/1.3	Non-sig
Rho	17.9/1.5	15.2/1.3	Non-sig
Total Activity	8545/1102	8096/1162	Non-sig
Total Dark Activity	7850/1237	7045/965	Non-sig
Total Light Activity	695/158	1052/214	Non-sig
% Light Activity	9.4/3.5	12.8/1.3	Non-sig
Chi-square Periodogram Peak (Hours)	24/0.0	24/0.0	Non-sig
Chi-square Periodogram Peak (Amplitude)	855/76	776/52	Non-sig
Phase of entrainment	0.2/0.3	0.2/0.4	Non-sig
Total Activity Bouts	5.4/0.4	6.1/1.2	Non-sig

Table 3.10: Circadian and locomotion parameters analysed for each genotype. Statistical differences illustrated in red. Table 3.10 corresponds to days 2 to 16 from figure 3.19. Mean ± SEM values for each circadian parameter of each genotype are also presented (n= 4 KO, n= 3 WT).

Table 3.11

DD Period

Parameter	Parkin KO (mean/SEM)	Parkin WT (mean/SEM)	P-value
Tau	23.7/0.1	23.8/0.1	Non-sig
Total Activity	9895/2375	8125/1486	Non-sig
Chi-square Periodogram Peak (Hours)	23.8/0.0	23.7/0.1	Non-sig
Chi-square Periodogram Peak (Amplitude)	741/156	702/64	Non-sig
Total Activity Bouts	5.2/0.3	6.8/1.6	Non-sig

Table 3.11: Circadian and locomotion parameters analysed for each genotype. Statistical differences illustrated in red. Table 3.11 corresponds to days 31 to 45 from figure 3.19. Mean ± SEM values for each circadian parameter of each genotype are also presented (n= 4 KO, n= 3 WT).

Table 3.12

LL Period

Parameter	Parkin KO (mean/SEM)	Parkin WT (mean/SEM)	P-value
Tau	25.3/0.1	25.3/0.1	Non-sig
Total Activity	6475/2144	5148/1324	Non-sig
Chi-square Periodogram Peak (Hours)	25.3/0.1	25.4/0.1	Non-sig
Chi-square Periodogram Peak (Amplitude)	344/50	410/51	Non-sig
Total Activity Bouts	4.5/0.4	4.7/0.4	Non-sig

Table 3.12: Circadian and locomotion parameters analysed for each genotype. Statistical differences illustrated in red. Table 3.12 corresponds to days 46 to 57 from figure 3.19. Mean ± SEM values for each circadian parameter of each genotpe are also presented (n= 4 KO, n= 3 WT).

Mild variation in activity levels was observed in the KO (Tables 3.10-3.12). Non-motor circadian parameters such as tau remained largely unaltered. Despite the absence of significance in total activity levels in the KO, significant early scotophase hyperactivity was detected (Tables 3.10-3.12, Figure 3.20). Additionally, the hyperactive phenotype increased in the KO during the early scotophase as the screen progressed (Figure 3.20: A→C). Fragmentation remained largely unchanged throughout the circadian screen (Tables 3.10-3.12).

For examination of the short-term retinal input signalling pathways of each PD model, a 1hr light pulse, 150lux at ZT14 (during the subjective night-active phase for nocturnal rodents) was administered (negative masking).

Figure 3.21: Negative masking effects of photic stimulation on day of pulse administration on each genotype

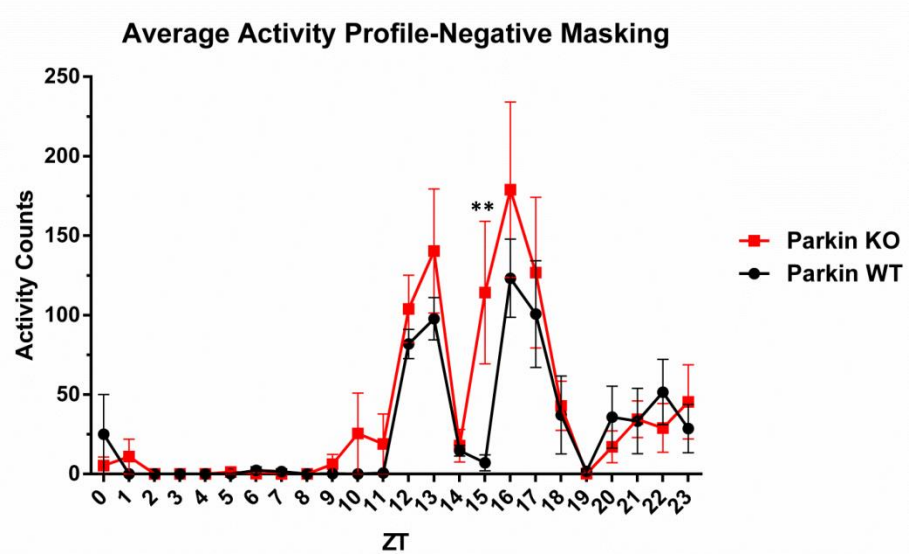

Figure 3.21: Average activity profiles for both genotypes on day of 1hr 150 lux pulse administration at ZT14. Data presented as mean ± SEM (n= 4 KO, n= 3 WT). No significant difference between genotypes was recorded.

Both genotypes responded to nocturnal photic stimulation by a negative masking (suppression of activity) effect, suggesting functional retinal inputs to the visual system (Figure 3.21). However, the WT exhibited abnormal short-term photic sensitivity as illustrated by the extended suppression of activity for ZT14 and ZT15. The KO recorded a normal response to abrupt photic stimulation.

Figure 3.22: Phase advance observed in both genotypes during the 6hr phase shift

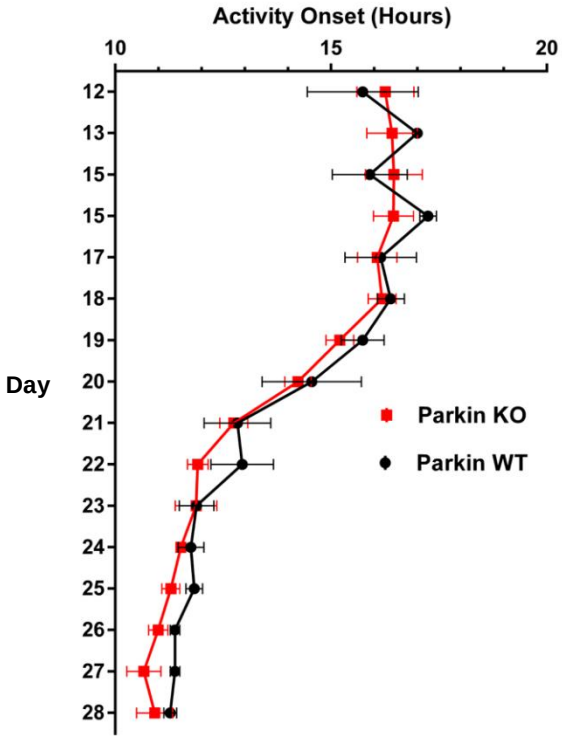

Figure 3.22: Illustrates the phase advance curve of Parkin KO versus Parkin WT during a 6hr phase shift. Data presented as mean ± SEM (n= 4 KO, n= 3 WT). No significant difference between genotypes was recorded.

Both genotypes exhibited similar phase advance curves, suggesting no circadian abnormalities during phase shifts (Figure 3.22). Increased variability in the onset of activity in the WT (Figure 3.22) resulted from the cessation of activity in a few mice as a result of

technical issues (partial rotation blockage of the circadian wheel due to excessive cage bedding; was corrected as soon as discovered).

A DD activity onset plot was also constructed in order to graphically illustrate the functionality of the SCN light-independent core clock (Figure 3.23).

Figure 3.23: DD phase onset plots

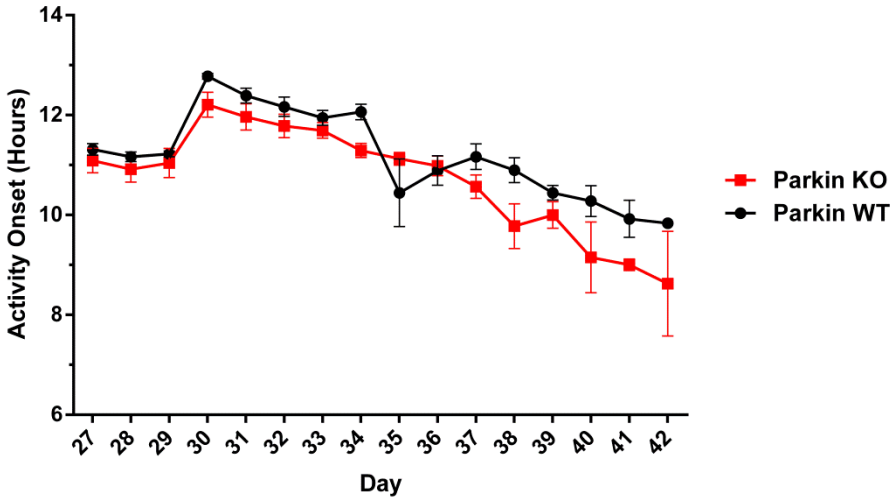

Figure 3.23: Illustrates the DD activity onset of Parkin KO versus Parkin WT during constant darkness conditions. Data presented as mean ± SEM (n= 4 KO, n= 3 WT). No significant difference between genotypes was recorded.

Similar DD activity onsets between genotypes suggest no core clock abnormalities under constant lighting conditions (Figures 3.23, 3.24, 3.25).

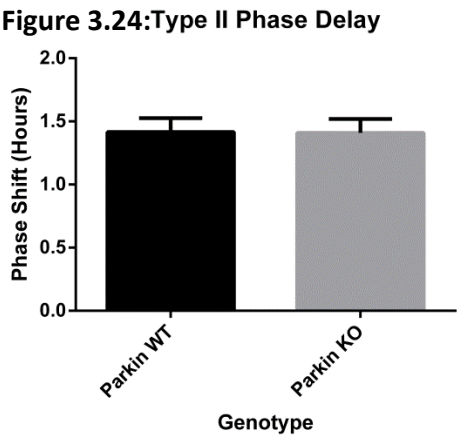

Figure 3.24: Type II Phase Delay graph of Parkin KO versus Parkin WT. Graph illustrates the ability of each genotype to phase shift following an acute photic stimulus in the subjective night of the preceding day. No significant difference between genotypes was recorded. Data presented as mean ± SEM (n= 4 KO, n= 3 WT).

Figure 3.25: Representative double-plotted actograms of the DD paradigm

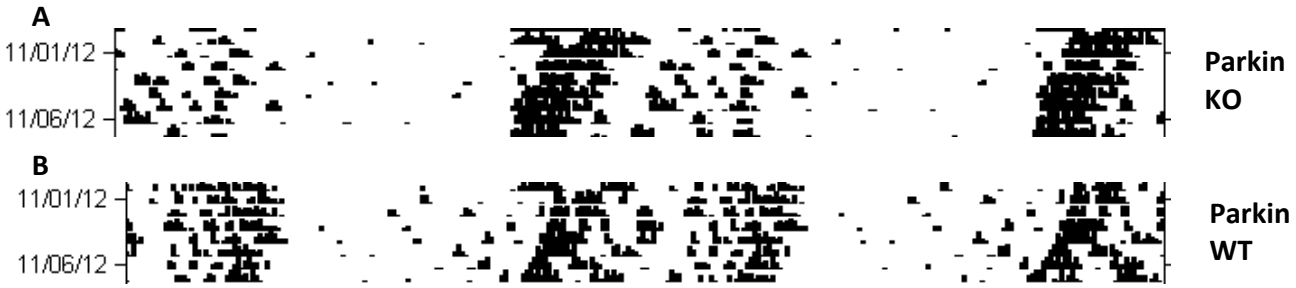

Figure 3.25: Double-plotted actograms of Parkin KO vs Parkin WT under DD paradigm. Black spikes represent activity data recorded from each individual mouse and each line represents 48h with dates presented on the left hand side of each diagram. (**A**) Illustrates the DD activity profile of a representative Parkin KO mouse (**B**) illustrates the DD activity profile of a representative Parkin WT mouse.

Finally, a LL activity onset profile was also constructed to report on clock functionality under constant 150lux lighting conditions (Figure 3.26).

Figure 3.26: LL phase onset plots

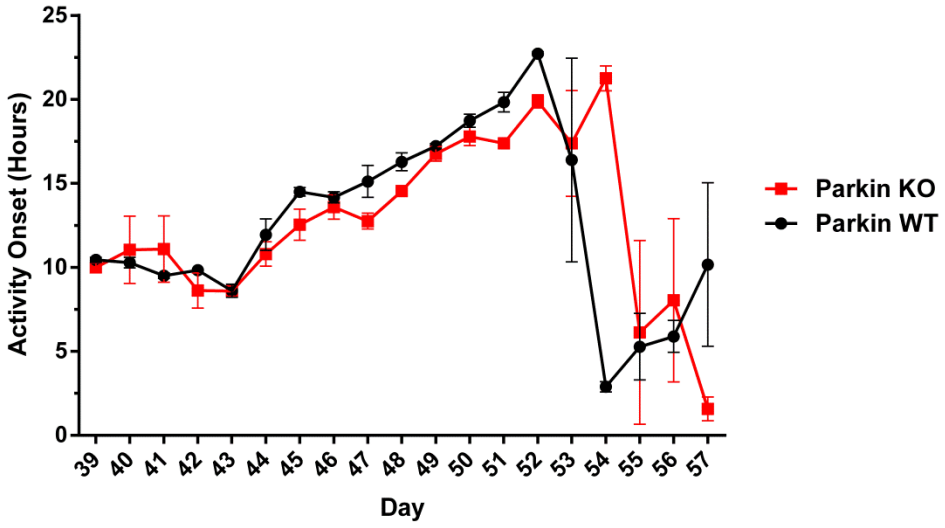

Figure 3.26: Illustrates the LL activity onset of Parkin KO versus Pakin WT. Data presented as mean ± SEM (n= 4 KO, n= 3 WT). No significant difference between genotypes was recorded. LD began at day 59.

Similar LL activity onsets in both genotypes were recorded suggesting absence of clock abnormalities under constant lighting conditions (Figure 3.26). A summary table of the screen is presented.

Table 3.13: Summary table of screened Parkin mice

Genotype	Activity Levels	Fragmentation Pattern	LD entrainment	Negative masking	Phase Advance	DD	LL
Parkin KO	↑	-	✓	✓	✓	✓	✓
Parkin WT	-	-	✓	✓	✓	✓	✓

↑: Mild Up-regulation; ✓: Normal Response; - :Baseline Level

Table 3.13: Table summarises activity levels, fragmentation pattern and circadian response of each genotype.

3.10 Discussion on PD/FTDP-17 mouse models

3.10.1 BAC SNCA Overview

In summary, using running-wheel behavioural analysis, all of the BAC SNCA mouse models displayed normal LD entrainment and re-entrainment as well as normal negative masking, DD and LL periods. Period length (tau) under constant conditions was not significantly different among lines (DD: tau <24h, LL: tau>24h). However, OVX and A30P mutant lines displayed a hyperactive wheel phenotype localised during the scotophase period compared to WT/KO controls (Figures 3.2-3.3). Photophases did not yield any significant motor variation among the lines (Table 3.2). Variation in rhythm stability and consistency were documented between OVX and controls. In particular, the OVX exhibited a reduced fragmentation activity pattern, decreased IV and increased IS; all of these are signs associated with increased rhythm stability (Figures 3.4-3.5).

Due to the OVX/A30P hyperactivity observed by wheel-running, additional locomotor activity testing was undertaken (Taylor *et al*., 2014). Utilisation of a running-wheel as an activity measure could potentially bias the results due to the selective nature of data collection (wheel rotation) (Fisher *et al*., 2012; Careau *et al*., 2012). Interestingly, locomotor activity cage testing of the same cohort of mice screened in the wheels did not report any significant activity variations (Taylor *et al*., 2014). Fragmentation differences could arise from wheel-running, suggesting that KO and SNCA-WT mice did not display actual fragmentation but were active in regions of the cage not spatially close to the wheel (Zombeck *et al*., 2011; Careau *et al*., 2012; Fisher *et al*., 2012). Indeed wheel-running exercises motivational reinforcement on mouse behavioural activity patterns (Careau *et al*., 2012). Interestingly, dopamine deficits in PD have been implicated in reward-related impulsivity and increased

wheel-running in the BAC PD models could potentially reflect that phenotype (Aarts *et al*., 2012). Moreover, activity variations could also arise due to the fact that locomotor activity cage testing was only conducted during the initial 4 hour scotophase period (Figure 3.3). Furthermore, activity data collected on the first day of wheel-running also recorded no significant activity differences among lines. Due to the short duration of locomotor activity cage testing (only 4 hours) it could perhaps be classified partially as an anxiety test as well as an activity test. Therefore, running-wheel data illustrate the power of long–term activity monitoring versus short-term data collection.

Indeed, behavioural experiments have demonstrated variations between wheel-running and open-field testing in activity levels registered (Careau *et al*., 2012). For example, HR (Higher-Runner Hsd:ICR strain) mice typically run 3-fold more than C lines (Control Hsd-ICR strain) in their home/wheel-running environment (Malisch *et al*., 2009; Careau *et al*., 2012). However, during open-field testing no such activity deficit in C mice is registered. This suggests that home-running and wheel-running activity is better correlated versus open-field testing (an anxiety test) (Stanford, 2007; Careau *et al*., 2012). Therefore, it is vital to consider differences and limitations in each behavioural test.

A potential refinement empirically addressing the LMA/circadian screen variation would utilise infrared video tracking of cage activity. This could record the nocturnal wheel-independent mobility/immobility ratio. Recent studies focus on rapid high-throughput behavioural screening via automated non-invasive video tracking (Fisher *et al*., 2012). Data suggest a high correlation with EEG measurements under baseline, light and pharmacologically modified behavioural states (Fisher *et al*., 2012). Fundamental advantages of this approach include rapid non-invasive assessment that allows detection of potential

behavioural deficits by analysing total distance travelled and preferred cage locations (Fisher *et al*., 2012).

3.10.2 BAC OVX versus ASO

Emerging wheel-running data from the conventional Thy-1 driver ASO (human α-synuclein over-expressing) PD model suggest progressive motor and non-motor dysfunctions. ASO mice display 15-fold up-regulation of SNCA in the SCN, striatum and substantia nigra (Kudo *et al*., 2011; Willison *et al*., 2013). Conversely, BAC OVX mice display roughly a 2-fold increase in endogenous human SNCA versus endogenous mouse levels, a spatio-temporal expression pattern closer resembling duplications of the SNCA locus in PD patients (Janezic *et al*., 2013).

Thy-1-controlled ASO mice display progressive motor deficits and increased rhythm fragmentation in wheel-running experiments (Kudo *et al*., 2011) as well as early (at 3 months) progressive motor and non-motor deficits including olfactory and cognitive deterioration (Fleming and Chesselet, 2009; Kudo *et al*., 2011). This is in contrast to our findings on the BAC SNCA mice that display scotophase hyperactivity.

Despite normal *Per2* clock gene expression in the ASO line, a weakened circadian output is displayed due to decreased spontaneous SCN firing rate of mutant mice at ZT 4-8 (Kudo *et al*., 2011; Willison *et al*., 2013). There were no LD entrainment deficits and DD tau in the ASO line appeared normal (Kudo *et al*., 2011). This overlaps with our findings on the BAC SNCA mice that lack circadian deficits (normal LD entrainment, DD and LL period length). Importantly, the ASO line displayed circadian electrical deficits prior to dopaminergic loss

occurring at 14 months of age (Kudo *et al*., 2011). Video-recordings of 6 months-old ASO mice also recorded a delay in sleep onset (Willison *et al*., 2013).

BAC OVX display evoked dopaminergic release deficits from an early age (3 months old) that persist throughout their lifespan (Janezic *et al*., 2013). Importantly, motor function tests display a progressively deteriorating phenotype associated with impaired motor coordination rather than muscle wasting (Janezic *et al*., 2013). The hyperactive wheel phenotype present here also suggests the absence of muscle weakness in the BAC OVX mice. Motor pathology is complemented by age-dependent dopaminergic loss of substantia nigra neurons at 18 months (Janezic *et al*., 2013). Interestingly, wheel-running data report hyperactivity and increased rhythm stability in the BAC OVX instead of deterioration as in the ASO line. Both models display circadian abnormalities (alterations in fragmentation patterns) reminiscent of PD pathology (Willison *et al*., 2013; Janezic *et al*., 2013). This would suggest that PD pathology is associated with circadian abnormalities (Willison *et al*., 2013).

The main feature of the BAC models is the identification of regional prodromal dopaminergic alterations. Indeed, dopamine depletion is associated with circadian rhythm de-synchronisation in PD patients (Imbesi *et al.,* 2009; Hampp *et al*., 2008; Hood *et al*., 2010). *Per2* gene expression appears to have a direct effect on dopaminergic circuitry by participating in striatal metabolic processes (Hampp *et al*., 2008; Rutten *et al*., 2012). In addition, agonists of dopamine receptors have an impact on striatal core clock period gene expression (Imbesi *et al*., 2009; Rutten *et al*., 2012). These findings are critical due to recent findings concerning core clock gene (Bmal 1/2) de-regulation in total leukocytes in human PD patients during night-time periods (Ding *et al*., 2011). This underscores how molecular clock deficits can potentially link to dopaminergic alterations.

OVX/A30P scotophase hyperactivity could be associated with exposure to wheel-running. However, altered rest/activity fragmentation, altered IV and IS could partially reflect the circadian pathology observed in PD patients and confirms the original hypothesis (see Hypotheses section). Recently, OVX mice have been shown to exhibit progressive dopaminergic nigrostratial neuronal loss (Janezic *et al*., 2013). Moreover, prodromal neurotransmitter deficits at dopaminergic axons, coupled to electrical abnormalities of substantia nigra neurons, increase considerably the face validity of the model (Janezic *et al*., 2013). Additionally, motor pathology and non-motor pathology coupled to potential activity fragmentation during wheel-running is present (Janezic *et al*., 2013; Taylor *et al*., 2014). Therefore, the BAC SNCA OVX mice could represent a unique model for uncovering the pathological events underlying PD.

3.10.3 BAC MAPT Overview

In summary, using running-wheel behavioural analysis, all of the BAC MAPT mouse models displayed normal LD entrainment and re-entrainment as well as normal negative masking, DD and LL periods. Period length under constant conditions was not significantly different among lines (DD: tau <24h, LL: tau>24h). The N51 mutant lines compared to WT/KO controls displayed a mild hyperactive wheel phenotype localised during the early scotophase period (Figure 3.10). Photophases did not yield any significant motor variation among the lines (Table 3.6). No variations in rhythm stability and fragmentation pattern were documented (Tables 3.6-3.8).

Preliminary longitudinal phenotypic characterisation of the BAC MAPT N51 mice identified a non-motor depression phenotype at 6 months of age (increased immobility time

at the tail suspension test) (Wobst *et al*., 2014; unpublished data; Egashira *et al*., 2005). Subsequent behavioural testing via accelerating rotarod and locomotor chambers reported mild hyperactivity in the BAC N51 mice (n= 25) (Wobst *et al*., 2014; unpublished data). Using running-wheels the BAC N51 line also registered a mild hyperactive phenotype primarily during the early scotophase period (Figure 3.10). Mild hyperactivity in a variety of motor function tests could be indicative of elevated anxiety levels. However, anxiety tests were inconclusive with elevated plus maze registering higher levels in the BAC WT, while light/dark box transitions were not different between lines (Wobst *et al*., 2014; unpublished data). Finally, no gastrointestinal dysfunction was present and no spatial working memory deficits were reported as assessed by T maze (Wobst *et al*., 2014; unpublished data). The behavioural data do not recapitulate the pathology observed in tauopathic patients despite mild hyperactivity in different motor function tests.

The original hypothesis predicted that PD models investigated would display possible circadian (fragmentation differences) rhythm abnormalities in activity profiles reminiscent of PD pathology in patients. Although this was not observed, both BAC SNCA A30P and BAC MAPT N51 mis-sense mutants displayed hyperactivity when compared to controls. This activity difference was consistently detected during the early scotophase, illustrating a common behavioural phenotype in BAC models of PD/FTDP-17 (Figures 3.3 and 3.10) (Wills *et al*., 2010; Wills *et al*., 2011).

3.10.4 MAPT mutants

Cell culture experiments have investigated the MAPT N296H mutation (Yoshida *et al*., 2002). These constructs expressed a single isoform (4 Tandem repeat variant) human tau cDNA construct (Yoshida *et al*., 2002). The group demonstrated that the mutation impaired MAPT to interact with microtubules. This exon 10 specific mutation decreased MAPT assembly (Yoshida *et al*., 2002).

Recent mouse work on FTDP-17 reported a human mis-sense intronic MAPT mutant that promotes up-regulation of the pathogenic exon 10 isoform (Umeda *et al*., 2013). The mice exhibited progressive altered MAPT phosphorylation, synaptic deficiencies, cognitive impairment, Neurofibrillary Tangle (NFT) formation and neurodegeneration (Umeda *et al*., 2013). Hippocampal mossy staining of the intronic mutant displayed abnormal phospho-Tau expression at 6 months of age (Umeda *et al*., 2013). Importantly, neuronal loss was apparent at 24 months, alongside NFT formation (Umeda *et al*., 2013). Toxic tau substrates contributed to synaptic and cognitive dysfunction as assessed by Morris water maze testing (Umeda *et al*., 2013). This *in vivo* work assessed how up-regulation of the neuropathological MAPT variant contributes to both neurodegeneration and behavioural alterations.

Human N297K mis-sense cDNA mutants under the PrP promoter expressing the 4 tandem repeat MAPT variant displayed open-field hyperactivity and PPI at 12 months of age (pre-pulse inhibition) deficits (Taniguchi *et al*., 2005). Additionally, the mutant mice exhibited impaired spatial learning memory as assessed by Morris water maze testing (Taniguchi *et al*., 2005). Histological analysis lacked NFTs, and behavioural alterations appeared to precede tau accumulation (Taniguchi *et al*., 2005). Interestingly, the N297K MAPT mutation is located one amino acid position further to the BAC MAPT-N51 line investigated here (N296H). However,

deducing a correlation between observed open-field hyperactivity in cDNA N297K Tg MAPT mice and wheel-running hyperactivity in BAC MAPT N296H mice involves differences in construct and methodological approaches (Careau *et al*, 2012; Umeda *et al*., 2013). Nevertheless, it is noteworthy that a MAPT mutation spatially relevant to the one investigated here generated a hyperactive phenotype similar to our own.

Dawson *et al* recently generated PAC (P1-derived artificial chromosome) transgenic MAPT mice that display a 2-fold protein expression of the 3 and 4 Tandem repeat human Tau variant (1:1 ratio) (Dawson *et al*., 2007). The presence of the exon 10 N279K mis-sense mutation increased expression of the pathogenic isoform, leading to tau aggregation and behavioural deficits (Dawson *et al*., 2007). The PAC MAPT N279K displayed motor impairments at 3 weeks as assessed by rotarod and memory impairment in the radial arm water maze test (Dawson *et al*., 2007). Therefore, exon 10 mutations under physiologically relevant spatio-temporal expression levels also promote FTDP-17 neuropathology.

In summary, MAPT mouse work to date has demonstrated how up-regulation of the exon 10 isoform, with an exonic or intronic mutation, progresses to NFTs, neuronal cell loss and behavioural pathology (Dawson *et al*., 2007; Umeda *et al*., 2013). Additionally, exon 10 N297K cDNA mice display hyperactivity reminiscent of the phenotype exhibited by the BAC MAPT N51 examined here. The N51 scotophase hyperactivity alongside a depression-like phenotype display alterations identified by other FTDP-17 mouse models. Further molecular and electrophysiological longitudinal characterisation of the BAC MAPT model would address its value as an FTDP-17 model.

3.10.5 *Parkin* KO Overview

In summary, using running-wheel behavioural analysis, the *Parkin*$^{-/-}$ mouse model displayed normal LD entrainment and re-entrainment as well as normal negative masking, DD and LL periods. Period length (tau) under constant conditions was not significantly different between genotypes (DD: tau <24h, LL: tau>24h). The KO compared to WT control displayed a mild hyperactive wheel phenotype localised during the early scotophase period (Figure 3.20). Additionally, the hyperactive phenotype increases in the KO during early scotophase period as the screen progresses (Figure 3.20: A→C). Photophases did not yield any significant motor differences between genotypes (Figure 3.20). No variations between genotypes in rhythm stability and fragmentation patterns were observed (Table 3.10) and therefore the original PD hypothesis is not confirmed (see Hypotheses section).

Previous findings on the *Parkin*$^{-/-}$ (exon 3 deleted) line have demonstrated significant behavioural impairments in locomotor activity as well as memory impairments in T-maze alternations (Itier *et al*., 2003). Moreover, another group reported, in the exon 3 deleted *Parkin*$^{-/-}$, motor deficits when using a beam traversal task (Goldberg *et al*., 2003). Somatosensory impairments via an adhesive removal test were also reported.

Table 3.14: Behavioural abnormalities in *Parkin*$^{-/-}$ mouse models of PD

Mouse	Mutation	Behavioural Impairments
Parkin knockout	Exon 3 deletion No Parkin protein expressed	Locomotor activity, alternation in T maze
Parkin knockout	Exon 3 deletion No Parkin protein expressed	Challenging beam, response to sensory stimuli
Parkin knockout	Exon 7 deletion No Parkin protein expressed	Startle response
Parkin knockout	Exon 2 deletion No Parkin protein expressed	None detected in tests used

Table 3.14: Exon-specific *Parkin* deletions and corresponding mouse behavioural impact.

Fleming *et al*., 2005

As discussed above, a comparison of activity between different behavioural tests is not appropriate. Behavioural experiments have demonstrated variations between wheel-running and open-field testing in activity levels registered (Careau *et al*., 2012). Interestingly, our data displayed a potential hypersensitivity in the WT following negative masking (Figure 3.21). The WT, unlike the KO mice, maintained suppressed activity for an additional hour following a nocturnal light pulse at ZT14 (Figure 3.21). Finally, end-stage LD cycles (after LL) displayed the greatest scotophase activity variation between genotypes (Figure 3.19-3.20). However, due to the limited power of the screen (limited sample size) it is difficult to identify the causal factor for this variation.

Age-related effects could also potentially have an impact on the mammalian circadian axis and contribute to this progressive activity variation between genotypes (Figure 3.20). Age-dependent progressive motor deterioration has previously been observed (Peng and Kang, 1984; Colwell *et al*., 2011). Axonal conduction velocity in motor neurons also appears significantly reduced due to ageing (Engelhardt *et al*., 1989; Fujimaki *et al*., 2009; Thakur *et al*., 2010). Additionally, aged animals display a damped neuroendocrine output as a result of

reduced neurotransmitter (VIP, AVP) levels (Singletary and Naidoo, 2011, Nakamura *et al*., 2011, Sellix *et al*., 2012). Moreover, aged animals exhibit slower re-entrainment of peripheral oscillators, during phase shifts, due to the lower SCN amplitude rhythms (Sellix *et al*., 2012). Therefore, ageing leads to a reduced electrical and neuropeptide SCN output (Sellix *et al.*, 2012). Parkin's neuroprotective role in the survival of dopaminergic neurons has previously been reported (Lucking *et al*., 2000; Solano *et al*., 2008). Additionally, glial dysfunction has been documented in *Parkin*$^{-/-}$ cell cultures and is augmented with ageing (Solano *et al*., 2008). Therefore, longitudinal activity monitoring of *Parkin*$^{-/-}$ mice via wheel-running could possibly reveal interesting variations.

4 Results II: Circadian screening of *Npc* and *Hexb* KO mice

4.1 NPC and neurodegeneration

Niemann-Pick C (NPC) disease is a fatal, recessive metabolic disorder due to the accumulation of glycolipids and cholesterol (Vanier, 2010). Neurological progression and severity exhibit heterogeneity with time of disease onset constituting a major factor (Vanier, 2010). Common clinical neurological symptoms include neurodevelopmental motor impairments in the early infantile form, while cataplexy, ataxia and psychiatric disturbances are more often encountered in the juvenile and adult variants of the disorder (Vanier, 2010). Importantly, recent clinical work on children with metabolic and endocrine disorders has identified sleep/wake abnormalities potentially due to the cross-talk between peripheral metabolic organs and the master SCN circadian clock (Alonso and Sheldon, 2010). The endocrine system is regulated by the circadian process (Alonso and Sheldon, 2010). Hence, circadian disturbances alter hormone secretion. Similarly, circadian disturbances leading to sleep abnormalities can arise from endocrine and metabolic dysfunction (Alonso and Sheldon, 2010). Importantly, the clinical manifestations of NPC are mutation dependent.

Interestingly, circadian rhythm alterations such as unstable periodicity and activity fragmentation have previously been documented in a LSD mucopolysaccharidosis VII mouse model (Ross *et al*., 2000; Yan *et al*., 2008; Parente *et al*., 2012). Additionally, urotensin II was up-regulated which is known to have an effect on cholinergic neurons during REM sleep (Huitron-Resendiz *et al*., 2005; de Lecea and Bourgin, 2008; Ono *et al*., 2008; Parente *et al*., 2012).

Figure 4.1: Clinical signs of NPC patients with varying disease onset

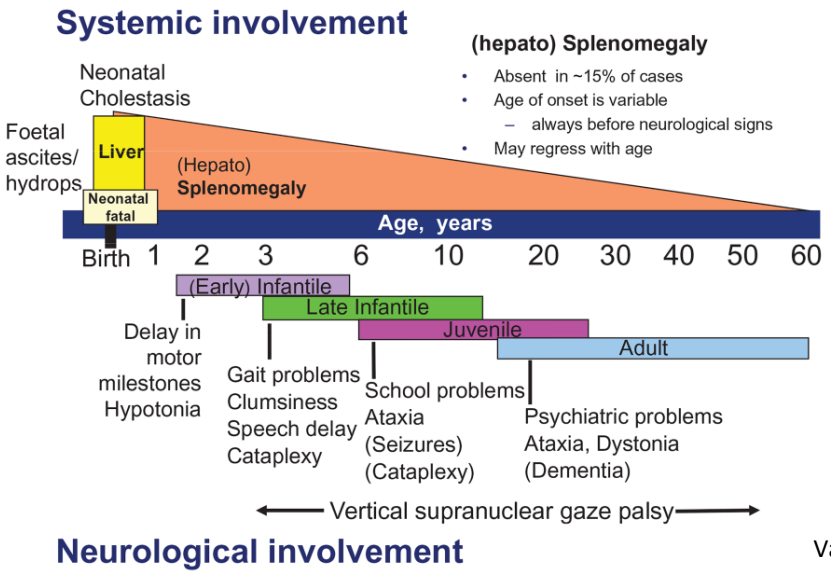

Vanier, 2010

Figure 4.1: Schematic illustrates NPC clinical symptoms.

NPC is a progressive neurodegenerative disorder characteristed by the accumulation of unesterified cholesterol and a wide variety of glycolipids in the endolysosomal organelles (Patterson *el al*., 2001; Schuzle and Sandhoff, 2011). Mutations harboured in NPC1 or NPC2 proteins lead to lipid-transporting defects within the exocytotic pathway (Schulze and Sandhoff, 2011). Low-density lipoprotein (LDL) uptake and subsequent hydrolysis via cholesterol esterases yields fatty acids and cholesterol (Brown and Goldstein, 1986; Schulze and Sandhoff, 2011). NPC1 and NPC2 proteins are vital components in the exocytotic machinery of transporting cholesterol out of the late endosome (Schulze and Sanhoff, 2011). NPC1 is a transmembrane cholesterol-binding glycoprotein while NPC2 is a glycosylated and mobile cholesterol-binding counterpart (Carstea *et al*., 1997; Naureckiene *et al*., 2000; Infante *et al*., 2008; Schulze and Sandhoff, 2011). Current models propose mobile NPC2 binding cholesterol from inner lysosomal spaces and transporting it to the transmembrane NPC1 for cholesterol exocytosis (Karten *et al*., 2009; Storch and Xu, 2009; Schulze and Sandhoff, 2011).

4.2 HEXA/B and neurodegeneration

Sandhoff disease is a fatal, recessive metabolic lipidosis disorder (Sango *et al*., 2008). Two functionally interacting genes HEXA and HEXB (α- and β-hexosaminidase) are each responsible for Tay-Sachs (HEXA mutations) and Sandhoff disease (HEXB mutations) (Sandhoff, 2001; Sango *et al*., 2008). In humans, absence of either subunit of the HEX enzyme leads to accumulation of GM2 gangliosides in the lysosomes of neuronal bodies (Sandhoff, 2001; Sango *et al*., 2008). Neurological progression and the severity of these two disorders are similar, irrespective of infantile or late-onset pathology (Gravel *et al*., 2001; Sango *et al*., 2008). Common clinical symptoms in the infantile form include progressive motor impairments, blindness and cognitive defects with a fatal outcome (Gravel *et al*., 2001; Sango *et al*., 2008).

Figure 4.2: Shared biochemistry in Tay-Sachs and Sandhoff diseases

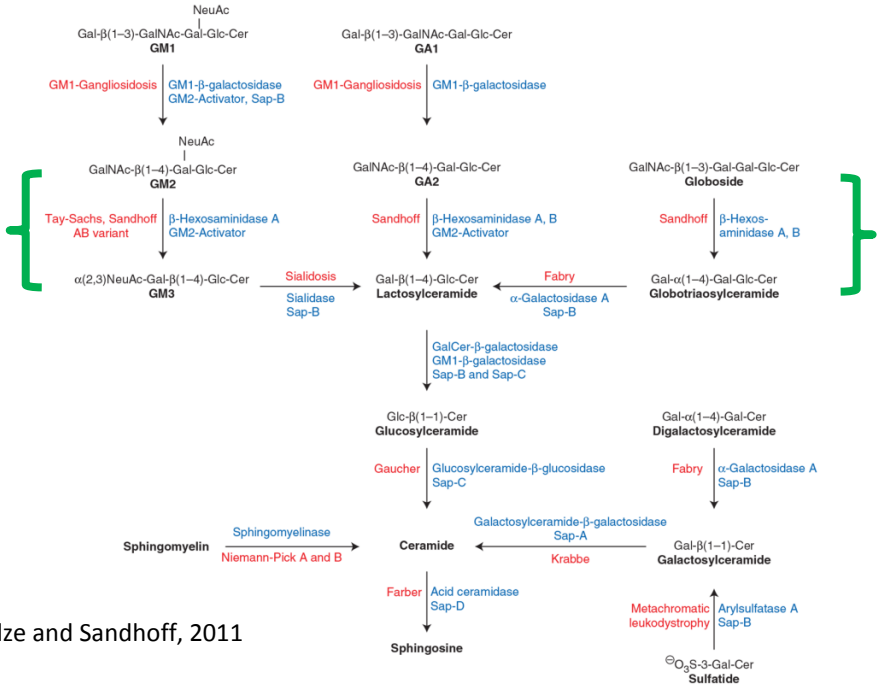

Schulze and Sandhoff, 2011

Figure 4.2: Figure illustrates lysosomal degradation pathways of sphingolipids in the cell. Shared biochemical pathways between disorders (green brackets) generate overlapping clinical signs in patients.

HEXA activity defects (unaffected HEXB expression or function) due to HEXA genetic mutations give rise to Tay-Sachs disease, while loss of both α and β subunit enzymatic activities due to HEXB mutations generate Sandhoff pathology (Conzelmann and Sandhoff, 1978; Hechtman *et al*., 1982; Phaneuf *et al*., 1996). A third GM2 gangliosidosis arises from GM2 activator loss (Hechtman *et al*., 1982; Phaneuf *et al*., 1996). The GM2 activator is a 17.6 kDa glycoprotein that is vital during ganglioside catabolism (Conzelmann and Sandhoff, 1978; Sandhoff *et al*., 2001; Kolter and Sandhoff, 2010).

Clinically, central nervous system and retinal atrophy is widespread in Sandhoff pathophysiology (Brownstein *et al*., 1980; Sango *et al*., 2008). An overall brain weight is observed due to excessive gliosis and glycolipid accumulation alongside axonal defects and spheroid bodies (Volk *et al*., 1975; Cox and Cachon-Gonzalez, 2012). Intermediate by-products of glycosphingolipid degradation pathways, such as GM2 gangliosides, accumulate systemically in these patients, generating mega-lysosomal organelles filled with membranous structures (Cox and Cachon-Gonzalez, 2012). The overall lipid ‘‘traffic-jam’’ shares clinical overlaps with other metabolic disorders but in each disorder the primary causal genetic defect varies (Simons and Gurenberg, 2000; Schulze and Sandhoff, 2011).

4.3 *Npc1* KO mouse model

Npc1 and *Npc2* mouse models exhibit the equivalent of the late infantile variant of the human disease (Walkley and Suzuki, 2004). BALB/c *Npc1*$^{-/-}$ is characterised by cholesterol accumulation and sphingomyelin tissue deposition (Morris *et al*., 1982; Walkely and Suzuki, 2004). The model exhibits hypomyelination, neuronal storage, and neurodegernation (Walkley and Suzuki, 2004). However, no neurofibrillary tangles are present, unlike human cases of NPC (Walkley and Suzuki, 2004). Myelin degeneration is apparent after 2 months,

possibly following axonal spheroid formation and subsequent degeneration (Weintraub *et al*., 1987; Higashi *et al*., 1991; Walkley and Suzuki, 2004). Central nervous system heterogeneity is considerable, with hypomyelination reported in the corpus callosum, while brain stem and spinal cord show less pathology (Walkley and Suzuki, 2004). Similarly to human cases, *Npc1*$^{-/-}$ mice exhibit GM2 and GM3 ganglioside localisation, demonstrated immunocytochemically (Sleat *et al*., 2004; Zervas *et al*., 2001; Walkley and Suzuki, 2004). Neuronal storage is mostly prominent in neuronal populations of the brainstem and thalamus (Walkley and Suzuki, 2004).

A prominent feature of *Npc1*$^{-/-}$ mice is the neurodegeneration involved. Mutant mice brains are 65% the size of wild-type at 40 days, while progressive atrophy, mostly in cerebellar Purkinje cells and thalamus, exacerbate the pathology (Tanaka *et al*., 1988; Higashi *et al*., 1993; German *et al*., 2001; Yamada *et al*., 2001; Walkley and Suzuki, 2004). Attempts to halt the degenerative phenotype pharmacologically and genetically by reducing the cholesterol content have been largely unsuccessful (Patterson *et al*., 1993; Erickson *et al*., 2000). However, inhibitors of glycosphingolipid synthesis prolonged Purkinje survival rates and delayed clinical onset in the *Npc1*$^{-/-}$ mice (Zervas *et al*., 2001; Walkley and Suzuki, 2004). Interestingly, introducing wild-type Npc1 protein to the *Npc1*$^{-/-}$ mice rescued neurodegeneration, directly establishing the correlation between NPC1 and neuropathology (Loftus *et al*., 2002; Walkley and Suzuki, 2004).

Npc1$^{-/-}$ have undergone extensive behavioural assessment. In summary, retarded growth was observed between 25 and 45 days of age, while weight was similar to controls until day 45, before declining rapidly (Voikar *et al*., 2002). Coordination tests including beam balancing and rotating rod indicated significant motor impairment of the *Npc1*$^{-/-}$ between 28-40 days of age, before visible ataxia was observable (Voikar *et al*., 2002). Open-field tests

revealed elevated anxiety in the mutant mice due to their decreased exploratory activity (Voikar *et al*., 2002). Cognitive impairment was highly prevalent, as revealed by their impaired spatial learning memory in the water maze task (Voikar *et al*., 2002).

4.4 Tay-Sachs and Sandhoff KO mouse models

Tay-Sachs and Sandhoff mouse models exhibit vastly different phenotypes between them (Phaneuf *et al*., 1996). Although both *Hexa*$^{-/-}$ and *Hexb*$^{-/-}$ mice accumulate GM2 gangliosides *Hexa*$^{-/-}$ do not report any overt behavioural or neurological defect (Phaneuf *et al*., 1996). On the other hand, *Hexb*$^{-/-}$ mice develop fatal neurodegeneration coupled with tremor and ataxia (Phaneuf *et al*., 1996).

It is proposed that *Hexa*$^{-/-}$ mouse models are able to relieve the accumulated GM2 load via G_{A2} (asialo-GM2) catabolism through the dual action of sialidase and hexosaminidase (Phaneuf *et al*., 1996). While *Hexa*$^{-/-}$ brains showed limited GM2 distribution in the hippocampus and cerebral cortex, in the *Hexb*$^{-/-}$ mice the glycolipid deposition is widespread in the thalamus, cerebral cortex, hippocampus, substantia nigra pas compacta and striatum (Phaneuf *et al*., 1996). Furthermore, *Hexb*$^{-/-}$ exhibit extensive cerebellar pathology when compared to *Hexa*$^{-/-}$ (Phaneuf *et al*., 1996). This allows *Hexa*$^{-/-}$ to exhibit late-onset neuropathology, a mild phenotype and normal lifespan (Yamanaka *et al*., 1994; Miklyaeva *et al*., 2004; Sango *et al*., 2008). *Hexb*$^{-/-}$ mice report progressive motor deterioration at 3 months of age with a lifespan of about 5 months. *Hexb*$^{-/-}$ mice have high face validity as they replicate the neuropathology and biochemical defect of the GM2 gangliosidoses as well as the behavioural impairments of SD (Sango *et al*., 1995; Wada *et al*., 2000; Yamaguchi *et al*., 2004; Cachon-Gonzalez *et al*., 2006; Lee *et al*., 2007a; Sango *et al*., 2008).

A prominent feature of *Hexb*$^{-/-}$ mice is the myelin sheath collapse and axonal loss in the spinal cord (Phaneuf *et al*., 1996). *Hexb*$^{-/-}$ show extensive disruption of the spinal cord circuitry leading to a motor system collapse (Phaneuf *et al*., 1996). Moreover, *Hexb*$^{-/-}$ reported large structural abnormalities in the liver and kidney when compared to *Hexa*$^{-/-}$ (Phaneuf *et al*., 1996). Extensive vacuolation was evident in both liver parenchymal cells and epithelial cells in the proximal tubules of kidneys (Phaneuf *et al*., 1996). Importantly, the generation of membranous cytoplasmic bodies (MCBs) through glycolipid storage progresses independently to neurodegeneration, and underscores the spatio-temporal disease mechanisms in *Hexb*$^{-/-}$ that need to be addressed (Cox and Chachon-Gonzalez, 2012).

Hexb$^{-/-}$ mice have undergone extensive behavioural assessment. In summary tremor, ataxia, defects in motor reflex as well as balance impairments have been well characterised (Andersson *et al*., 2004; Denny *et al*., 2006; Denny *et al*., 2007; Gullinello *et al*., 2008). Cognitive working-memory defects were observed after 2.5 months of age in addition to increased anxiety, as exhibited by reduced locomotor activity in open-field tests (Gullinello *et al*., 2008). Cognitive impairment was prevalent as revealed by their impaired working-memory in the novel object recognition test (Gullinello *et al*., 2008). Coordination tests including beam balancing and rotating rod indicated significant motor coordination defects of the *Hexb*$^{-/-}$ from 2.5 months of age, before visible ataxia was observable (Gulinello *et al*., 2008).

4.5 Objectives

Diagnosis of metabolic disorders integrally relies on systemic involvement and may include classical motor symptoms such as gait problems. However, increasingly non-motor symptoms such as sleep disorders and psychiatric manifestations are recognised as critical for early diagnosis and therapeutic intervention, especially due to their impact on patient morbidity. Based on the two-process model, the circadian regulation of sleep is distinct from the homeostatic drive (Borbely, 1982). Additionally, circadian rhythms exhibit a strong 24h period independent of prolonged wakefulness. Therefore, circadian rhythms, as measured by running-wheel activity, represent a robust quantifiable biomarker that can reliably reflect sleep disruption in pathology. In addition, such measurements may facilitate the detection of new activity measures during progression of the neuropathology.

The *Npc*1$^{-/-}$ and *Hexb*$^{-/-}$ mouse models display widespread CNS neurodegeneration and motor deficits. This screen would study the effects of *Npc1* and *Hexb* on the circadian axis. Rest/activity cycles in the *Npc1*$^{-/-}$ and *Hexb*$^{-/-}$ mice would be investigated at an early pre-symptomatic stage to possibly establish circadian non-motor/motor symptom progression in NPC and SD. Therefore, the main objective of this work is to:

- Study circadian rest/activity behavioural phenotypes in the *Npc1*$^{-/-}$ and *Hexb*$^{-/-}$ mice models.

4.6 Materials and Methods

4.6.1 Clocklab/Matlab

A behavioural circadian screen adapted from previous work on the PD mice covering the most commonly employed circadian paradigms was utilised. 22 *Npc1*$^{-/-}$ (n= 11 KO and 11 WT) and 13 *Hexb*$^{-/-}$ mice (n= 7 KO and 6 WT) at 7 weeks of age, age-matched male mice were individually housed in large cages (44x26x12cm) with running-wheels. Student's t-tests were used in cases of direct comparison across one categorical variable with no more than two groups, and one dependent measurement. ANOVAs were used in the case of one categorical variable with more than two groups.

4.6.2 Circadian Screen

A number of circadian paradigms (Figures 4.3-4.4) were completed including 12:12hr Light-Dark (LD) cycle, phase shift (6 hours phase advance) and a Dark-Dark (constant dark conditions-DD). The circadian screens were fragmented and repeated twice due to the limited lifespan of these models. Light conditions were maintained at 150 lux.

Figure 4.3: Circadian paradigms employed for *Npc1*$^{-/-}$ mice

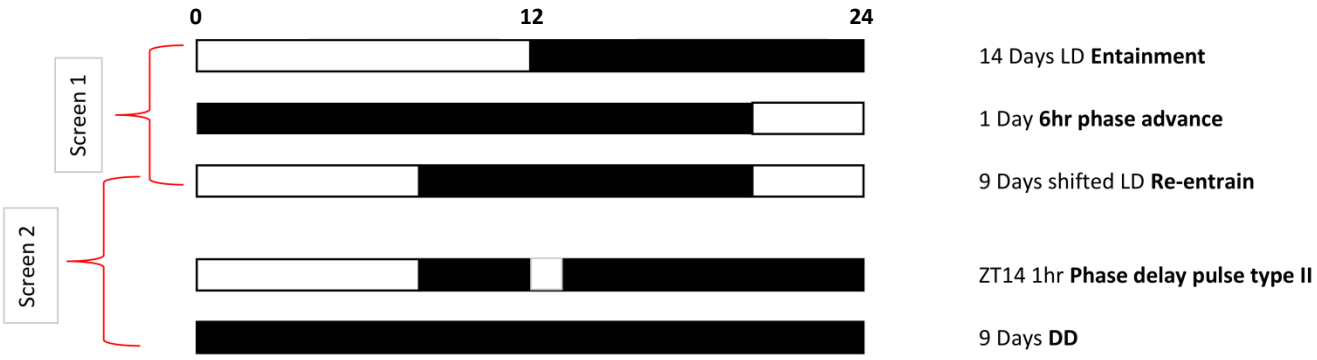

Figure 4.3: The numbers along the top denote Zetigeber Time (ZT) under the initial 12:12hr Light-Dark (LD) cycle. All environmental lighting changes are stated in the brief description of a given paradigm (right). The black (dark) and white (light) bars graphically represent the changing light environment as the screen progresses. Screen 1 included an LD, phase advance and LD re-entrainment protocol while screen 2 included an LD, Negative masking and DD paradigm. All lights were set at an intensity of 150lux. Further abbreviations-DD: 24 hour Dark.

Figure 4.4: Circadian paradigms employed for *Hexb*$^{-/-}$ mice

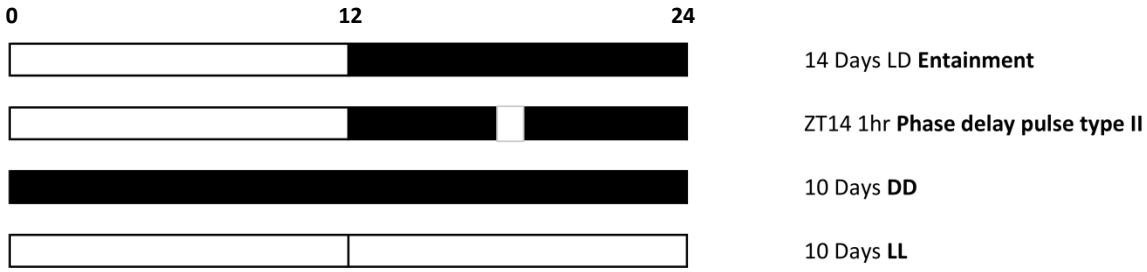

Figure 4.4: The numbers along the top denote Zetigeber Time (ZT) under the initial 12:12hr Light-Dark (LD) cycle. All environmental lighting changes are stated in the brief description of a given paradigm (right). The black (dark) and white (light) bars graphically represent the changing light environment as the screen progresses. Screen included LD entrainment, a DD and LL paradigm. All lights were set at an intensity of 150lux. Further abbreviations-DD: 24 hour Dark and LL: 24 hour Light.

4.7 Circadian data of *Npc1* KO mouse model

Npc1$^{-/-}$ and WT (+/+) controls were screened for rest/activity profiles from 7 weeks of age (Figure 4.5). Due to the limited lifespan of this model, modified shorter screens were pursued.

Figure 4.5: Representative double-plotted actograms of the screen for each genotype

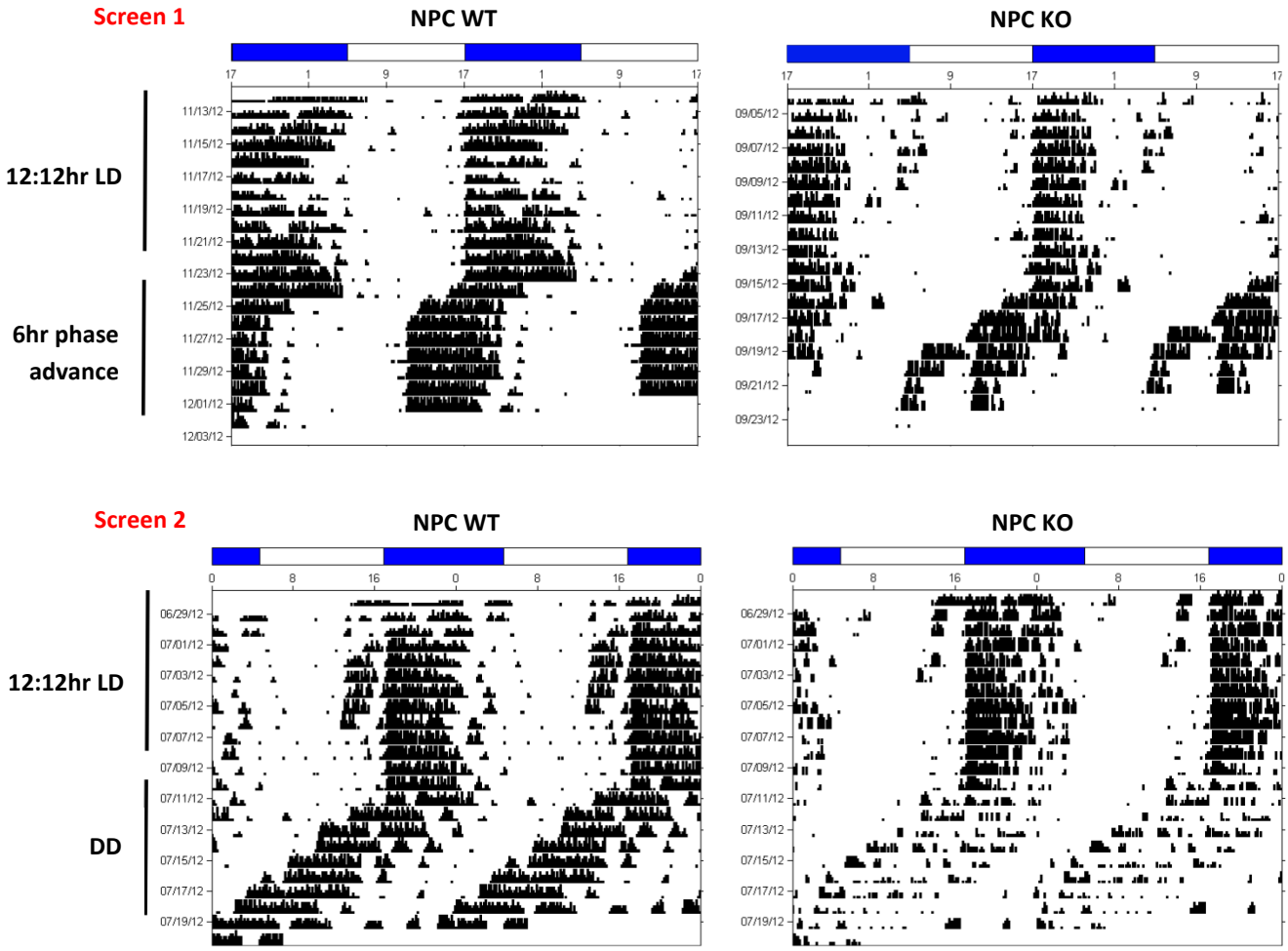

Figure 4.5: Blue bars indicate the dark phase and white bars the light phase (this reflects only the starting 12:12hr LD cycle and not 6hr phase advanced or DD paradigms). Black spikes represent activity data recorded from each individual mouse and each line represents 48h with dates presented on the left hand side of each diagram. Alternative circadian paradigms and their respective duration are represented on the left hand side of actograms.

Entrainment to a 12:12hr Light-Dark cycle was observed in both genotypes (Figure 4.5). However, the *Npc1*$^{-/-}$ exhibited significant hypoactivity (Figure 4.5). A *count by day* plot

of the entire circadian screen illustrates the activity variation associated with each circadian paradigm (Figure 4.6).

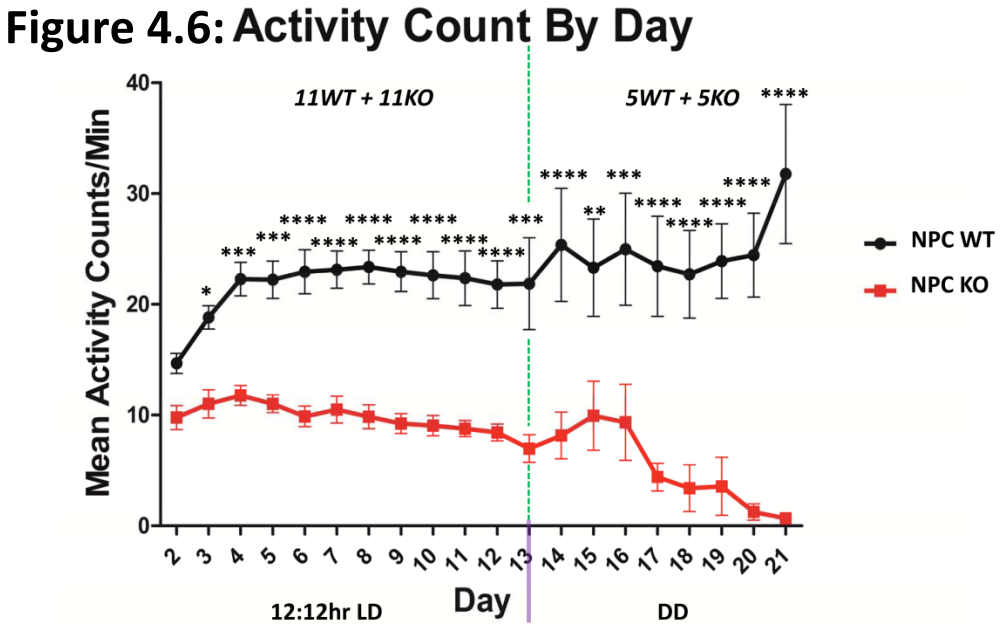

Figure 4.6: The graph illustrates mean activity counts per min for each day of the 21 days of the circadian screen. X-axis represents each day clustered in circadian paradigms. Data presented as mean ± SEM (n= 11 KO, n= 11 WT for LD paradigm while for DD paradigm n= 5 KO, n= 5 WT). Significant hypoactivity is recorded for the NPC KO versus the NPC WT control. Appendix 8.4 contains further information regarding the mouse models.

Severe hypoactivity of the KO versus WT is shown throughout most of the circadian screen (Figure 4.6). Days 2 to 20 illustrate progressive increase in activity counts by day in WT mice. However, the KO activity counts rapidly decline as the pathology begins to manifest itself. Activity suppression in the KO persisted during a 24 hour Dark paradigm (DD-days 14 to 21), in comparison to the increasing activity trend of the WT mice. Activity variation between genotypes was also present under a LD/6hr phase advance paradigm (screen 1-data not shown).

Figure 4.7: LD activity profiles over 11 days

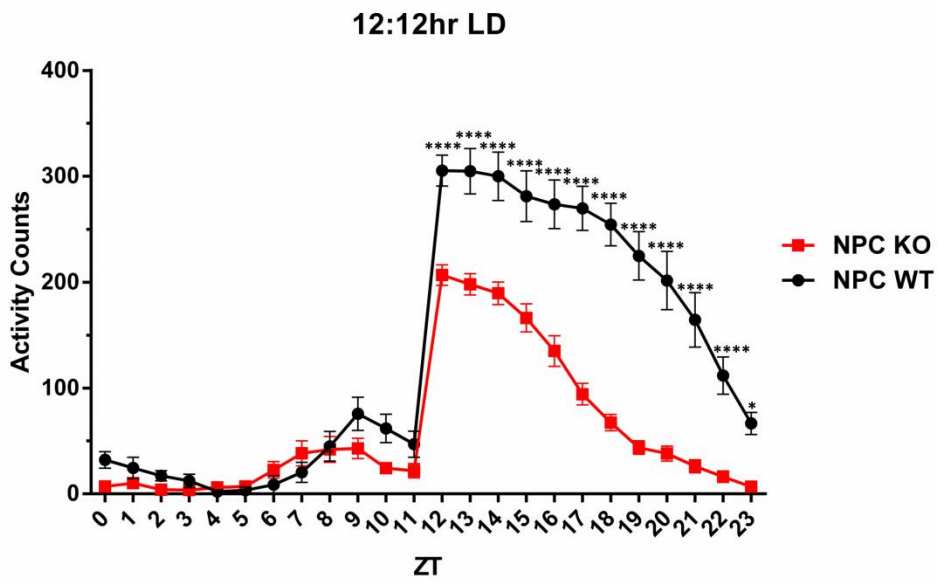

Figure 4.7: Activity profile over 11 days during a 12:12hr LD paradigm (days 2 to 12-figure 4.6). Data presented as mean ± SEM (n= 11 KO, n= 11 WT). Significant hypoactivity is recorded for the NPC KO versus the NPC WT control.

Scotophase-specific KO hypoactivity is shown versus WTs (Figure 4.7). No difference was detected during photophase epochs. Importantly, wheel-running reported this activity deficit as consistent with other motor function tests (Voikar *et al*., 2002). A numerical summary of the circadian parameters per paradigm illustrates any potential significance (Tables 4.1-4.3).

Table 4.1

12:12hr LD Cycle

Parameter	NPC KO (mean/SEM)	NPC WT (mean/SEM)	P-value
Tau	24.0/0.1	24.0/0.1	Non-sig
Tau Onset Error	1.6/0.2	1.5/0.4	Non-sig
Total Activity	14178/1050	31083/2031	<0.05
Total Dark Activity	11707/827	27311/2026	<0.05
Total Light Activity	2471/545	3772/691	Non-sig
% Light Activity	16.6/3.2	12.3/2.2	Non-sig
Chi-square Periodogram Peak (Hours)	23.8/0.2	23.9/0.2	Non-sig
Chi-square Periodogram Peak (Amplitude)	846/52	951/68	Non-sig
Phase of entrainment	1.3/0.4	0.9/0.3	Non-sig
Total Activity Bouts	4.6/0.2	3.7/0.3	Non-sig

Table 4.1: Circadian and locomotion parameters analysed for each genotype. Statistical differences illustrated in red. Table 4.1 corresponds to days 2 to 12 from figure 4.6. Mean ± SEM values for each circadian parameter of each genotype are also presented (n= 11 KO, n= 11 WT).

Table 4.2

6hr Phase Advance

Parameter	NPC KO (mean/SEM)	NPC WT (mean/SEM)	P-value
Tau	22.9/0.1	23/0.1	Non-sig
Tau Onset Error	2.9/0.7	2.4/0.2	Non-sig
Total Activity	4497/1197	25611/3916	<0.05
Total Dark Activity	4489/1199	25518/3903	<0.05
Total Light Activity	8.0/4.3	93/17	<0.05
% Light Activity	0.7/0.5	0.4/0.05	Non-sig
Chi-square Periodogram Peak (Hours)	23.1/0.1	23.4/0.2	Non-sig
Chi-square Periodogram Peak (Amplitude)	366/81	712/105	<0.05
Total Activity Bouts	2.9/0.4	2.8/0.6	Non-sig

Table 4.2: Circadian and locomotion parameters analysed for each genotype. Statistical differences illustrated in red. Table 4.2 corresponds to days 14 to 21 from screen 1 (data not shown). Mean ± SEM values for each circadian parameter of each genotype are also presented (n= 6 KO, n= 6 WT).

Table 4.3

DD Period

Parameter	NPC KO (mean/SEM)	NPC WT (mean/SEM)	P-value
Tau	21.9/0.6	22.5/0.2	Non-sig
Tau Onset Error	5.8/0.9	2.4/1.1	<0.05
Total Activity	7826/2585	36485/6293	<0.05
Chi-square Periodogram Peak (Hours)	21.3/0.2	22.2/0.2	<0.05
Chi-square Periodogram Peak (Amplitude)	263/15	494/94	<0.05
Total Activity Bouts	4.2/1.0	5.1/1.2	Non-sig

Table 4.3: Circadian and locomotion parameters analysed for each genotype. Statistical differences illustrated in red. Table 4.3 corresponds to days 14 to 21 from figure 4.6. Mean ± SEM values for each circadian parameter of each genotype are also presented (n= 5 KO, n= 5 WT).

Significant deficits in activity levels were observed in the KO (Tables 4.1-4.3). Tau remained largely unaltered (Table 4.1). Fragmentation remained largely unchanged throughout the circadian screen (Tables 4.1-4.3). However, the KO exhibited reduced rhythm stability towards the end of the screen (Tables 4.2-4.3).

Due to the early pathology and limited lifespan of the *Npc1*$^{-/-}$ mice many circadian parameters deviated considerably as the sample size decreased towards the end of the screen. Importantly, KO activity deficits in rotating rod and beam balancing tests have been identified by independent groups (Voikar *et al*., 2002). Interestingly, our screen also recorded activity deficits in the KO as consistent with other studies (Voikar *et al*., 2002). It is also noteworthy to point out the consistency of the KO's hypoactivity during the 21 days of screening.

In addition to the circadian parameters presented (Tables 4.1-4.3), activity onset under different lighting conditions constitutes a fundamental circadian marker of the functionality of input, core clock and output signalling (LeGates and Altimus, 2011). For examination of the short-term retinal input signalling pathways, a 1hr light pulse, 150lux at ZT14 (during the subjective night-active phase for nocturnal rodents) was administered (negative masking).

Figure 4.8: Negative masking effects of photic stimulation on day of pulse administration on each genotype

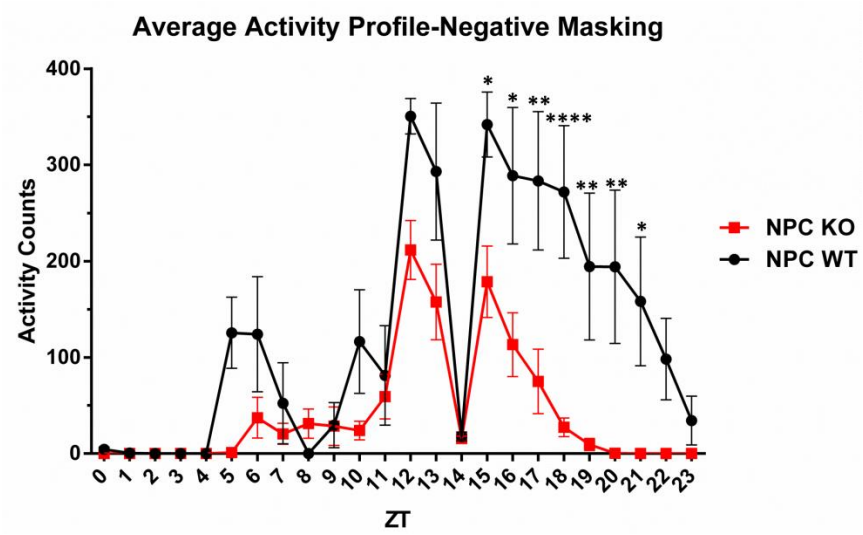

Figure 4.8: Average activity profiles for both lines on day of 1hr 150 lux pulse administration at ZT14. Data presented as mean ± SEM (n= 5 KO, n= 5 WT). No significant difference between lines was recorded.

Both genotypes responded to nocturnal photic stimulation by a negative masking (suppression of activity) effect, suggesting functional retinal input pathways (Figure 4.8). Similarly, phase shift curves were constructed for each circadian paradigm (6hr phase advance, DD and LL) in order to establish the functionality of the endogenous core clock and the SCN output.

Figure 4.9: Phase advance observed in both genotypes during the 6hr phase shift

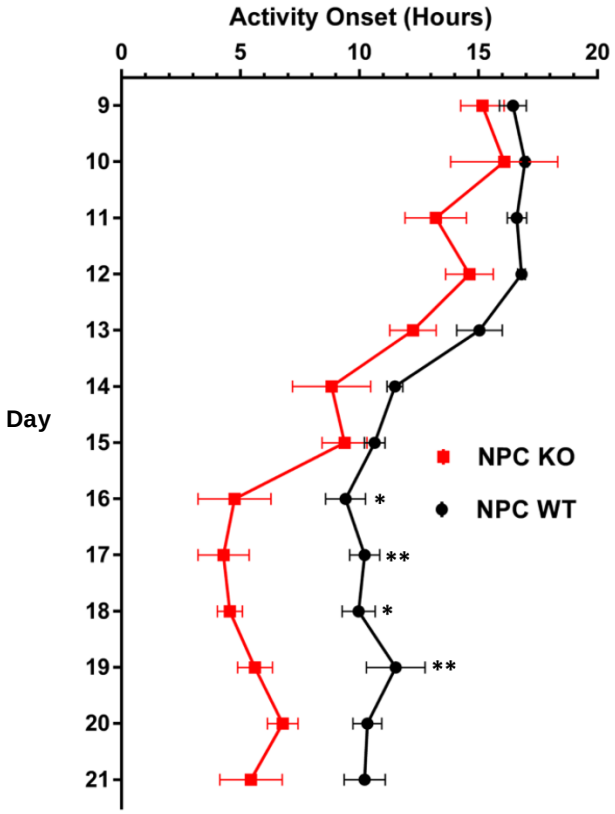

Figure 4.9: Illustrates the phase advance curve of NPC KO versus NPC WT during a 6hr phase shift. Data presented as mean ± SEM (n= 4 KO, n= 6 WT). Onset variations between genotypes in the latter half (Days 16-19) of the phase shift were observed.

Both genotypes exhibited similar phase advance curves until day 15, suggesting no circadian abnormalities during phase shifts (Figure 4.9). However, increasing onset variability in the KO reported re-entrainment deficits (Figure 4.9). On the other hand, considerable rhythm instability of the KO mice due to poor health is a factor that needs to be considered. Finally, technical issues (partial rotation blockage of the circadian wheel due to excessive cage bedding) could also contribute to this variation.

Figure 4.10: Representative double-plotted actograms of the 6hr phase shift

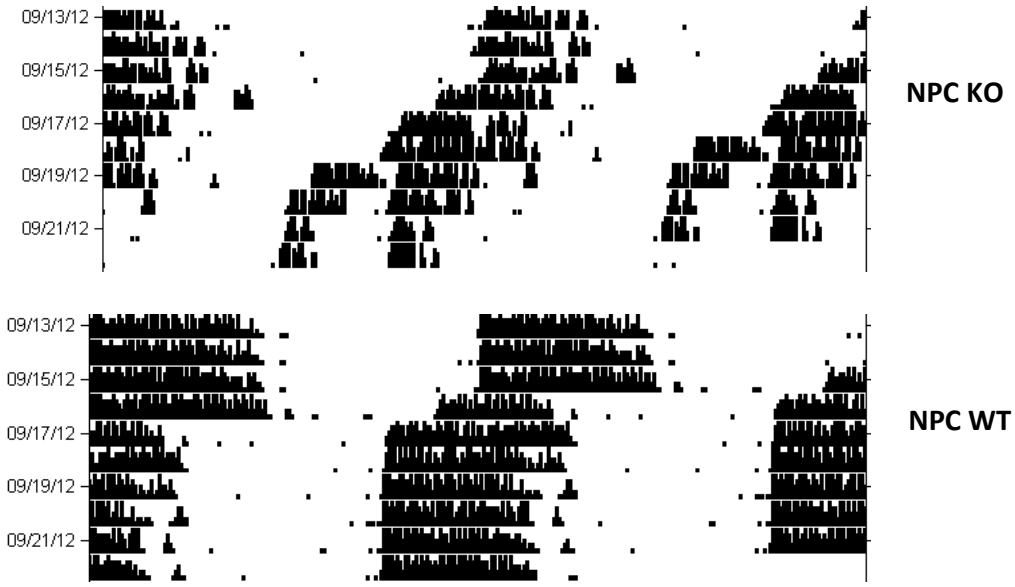

Figure 4.10: Double-plotted actograms of 6hr phase advance. Black spikes represent activity data recorded from each individual mouse and each line represents 48h with dates presented on the left hand side of each diagram.

A DD activity onset plot was also constructed in order to graphically illustrate the functionality of the SCN light-independent core clock (Figure 4.11).

Figure 4.11: DD phase onset plots

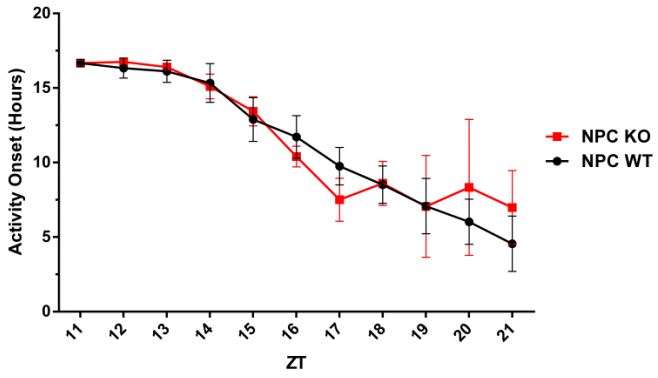

Figure 4.11: Illustrates the DD activity onset of NPC KO versus NPC WT during constant darkness conditions. Data presented as mean ± SEM (n= 5 KO, n= 5 WT). No significant difference between genotypes was recorded.

Similar DD activity onsets between genotypes suggest no core clock abnormalities under constant lighting conditions (Figures 4.11 and 4.12).

Figure 4.12: Representative double-plotted actograms of the DD paradigm

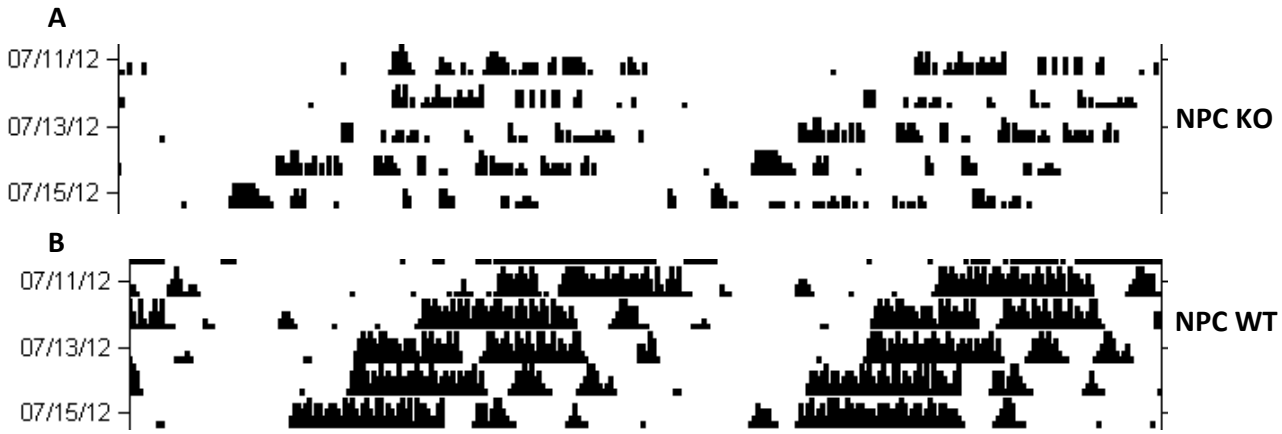

Figure 4.12: Double-plotted actograms of NPC KO versus NPC WT under DD paradigm. Black spikes represent activity data recorded from each individual mouse and each line represents 48h with dates presented on the left hand side of each diagram. (**A**) Illustrates the DD activity profile of a representative NPC KO mouse (**B**) illustrates the DD activity profile of a representative NPC WT mouse.

A summary table of the screen is presented.

Table 4.4: Summary table of screened NPC mice

Genotype	Activity Levels	Fragmentation Pattern	LD entrainment	Negative masking	Phase Advance	DD
NPC KO	↓↓	-	✓	✓	✗	✓
NPC WT	-	-	✓	✓	✓	✓

↓↓: Significant Down-regulation; ✓: Normal Response; - :Baseline Level; ✗: Abnormal Response

Table 4.4: Table summarises activity levels, fragmentation pattern and circadian response of each genotype.

4.8 Circadian data of *Hexb* KO mouse model

Hexb$^{-/-}$ and WT (+/+) controls were screened for rest/activity profiles from 7 weeks of age (Figure 4.13). Due to the limited lifespan of this model, modified shorter screens were pursued.

Figure 4.13: Representative double-plotted actograms of the screen for each genotype

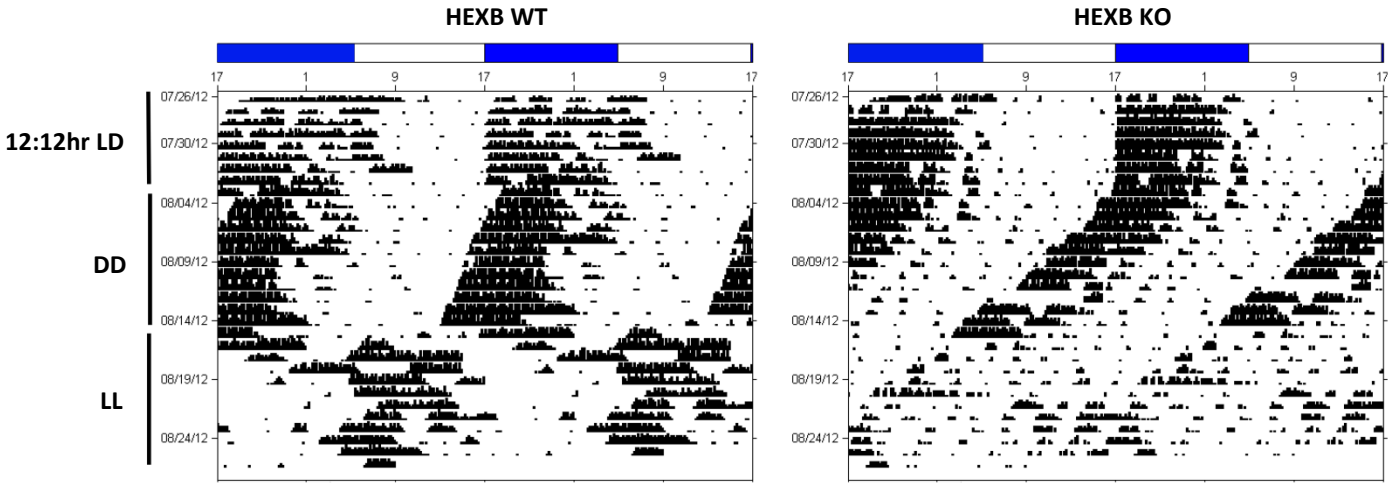

Figure 4.13: Blue bars indicate the dark phase and white bars the light phase (this reflects only the starting 12:12hr LD cycle and not 6hr phase advanced or DD paradigms). Black spikes represent activity data recorded from each individual mouse and each line represents 48h with dates presented on the left hand side of each diagram. Alternative circadian paradigms and their respective duration are represented on the left hand side of actograms.

Entrainment to a 12:12hr Light-Dark cycle was observed in both genotypes (Figure 4.13). However, the *Hexb*$^{-/-}$ exhibited significant free-running period (mean tau= 23.2h) variation versus WTs (mean tau= 23.6h) under constant DD and LL paradigms (Figure 4.13). Importantly, a range of free-running periods was recorded in both genotypes (Figure 4.17). Additionally, mild hypoactivity versus WTs is exhibited by the *Hexb*$^{-/-}$ (Figure 4.13). A *count by day* plot of the entire circadian screen illustrates the activity variation associated with each circadian paradigm (Figure 4.14).

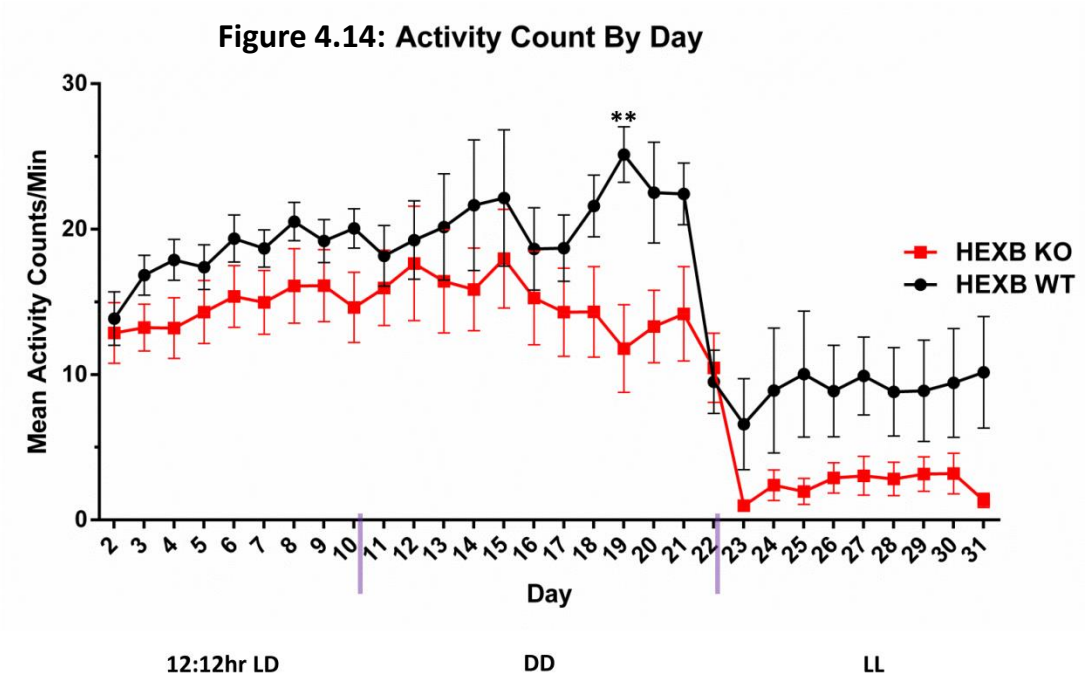

Figure 4.14: The graph illustrates mean activity counts per min for each day of the 31 days of the circadian screen. X-axis represents each day clustered in circadian paradigms. Data presented as mean ± SEM (n= 7 KO and n= 6 WT). Mild hypoactivity is recorded by the HEXB KO versus the HEXB WT control. Appendix 8.4 contains further information regarding the mouse models.

Mild hypoactivity of the KO versus WT is shown throughout most of the circadian screen (Figure 4.14). Days 2 to 20 illustrate progressive increase in activity counts by day in WT. However, the KO activity counts decline as the pathology begins to manifest itself. Activity suppression in the KO persisted during a 24 hour Dark paradigm (DD-days 11 to 21) in comparison to the increasing activity trend of the WT mice. Finally, the observed mild hypoactivity in the KO was also recorded under a 24 hour Light paradigm (LL-days 23 to 31).

Figure 4.15: LD activity profiles over 7 days

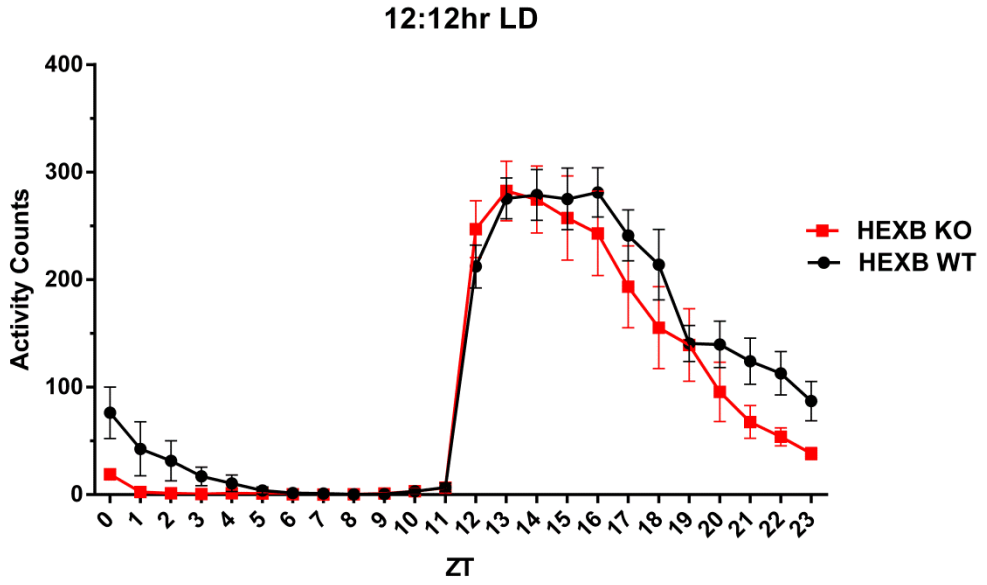

Figure 4.15: Activity profile over 8 days during a 12:12hr LD paradigm (days 2 to 9-figure 4.14). Data presented as mean ± SEM (n= 7 KO, n= 6 WT). Mild hypoactivity is recorded by the HEXB KO versus the HEXB WT control.

Scotophase-specific mild KO hypoactivity is shown versus WTs (Figure 4.15). Mild KO hypoactivity was also detected during photophase epochs. However, activity variations between genotypes were not significant. A numerical summary of the circadian parameters per paradigm illustrates any potential significance (Tables 4.5-4.7).

Table 4.5

12:12hr LD Cycle

Parameter	HEXB KO (mean/SEM)	HEXB WT (mean/SEM)	P-value
Tau	24.0/0.0	23.9/0.0	Non-sig
Tau Onset Error	0.2/0.1	0.4/0.1	Non-sig
Alpha	8.3/2.2	10.0/2.0	Non-sig
Rho	15.6/2.2	13.9/2.0	Non-sig
Total Activity	20847/2934	25767/1311	Non-sig
Total Dark Activity	20282/2960	23709/1650	Non-sig
Total Light Activity	565/100	2058/817	Non-sig
% Light Activity	3.3/1.1	8.2/3.4	Non-sig
Chi-square Periodogram Peak (Hours)	23.8/0.0	23.9/0.0	Non-sig
Chi-square Periodogram Peak (Amplitude)	740/48	654/56	Non-sig
Phase of entrainment	0.1/0.1	-0.1/0.0	Non-sig
Total Activity Bouts	3.5/0.4	3.3/0.2	Non-sig

Table 4.5: Circadian and locomotion parameters analysed for each genotype. Statistical differences illustrated in red. Table 4.5 corresponds to days 2 to 8 from figure 4.14. Mean ± SEM values for each circadian parameter of each genotype are also presented (n= 7 KO, n= 6 WT).

Table 4.6

DD Period

Parameter	HEXB KO (mean/SEM)	HEXB WT (mean/SEM)	P-value
Tau	23.2/0.1	23.6/0.1	<0.05
Tau Onset Error	0.6/0.2	0.8/0.3	Non-sig
Total Activity	22522/4231	29030/3998	Non-sig
Chi-square Periodogram Peak (Hours)	23.2/0.1	23.6/0.1	<0.05
Chi-square Periodogram Peak (Amplitude)	933/81	820/87	Non-sig
Total Activity Bouts	4.2/0.5	3.7/0.4	Non-sig

Table 4.6: Circadian and locomotion parameters analysed for each genotype. Statistical differences illustrated in red. Table 4.6 corresponds to days 11 to 21 from figure 4.14. Mean ± SEM values for each circadian parameter of each genotype are also presented (n= 7 KO, n= 6 WT).

Table 4.7

LL Period

Parameter	HEXB KO (mean/SEM)	HEXB WT (mean/SEM)	P-value
Tau	23.7/0.4	24.8/0.3	Non-sig
Total Activity	5179/949	13413/4769	Non-sig
Chi-square Periodogram Peak (Hours)	24.9/0.9	26.1/1.4	Non-sig
Chi-square Periodogram Peak (Amplitude)	298/32	328/41	Non-sig
Total Activity Bouts	4.6/0.5	3.6/0.7	Non-sig

Table 4.7: Circadian and locomotion parameters analysed for each genotype. Statistical differences illustrated in red. Table 4.7 corresponds to days 23 to 30 from figure 4.14. Mean ± SEM values for each circadian parameter of each genotype are also presented (n= 7 KO, n= 6 WT).

No significant differences in activity levels were observed in the KO (Tables 4.5-4.7). Non-motor circadian parameters such as alpha/rho remained unaltered (Table 4.5). However, tau varied between genotypes in both DD and LL paradigms (Table 4.6-4.7). Tau under LD cycles was comparable between genotypes (Table 4.5). Fragmentation remained largely unchanged throughout the circadian screen (Tables 4.5-4.7).

Due to the early pathology and limited lifespan of the *Hexb*$^{-/-}$ mice, many circadian parameters deviate considerably as the sample size decreased towards the end of the screen. Importantly, KO activity deficits in rotating rod and open-field tests have been identified by independent groups (Gulinelo *et al*., 2008). It is also noteworthy to point out the consistency of the KO's hypoactivity during the 31 days of screening.

For examination of the short-term retinal input signalling pathways a 1hr light pulse, 150lux at ZT14 (during the subjective night-active phase for nocturnal rodents) was administered (negative masking).

Figure 4.16: Negative masking effects of photic stimulation on day of pulse administration on each genotype

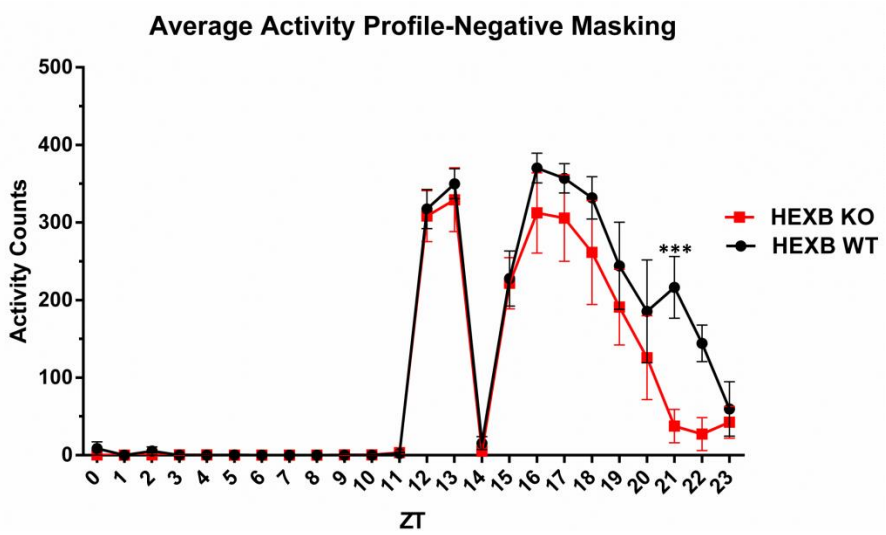

Figure 4.16: Average activity profiles for both lines on day of 1hr 150 lux pulse administration at ZT14. Data presented as mean ± SEM (n= 7 KO, n= 6 WT). No significant difference between lines was recorded.

Both genotypes responded to nocturnal photic stimulation by a negative masking (suppression of activity) effect, suggesting functional retinal input pathways (Figure 4.16). A DD activity onset plot was also constructed in order to graphically illustrate the functionality of the SCN light-independent core clock (Figure 4.17).

Figure 4.17: DD phase onset plots

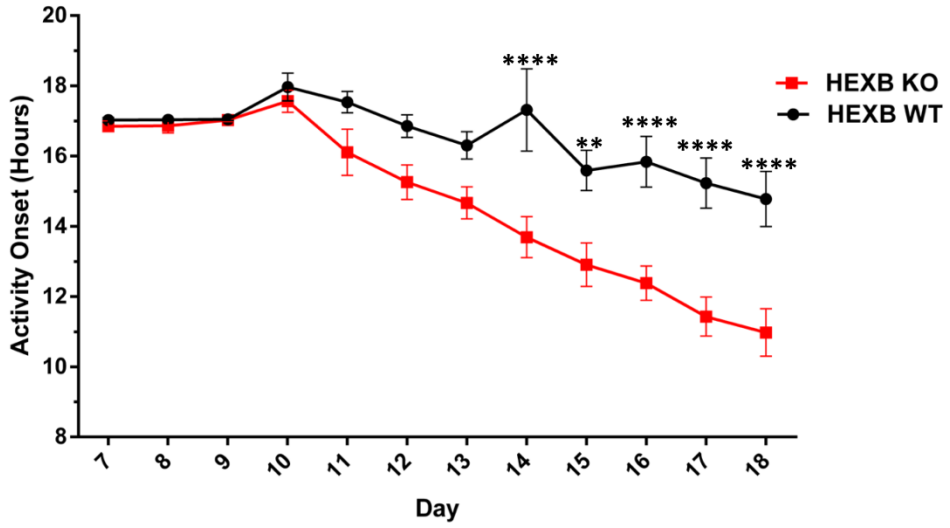

Figure 4.17: Illustrates the DD activity onset of HEXB KO versus HEXB WT during constant darkness conditions. Data presented as mean ± SEM (n= 7 KO, n= 6 WT). The HEXB KO exhibits shorter free-running periods versus HEXB WTs.

The KO exhibit a shorter free-running period versus WT controls (Figure 4.17). Importantly, a range of free-running periods was observed in both genotypes (Figure 4.17). This suggests possible core clock deficits in the *Hexb*$^{-/-}$ mice.

Figure 4.18:Type II Phase Delay

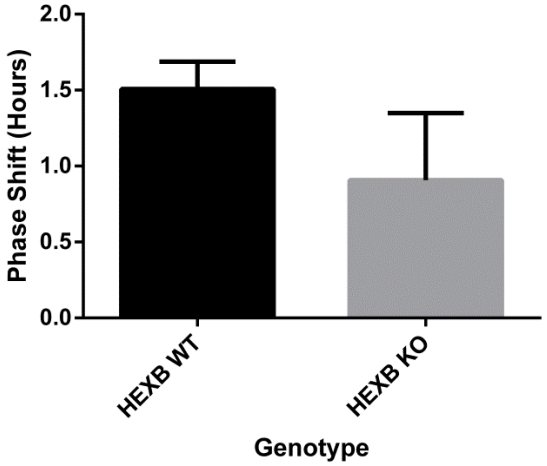

Figure 4.18: Type II Phase Delay graph of HEXB KO versus HEXB WT. Graph illustrates the ability of each genotype to phase shift following an acute photic stimulus in the subjective night of the preceding day. No significant difference between genotypes was recorded. Data presented as mean ± SEM (n= 7 KO, n= 6 WT).

Figure 4.19: Representative double-plotted actograms of the DD paradigm

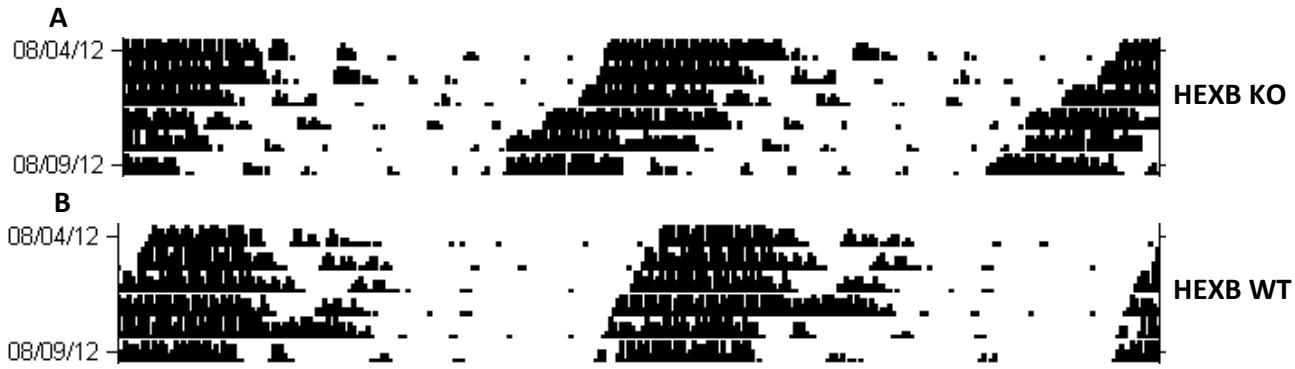

Figure 4.19: Double-plotted actograms of HEXB KO vs HEXB WT under DD paradigm. Black spikes represent activity data recorded from each individual mouse and each line represents 48h. (**A**) Illustrates the DD activity profile of a representative HEXB KO mouse (**B**) illustrates the DD activity profile of a representantive HEXB WT mouse.

Possible core clock deficits were exhibited by the *Hexb*$^{-/-}$ (Figure 4.19). Finally, a LL activity onset profile was also constructed to report on clock functionality under constant 150lux lighting conditions (Figure 4.20).

Figure 4.20: LL phase onset plots

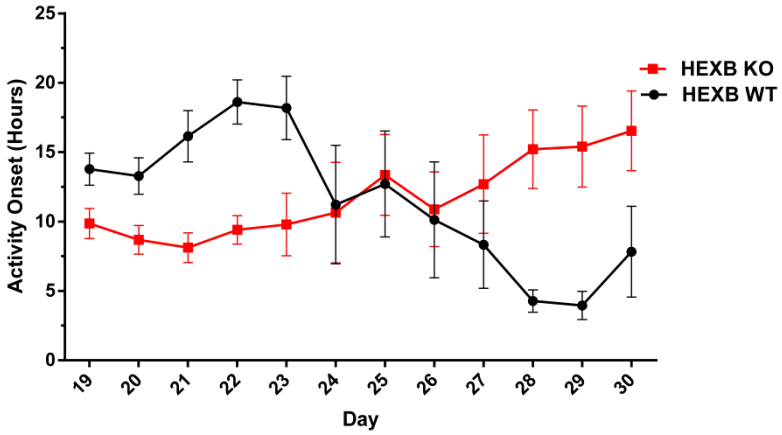

Figure 4.20: Illustrates the LL activity onset of HEXB KO versus HEXB WT. Data presented as mean ± SEM (n= 7 KO, n= 6 WT). The HEXB KO exhibits shorter free-running photoperiods versus HEXB WTs.

Dissimilar LL activity onsets between genotypes were recorded in the *Hexb*$^{-/-}$ mice (Figure 4.20). Interestingly, the KO exhibited a period shorter than 24h, which might indicate potential end-stage retinal input dysfunction.

Figure 4.21: Representative double-plotted actograms of the LL paradigm

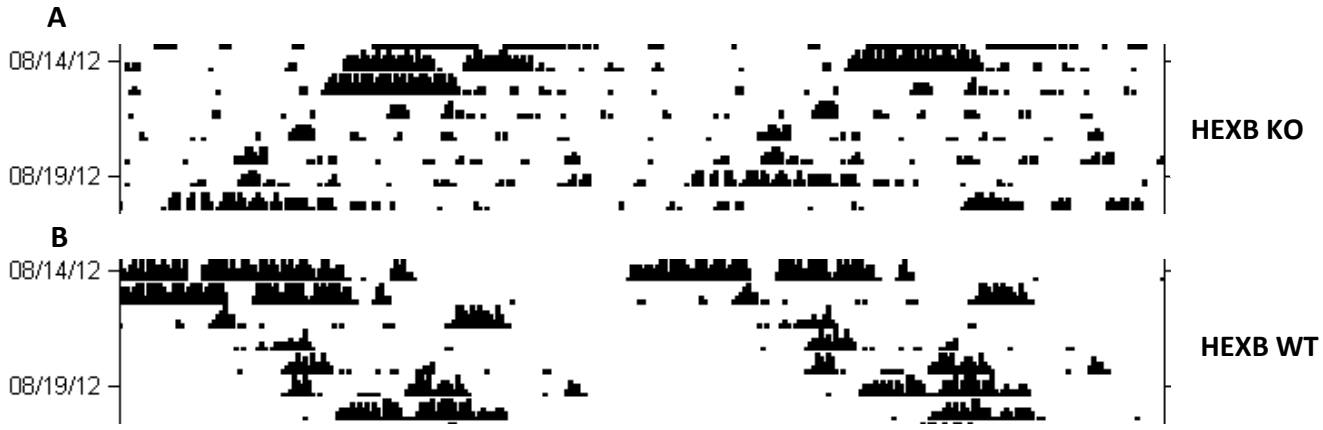

Figure 4.21: Double-plotted actograms of HEXB KO versus HEXB WT under LL paradigm. Black spikes represent activity data recorded from each individual mouse and each line represents 48h. (**A**) Illustrates the LL activity profile of a representative HEXB KO mouse (**B**) illustrates the LL activity profile of a representative HEXB WT mouse.

Dissimilar LL activity onsets in both genotypes were recorded, suggesting potential clock pathology under constant lighting conditions (Figure 4.21). Despite activity suppression in both genotypes under an LL paradigm the endogenous *Hexb*$^{-/-}$ core clock is unable to free-run according to Aschoff's rule (LL: tau>24h). A summary table of the screen is presented.

Table 4.8: Summary table of screened *Hexb* mice

Genotype	Activity Levels	Fragmentation Pattern	LD entrainment	Negative masking	DD	LL
HEXB KO	↓	-	✓	✓	✖	✖
HEXB WT	-	-	✓	✓	✓	✓

↓: Mild Down-regulation; ✓: Normal Response; - :Baseline Level; ✖: Abnormal response

Table 4.8: Table summarises activity levels, fragmentation pattern and circadian response of each genotype.

4.9 Discussion on *Npc1* KO

In summary, using running-wheel behavioural analysis, the *Npc1*$^{-/-}$ mouse model displayed normal LD entrainment, negative masking and DD periods. Period length under constant conditions was not significantly different between genotypes (DD: tau <24h). However, during a 6hr phase advance paradigm abnormal re-entrainment in the *Npc1*$^{-/-}$ was recorded. The KO compared to WT control displayed a severe hypoactive wheel phenotype localised during the scotophase period (Figure 4.7). Photophases did not yield any significant motor variation between genotypes (Figure 4.7). No variations between genotypes in fragmentation patterns were observed (Tables 4.1-4.4).

Previous findings on *Npc1*$^{-/-}$ by 1 month of age have demonstrated significant motor deficits in locomotor activity (beam balancing, rotating rod) as well as cognitive impairments in the water maze test (Voikar *et al*., 2002). Additionally, progressive weight loss occurs in the KO after 1.5 months of age (Voikar *et al*., 2002). Decreased exploratory behaviour in the open-field testing was exhibited by the *Npc1*$^{-/-}$ (Voikar *et al*., 2002). The group reported learning impairment independent of progressive motor pathology in the *Npc1*$^{-/-}$. Extensive corpus callosum neuropathology in the KO mice, a region involved in spatial learning, as well as cerebellar Purkinje loss, complement the behavioural data (Weintraub *et al*., 1987; Middleton and Strick, 1998; German *et al*., 2001). Our running-wheel activity data also reported severe hypoactivity in the *Npc1*$^{-/-}$ consistent with published studies (Voikar *et al*., 2002). This suggests wheel-running is a reliable method for motor function assessment. Importantly, there was progressive deterioration of motor function in an age-dependent manner (Figure 4.6).

A 6hr phase advance reported abnormal end-stage re-entrainment onsets in the *Npc1*$^{-/-}$ versus the WT (Figure 4.9). Importantly, short-term retinal input pathways appeared normal in both genotypes (Figure 4.8). Both genotypes responded to a negative masking effect via activity suppression during application of a nocturnal light pulse at ZT14 (Figure 4.8). Circadian work on phase re-entrainment in voltage gated ($Ca_v2.1$) calcium channel mutant mice reported circadian deficits (van Oosterhout *et al*., 2008). The R192Q mutation induces calcium inflow and enhances neurotransmitter release (van Oosterhout *et al*., 2008). The $Ca_v2.1$ channels are pre-synaptically localised and ubiquitously expressed throughout the CNS (Cloues *et al*., 2003; van den Maagdenberg *et al*., 2004; van Oosterhout *et al*., 2008). The knock-in mis-sense mutant mice exhibit rapid re-entrainment to phase advanced cycles (van Oosterhout *et al*., 2008). Importantly, retinal input pathways appeared normal (van Oosterhout *et al*., 2008). However, synaptic excitability in the dorsal SCN was enhanced and EEG parameters displayed enhanced phase shifting of rest/activity cycles, suggesting extra-SCN areas impact on SCN re-entrainment (van Oosterhout *et al*., 2008). Importantly, tau under DD or LL paradigms remained unaltered between genotypes (van Oosterhout *et al*., 2008). In summary, deficits in re-entrainment during 6hr phase advance in the $Ca_v2.1$ mutant mice were potentially the result of calcium-mediated synaptic dysfunction (van Oosterhout *et al*., 2008).

Recent work has implicated de-regulation of calcium homeostasis in NPC leading to additional cholesterol accumulation (Lloyd-Evans *et al*., 2008). Importantly, pharmacological agents that elevated calcium levels rescued the NPC cellular phenotype (Lloyd-Evans *et al*., 2008. Application of the same agents in the *Npc1* mouse improves performance and lifespan (Lloyd-Evans *et al*., 2008). Interestingly, calmodulin inhibitors are able to recapitulate NPC cellular pathology (Masson *et al*., 1992; Lloyd-Evans *et al*., 2008). Defects in synaptic

trafficking that are regulated by calcium and calcium-binding factors promote the NPC disease phenotype (Lloyd-Evans *et al*., 2008).

In summary, our *Npc1*$^{-/-}$ mice exhibit a potentially enhanced behavioural phase resetting during a 6hr LD advance. Altered calcium homeostasis in *Npc1*$^{-/-}$ mice could potentially have an impact on SCN re-entrainment during phase shifts. Additionally, severe hypoactivity localised in the scotophase was recorded and was consistent with previous studies (Voikar *et al*., 2002). Further investigation of phase re-entrainment in NPC mice is necessary to confirm the finding. However, these results do not confirm the original hypothesis regarding potential core clock defects in LSDs (see Hypotheses section).

4.10 Discussion on *Hexb* KO

In summary, using running-wheel behavioural analysis, the *Hexb*$^{-/-}$ mouse model displayed normal LD entrainment and a negative masking response. However, *Hexb*$^{-/-}$ exhibited shorter free-running periods versus WTs under constant DD and LL paradigms. Importantly, a range of free-running periods was observed in both genotypes (Figure 4.17). Additionally, the *Hexb* WT mice exhibited comparable free-running periods to C57BL/6 mice from other circadian studies (Schwartz and Zimmerman, 1990). Compared to WT control, the KO displayed a mild hypoactive wheel phenotype localised during the scotophase (Figure 4.15). No variations between genotypes in fragmentation patterns were observed (Tables 4.5-4.7).

Previous findings on the *Hexb*$^{-/-}$ mice have demonstrated significant behavioural impairments in open-field locomotor activity as well as cognitive impairment in the novel object recognition test (Gullinello *et al*., 2008). Motor coordination was also significantly impaired in an age-dependent manner; a finding that overlaps with the data generated via

wheel-running. Given the extensive spinal cord neuronal disruption present in the *Hexb*$^{-/-}$, locomotor variations between genotypes are expected (Phaneuf *et al*., 1996). More recently, an inducible mouse model of *Hexb*$^{-/-}$ under the mouse *Hexb* promoter, illustrated that *Hexb* silencing after 5 weeks induced progressive neurodegeneration reminiscent of a GM2 gangliosidosis (Sargeant *et al*., 2012). Acute spinal cord pathology and glycolipid storage was present in this adult-inducible *Hexb*$^{-/-}$ model (Sargeant *et al*., 2012). Screening inducible *Hexb*$^{-/-}$ mice could correlate spatio-temporal *Hexb*$^{-/-}$ expression data to circadian axis functionality. Attenuated *Hexb* models might facilitate further understanding of circadian deficits in GM2 gangliosidosis.

Importantly, *Hexb*$^{-/-}$ mice responded to a nocturnal light pulse by suppression of activity (Figure 4.16). However, under constant DD and LL paradigms, free-running period was significantly shorter in the KOs versus WTs (Figures 4.17 and 4.20). This suggests potential core clock deficits prior to extensive neurodegeneration and could represent a significant prodromal phenotype in SD. Finally, activity suppression under LL was comparable between genotypes (Figure 4.14). Previous work has indicated that circadian rhythms are able to synchronise via light in mice lacking rods and cones (Nelson and Zucker, 1981; Freedman *et al*., 1999). Mice were generated that lacked rods and cones and were visually blind but achieved proper LD entrainment (Freedman *et al*., 1999). A parallel versus a serial input pathway circadian model in mice has been theorised (Güler *et al*., 2008). Güler *et al* demonstrated intrinsically photosensitive melanopsin-containing retinal ganglion cells (ipRGCs) as the only input pathway in circadian entrainment. Image formation was still possible, despite circadian photoentrainment deficits, in these genetically ablated ipRGCs mice thereby dissociating pattern vision from circadian mechanisms (Güler *et al*., 2008).

Figure 4.22: Light-dependent retinal input pathways separating the visual from the circadian system

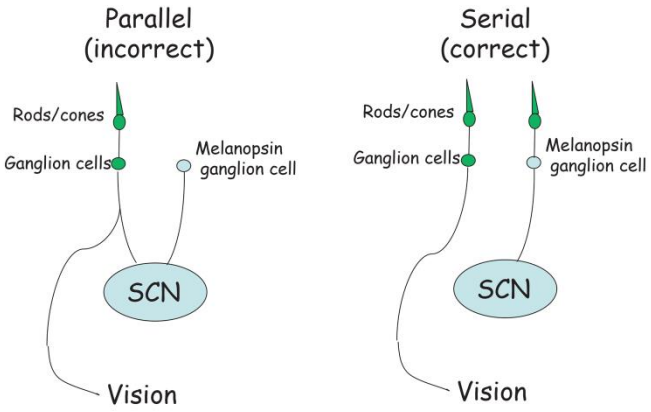

Figure 4.22: Parallel versus Serial retinal input model in mammals. *Hexb*$^{-/-}$ exhibit shorter than 24hr tau under LL while activity suppression under LL indicates functional non-clock input pathways

Based on Güler *et al.,* 2008

Studies on *Hexb*$^{-/-}$ mice have illustrated the extensive GM2 deposition in retinal ganglion cells, vacuolation in retinal neurons and disruption of the retinal pigment epithelium (Sango *et al*., 2005; Sango *et al*., 2008). Amacrine and retinal ganglion cells appear to contain several inclusions (Nagashima *et al*., 1981; Sango *et al*., 2008). Neuronal apoptosis has previously been documented in the thalamus, brain stem and spinal cord in the *Hexb*$^{-/-}$ mice at 3 months of age (Wada *et al*., 2000; Sango *et al*., 2008). Similarly, retinal ganglion cells in the *Hexb*$^{-/-}$ undergo apoptosis as visualised by electron microscopy (Sango *et al*., 2008). Previous studies have identified the increased susceptibility of retinal ganglion cells to glycolipid storage versus other retinal structures (Sango *et al*., 2008). These findings overlap in both the motor and non-motor pathology identified by our screen on the *Hexb*$^{-/-}$ mice. Hence, our data suggest mild scotophase hypoactivity coupled to prodromal light-independent SCN core clock pathology with potential end-stage retinal ganglion disruption in the *Hexb*$^{-/-}$ mice. These results confirm the original hypothesis regarding potential core clock defects in LSDs (see Hypotheses section).

5 Results III: Proteomic profiling of the *Bdr* SCN

5.1 *Snap-25* and the *Bdr*

SNARE proteins are important factors participating in vesicle-trafficking and recycling (Johnson *et al*., 2008). SNAP-25 is a SNARE factor participating in neurotransmitter release via vesicle fusions with the pre-synaptic membrane (Johnson *et al*., 2008; Corradini *et al*., 2009). GWAS studies have identified the SNAP-25 chromosomal area to be a strong candidate risk gene for schizophrenia (Johnson *et al*., 2008). Recently, TSNARE1 has been identified as a new susceptibility locus associated with schizophrenia and bipolar disorder, suggesting synaptic trafficking mechanisms as vital in neuropsychiatric conditions (Sleiman *et al*., 2013). Importantly, *Snap-25* is expressed in rodent SCN and is important in maintaining circadian rhythm oscillations (Deery *et al*., 2009).

Using an ENU mutant model, the blind-drunk (*Bdr*), the effects of *Snap-25* on schizophrenic endophenotypes may be investigated (Jeans *et al*., 2007). The *Bdr* mutants harbour a mis-sense dominant gain-of-function mutation on isoform *Snap-25b*. This induces a single amino acid substitution at position 67 (isoleucine to threonine). The *Bdr* mice display impaired cortical glutamate transmission due to retarded exocycotic vesicle recycling rates (Jeans *et al*., 2007). The mutation induces increased binding affinity of the SNARE complex eventually reducing the mobilisation of reserve pool vesicles (Jeans *et al*., 2007). Behaviourally, the *Bdr* exhibit impaired sensorimotor gating (PPI deficits), a schizophrenic endophenotype that is aggravated via pre-natal stress (PNS) and rescued by antipsychotic drugs (Oliver and Davies, 2009).

Circadian behavioural data suggested that the light input pathway via RHT is likely to be unaffected (Figures 1.8B & 1.8D) but the 6hr phase advance under LD conditions (Figure 1.9A) in *Bdr* required further investigation. The endogenous core clock appears unaffected (Figure 1.9C), suggesting disruption of critical output signalling in the *Bdr*. To investigate this at a molecular level, an expression analysis via microarray at three time points (ZT6/ZT11/ZT13) complemented by ISH and IHC data was conducted. Microarray data reveal a small subset of SCN output neurotransmitter factors (AVP, Neurotensin, Substance P) are temporally de-regulated. ISH and IHC data confirmed the desynchronised expression levels of SCN output factors (Oliver *et al*., 2012). Moreover, AVP regulates corticosterone release via the hypothalamic-pituitary-adrenal axis (HPA axis) (Dickmeis, 2009; Oliver *et al*., 2012). Plasma corticosterone levels appear phase advanced in the *Bdr*, suggesting a perturbed HPA axis in this schizophrenic mouse model (Oliver *et al*., 2012). Indeed, SNAP-25 is expressed in the adrenal medulla supporting this hypothesis (Grant *et al*., 1999).

Therefore, mutations in the schizophrenic risk gene *Snap-25* disrupt SCN output synaptic connectivity and glutamatergic cortical neurotransmission, promoting schizophrenic endophenotypes like impaired sensorimotor gating (PPI deficits) and circadian disruption (Figure 5.1).

Figure 5.1: Circadian axis operation in *Bdr* versus WT

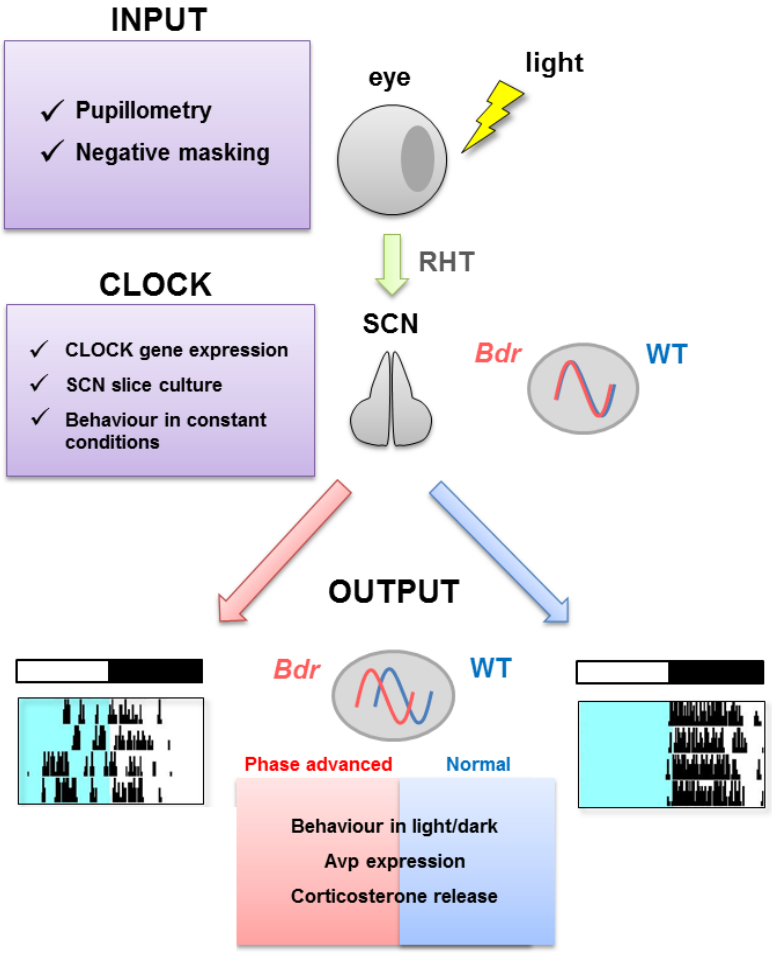

Figure 5.1: Circadian axis investigation in *Bdr* versus WT. Retinal input pathways via RHT appear normal, as indicated by behavioural and molecular negative masking experiments as well as pupillometry data. Core clock gene expression appears unaffected and is complemented by normal free-running periods during DD circadian screening. However, under LD cycles *Bdr* mice exhibited considerable phase advance in activity onset. An array conducted at ZT6/ZT11/ZT13 and confirmed by ISH/IHC revealed output AVP de-synchrony, HPA axis perturbation and corticosterone temporal de-regulation.

The *Bdr* mouse allows investigation of the functional cross-talk between circadian disruption and schizophrenic endophenotypes. Despite identification of neurotransmitter systems (AVP, NT) associated with schizophrenic pathology, the underlying mechanisms promoting circadian disruption are not well understood (De Wied and Sigling, 2002; Caceda *et al*., 2006; Oliver *et al*., 2012). Moreover, circadian pacemaking is principally dependent on

coordinating transcriptional and post-transcriptional networks (Reppert and Weaver, 2002; Hastings *et al*., 2003; Deery *et al*., 2009; McGlincy *et al*., 2012). SCN proteomic studies in WT mice by 2D-DIGE reported considerable disparity between transcriptional and post-transcriptional rhythms (Ueda *et al*., 2002; Deery *et al*., 2009; Robles and Mann, 2013). It is estimated that roughly 10% of soluble SCN proteins display diurnal oscillations, while roughly 25% of the proteome detected exhibited synchronous transcriptional rhythmicity (Deery *et al*., 2009; Robles and Mann, 2013). This would suggest that the majority of cycling proteins (~75%) exhibit de-synchronous transcriptional and post-transcriptional daily rhythms (Deery *et al*., 2009; Robles and Mann, 2013). This disparity may rise from multiple isoforms being expressed, but with only some under circadian control (Deery *et al*., 2009). Additionally, it has been shown in multiple studies that complex neuropsychiatric conditions often involve global proteomic alterations that are temporally and spatially regulated (English *et al*., 2011). There have been numerous proteomic investigations on the dorsolateral prefrontal cortex (dlPFC), anterior cingulate cortex and the insular cortex of schizophrenics (Johnston-Wilson *et al*., 2000; Prabakaran *et al*., 2004; Beasley *et al*., 2006; Clark *et al*., 2006; Pennington *et al*., 2007). Data from these studies revealed that 262 proteins were differentially expressed (English *et al*., 2011). Importantly, 20 of these targets have been previously implicated at the transcriptomic level in schizophrenia (e.g. GAP-43, SNAP-25) while 9 proteins have also been identified in bipolar disorder (Welckert *et al*., 2001; Clinton *et al*., 2004). Taken together, these findings suggest that circadian synaptic trafficking in neuropsychiatric conditions involves a complex rhythmic and non-rhythmic proteomic network. Therefore, circadian proteomic investigation of the *Bdr* model of synaptic dysfunction may identify potential schizophrenic biomarkers relevant to diurnal cycle mechanisms.

Despite the utility of 2D gels, shotgun proteomics through the increasing availability of high-resolution MS instruments (e.g. Q Exactive) offer the possibility of investigating the proteomic oscillatory network in complex diseases (Tian *et al*., 2011; Mitchell *et al*., 2011; English *et al*., 2011; Robles and Mann, 2013; Lee *et al*., 2013). Tian *et al* for the first time deployed an automated sample processing stage coupled to LC-MS/MS that allowed the simultaneous quantification of roughly 2100 proteins (Tian *et al*., 2011). In contrast, 2D-PAGE gels depth of information is mainly limited to roughly 50 targets excised and identified by LC-MS/MS (liquid chromatography and tandem mass spectrometry) (Deery *et al*., 2009; Robles and Mann, 2013). Finally, 2D-PAGE limitations include gel-to-gel reproducibility, poor resolving power for high MW targets, relatively poor sensitivity for detecting rare or low abundance targets as well as ineffective separation of hydrophobic or basic proteins (English *et al*., 2011; Leung *et al*., 2012). Given the presumed functional, genetic and pathological cross-talk between circadian disruption, schizophrenia and synaptic dysfunction in the *Bdr* mouse, a 24hr LD proteomic investigation was undertaken. We hypothesised that the de-regulation of neurotransmitters detected in the *Bdr* SCN, promoting HPA axis perturbation, would be mechanistically revealed when the post-transcriptional network is investigated.

5.2 Objectives

- Investigate light-mediated retinal input pathways to the central pacemaker, the SCN. The aim was to identify defective elements of the circadian axis.

- Conduct a 24hr (6 time points) peptidomic and proteomic SCN expression analysis in the SCN of WT versus *Bdr* mice. The aim was to identify proteins under circadian control de-regulated in the *Bdr*.

- Confirm expression changes of proteomic SCN targets.

5.3 Materials and Methods

5.3.1 Acute light-induced SCN IEGs profiling/qRT-PCR/ISH

As previously stated (see pages 63-70)

5.3.2 SCN proteomics-MS optimisation/quantitation/validation

As previously stated (see pages 71-79)

5.4 Results

5.4.1 Acute light-induced SCN IEGs

Previous circadian screening (Figure 1.9-negative masking) on *Bdr* mice suggested the absence of any deleterious effect on the light input pathways to the SCN (Oliver *et al*., 2012). Follow-up molecular work was necessary to confirm this finding (Figures 5.2-5.4). The light induction of IEGs was utilised as molecular markers of neuronal activity of the SCN (Morris *et al*., 1998). IEGs (*c-fos* and *jun-B*) as well as core clock genes *Per1* & *2*, SCN tissue punch validating control (*Six-6*) and *VIP* circadian timekeeper control (immune to photic stimulation) were investigated.

Figure 5.2: qRT-PCR of IEGs, *Per1- 2*, *Six-6* and *VIP* on WT versus *Bdr* SCN

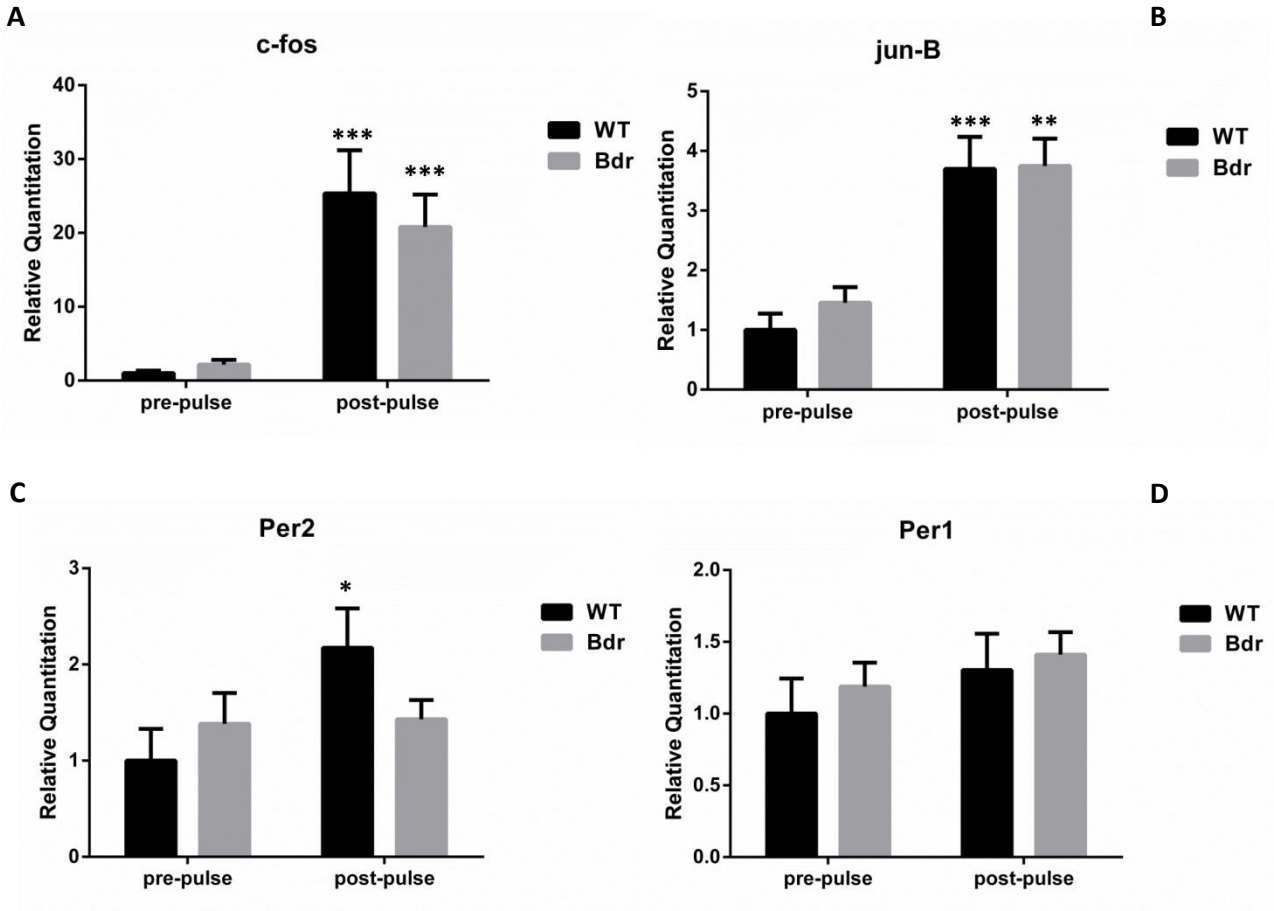

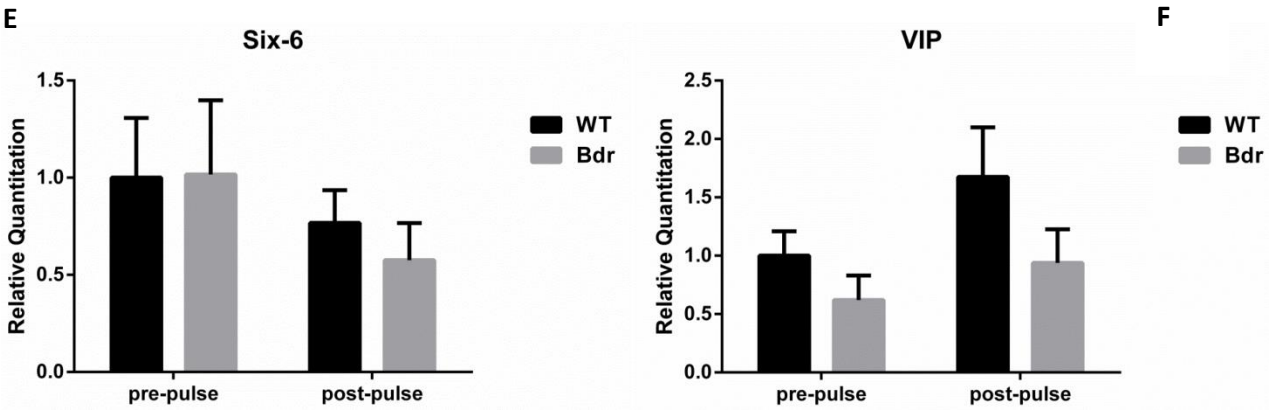

Figure 5.2: (**A, B**) Relative quantitation of IEGs *c-fos* and *jun-B* show induction following 150lux 30min photic stimulation. Both *Bdr* and WT generate this expression pattern (**C**) Core clock *Per2* shows induction following 150 lux 30min photic stimulation only in WT (**D**) *Per1* shows no statistically significant induction in either genotype (**E, F**) No significant difference in *Six-6* or *VIP* was detected following the 150 lux 30min light pulse at ZT16. Data plotted as mean ± SEM (n= 4 per genotype). RINs (RNA Integrity Number) of samples > 6.5.

qRT-PCR data confirm normal light input signalling via RHT to the SCN by subjecting WT and *Bdr* mice to a 150 lux light pulse at ZT16 for 30 minutes (Figure 5.2). qRT-PCR data (Figure 5.2) suggest that the light input pathways to the SCN are not defective in *Bdr* mice because of comparable IEGs expression between genotypes following nocturnal photic stimulation (Figure 5.2). *Per 1* and *2* genes show only minor up-regulation following the light pulse (Figure 5.2). ISH was also conducted to confirm these findings. Induction of *c-fos* and *jun-B* was also observed via ISH following 150 lux 30min photic stimulation at ZT16 in both WT and *Bdr* mice (Figures 5.3 & 5.4).

Figure 5.3: Representative i*n situ* of pre-pulse and post-pulse WT SCN *c-fos* induction

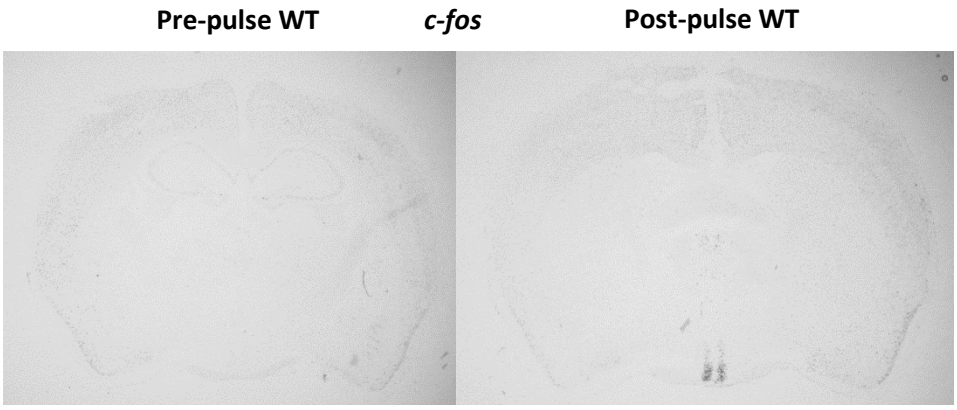

Figure 5.3: Representative low magnification image of *c-fos* induction in WT SCN after 30 minutes of 150 lux light pulse at ZT16.

Figure 5.4: ISH of *c-fos*, *jun-B* and *VIP* targets on WT and *Bdr* SCN

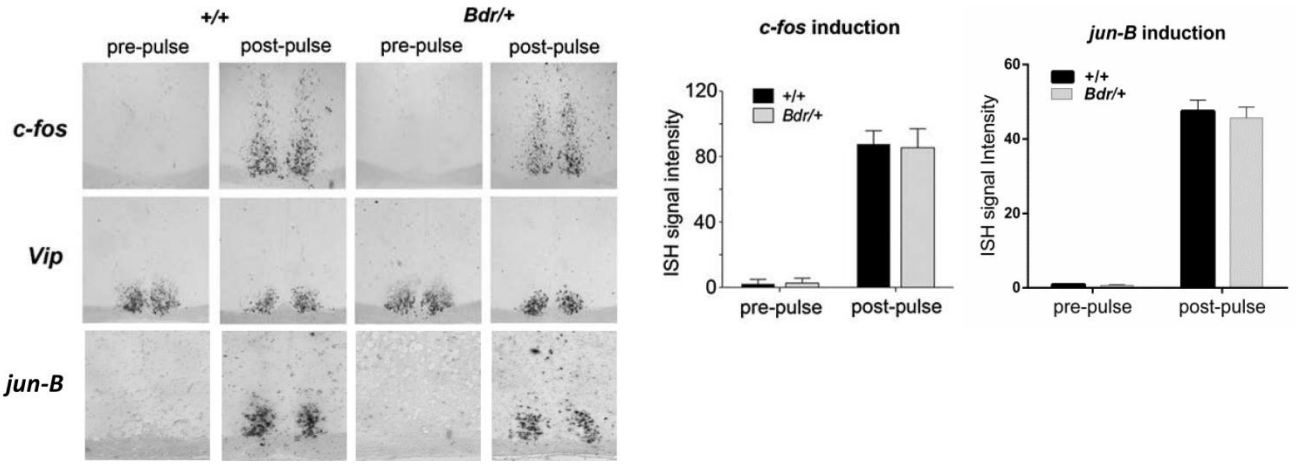

Figure 5.4: Representative high magnification ISH SCN images of *c-fos* and *jun-B* pre-pulse and post-pulse after 30 minutes 150 lux light pulse at ZT16 in WT versus *Bdr*. IEGs show induction in both genotypes, while *VIP* remains unaltered in pre-pulse and post-pulse conditions. Quantification of *c-fos* and *jun-B* levels pre-pulse and post-pulse in WT and *Bdr* SCN show comparable expression (n= 3-4 per genotype).

ISH data (Figures 5.3 & 5.4) confirm qRT-PCR data (Figure 5.2), suggesting the absence of any deleterious effect on the light input pathways in *Bdr* mice. Period genes were not investigated via ISH. Next, investigation of SCN protein expression levels via mass spectrometry was undertaken. The aim was to identify proteins under circadian control de-regulated in the *Bdr*.

5.4.2 SCN proteomics-MS optimisation

A range of molecular experiments have reported the significance of the post-transcriptional rhythms in endogenous circadian homeostasis (Deery *et al*., 2009; Tian *et al*., 2011; McGlincy *et al*., 2012; Lee *et al*., 2013; Robles *et al*., 2014; Mauvoisin *et al*., 2014). The first aim was to optimise the yield and nature of neuropeptidome/proteome extracted from SCN tissue punches using a set of alternative reagents and methodologies. Single 1mm and 2mm SCN tissue punches from WT mice were acquired and peptidome/proteome extracted using different chaotropic agents and detergents (CHAPS, Lauryl Maltoside, Invitrosol, Urea) (Figure 5.5). A gel-free MS-based method was utilised due to straightforward sample handling and superior proteome coverage (English *et al*., 2011). Size-exclusion ultrafiltration using 10kDa centrifugal filters was utilised for separating the endogenous peptidome from the proteome (Lee *et al*., 2013). SCN specific spatio-temporal controls could then be quantified using the endogenous peptidome.

Figure 5.5: Proteomic yield of alternative buffers and increasing tissue quantity

A

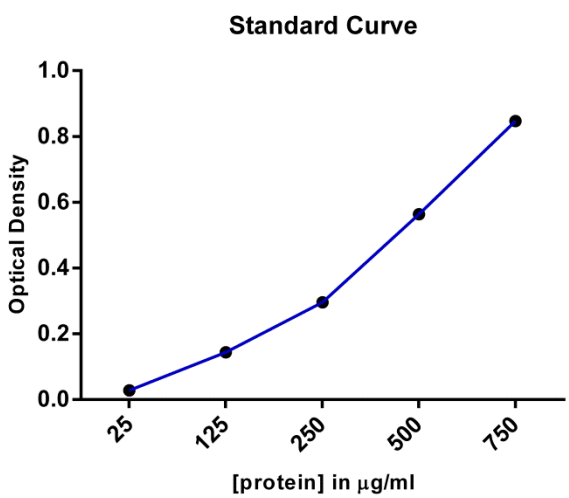

B

Buffer	Tissue Quantity	Optical Density	[Protein] µg/ul
Maltoside (1%-4%)	1mm-2mm	0.2-0.32	125-250
Urea (8M)	1mm-2mm	0.18-0.28	125-250
Invitrosol (1x)	1mm-2mm	0.2-0.29	125-250
CHAPS (1%-4%)	1mm-2mm	0.16-0.29	125-250

Figure 5.5: (**A**) Representative Optical Density/Concentration standard curve of increasing albumin (BSA) standards (**B**) Optimisation table reporting [Protein] under alternative buffer concentrations and SCN tissue quantity in order to discover the optimal reagent in the extraction/MS compatibility ratio. Absorbance data suggest that tissue quantity represents the limiting factor for quantitative efficiency of protein extraction. However, MS data suggest that buffer type represents the limiting factor for qualitative efficiency of protein extraction (Table 5.1, Figure 5.6).

A starting [protein] of around 0.6 mg/ml – 1 mg/ml (sample initially diluted in a 1:5 ratio) for a 1mm SCN tissue punch was generated (Figure 5.5). Alternative buffers did not seem to generate any significant increase in terms of extraction efficiency (tissue quantity and not buffer type was the limiting factor) and therefore 8M Urea was selected due to its MS compatibility under a label-free quantification approach. Moreover, Urea has been previously utilised in similar SCN proteomic studies (Deery *et al*., 2009; Robles *et al*., 2014;

Mauvoisin *et al*., 2014). MS studies on the effect of alternative buffers on the SCN peptidome/proteome were conducted, further validating the selection of Urea buffer (Table 5.1, Figure 5.6). Single 1mm WT SCN tissue punches were subjected to protein extraction using 8M Urea, 1% Lauryl Maltoside and 1X Invitrosol. The samples were subsequently fractionated (between below and above 10kDa) using 10kDa centrifugal filters. Neuropeptide targets such as secretogranin-2 and proenkephalin-A suggested that the 8M Urea buffer was most appropriate to this investigation (Table 5.1, Figure 5.6).

Table 5.1: Neuropeptides identified from 1mm WT SCN tissue punch via label-free MS/MS

Peptide	Observed m/z	Sequence
Proenkephalin-A	1385.67	SPQLEDEAKELQ
Secretogranin-2	1040.55	PELLNTNQL
	1157.52	SGQLGLPDEEN
	1382.7	IPVGSLKNEDTPN
Vascular endothelial cadherin	729.35	AGPNFPQ
Somatostatin-28	1243.56	SANSNPAMAPRE
Neurogenic locus notch homolog protein 1	1462.58	MSAMAPTPPQGEVD
	1504.93	GVLLSRKRRRQH
Brain-specific angiogenesis inhibitor-1 associated protein 2	1565.75	ASESQGSKELGDVLF
Somatostatin precursor	1243.56	SANSNPAMAPRE
	1414.81	KSLAAATGKQELAK
Multi-sensor signal transduction histidine kinase	525.2	GAEYS
	1682.88	VCPNDIGLVMIDAPKV
Bifunctional sulphur carrier protein/thiazole synthase protein	1710.96	SVADLVRSLELDPAKV
Cocaine-and amphetamine-regulated transcript protein	1951.12	APGAMLQIEALQEVLKKL
	2166.25	APGAMLQIEALQEVLKKLKS
Macrophage migration inhibitory factor	2886.5	PMFIVNTNVPRASVPEGFLSELTQQL
Calmodulin	1773.81	GQVNYEEFVQMMTAK
Peptidyl-prolyl cis-trans isomerase A	2338.15	VNPTVFFDITADDEPLGRVSF
	2727.34	VNPTVFFDITADDEPLGRVSFELF
ProSAAS	1812	SLSAASAPLVETSTPLRL
	2531.31	GEAAGAVQELARALAHLLEAERQE
	2954.57	AVPRGEAAGAVQELARALAHLLEAERQE
Corticotropin-releasing factor-binding protein	2432.27	RYLEVQEAAVYDPLLLFSANL

Table 5.1: Representative Neuropeptides identified in the below 10kDa SCN, the sequence ID and their observed MW. In **red** 8M Urea samples, in **green** the 1X Invitrosol samples, in **orange** the 1% Lauryl Maltoside samples and in **blue** overlap in hits for both Invitrosol (**green**) and Maltoside (**orange**) samples.

A range of neuropeptides (Proenkephalin-A, Somatostatin) were identified in the below 10kDa fraction using the 8M Urea (Table 5.1, Figure 5.6). Additionally, secretogranin-2 has been implicated in sorting neuroendocrine secretory factors, a mechanism potentially important when examining synaptic mutants like the *Bdr* model (Table 5.1). Optimisation studies were focused on the endogenous peptidome as the amount of SCN tissue available was not limiting for detection of the above 10kDa (proteome) abundance. Numerous targets identified (Table 5.1) overlap with previous literature reports of SCN proteomics, suggesting that tissue punches were accurately taken and subsequently protein extracted (e.g. ProSAAS, Proenkephalin-A, Somatostatin) (Hatcher *et al*., 2008; Bora *et al*., 2008; Lee *et al.,* 2010; Lee *et al*., 2013). Alternative buffers including organic compounds (acetic acid and acidified acetone) and heat treatments were also tested but did not yield any significant improvement in the number of proteins identified (similar targets were detected). Organic compounds are more suitable for neuropeptide extraction when tissue quantity is not a limiting factor (Bora *et al*., 2008). However, proteomic extraction was the main focus of this investigation and therefore these compounds were excluded as potential buffers.

Figure 5.6: Representative SCN neuropeptides extracted from different buffers

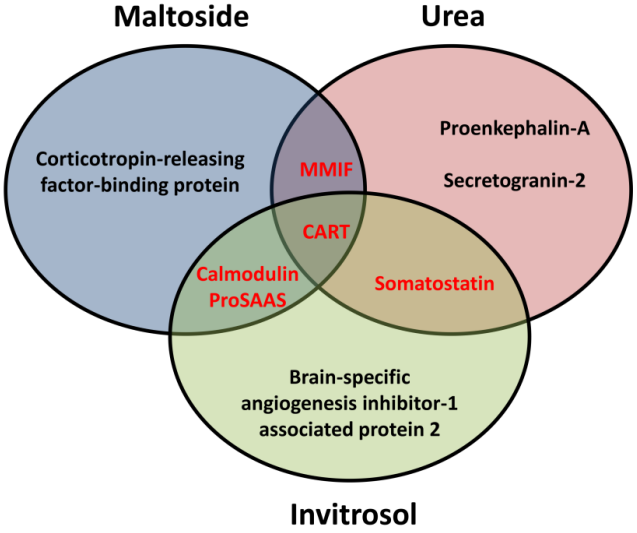

Figure 5.6: Venn diagram illustrating Urea, Maltoside and Invitrosol buffers and corresponding SCN neuropeptides identified. Further abbreviations–MMIF: Macrophage Migration Inhibitory Factor, CART: Cocaine-and Amphetamine-Regulated Transcript Protein.

5.4.3 SCN proteomics-MS data

A comparative proteomic LD screen (every 4hr) between WT and *Bdr* SCN was conducted using label-free MS/MS. MS quantitation of endogenous neuropeptides yielded roughly 70 endogenous peptides (below 10kDa targets) while over 2000 proteins (above 10kDa targets) were identified with our methodology (ten pooled SCNs per genotype per ZT- see Methods/Proteomic 24hr circadian molecular profiling section). Data generated were reported in an ion intensity map (Figure 5.7) where the peptide features were identified using Mascot and chromatographically aligned and quantified using Progenesis LC-MS.

Figure 5.7: Representative SCN ion intensity map

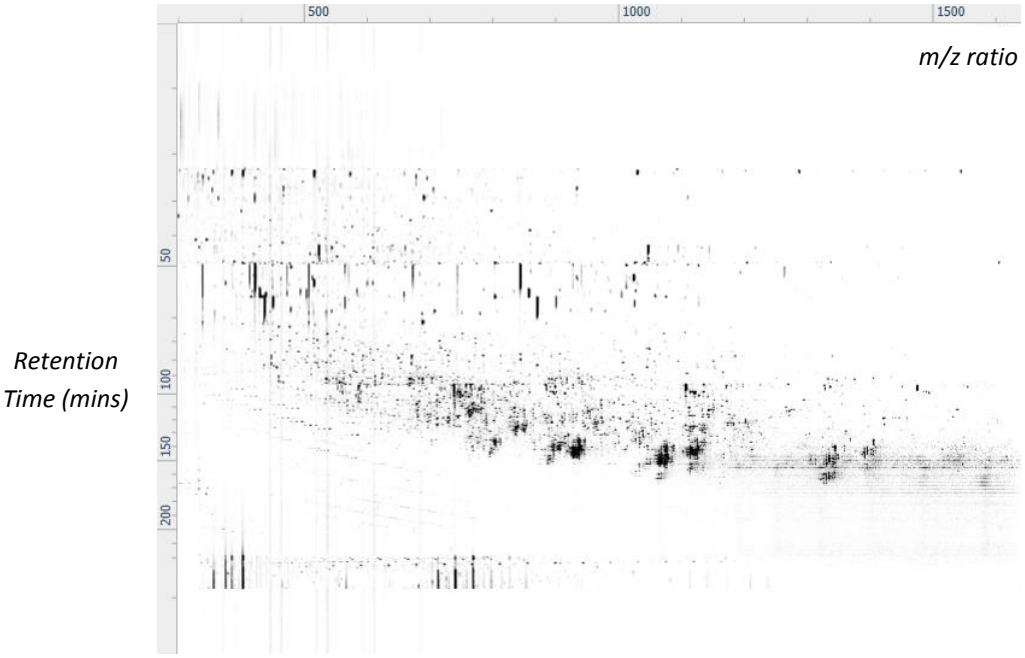

Figure 5.7: Ion intensity map resolved along m/z ratio x-axis and chromatographic retention time (minutes) y-axis.

A reference map was selected and all chromatograms were aligned and fitted to the reference dataset by Progenesis LC-MS. This was conducted separately for the proteomic (above 10kDa) dataset (technical duplicates) and the peptidomic (below 10kDa) dataset (no replicates).

5.4.4 SCN proteomics-MS analysis

Alignment and Normalisation of 2D ion intensity maps: A single reference ion intensity map is selected to align the remaining runs (the process can be repeated with different reference runs to cross-validate findings). This allows for calibration of data between different samples. Peptide ions between runs are often aligned to middle runs to account for retention time drifts. Additionally, a normalisation factor is selected using the quantitative abundance ratio between the reference run and the normalised run. The normalisation factor is then calculated from the mean of the upper and lower robust estimation limits, which are deduced from the median of the logarithmic abundance ratio of the up-regulated and down-regulated features respectively. In summary, this aids in the minimisation of experimental variation between samples and allows for the generation of comparative graphs.

Quantitation and Identification: Protein abundance is calculated from the sum of all unique normalised abundances for a specific protein on each run (Figure 5.8). Alignment and co-detection of features mean that the same number of quantified peptides is maintained across all runs so the sum of ion abundances between groups can be compared.

Figure 5.8: Quantification Protocol by Progenesis LC-MS

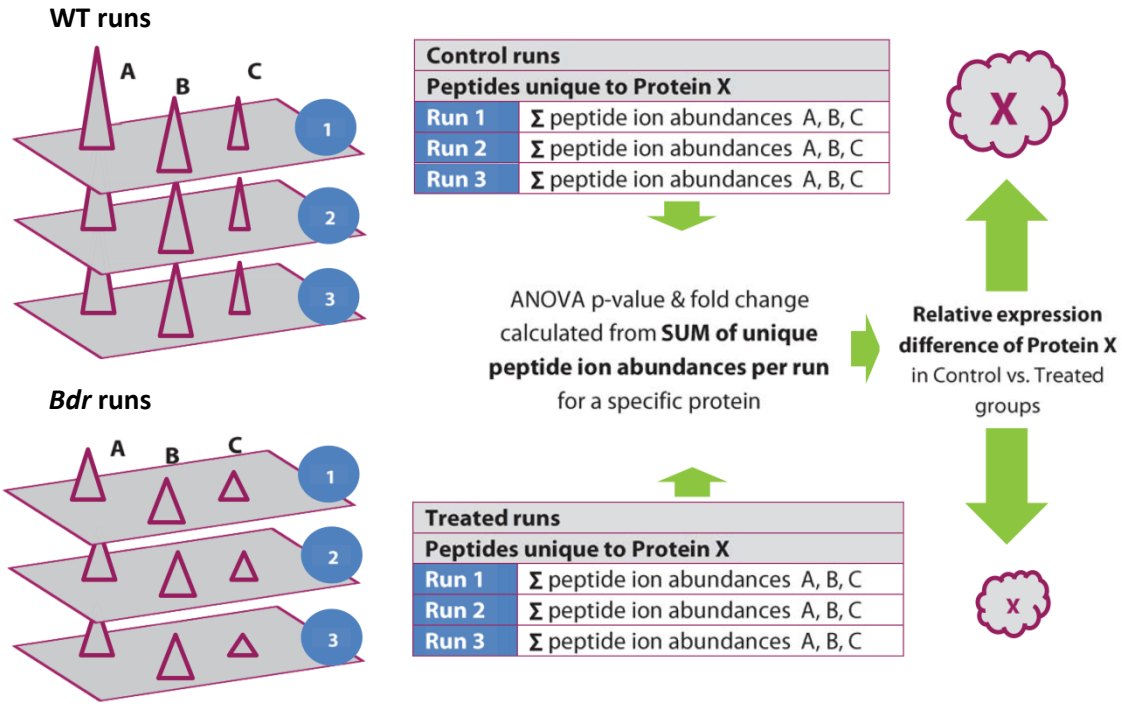

Figure 5.8: Co-detection of features in WT versus *Bdr* runs is presented on the left hand side. Summing unique peptide ion abundances for each run to a final confidence value makes the protein quantitation more reliable as higher signal peptides have greater influence upon the final value (middle and right hand side). Common peptides between proteins are removed from the final protein quantitation as unique peptides only are used for quantitation.

Additionally, spectral counts (or peptide counts) quantitation, defined as the total number of spectra identified for a protein, was utilised due to the complexity and experimental design of the proteomic screen. Spectral counting is heavily dependent on peptide identification. As such, filtering criteria prior to peptide counting can influence the final spectral values. Mascot cutoff score was set to 30 as default standard. Identified proteins with at least two unique peptides and presence in both technical replicas were preserved.

Although quantitation by MS intensity out-performs spectral counting, it relies heavily on a high degree of retention time alignment for confident quantitation. Some errors derived from ion intensity misalignment can be partially cross-checked using spectral counts (semi-quantitative) (Lundgren *et al*., 2010). Therefore, utilising a combined approach between MS ion intensity and spectral counting is considered practical in the analysis of experimentally challenging datasets (Zhu *et al*., 2010; Lundgren *et al*., 2010).

Grouping protein patterns: Protein data can then be subsequently categorised in dendograms (a visual representation of correlation data) and the lower the dendogram value, the greater the correlation (Figure 5.9A). Highly correlated expression clusters belong at the bottom of the dendogram data cluster (e.g. highlighted protein cluster in red-Figure 5.9A). Additionally, highly correlated clusters display similar abundance profiles (Figure 5.9B), while low correlated clusters belong at the top of the dendogram and show dissimilar abundance profiles. This approach is particularly useful for identifying protein groups with characteristic expression patterns across the 24h period. Additionally, validated targets that belong to particular protein clusters can be compared to other similarly phased candidates based on their dendogram value.

Figure 5.9: Dendogram profile of Proteins

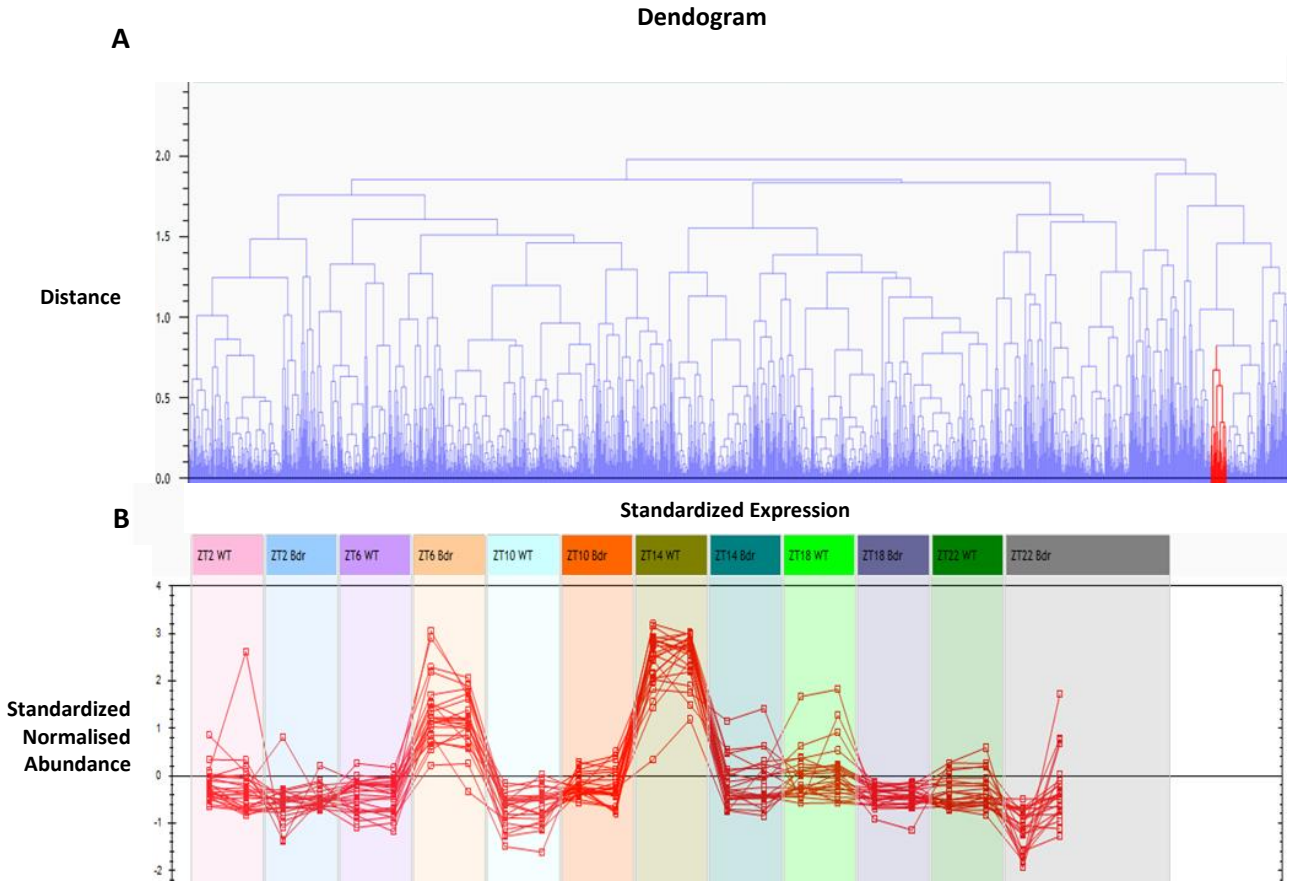

Figure 5.9: (**A**) Global proteomic dendogram profile. Highlighted in red is a particular protein cluster (**B**) Subsequent standardized expression pattern of the highlighted protein cluster illustrating up-regulation of proteins at ZT6 *Bdr* and ZT14 WT.

Therefore, the main criteria for selecting candidate proteins for further investigation were:

- Significant fold change between WT and *Bdr* at a single timepoint (minimum of 3-fold change).
- Confident quantification of specific candidates (illustrated by the confidence values).
- Phase advanced rhythmic pattern of *Bdr* proteins that corresponds to previous wheel-running data.

- Functional role in synaptic trafficking mechanisms, circadian and/or disease biomarkers.
- Selecting candidates with peptide counts of 10-30. Validation via IHC/WB might be challenging for low abundant targets (below 10 peptides), due to the lower MS quantification confidence, whereas highly abundant targets might saturate the signal without producing any detectable differences (above 30 peptides) (Hauck *et al*., 2010).
- Selecting candidates that display maximum expression in underloaded runs from the dataset. This would suggest that if all runs were equally loaded the selected candidate would still represent the expression peak of the dataset.
- Selecting candidates with highly correlated protein abundance and spectral count values for additional confidence.
- Selecting candidates that display similar expression profiles independent of the original alignment reference run. Therefore, repeat analysis with different alignment references and identify targets that maintain their rhythmicity across all analysis rounds.

Initially, to confirm that the tissue punches were anatomically correct and that the lighting conditions prior to tissue collection were set correctly, MS data were mined for neuropeptides and proteins with known circadian fluctuations in the SCN (Table 5.2, Figure 5.10).

Table 5.2: MS data table of proteomic WT spatio-temporal controls

Description	Peptide count	Peptides used in quantitation	Confidence	ANOVA (p)	Max fold change	Highest mean condition	Lowest mean condition
Alpha-enolase	47	38	3872	5.95E-07	2.57	ZT2 WT	ZT10 WT
Fructose-bisphosphate aldolase A	35	32	2781	9.56E-09	7.92	ZT14 WT	ZT10 WT
Gamma-enolase	38	29	3353	4.13E-05	2.47	ZT2 WT	ZT10 WT
14-3-3 protein zeta/delta	33	21	2360	3.37E-06	2.52	ZT2 WT	ZT10 WT
Fructose-bisphosphate aldolase C	23	19	1693	3.33E-07	4.06	ZT14 WT	ZT10 WT
Beta-soluble NSF attachment protein	26	22	1567	0.009279	2.11	ZT14 WT	ZT6 WT
Heat shock 70kDa protein 12A	14	13	957	5.18E-05	4.14	ZT2 WT	ZT14 WT
Stress-induced-phosphoprotein 1	5	4	311	3.04E-06	3.71	ZT14 WT	ZT22 WT
Proteasome subunit alpha type-6	2	2	174	0.000296	15.64	ZT10 WT	ZT14 WT

Table 5.2: Spatio-temporal WT proteomic controls confirmed by Deery *et al*., 2009. Table displays the peptide count (total number of peptides identified per protein), peptides used in quantitation, the overall identification confidence value, ANOVA (p-value) and the maximum fold change between highest and lowest mean condition. Confidence values represent the sum of all peptide mascot identification values per protein.

Figure 5.10: WT SCN spatio-temporal controls quantified over 24h

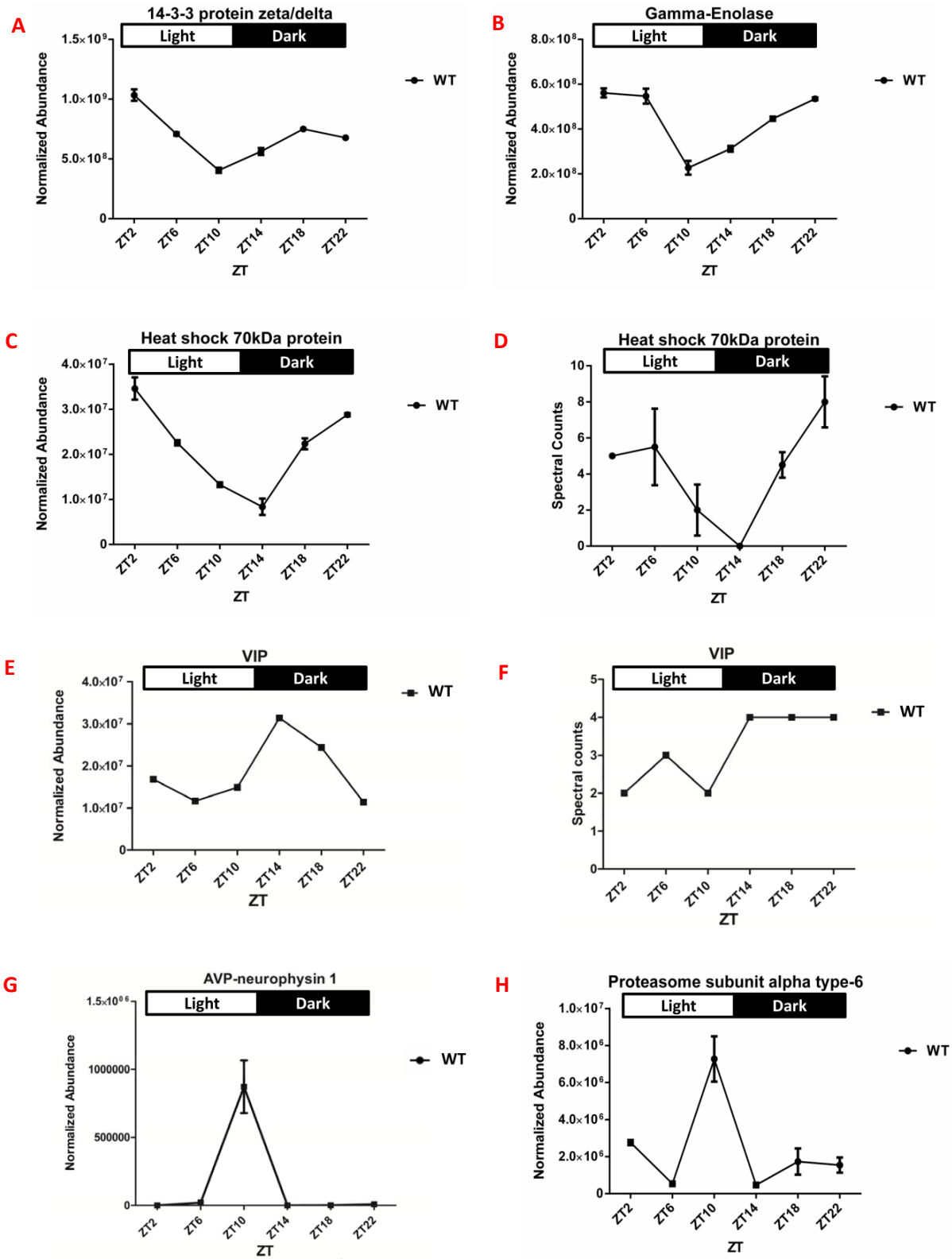

Figure 5.10: (**A**) MS WT SCN 14-3-3 protein zeta/delta normalised abundance across an LD cycle (**B**) MS WT SCN Enolase normalised abundance across an LD cycle (**C, D**) MS WT SCN Heat shock 70kDa protein normalised abundance and spectral counts across an LD cycle (**E, F**) MS WT VIP normalised abundance and spectral counts across an LD cycle (**G**) MS WT SCN AVP-neurophysin 1 normalised abundance across an LD cycle (**H**) MS WT SCN Proteasome subunit normalised abundance across an LD cycle. Data plotted as mean ± SEM (Bessel's correction (n-1) applied due to small sample sizes).

Previously published protein expression studies confirm the WT control data generated in this work (Ban *et al*, 1997; Hatcher *et al*., 2008; Deery *et al*., 2009; Oliver *et al*., 2012). For example, WT Vasoactive intestinal peptide (VIP) shows an up-regulation during the night-time period (Ban *et al*., 1997; Cayetanot *et al*., 2005) and WT AVP neuropeptides detected via MS follow the expression pattern previously published by our own group as well as independent MS studies (Figure 5.10) (Hatcher *et al*., 2008; Oliver *et al*., 2012). Importantly, there is positive correlation between spectral counting and ion abundance (Pearson correlation coefficient= 0.7; for *Bdr* and WT samples). In addition, identical phase of expression patterns were observed between our MS-generated data and previously published SCN proteomic data via 2D gels (enolase, proteasome subunit) (Deery *et al*., 2009).

However, some targets with 24 hour profiles that did not overlap with previously published reports were also recorded (Figure 5.11, Table 5.3). Septin 11 and alpha neurexin show some expression differences when compared to previously published reports (Deery *et al*., 2009). Protein fragmentation, due to MS, and multiple isoforms (e.g. alpha/beta/gamma-soluble NSF attachment protein) could alter expression patterns for specific targets across an LD cycle (Figure 5.11). This post-transcriptional complexity in the SCN has been previously identified as an important regulatory mechanism in diurnal rhythms (Deery *et al*., 2009). A limitation of MS quantitation is poor isoform differentiation which may lead to some non-overlapping targets when compared to other proteomic platforms (English *et al*., 2011). For example, the beta-soluble NSF attachment protein isoform shows overlap with other protemic studies while the alpha/gamma isoforms exhibit no such correlation (Figure 5.11) (Deery *et al*., 2009).

Figure 5.11: WT SCN non-overlapping targets versus control

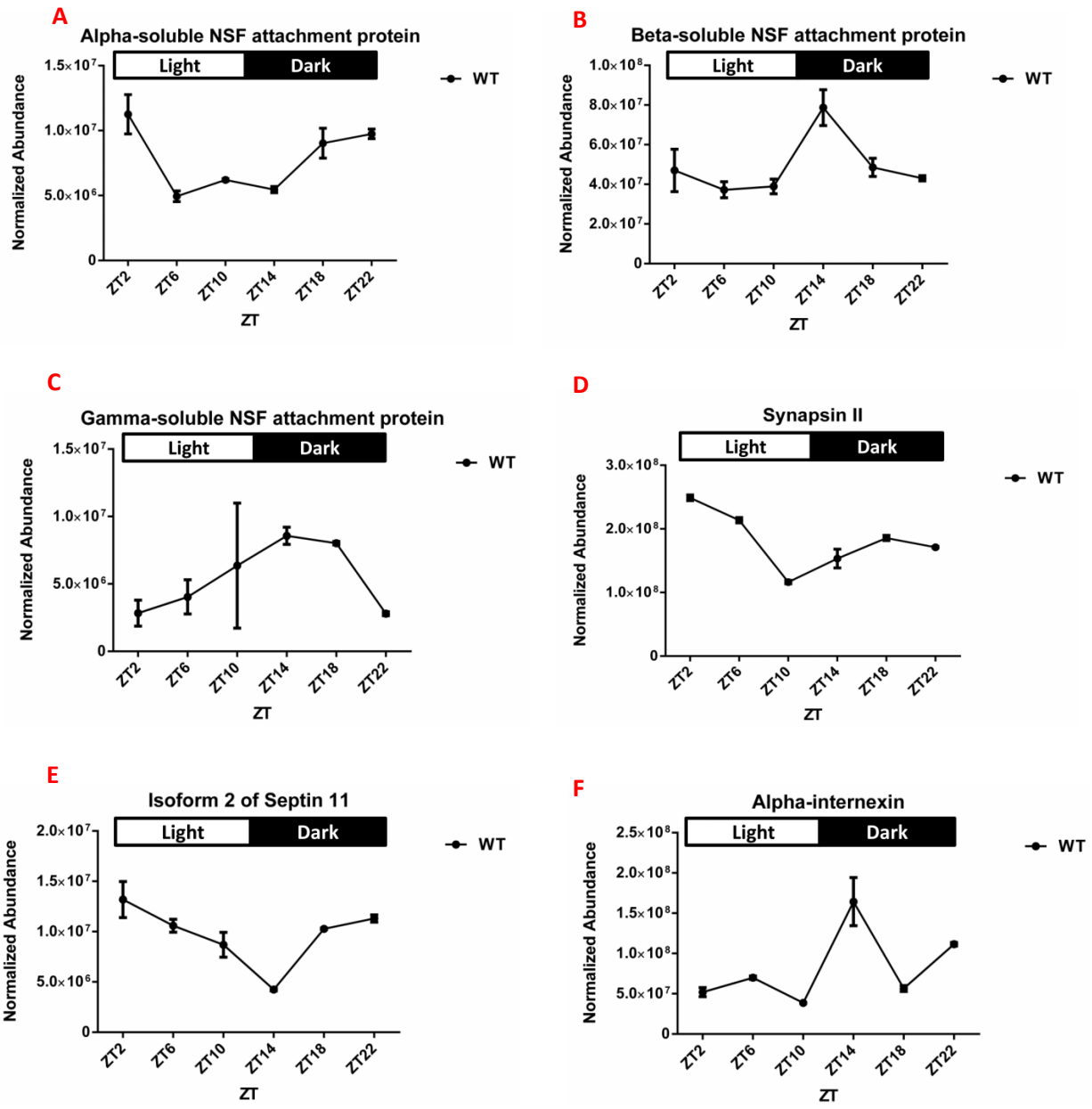

Figure 5.11: (**A**) MS WT SCN alpha-soluble NSF attachment protein normalised abundance across an LD cycle (**B**) MS WT SCN beta-soluble NSF attachment protein normalised abundance across an LD cycle (**C**) MS WT SCN gamma-soluble NSF attachment protein normalised abundance across an LD cycle (**D**) MS WT SCN synapsin II normalised abundance across an LD cycle (**E**) MS WT SCN isoform 2 of septin 11 normalised abundance across an LD cycle (**F**) MS WT SCN alpha-internexin normalised abundance across an LD cycle. Data plotted as mean ± SEM (Bessel's correction (n-1) applied due to small sample sizes).

Note: Only the Beta-soluble NSF attachment protein (control) shows similar expression data with other studies (Table 5.2; Deery *et al.*, 2009). All other isoforms do not overlap (Table 5.3).

Table 5.3: WT SCN non-overlapping proteomic targets

Description	Peptide count	Peptides used in quantitation	Confidence	ANOVA (p)	Max fold change	Highest mean condition	Lowest mean condition
Alpha-soluble NSF attachment protein	9	5	475	0.000335	2.28	ZT2 WT	ZT6 WT
Gamma-soluble NSF attachment protein	6	6	296	0.083322	3.07	ZT14 WT	ZT22 WT
Synapsin II	23	18	1668	2.35E-05	2.14	ZT2 WT	ZT10 WT
Isoform 2 of Septin 11	10	6	607	0.000125	3.11	ZT2 WT	ZT14 WT
Alpha-internexin	24	19	1471	3.49E-05	4.26	ZT14 WT	ZT10 WT

Table 5.3: Non-overlapping WT targets when compared to Deery *et al*., 2009. Table displays the peptide count (total number of peptides identified per protein), peptides used in quantitation, the overall identification confidence value, ANOVA (p-value) and the maximum fold change between highest and lowest mean condition. Confidence values represent the sum of all peptide mascot identification values per protein.

Next, the MS data obtained from both *Bdr* and WT SCNs was compared to identify differentially expressed proteins. Interestingly, previous microarray SCN data have suggested potential de-synchrony in WT versus *Bdr* for *Tac1* at ZT6 (Oliver *et al*., 2012). A similar variation at the peptide level is recorded via this screen. Importantly, temporal de-synchrony is detected in Tac1 with abundance peaks different between WT (ZT10) and *Bdr* (ZT6) (Figure 5.12). That would be consistent with disruption of critical output signalling in the *Bdr* (Oliver *et al*., 2012). Similarly, aldolase A represents a significant spatio-temporal control in the WT SCN (Deery *et al*., 2009) that shows potential de-synchrony in the *Bdr* model (Figure 5.12).

Figure 5.12: WT/*Bdr* SCN spatio-temporal controls quantified over 24hr

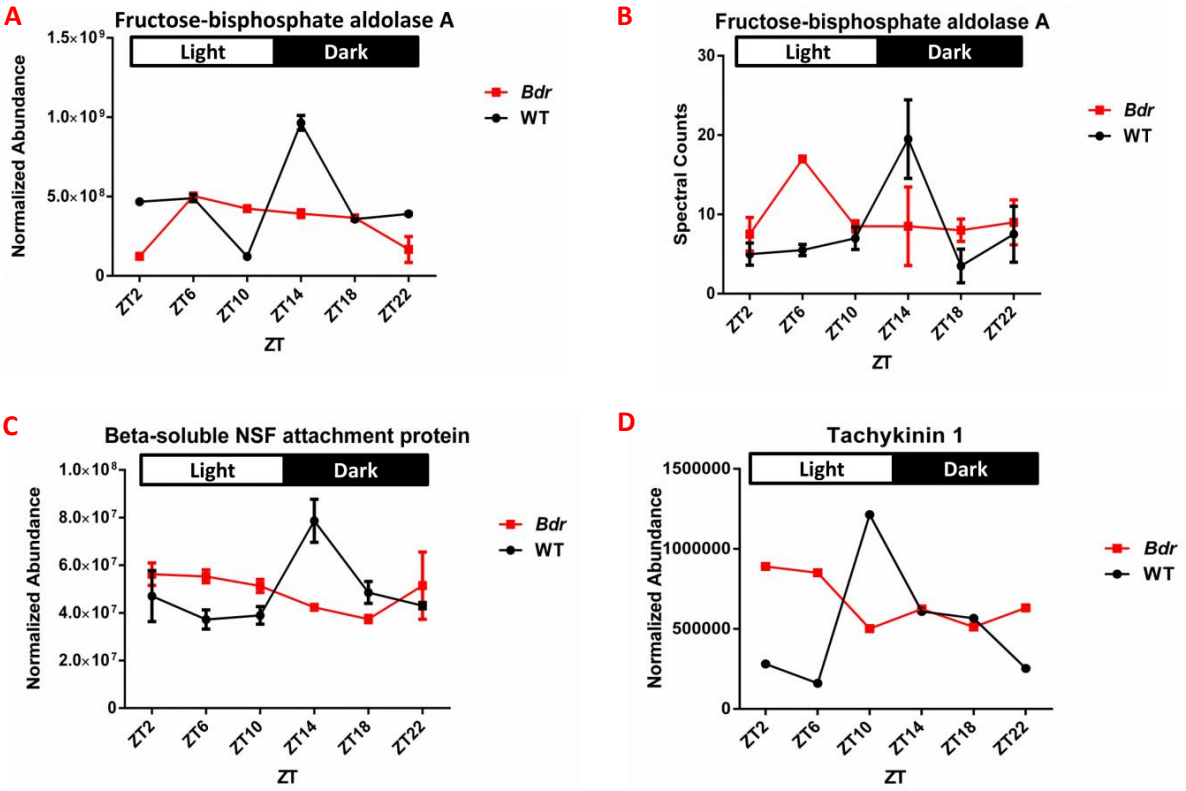

Figure 5.12: (**A, B**) MS WT and *Bdr* SCN Fructose-bisphosphate aldolase A normalised abundance and spectral counts across an LD cycle (**C**) MS WT and *Bdr* SCN Beta-soluble NSF attachment protein normalised abundance across an LD cycle (**D**) MS WT and *Bdr* Tachykinin 1 normalised abundance across an LD cycle. Data plotted as mean ± SEM (Bessel's correction (n-1) applied due to small sample sizes).

Beta-soluble NSF attachment protein is an important WT spatio-temporal control in the SCN with a peak at ZT14 (Figure 5.12; Deery *et al*., 2009) and shows some potential differential expression in the *Bdr*. Interestingly, possible temporal differences in metabolic proteins (Figure 5.12) previously unidentified via a microarray could potentially suggest a wider network de-regulation in the *Bdr*. Therefore, a list of targets temporally de-regulated targets was constructed when significance was achieved in ion intensity values (Tables 5.4, 5.5 and 5.6). Normalised protein abundance graphs and raw spectral count graphs of specific de-regulated targets were subsequently generated (Figure 5.14).

Table 5.4: MS data table of potentially de-regulated endogenous peptidomic targets

Description	Peptide count	Peptides used in quantitation	Confidence	Max fold change	Highest mean condition	Lowest mean condition
Secretogranin-2	12	12	772	6.17	ZT2 *Bdr*	ZT10 WT
Proprotein convertase subtilisin/kexin type 1 inhibitor	11	11	611	28.29	ZT2 *Bdr*	ZT10 *Bdr*
Proenkephalin-A	8	8	349	5.94	ZT2 *Bdr*	ZT6 *Bdr*
Secretogranin-1	6	6	317	32.97	ZT2 *Bdr*	ZT6 *Bdr*
Prothyroliberin	6	6	253	7861.47	ZT2 *Bdr*	ZT6 *Bdr*
Chromogranin-A	5	5	171	112.19	ZT2 WT	ZT6 *Bdr*
Proprotein convertase subtilisin/kexin type 1	3	3	114	3.62	ZT10 *Bdr*	ZT2 *Bdr*
Somatostatin	3	3	158	7.87	ZT6 *Bdr*	ZT22 *Bdr*
Tachykinin 1	2	2	100	7.54	ZT10 WT	ZT6 WT

Table 5.4: Potentially de-regulated endogenous peptidomic candidates. Peptidomic SCN targets reveal a more extensive de-regulation in the *Bdr* that was previously undetected.

Figure 5.13: Representative Prothyroliberin peptide in ion intensity maps

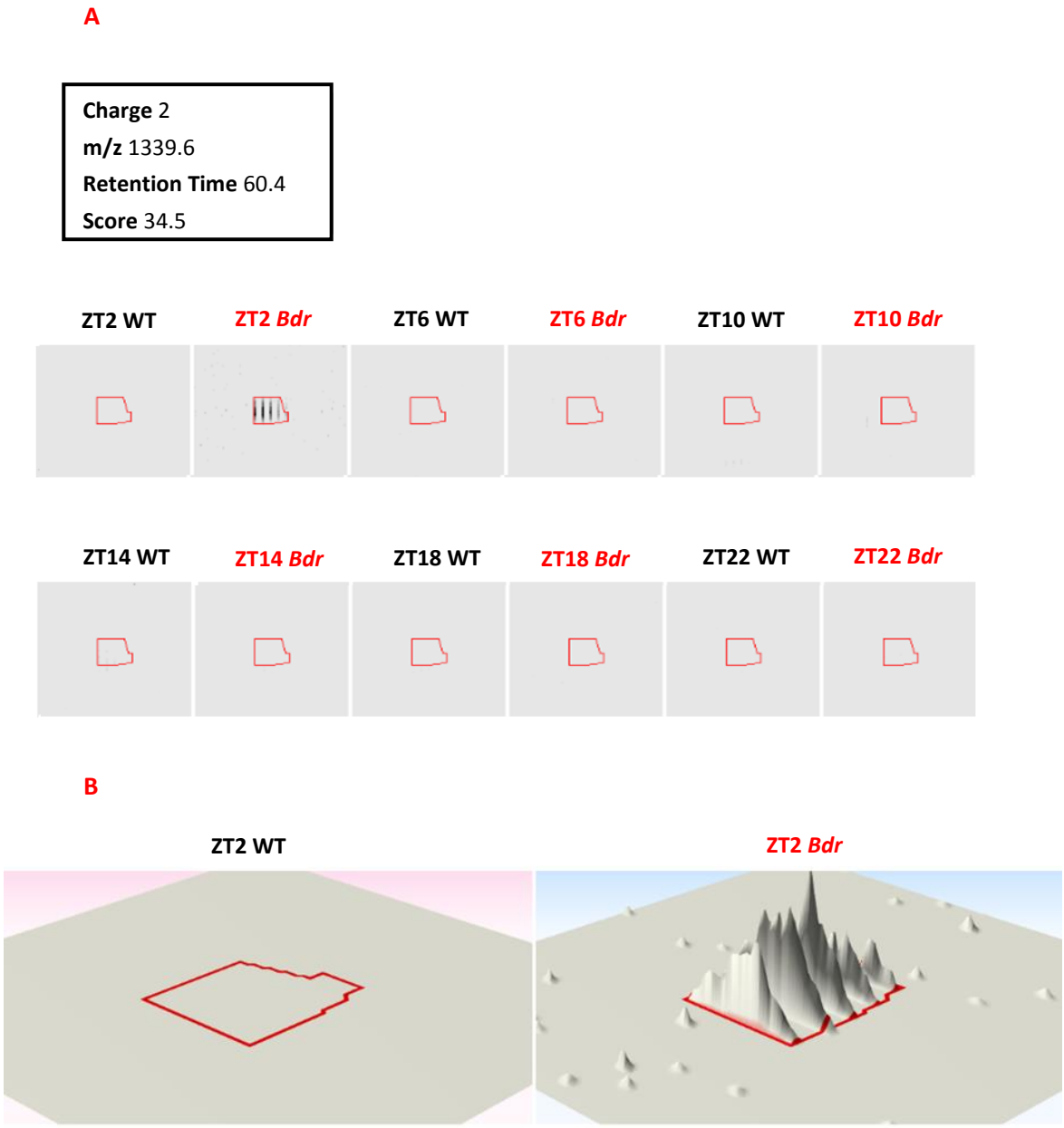

Figure 5.13: (**A**) Prothyroliberin SCN peptide displaying temporal up-regulation in *Bdr* versus *WT* in the light phase. The peptide achieved a confident identification score (34.5) (**B**) 3D image of ion intensity maps displaying up-regulation of prothyroliberin at ZT2 *Bdr.*

Our MS data suggest potential metabolic deficits in the *Bdr* model, as illustrated by de-regulated prothyroliberin or thyrotropin-releasing factor (TRF), which is involved in the release of TSH (thyroid-stimulating hormone); a factor that stimulates systemic metabolic processes (Taylor *et al*., 1990; Pierpaoli, 2013).

Table 5.5: MS data table of potentially de-regulated SCN proteomic targets

Description	Peptide count	Peptides used in quantitation	Confidence	ANOVA (p)	Max fold change	Highest mean condition	Lowest mean condition
Alpha-internexin	24	19	1471	3.86E-08	4.62	ZT14 WT	ZT2 *Bdr*
Tenascin-R	19	19	1330	1.01E-06	6.21	ZT2 WT	ZT22*Bdr*
Calmodulin	21	21	1869	4.70E-06	10.25	ZT10 WT	ZT22 *Bdr*
Calretinin	28	27	1886	1.27E-14	10.30	ZT2 *Bdr*	ZT22 *Bdr*
Septin-5	14	13	796	1.99E-05	6.09	ZT14 WT	ZT22 *Bdr*
Peroxiredoxin-2	11	11	794	4.78E-07	8.42	ZT2 WT	ZT22 *Bdr*
Protein kinase C and casein kinase substrate in neurons protein 1	12	12	707	0.035484	2.36	ZT14 WT	ZT6 WT
Isoform 2 of Alpha-synuclein	9	6	746	4.72E-06	11.01	ZT2 *Bdr*	ZT14 *Bdr*
Isoform C of Prelamin-A/C	10	9	625	1.07E-05	4.98	ZT14 WT	ZT6 WT
ProSAAS	8	8	521	0.022904	3.69	ZT14 WT	ZT2 WT

Table 5.5: Potentially de-regulated proteomic candidates. Proteomic SCN targets reveal a more extensive de-regulation in the *Bdr* that was previously undetected.

Figure 5.14: Temporally de-regulated SCN proteomic targets in *Bdr* versus WT

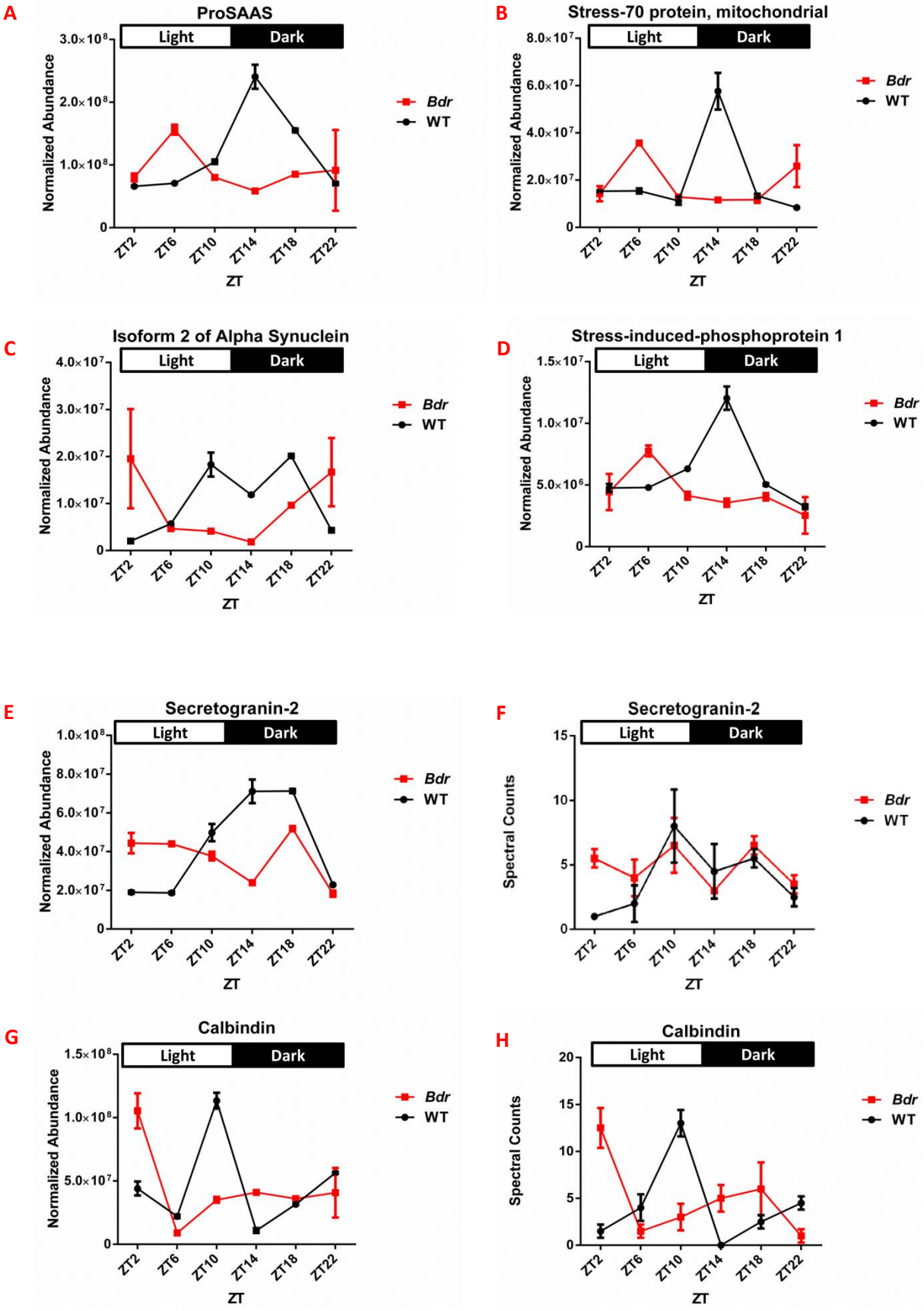

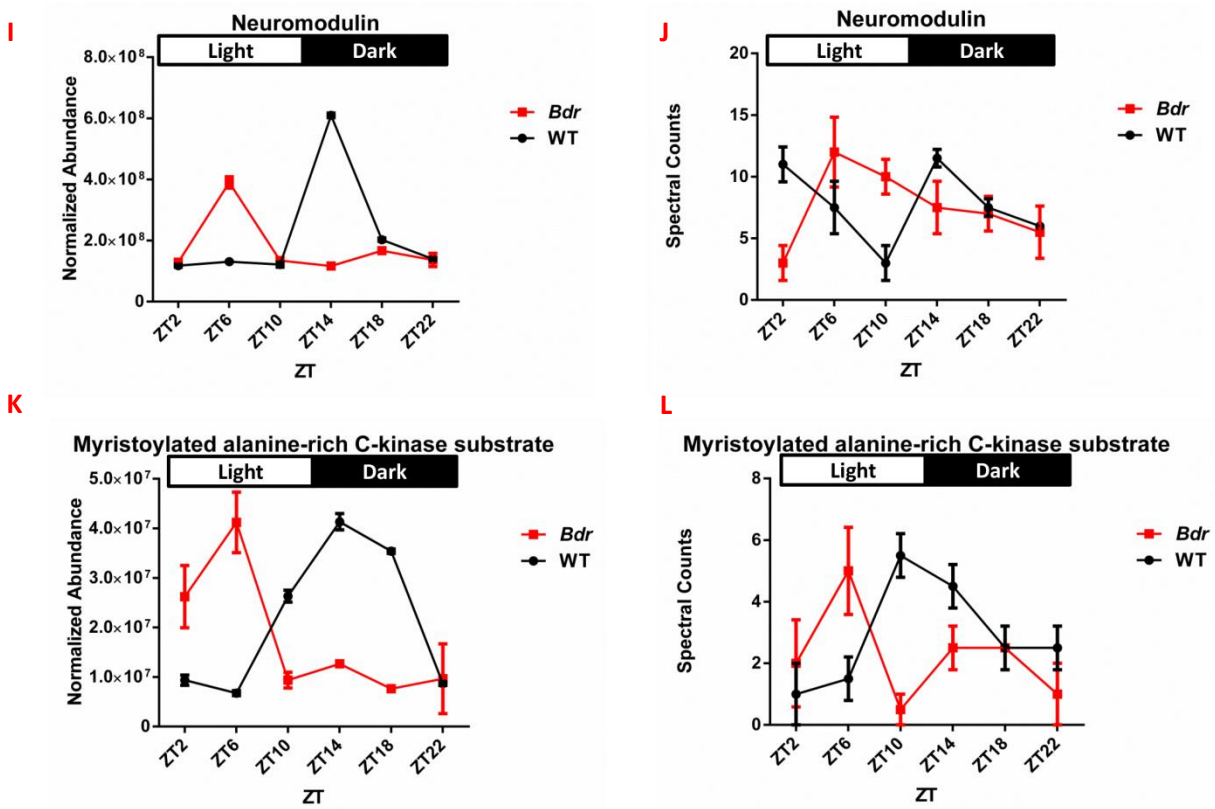

Figure 5.14: (**A**) MS WT and *Bdr* SCN ProSAAS normalised abundance across an LD cycle (**B**) MS WT and *Bdr* SCN Stress-70 protein, mitochondrial normalised abundance across an LD cycle (**C**) MS WT and *Bdr* SCN Isoform 2 of Alpha-Synuclein normalised abundance across an LD cycle (**D**) MS WT and *Bdr* SCN Stress-induced-phosphoprotein 1 normalised abundance across an LD cycle (**E, F**) MS WT and *Bdr* SCN Secretogranin-2 normalised abundance and spectral counts across an LD cycle (**G, H**) MS WT and *Bdr* SCN Calbindin normalised abundance and spectral counts across an LD cycle (**I, J**) MS WT and *Bdr* SCN Neuromodulin/GAP-43 normalised abundance and spectral counts across an LD cycle and (**K, L**) MS WT and *Bdr* SCN Myristoylated alanine-rich C-kinase substrate (MARCKS) normalised abundance and spectral counts across an LD cycle. Data plotted as mean ± SEM (Bessel's correction (n-1) applied due to small sample sizes). ANOVA p-values were calculated between each group (WT vs *Bdr*) using the summed peptide ion abundances.

Temporally de-regulated proteomic targets involved in synaptic trafficking, calcium signalling and neurodevelopment were identified from examining both normalised abundance and spectral counts (Figure 5.14, Table 5.6). Four of these (Secretogranin-2, Calbindin, GAP-43/Neuromodulin and MARCKS) were selected for further analysis and confirmation.

Table 5.6: MS data table of followed-up de-regulated proteomic targets

Description	Peptide count	Peptides used in quantitation	Confidence	ANOVA (p)	Max fold change	Highest mean condition	Lowest mean condition
Secretogranin-2	19	19	1289	8.24E-10	3.82	ZT14 WT	ZT22 *Bdr*
Calbindin	18	17	1270	2.99E-09	10.27	ZT2 *Bdr*	ZT6 *Bdr*
Neuromodulin	25	25	1891	3.02E-10	5.71	ZT14 WT	ZT10 WT
MARCKS	11	11	745	0.000345	12.57	ZT14 WT	ZT6 WT

Table 5.6: Followed-up de-regulated proteomic targets. Table displays the peptide count (total number of peptides identified per protein), peptides used in quantitation, the overall identification confidence value, ANOVA (p-value) and the maximum fold change between highest and lowest mean condition. Confidence values represent the sum of all peptide mascot identification values per protein. ANOVA p-values were calculated between each group (WT vs *Bdr*) using the summed peptide ion abundances.

Four novel potentially de-regulated proteomic targets between *Bdr* and WT SCN were followed-up via IHC. All four (Secretogranin-2, Calbindin, Neuromodulin and MARCKS) targets recorded sufficient (between 10-30 peptide counts per protein) peptides for confident identification and quantitation. Low abundant proteins (below 10 peptides) might not be validated via IHC/WB, due to the lower MS quantification confidence, whereas highly abundant targets might saturate the signal without producing any detectable difference (above 30 peptides) (Hauck *et al*., 2010). Representative isotopic distributions of two different MARCKS peptides following Progenesis LC-MS analysis displayed expression differences between WT and *Bdr* (Figure 5.15).

Figure 5.15: Representative MARCKS peptide in ion intensity maps

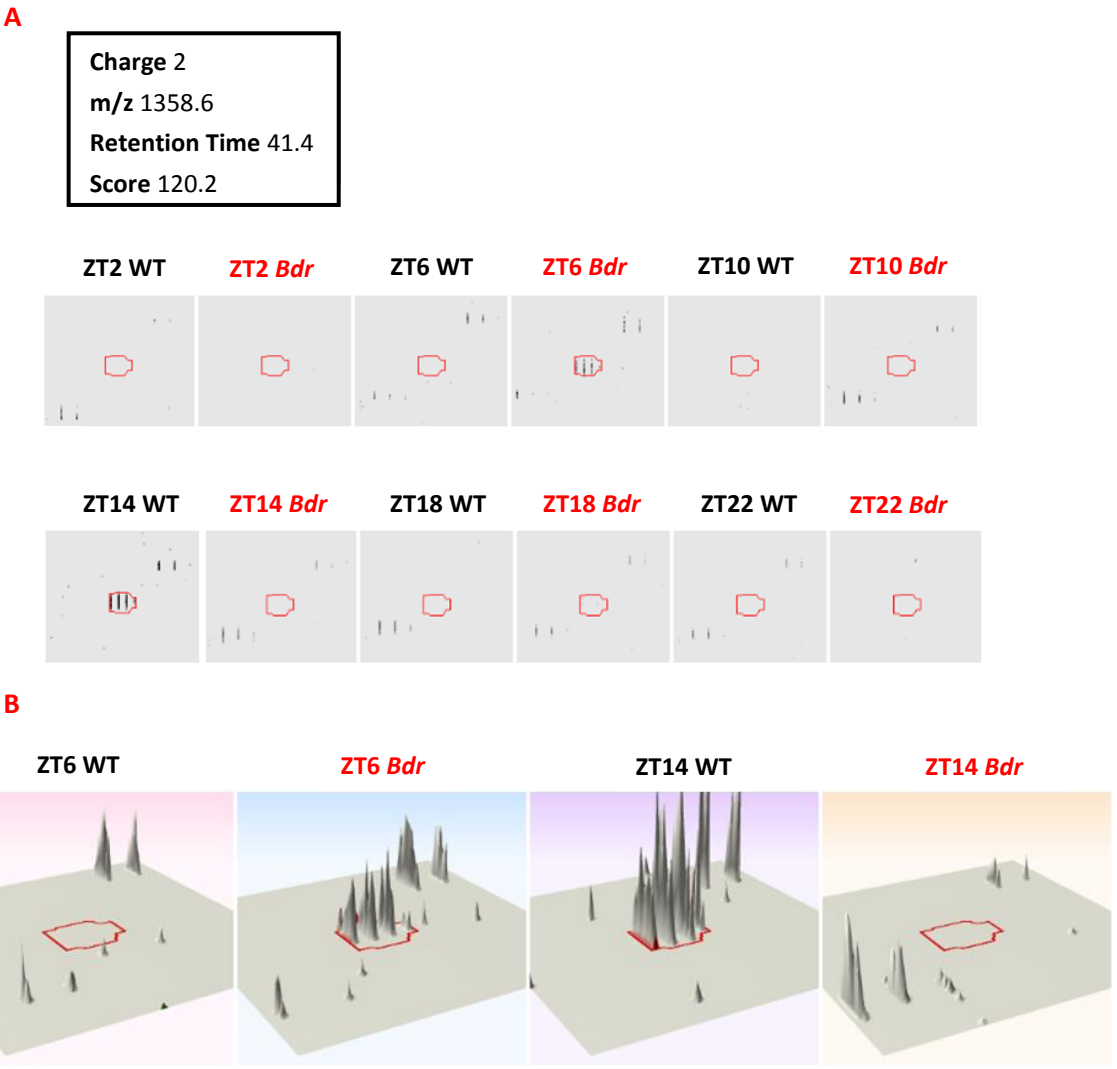

Figure 5.15: MARCKS SCN peptide displaying temporal de-regulation in WT versus *Bdr* in the light and dark phase. The peptide achieved a confident identification score (120.2) (**B**) 3D image of ion intensity maps displaying up-regulation of MARCKS at ZT6 *Bdr* and down-regulation at ZT14.

MARCKS SCN peptide displays temporal de-regulation with a genotype-specific effect (Figure 5.15). The peak areas for quantification were automatically selected following retention drift corrections for each individual sample. However, given the complex data mining process and associated variations introduced via computational methodologies, it was still necessary to confirm these MS findings to avoid false positives.

5.4.5 SCN proteomics-IHC/WB/ELISA validation

Progenesis LC-MS has previously demonstrated a high degree of correlation between MS and IHC/WB data (Abdul-Salam *et al*., 2010; Hauck *et al*., 2010). Therefore, 4 proteomic (Calbindin, MARCKS, Neuromodulin and Secretogranin-2) targets and Tac1/SP (Tachykinin 1/Substance P) (Figure 5.12; similar findings between our MS data and previous microarray results) were further investigated via a 24h IHC/WB screen.

Figure 5.16: IHC SCN confirmation of proteomic de-regulation over 24h in WT versus *Bdr*

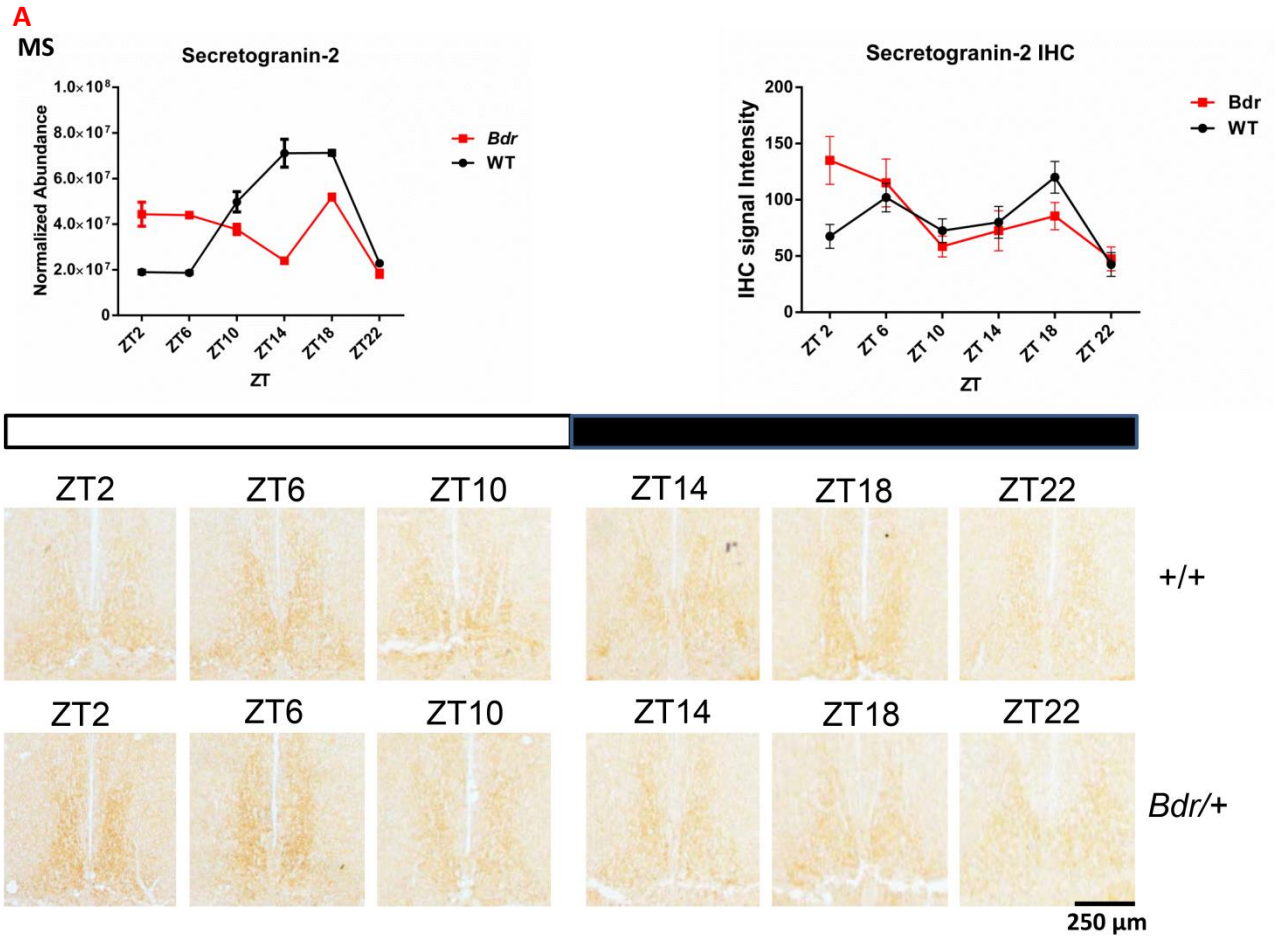

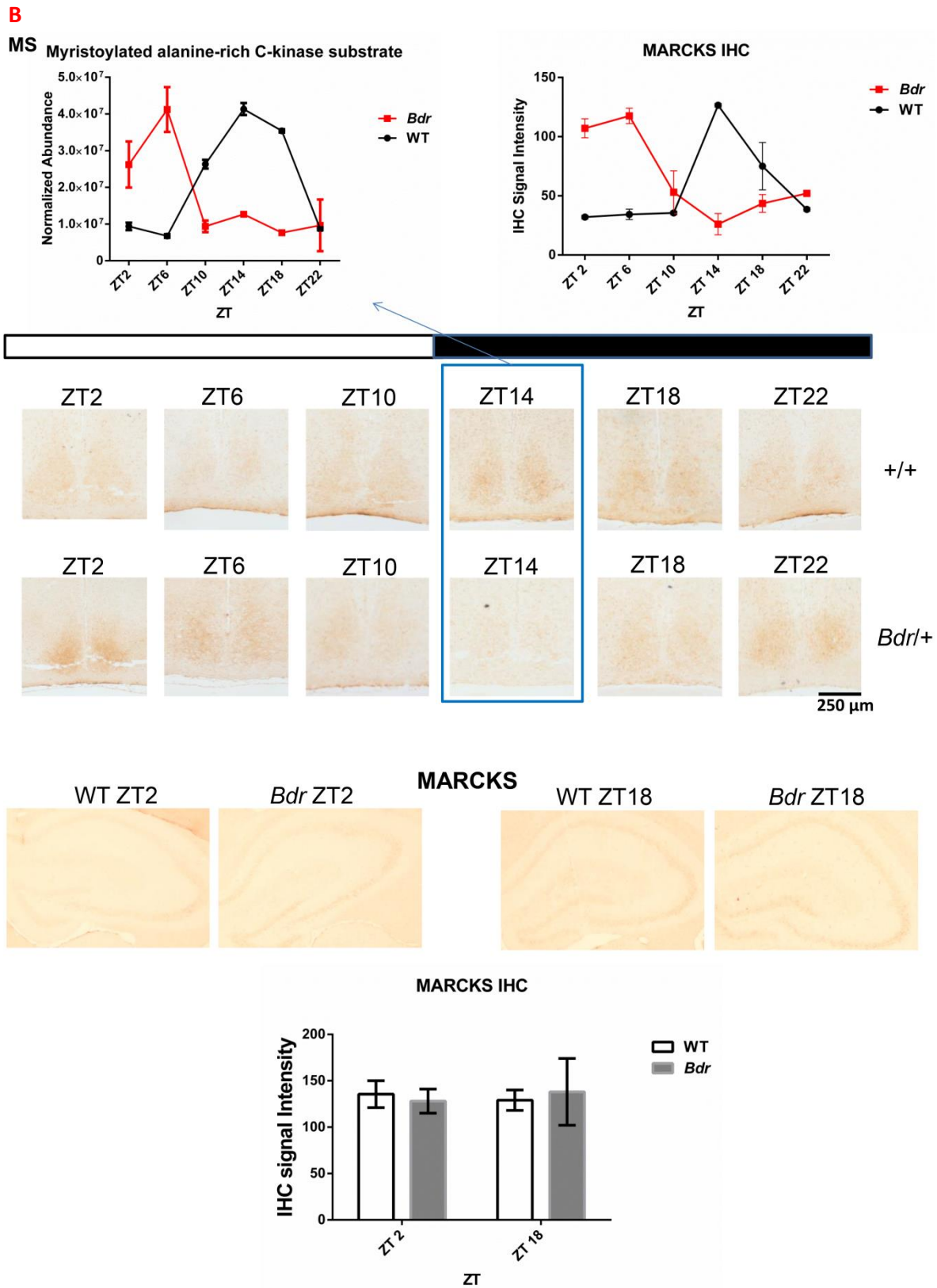

Figure 5.16: (**A**) 24h SCN IHC Secretogranin-2 +/+ versus *Bdr*/+ and MS normalised abundance protein profile. IHC WT quantification shows similar phase with MS data (**B**) 24h SCN IHC MARCKS +/+ versus *Bdr*/+ and MS normalised abundance protein profile suggests temporal de-regulation in *Bdr* MARCKS. Also depicted ZT2, ZT18 Hippocampus MARCKS staining and quantification suggesting hippocampal MARCKS levels remain unaltered. GAP-43/Neuromodulin and Calbindin/Tac1 IHC not shown as non-specific SCN antibody binding pattern prompted WB testing (n= 2-3 per genotype).

Our IHC data showed the presence of secretogranin-2 in WT and *Bdr* SCN (Figure 5.16). IHC of secretogranin-2 failed to detect any robust rhythmicity as reported by the MS data (Figure 5.14). Secretogranin-2 exhibited the smallest MS fold change from all the targets further investigated (Table 5.6); a factor that could have challenged the confirmation process. Despite the lack of IHC confirmation other MS studies have demonstrated an up-regulation of secrotagranin-2 during the dark phase (ZT18) in WT SCN (Lee *et al*., 2013). Therefore, our MS secretogranin-2 data were confirmed by an independent proteomics study (Lee *et al*., 2013).

Tac1/Sp MS data reported MS differences at ZT6 (Figure 5.12). These differences were similar to previous ZT6 microarray data suggesting that Tac1/Sp is an important spatio-temporal control and a potentially de-regulated target in *Bdr* SCN (Oliver *et al*., 2012). Mixed IHC results were generated (data not shown) due to the endogenous heterogeneous hypothalamic distribution of this particular target. Hence, further investigation of this candidate was not undertaken (Tac1/Sp qRT-PCR confirmation was also not accomplished) (Oliver *et al*., 2012).

MARCKS and pMARCKS displayed both specific antibody staining and SCN temporal de-regulation in *Bdr* (Figures 5.16 and 5.18). Importantly, MARCKS SCN de-regulation does not occur in all brain regions as MARCKS hippocampal staining of *Bdr* and WT at ZT2 and ZT18 did not reveal any expression differences (Figure 5.16). Given the role of MARCKS and pMARCKS in vesicle-trafficking pathways, neuronal plasticity, the Protein Kinase C pathway (PKC) and calcium signalling neuromodulin/GAP-43 and calbindin were also investigated via WB (Figure 5.17). Initially, a WB on WT SCN GAP-43 was conducted in order to assess antibody quality and the ultrafiltration process (Figure 5.17A). WT/*Bdr* SCN Calbindin and GAP-43 were subsequently probed at ZT10/ZT14 (Figures 5.17B-F). GAP-43 and Calbindin

WBs confirmed the expression pattern originally quantified by MS (Figure 5.14). However, both targets failed to achieve significance via WB. This could be due to the endogenous heterogeneous hypothalamic distribution of both targets introducing variations during tissue punch collection (data not shown). Finally, the expression differences in MS data for these two targets were smaller compared to MARCKS (Table 5.6).

Figure 5.17: WB SCN confirmation of proteomic de-regulation in WT versus *Bdr*

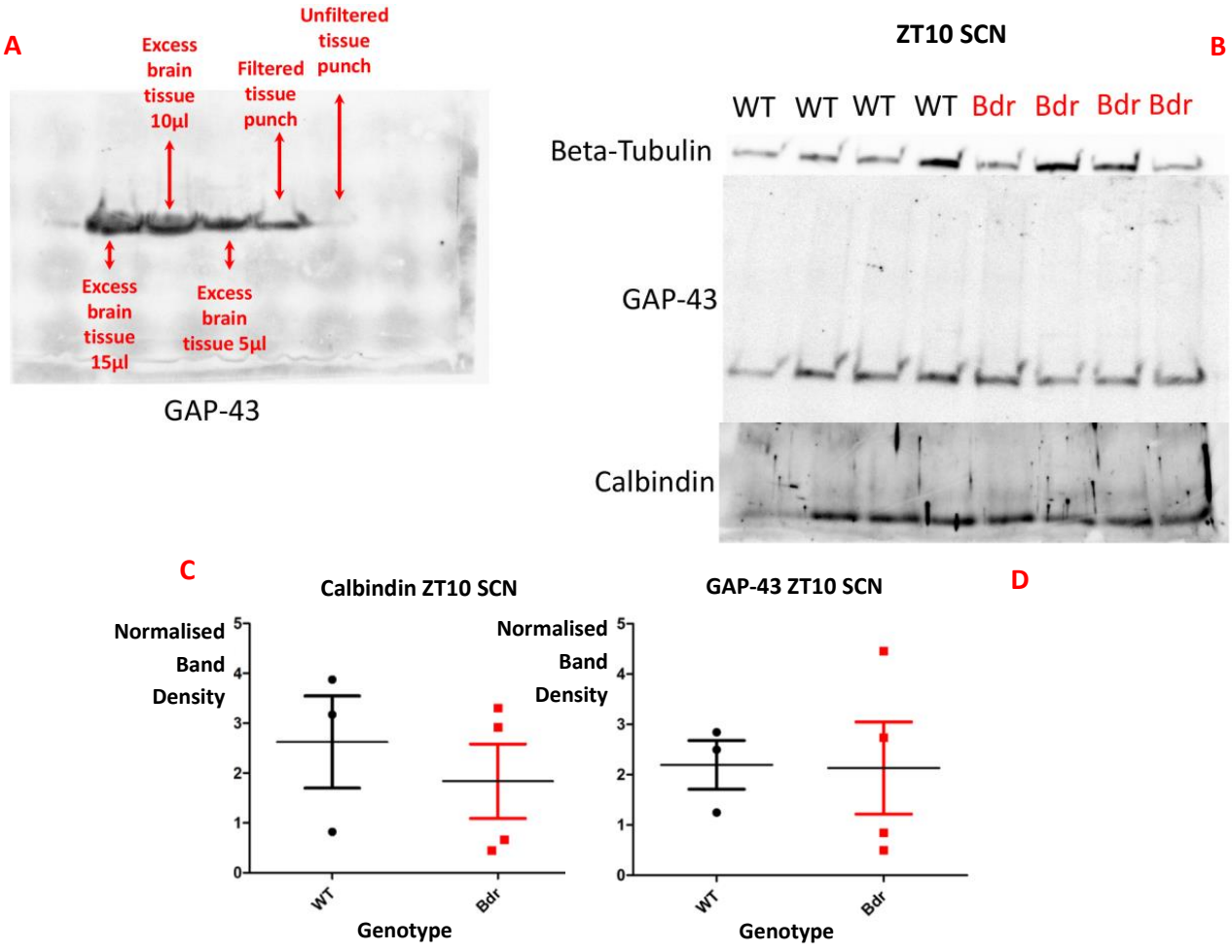

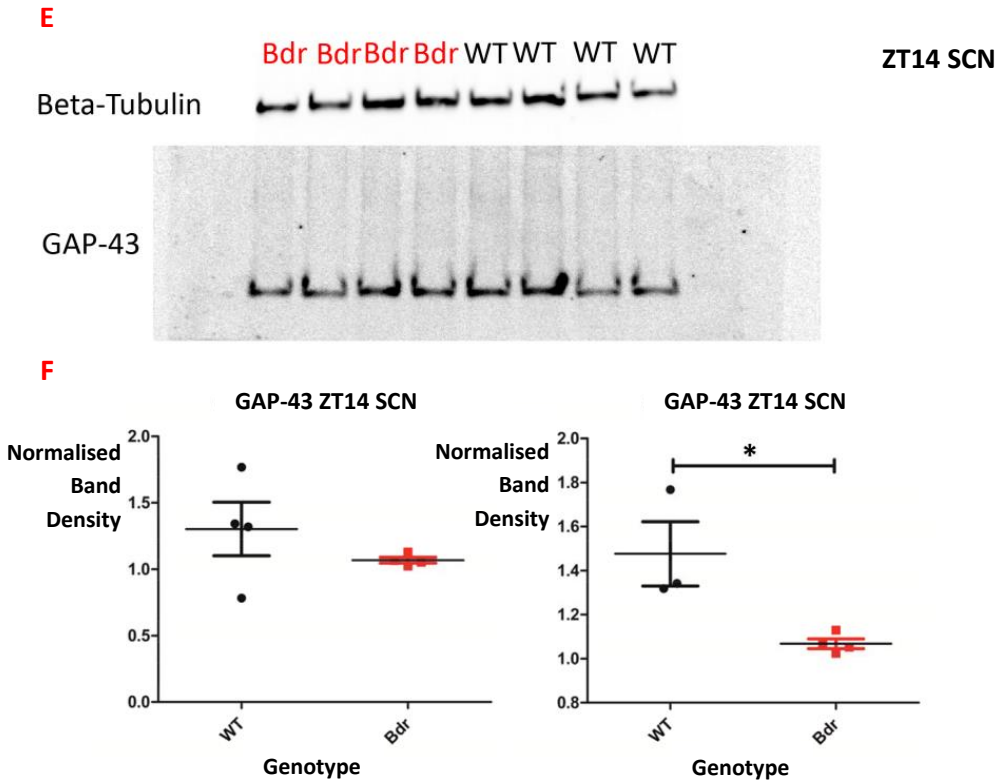

Figure 5.17: (**A**) GAP-43 WB WT control on unfiltered SCN tissue punch, filtered SCN tissue punch and increasing concentrations of brain homogenate (**B**) ZT10 SCN WB Calbindin and GAP-43/Neuromodulin in WT and *Bdr* (**C**) Calbindin ZT10 SCN WB profile. Data display a non-significant down-regulation in *Bdr* (**D**) GAP-43/Neuromodulin ZT10 SCN WB profile. Data display no difference between genotypes (**E**) ZT14 SCN WB GAP-43/Neuromodulin in WT and *Bdr* (**F**) GAP-43/Neuromodulin ZT14 SCN WB profile. Data display a non-significant down-regulation in *Bdr* which become statistically significant by excluding the lowest WT value (n= 3-4 per genotype).

Given the confirmed MARCKS de-regulation we subsequently probed for pMARCKS via IHC and PKC involvement via ELISA (Figure 5.18). Fitzgerald *et al* demonstrated up-regulation of pMARCKS in the prefrontal cortex of GluA1$^{-/-}$ mice displaying schizoaffective-like behaviour (Fitzgerald *et al*. 2010). Importantly, MARCKS is a PKC signalling target and often de-regulated in schizoaffective and bipolar disorder (Abrial *et al*., 2011; Le-Niculescu *et al*., 2013; Pinner *et al*., 2014).

Figure 5.18: IHC/ELISA SCN confirmation of pMARCKS/PKC activity de-synchrony

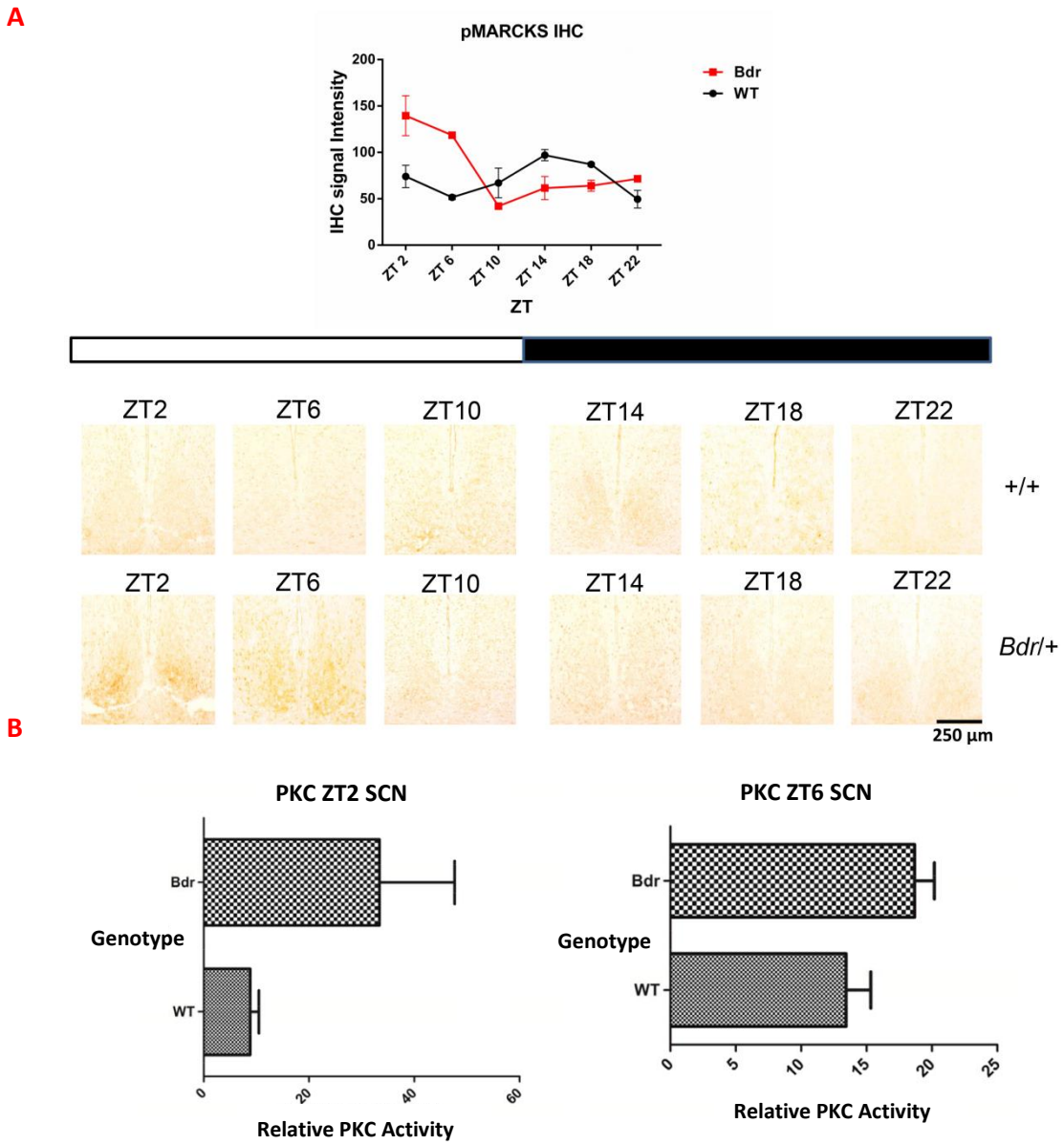

Figure 5.18: (**A**) 24h SCN IHC pMARCKS +/+ versus *Bdr*/+ protein profile. IHC quantification suggests de-regulation of this particular target and (**B**) SCN PKC relative activity for ZT 2, ZT 6 WT and *Bdr*. ELISA suggests up-regulation of PKC activity in *Bdr* SCN (n= 2-3 per genotype for IHC and n= 4 per genotype for ELISA).

IHC and ELISA demonstrate potential dysfunction of the PKC pathway in the *Bdr* SCN contributing to pMARCKS/MARCKS de-synchrony (Figure 5.18) that could potentially lead to the previously described AVP de-synchrony and subsequent HPA axis perturbation.

In summary, using quantitative proteomics of the SCN, a number of temporally de-regulated proteins were identified in the *Bdr* mice, some of which were confirmed using IHC or WB (Table 5.7).

Table 5.7: Summary data of proteomic SCN targets

Protein Target	Genotype	MS levels	Zeitgeber (ZT)	IHC confirmed	WB confirmed
Secretogranin-2	WT	↑	ZT 10-18	×	_
	Bdr	↑	ZT 2-6, 18	×	_
GAP-43	WT	↑	ZT 14	×	✓
	Bdr	↑	ZT 6	×	_
Calbindin	WT	↑	ZT 10	×	✓
	Bdr	↑	ZT 2	×	_
Tackykinin	WT	↑	ZT 10	×	_
	Bdr	↑	ZT 6	×	_
MARCKS	WT	↑↑	ZT 14-18	✓✓	_
	Bdr	↑↑	ZT 2-6	✓✓	_
pMARCKS	WT	?	ZT 14	✓	_
	Bdr	?	ZT 2-6	✓✓	_

↑↑: Overt Up-regulation; ↑: Moderate Up-regulation; ✓✓: Confident confirmation; ✓: Partial Confirmation ×: No confirmation; ?: Unknown; - : Not conducted

Table 5.7: Table summarises candidate proteomic SCN targets, MS levels, expression peak at particular ZT, IHC and WB confirmation.

5.5 Discussion

This body of work concluded functional *Bdr* retinal input pathways as identified by proper IEGs (*c-fos* and *jun-B*) induction as markers of recent neuronal activity (Oliver *et al*., 2012). This overlaps with functional activity suppression during negative masking experiments as well as normal pupillometry data (Oliver *et al*., 2012). Furthermore, core clock protein *Bdr* rhythms were maintained in the SCN (Oliver *et al*., 2012). Taken together, these data exclude the input and core clock pathways of the circadian axis as being defective.

It has been previously shown that LD circadian phase advance in the *Bdr* arises from synaptic perturbation of critical output signals (e.g. AVP) that impact on the HPA axis (Oliver *et al*., 2012). Additionally, Neurotensin (NT) also showed a de-synchronous pattern in the *Bdr* SCN (Oliver *et al*., 2012). Importantly, AVP, NT and Tac1/Sp have all been implicated as defective neurotransmitter systems in schizophrenia (Ma *et al*., 2006; Cilia *et al*., 2010). This suggests that circadian disruption is associated with schizophrenic pathology (Pritchett *et al*., 2012).

A 24h (6 time points) proteomic screen was therefore conducted in order to comprehend the underlying post-transcriptional mechanisms governing circadian disruption in the *Bdr* model. The proteomic data would also provide an important platform for the WT SCN rhythmic networks. The complexity and experimental challenges of the proteomic investigation demanded next-generation MS-sequencing (see Methods sections). Our MS data provided endogenous neuropeptide and proteomic spatio-temporal controls (Figure 5.10, Table 5.2). A gel-free MS-based method was utilised due to straightforward sample handling and superior proteome coverage versus 2D-gels (English *et al*., 2011). Despite the significant variation in the methodological platforms for dissecting proteomic SCN rhythms,

considerable overlaps exist between our data and previously published reports (Hatcher *et al*., 2008; Deery *et al*., 2009; Tian *et al*., 2011; Lee *et al*., 2010; Oliver *et al*., 2012; Lee *et al*., 2013). Moreover, the de-synchronies recorded were previously identified neuropeptides (Tac1/Sp) as well as previously unidentified metabolic controls (Fructose-bisphosphate Aldolase A) (Oliver *et al*., 2012). Importantly, our own MS data detected WT AVP peaking at ZT10 (Hatcher *et al*., 2008) but *Bdr* ZT6 AVP levels were below detection limit (Figure 5.10). However, some non-overlapping WT targets were recorded (Figure 5.11, Table 5.3). Methodological differences between MS and 2D gels contribute to some discrepancy, particularly for highly fragmented/multiple isoform targets, between expression patterns reported (Deery *et al*., 2009; English *et al*., 2011).

A series of temporally de-regulated candidates were identified (Tables 5.4-5.6). Integration of multiple analysis methods (MS ion intensity and spectral counting) aided in filtering potentially false positives. However, validation of MS-sequencing via antibody studies still presents a significant bottleneck in confirmation studies (Figure 5.19) (Mitchell *et al*., 2011).

Figure 5.19: Methodological variations between MS and IHC

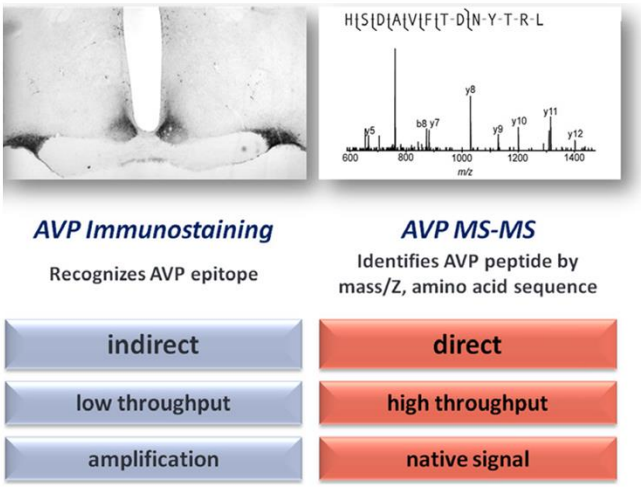

Mitchell *et al*., 2011

Figure 5.19: Experimental variations between high-throughput MS studies and low-throughput antibody based IHC experiments.

Five short-listed proteomic candidates were further investigated via IHC/WB (Secretogranin-2, Tachykinin1/Substance P, MARCKS, GAP-43/Neuromodulin and Calbindin). All these targets displayed variable levels of de-synchrony (Tables 5.4 and 5.6, Figures 5.12 and 5.14). Importantly, all these targets participate in synaptic trafficking events, synaptic plasticity, neurodevelopment and calcium signalling (Abrial *et al*., 2011).

Secretogranin-2 has been identified as a potential biomarker in neuropsychiatric disorders (Bartolomucci *et al*., 2010). Involvement of granin family biomarkers in neurological disorders such as Alzheimer's disease (AD), Frontal Temporal Dementia (FTD) and schizophrenia is well reported (Table 5.8) (Huang *et al*., 2006; Gros-Louis *et al*., 2009; Schrott-Fischer *et al*., 2009; Bartolomucci *et al*., 2010).

Table 5.8: Granin peptides in neurological disorders

Disorder	Impact	Stage
Alzheimer's disease (AD)	Lower levels in CSF (cerebrospinal fluid)	Potential Biomarker (Carrette *et al*., 2003; Pasinetti *et al*., 2006; Simonsen *et al*., 2007).
Frontotemporal dementia (FTD)	Lower levels in CSF	Potential biomarker (Ruetschi *et al*., 2005)
Amyotrophic lateral sclerosis	Lower levels in CSF and motor neurons	Pre-clinical (Zhao *et al*., 2008)
Schizophrenia/depression	Higher levels in CSF	Potential Biomarker (Huang *et al*., 2006; Huang *et al*., 2007)
Obesity/eating disorders	Orexin-dependent food intake increase	Pre-clinical (Bartolomucci *et al*., 2007; Toshinai *et al*., 2010)

Table 5.8: Numerous disorders in human or animal models associated with granin peptides.

Based on Bartolomucci *et al*., 2010

Secretogranin-2 has recently been shown to exhibit a 30% increase in the SCN during the night (Lee *et al*., 2013). This potentially identifies a wider functional SCN significance given the importance of this factor in sorting neuroendocrine secretory proteins (Fischer-Colbrie *et al*., 2005). Our data reported this night-time up-regulation in WT SCN but additionally recorded a potential expression variation when compared to the *Bdr* SCN (Figure 5.14 and Table 5.6). However, IHC validation of the detected MS variation did not confirm this finding. This could be due to the lack of sensitivity of IHC versus MS quantitation. Moreover, further methodological variations between techniques could contribute to this disparity (Figure 5.16). Additionally, secretogranin-2 recorded the smallest fold change from all factors further investigated and also did not display major spectral counts variations (Figure 5.14 and Table 5.6). Nevertheless, its functional impact on SCN rhythms is currently

an exciting finding, particularly due to its highly localised regional hypothalamic distribution and its potential biomarker status (Figure 5.16 and Table 5.8).

Tac1/Sp has been implicated in SCN synchronisation in response to photic stimulation (Abrahamson and Moore, 2001; Sterniczuk *et al*., 2010). Tac1/Sp has also been independently linked to schizophrenic pathology (Cilia *et al*., 2010). Neurotransmitter Tac1 SCN de-synchrony represents a potential pathway linking circadian disruption and schizophrenia in the *Bdr* model. Despite falling below significance in both transcriptomic and proteomic follow-up studies (qRT-PCR/IHC), its potential involvement in the disease process as a neurotransmitter system is significant. Additionally, given the retarded vesicle recycling rate in the *Bdr* model, potential SCN neurotransmitter de-synchronies support the existing data (Jeans *et al*., 2007; Oliver and Davies, 2009). Finally, other critical output neurotransmitter signals (AVP/NT) display temporally shifted SCN profiles in the *Bdr* and Tac1 may be associated with similar synaptic exocytosis pathways (Oliver *et al*., 2012).

Myristoylated alanine-rich C-kinase substrate (MARCKS) is an important vesicle-trafficking factor and is regulated by Ca^{2+}/Calmodulin and protein kinase C (Szabo *et al*., 2009). Transgenic mouse work on a MARCKS over-expressing line reported hippocampal-dependent learning deficits and impairment of long-term potentiation (McNamara *et al*., 2005). Importantly, the neurological phenotype was not attributed to PKC isozyme variation or variations in calmodulin expression (a MARCKS and Ca^{2+} binding partner) (McNamara *et al*., 2005). Hippocampal deficiencies and cognitive decline were associated with MARCKS over-expression (McNamara *et al*., 2005). Furthermore, heterozygous MARCKS mouse models (expressing 50% of MARCKS protein product) also exhibited spatial learning deficits and impairment of long-term potentiation (Hussain *et al*., 2006). MARCKS is a

developmentally regulated, PKC phosphorylated protein factor that co-localises with synaptic vesicles in order to define pre-synaptic and post-synaptic neuronal architecture (Hussain *et al*., 2006).

More recently, MARCKS has also been associated with sleep deprivation and neuropsychiatric disorders including bipolar disorder and schizophrenia (Szabo *et al*., 2009; Fitzgerald *et al*., 2010; Okuda *et al*., 2010; Abrial *et al*., 2011; Barkus *et al*., 2012; Trovò *et al*., 2013; Le-Niculescu *et al*., 2013; Pinner *et al*., 2014). pMARCKS, a marker of PKC activity, is up-regulated in the prefrontal cortex of amphetamine-treated mice or sleep-deprived animals (Szabo *et al*., 2009). Interestingly, lithium treatment of sleep-deprived animals can rescue the molecular pMARCKS up-regulation and alleviate the somatic impact (Szabo *et al*., 2009). Furthermore, ionotropic NMDA and AMPA receptors are also phosphorylation targets in sleep-deprived animals (Arnsten and Manji, 2008; Szabo *et al*., 2009). Importantly, this phosphorylation receptor pattern is also reversible via lithium treatment, providing the first mechanistic links between sleep-deprivation and neuropsychiatric disorders like schizophrenia that have an impact on the glutamatergic system (Szabo *et al*., 2009). Moreover, glutamate neurotransmission is critical in long-term potentiation and memory formation, functions compromised when MARCKS levels vary (McNamara *et al*., 2005; Hussain *et al*., 2006; Szabo *et al*., 2009).

Genetic variation in a schizophrenia-predisposing gene Dysbindin has been strongly associated with neuropathology (Benson *et al*., 2001; Straub *et al.*, 2002; Okuda *et al*., 2010). The dysbindin risk gene co-localises both pre-synaptically and post-synaptically and is involved in NMDA and GABAergic receptor trafficking (Okuda *et al*., 2010). Moreover, dysbindin over-expression induced glutamatergic hyper-activation in neuronal cell cultures

while dysbindin$^{-/-}$ mice display dopaminergic gain-of-function pathology (Okuda *et al*., 2010). MARCKS expression is regulated via the NF-YB/Dysbindin complex with schizophrenic brains exhibiting decreased dysbindin, MARCKS up-regulation and de-regulated neurotransmission (Okuda *et al*., 2010). Crucially, MARCKS actively participates in neurodevelopment such as synaptogenesis and axonal growth cones, thereby providing a mechanistic association between the schizophrenic neurodevelopmental hypothesis and molecular factors (Johnson *et al*., 2008; Okuda *et al*., 2010).

AMPA GluA1$^{-/-}$ mouse model of schizoaffective disorder displays prefrontal cortex pathology by up-regulation of pMARCKS and pNeuromodulin, which can be rescued by lithium administration (Fitzgerald *et al*., 2010; Barkus *et al*., 2012). Interestingly, lithium has been shown to have an impact on the amplitude and period of the circadian molecular mechanism (Klemfuss *et al*., 1992; Abe *et al*., 2000; Li *et al*., 2012). Finally, ageing also has an effect on MARCKS CNS levels (Trovò *et al*., 2013). Low PI (4, 5) P_2 (phosphoinositide) and phospholipase C_γ (PLC_γ) hippocampal levels in older mice impair long-term potentiation and cause memory deficits that can be rescued via chronic intraventricular perfusion of MARCKS peptides or AAV (Adeno-Associated Virus) induced over-expression of MARCKS (Trovò *et al*., 2013).

Studies in ovine anterior pituitary cells have demonstrated the impact of AVP neuropeptide on the phosphorylation status of MARCKS and its links to adrenocorticotropin (ACTH) secretion (Liu *et al*., 1994). This would suggest that AVP and MARCKS coordinate critical output signals. Moreover, it has been suggested that AVP mediates the release of ACTH via a PKC-dependent mechanism that could potentially involve a reversible MARCKS phosphorylation switch (Liu *et al*., 1992). Further evidence on the biosynthesis and secretion

of ACTH in the ovine anterior pituitary is established when experiments displayed a CRF (corticotropin-releasing factor)-dependent via PKA (Protein Kinase A) effect while AVP mediates its effect via PKC and together these two enzymes regulate ACTH biosynthesis (Liu *et al*., 1990). Importantly, the PKC-dependent effect on ACTH release has been also shown in rat anterior pituitary cells, thus demonstrating a cross-species mechanism of HPA axis regulation (Abou-Samra *et al*., 1986).

Kinase-dependent SCN pathways have been linked to photic synchronisation of the SCN (Butcher *et al*., 2002; Bonsall and Lall, 2013). Deficits in PKC activity have reported deficiencies in resetting the SCN and in the transcriptional machinery associated with circadian rhythms (Lee *et al*., 2007b; Robles *et al*., 2010; Bonsall and Lall, 2013). Several PKC isozymes have been identified. PKC isozymes are roughly divided into three groups depending on the activation substrate each group demands (Takai *et al*., 1979; Bonsall and Lall, 2013). Classical PKC enzymes (PKCα, PKCβ and PKCɣ) activate via a calcium- and DAG (diacylglycerol)-dependent mechanism (Bonsall and Lall, 2013). Novel PKC enzymes (PKCδ, PKCε, PKCη, and PKCθ) activate via a DAG substrate alone (Ono *et al*., 1998; Bonsall and Lall, 2013). Finally, atypical PKC enzymes (PKCζ and PKCι) activate via a calcium- and DAG-independent mechanism (Ono *et al*., 1989; Bonsall and Lall, 2013). The SCN appears to express all classical PKC isozymes as well as PKCε (Bult and Smale, 1999; Bonsall and Lall, 2013).

PKC signalling has been linked to functional input pathways to the SCN (Peirson *et al*., 2007; Lee *et al*., 2007b; Bansall and Lall, 2013). Indeed, $PKCz^{-/-}$ animals display attenuated phase shift responses to light pulses and deficits in light-induced SCN gene expression (Peirson *et al*., 2007). On the other hand, pharmacological inhibition of PKC does not

substantially alter IEGs induction in the SCN, suggesting that PKC does not couple light to rapid transcriptional activation (Lee *et al*., 2007b). Moreover, transient pharmacological disruption of basal PKC activity does not affect the pacemaking SCN activity in the absence of light (Lee *et al*., 2007b). Additionally, temporal regulation of PKC activity suggests a different response in light-induced clock entrainment across a 24h period (McArthur *et al*., 1997; Lee *et al*., 2007b; Bansall and Lall, 2013). Indeed, photic stimulation only during the subjective night results in induction of PKC activity in the SCN (Lee *et al*., 2007b).

Our data have demonstrated functional retinal input pathways in the *Bdr* as assessed by IEG (*c-fos* and *jun-B*) induction in the SCN (Figures 5.2-5.4). Additionally, MARCKS/pMARCKS levels maintain similar phases of expression across a 24h LD cycle (Figures 5.16 and 5.18). This suggests that PKC signalling might be an indirect contributor (related to the output and not the input component) to the *Bdr* circadian pathology due to the presence of temporally de-regulated PKC MARCKS substrates. Indeed, MARCKS expression changes have been associated with synaptic vesicle cycling alterations (McNamara *et al*., 2005; Okuda *et al*., 2010; Pinner *et al*., 2014). Additionally, phosphorylation of MARCKS alters its functional role allowing IP3 and DAG to initiate intracellular calcium release that activate the calmodulin/calcium pathway and phosphorylate CREB (West *et al*., 2001; Trovò *et al*., 2013). Therefore, PKC inhibition prior to the light phase might suppress pMARCKS levels in the *Bdr* (Figure 5.18). This could potentially result in appropriate sequestering of PI (4, 5) P_2 and prevent downstream intracellular cascades.

PKC inhibition has been associated with phase delays in response to light (Lee *et al*., 2007b; Bonsall and Lall, 2013). On the other hand, PKC$\alpha^{-/-}$ mice present decreased light-dependent phase delays (Shim et al., 2007; Bonsall and Lall, 2013). *In vitro* experiments on rat

SCN have demonstrated that PKC agonists can mimic the phase shift induced by melatonin on the SCN neuronal firing rate (McArthur *et al*., 1997). Importantly, the melatonin-induced phase advances can be rescued via administration of selective PKC inhibitors (calphostin C and chelerythrine chloride) (McArthur *et al*., 1997). Potential involvement of PKC-dependent mechanisms in the circadian pathology of the *Bdr* model has been identified (Figure 5.18). PKC specific drugs are currently investigated for their potential as mood-stabilising and anti-manic chemicals (Basta-Kaim *et al*., 2006; Abrial *et al*., 2013). Additionally, lithium appears to normalise disrupted PKC pathways in bipolar patients (Hahn *et al.*, 2005; Abrial *et al*., 2013). Clinical trials in bipolar patients have reported tamoxifen administration, an oestrogen receptor substrate, attenuated manic episodes by inhibiting PKC signalling pathways (Zarate *et al*., 2007; Amrollahi *et al*., 2010; Abrial *et al*., 2013).

Recent blood biomarker discovery in bipolar patients and schizophrenic/schizoaffective disorder patients has focused on predicting suicidal states (Le-Niculescu *et al*., 2013). Hospitalisation data suggest that MARCKS and MAP3K3 (mitogen activated kinase kinase kinase 3) reflect potentially crucial biomarkers for suicidality in mental health patients (Le-Niculescu *et al*., 2013). A list of blood biomarkers for suicidality following a convergent functional genomics (CFG) stratification analysis has been constructed (Figure 5.20).

Figure 5.20: CFG scoring of potential biomarkers in suicidality in mental health disorders

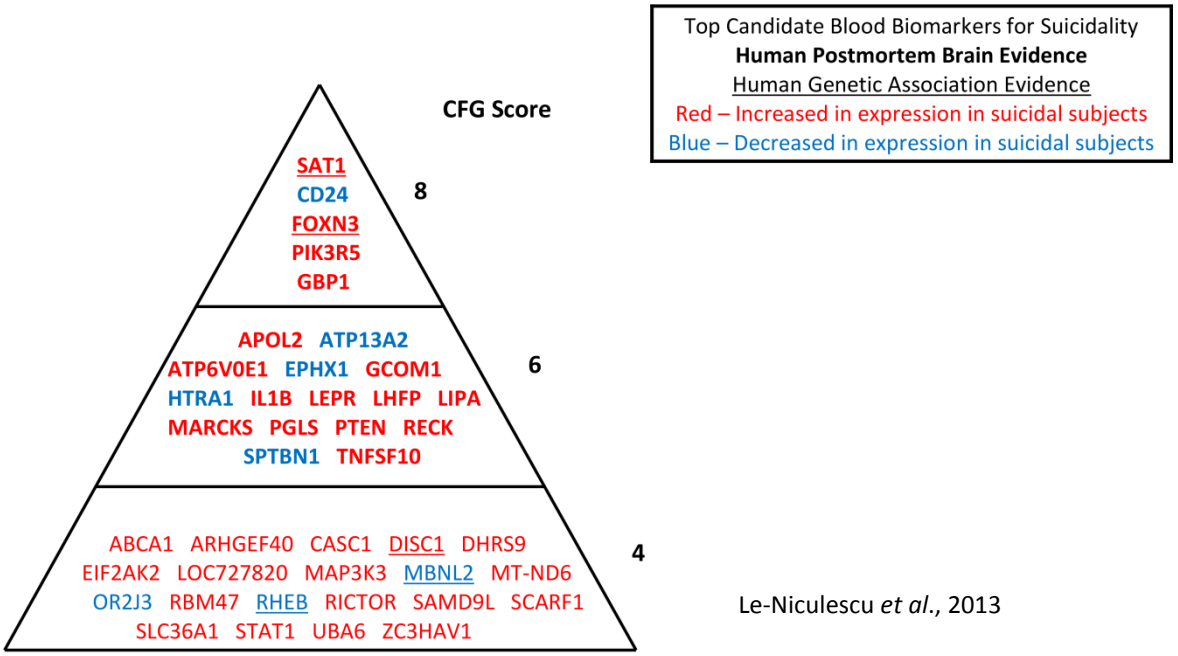

Figure 5.20: CFG scoring of potential suicidality biomarkers.

The biomarker potential of MARCKS in mental health disorders relating to suicidality receives a confident 6 point CFG score (Figure 5.20). Additionally, a number of post-mortem studies in mental health patients have investigated the alteration status of PKC activity and MARCKS (Wang and Friedman, 1996; Abrial *et al*., 2011). Furthermore, inhibiting the PKC pathway in amphetamine-induced hyperactivity rat models attenuated the activity increase (Abrial *et al*., 2013). Interestingly, the *Bdr* mice display mild ataxia and subsequent hypo-locomotion, yet their pMARCKS episodes can potentially manifest in a hypothalamic circadian setting.

GAP-43/Neuromodulin is also a PKC substrate involved in schizophrenia and is phosphorylated during long-term potentiation processes (Welckert *et al*., 2001; Fitzgerald *et al*., 2010). Neuromodulin alongside MARCKS is a potential PKC marker and GluA1$^{-/-}$ mice report up-regulation of both targets in the prefrontal cortex area (Szabo *et al*., 2009;

Fitzgerald *et al*., 2010). Importantly, lithium treatment, a PKC and circadian modulator, normalised expression patterns of PKC markers in the GluA1$^{-/-}$ mice (Fitzgerald *et al*., 2010). WB confirmation of initial MS-seq neuromodulin de-regulation only partially validated the findings (Figure 5.17). IHC of GAP-43/Neuromodulin was inconclusive due to the scattered non-SCN specific hypothalamic expression pattern of the target (data not shown). Therefore, given the heterogeneous expression, experimental validation of de-regulation was even more challenging. Despite the technical variation, WB suggested some temporal de-regulation of this target (Figure 5.17).

Calbindin is a Ca^{2+} sensor implicated in ion homeostasis in the SCN (Stadler *et al*., 2010). Interestingly, initial anatomical brain staining did not reveal hippocampal calbindin alterations in the *Bdr* mice (Jeans *et al*., 2007). Calbindin-D28K$^{-/-}$ mice display altered circadian properties as well as *Per2* core clock gene perturbations (Stadler *et al*., 2010). Synchronisation of the SCN depends on appropriate transmission of photic information via the RHT pathway (Shigeyoshi *et al*., 1997). Light pulses induce activation of the glutamatergic system via the RHT, which in turn triggers activation of ionotropic glutamate receptors and Ca^{2+} inflow (Schurov *et al*., 1999; Stadler *et al*., 2010). Subsequent activation of chromatin modifiers, IEGs, clock genes (Period 1 and 2) occurs (Crosio *et al*., 2000; Yan and Silver, 2002; Hirota and Fukada, 2004; Stadler *et al*., 2010). Consequently, phase advances or delays in activity onsets are reported in circadian studies (Albrecht *et al*., 2001; Tischkau *et al*., 2003; Stadler *et al*., 2010). IHC validation of Calbindin MS de-regulation was inconclusive due to the scattered non-specific hypothalamic expression pattern of the target (data not shown). WB confirmation of initial MS-seq calbindin de-regulation only reported a similar but non-significant up-regulation at WT ZT10 (Figure 5.17). However, WB of WT ZT14 calbindin reports down-regulation versus WT ZT10, a finding which overlaps with the initial proteomic

results (Figure 5.14). Interestingly, Calbindin SCN up-regulation in the *Bdr* co-occurs with PKC/pMARCKS up-regulation (Figures 5.17 and 5.18). Despite most short-listed proteomic candidates (Table 5.6) validated internally or externally as well as clustering in similar biological pathways the confirmed MARCKS/PKC de-synchronisation in the *Bdr* mice will be subject to further investigation by administration of a selective PKC inhibitor (chelerythrine chloride). Potentially, light-induced circadian PKC phosphorylation episodes in the *Bdr* (due to more PKC substrates present) that manifest as de-regulation of MARCKS/pMARCKS and neuropeptide (AVP/NT) output signals could contribute, to the circadian pathology of the model. Taken together, these findings confirm the original hypothesis regarding perturbed synaptic trafficking mechanisms in *Bdr* SCN (see Hypotheses section).

6 Main Discussion

6.1 Overview

A number of mouse models of neurological (schizophrenia and Parkinson's disease) and metabolic disorders (Sandhoff and NPC) were investigated for circadian behavioural parameters to ascertain whether known sleep disturbances in these disorders would be observed in mouse models. Additionally, elements of the circadian axis (input pathways, core clock mechanism) were molecularly investigated in the *Bdr* mouse in order to identify the cause-effect relationship of synaptic dysfunction on the circadian machinery.

Importantly, clinical studies have demonstrated the significant overlap between circadian disruption and neurological/metabolic disorders (Alonso and Sheldon, 2010; Bromundt *et al*., 2011; Wulff *et al*., 2012; Fernandez *et al*., 2012). Therefore, understanding the underlying circadian disruption can serve as a potential therapeutic intervention in a variety of disorders. For example, a Huntington's disease mouse model (R6/2 transgenic mouse) can display cognitive improvement via re-structuring the circadian axis landscape (Pallier *et al*., 2007; Maywood *et al*., 2010; Cuesta *et al*., 2011), suggesting that direct circadian regularisation alleviates CNS pathology. The R6/2 mice recapitulate the disrupted rest/activity cycles observed in Huntington's disease patients (Pallier *et al*., 2007; Maywood *et al*., 2010). By establishing robust, structured rest/activity cycles (for example through pharmacological treatments) in the R6/2 it was shown that cognitive decline may also slow following restoration of circadian rhythms (Pallier *et al*., 2007). In this way, the circadian axis is re-structured and regularised to a robust LD cycle in order to improve cognitive performance in the transgenic R6/2 mice.

BAC SNCA, MAPT and *Parkin*$^{-/-}$ mouse PD models were investigated for prodromal non-motor circadian deficits. All mouse lines underwent longitudinal 3-month circadian screening. Circadian paradigms included entrainment to a LD cycle, negative masking, a 6hr phase advance, DD, LL and re-entrainment to a LD cycle. All PD genetic lines displayed scotophase hyperactivity compared to controls, a finding that complements existing behavioural data on these models. It is known that the wheel-running exercises motivational reinforcement on mouse behavioural activity patterns (Careau *et al*., 2012). Interestingly, dopamine deficits in PD have been implicated in reward-related impulsivity, and increased wheel-running in the BAC PD models could potentially reflect that phenotype (Aarts *et al*., 2012). However, only the BAC OVX and A30P models displayed altered fragmentation patterns, confirming the original PD hypothesis that mouse models investigated could display possible circadian (fragmentation differences) rhythm abnormalities in activity profiles reminiscent of PD pathology in patients.

Hexb$^{-/-}$ and *Npc1*$^{-/-}$ mouse LSD models of Sandhoff and NPC disorders were investigated for prodromal non-motor circadian deficits. Due to reduced lifespans both mouse lines underwent modified shorter versions of longitudinal circadian screens. *Npc1*$^{-/-}$ mice displayed severe hypo-locomotion but remarkably no overt genotype-specific circadian pathology. Re-entrainment deficits in the *Npc1*$^{-/-}$ could be attributed to extensive end-stage CNS neuropathology. On the other hand, *Hexb*$^{-/-}$ mice displayed mild hypo-locomotion but also shorter free-running periods. Despite the severe CNS glycosphingolipid accumulation in both models, only the loss of the *Hexb* gene participated in rest/activity timing under constant conditions. Additionally, the *Npc1*$^{-/-}$ hypoactivity was recorded a week earlier than rotarod, following previously published reports, illustrating the sensitivity of running-wheel screening for motor pathology (Voikar *et al*., 2002). Taken together, these findings suggest

that the *Hexb*$^{-/-}$ mice confirm the original LSD hypothesis regarding potential core clock deficits.

Molecular experiments investigating IEGs in the *Bdr* suggest the absence of input defects. Moreover, previously confirmed neurotransmitter de-synchronies (AVP/NT) illustrate abnormal SCN function arising from disruption of critical output signals as a result of synaptic dysfunction (Oliver *et al*., 2012). An expanded post-transcriptional screen across the entire LD cycle (6 time points) investigated the temporal and mutation effects on circadian rhythms. Neuropeptide and proteomic spatio-temporal controls were recorded while several short-listed, temporally de-regulated SCN candidates were followed-up. Partial confirmation of most targets was achieved, with further emphasis placed on potential MARCKS/pMARCKS and PKC-dependent circadian de-synchrony. Taken together, these findings confirm the original hypothesis regarding perturbed synaptic trafficking mechanisms in the *Bdr*.

6.2 The *Bdr* model: Circadiomics

Circadiomics is a term reflecting the integrating process of genomic, transcriptomic, proteomic and metabolomic datasets regarding circadian processes (Patel *et al*., 2012). Our proteomic findings reflect part of this integrating effort in understanding circadian mechanisms through new technologies. We have identified for the first time a potential role for MARCKS peptides in the pathogenesis of circadian disruption in a mouse model of schizophrenia. Indeed MARCKS has mostly been associated with bipolar and schizoaffective disorder (Pandey *et al*., 2003; Ogden *et al*., 2004; Nock *et al*., 2008; Patel *et al*., 2010; Kurian *et al*., 2011; Le-Niculescu *et al*., 2013). Additionally, MARCKs/PKC signalling and glutamate receptors have been associated both in animal and human studies with complex mood-related disorders (Ambelas, 1979; Bannerman *et al*., 2004; Alt *et al*., 2006; Coyle *et al*., 2006;

Snyder *et al*., 2006; Lau *et al*., 2010; Kataoka *et al*., 2011; Fitzgerald *et al*., 2010). Indeed, the *Bdr* model appears to encapsulate major predisposition risk pathways in the pathophysiology of schizophrenia and mood-related disorders (Jeans *et al*., 2007; Oliver and Davies, 2009; Oliver *et al*., 2012). A recent convergent functional genomics (CFG) has given SNAP-25 a four point CFG score (Ayalew *et al*., 2012). Importantly, SNAP-25 has been functionally implicated in schizophrenic cortical circuitry disruption (Spellman *et al*., 2008). Additionally, altered levels in cerebellum and hippocampus from post-mortem schizophrenic studies all confirm its association with schizophrenia (Knable *et al*., 2004; Barr *et al*., 2006). Importantly, this provides an opportunity to investigate its possible functional implications in circadian disruption. The interplay between SNAP-25, MARCKS/pMARCKS, AVP, and PKC in the *Bdr* model suggests potential post-transcriptional disruption in the schizophrenic SCN.

Numerous proteomic studies from post-mortem mediodorsal thalamus, dorsolateral prefrontal cortex and anterior temporal lobe have indeed identified myelin basic protein, PKC, metabolic proteins, cytoskeletal proteins and GFAP (glial fibrillary acidic protein) as de-regulated targets in schizophrenic cohorts (Gattaz *et al*., 1990; Bassett *et al*., 1993; Horrobin *et al*., 1994; Lieberman *et al*., 1999; Lieberman *et al*., 2001; Martins-de-Souza *et al*., 2009, Martins-de-Souza *et al*., 2010). Many of these schizophrenic protein candidates including aldolase, GAP-43, 14-3-3 zeta, secretogranin-2 and MARCKS have been detected by our circadian proteomics screen. These findings further suggest that the *Bdr* model has relatively high face validity for investigating synaptic deficits associated with schizophrenia.

MARCKS/pMARCKS SCN functionality in relation to PKC, AVP, NMDA receptor trafficking and calcium homeostasis has been documented (Castren *et al*., 2005; Amadio *et al*., 2006; Pittenger *et al*., 2008; Tanis *et al*., 2007; Chen *et al*., 2010; Amrollahi *et al*., 2010; Abrial *et al*., 2011). Therefore, *in vivo* selective PKC inhibition by-passes the sedative effects

of antpsychotic treatment and has an impact on the specific rhythmic deficiency identified (Roth *et al*., 2008; Wine *et al*., 2009; McCornack, 2010, Muench and Hamer, 2010). PKC modulators are well tolerated with minimal side-effects and it would therefore be valuable to investigate their potential as a circadian modulator in the *Bdr* model (Bebchuk *et al*., 2000; Hahn *et al*., 2005; Dwivedi *et al*., 2005; Frey *et al*., 2006; Zarate *et al*., 2007; Einat *et al*., 2007; Yildiz *et al*., 2008; Galeotti *et al*., 2011; Hajek *et al*., 2012; Abrial *et al*., 2013).

Previously identified de-regulated targets quantified by our proteomic screen are key players participating in synaptic trafficking events and neuro-development (Martins-de-Souza, 2012; Patel *et al*., 2012). Interestingly, a novel function for MARCKS peptides in maintaining critical SCN output signalling has now been identified. Circadian disruption in neuropsychiatric animal models (e.g. *Vipr2, Nrg1* and *Dao*) draws from biological pathways characterising the entire spectrum of psychotic and mood-related disorders (Schurov *et al*., 2004; Wieczorek *et al*., 2004; Shirakawa *et al*., 2004; Gu *et al*., 2005; Scolnick *et al*., 2006; Bernstein *et al*., 2006; Carter, 2006; Boks *et al*., 2007; Dun *et al*., 2007; Diaz *et al*., 2007; Carter, 2007; Boucher *et al*., 2007; Morikawa *et al*., 2008; Sharif *et al*., 2009; Miyoshi *et al*., 2009). For example, the D-amino acid oxidase ($Dao^{-/-}$) knockout mice displayed increased fragmentation under LD, and deficits in negative masking as well as disruption of light-induced core clock gene expression in the SCN (Sobczyk *et al*., 2010; unpublished data). Heterozygous $Nrg1^{+/-}$ animals showed disrupted rest/activity rhythms and suppression of wheel-running activity when neuregulin was infused into the third ventricle (Johnson *et al*., 2002; Snodgrass-Belt *et al*., 2005). Some $Vipr2^{-/-}$ mice displayed circadian abnormalities including a shorter free-running period of roughly 22 hours (Hughes and Piggins, 2008). Another subset of $Vipr2^{-/-}$ mice displayed arrhythmia, suggesting a continuum of behavioural

phenotypes (Hughes and Piggins, 2008). Taken together, these findings illustrate the heterogeneity of circadian disruption in potential models of schizophrenia.

6.3 LSDs: Circadian Disruption and Metabolism

The mechanisms that couple metabolic processes to circadian rhythms are under active investigation (Asher and Schibler *et al*., 2011). Glucose homeostasis involves glycogen synthesis and break-down, a process governed by a large number of enzymes and hormones (Tzamaloukas *et al*., 2008; Agius, 2008; Lam *et al*., 2009; Asher and Schibler *et al*., 2011). Similarly, lipid metabolism is a metabolic process heavily reliant upon LSD enzymatic actions, trafficking pathways and vesicle recycling (Parente *et al*., 2012; Platt *et al*., 2012).

There has been a long-standing association between endogenous core clock gene disruption (*Clock/Npas2*, *Per1-3*, *Cry1-2*, *Bmal1* and *Rev-erba/Rev-erbb*) and metabolic pathology (Yamamoto *et al*., 1987; Rudic *et al*., 2004; Kudo *et al*., 2004; Turek *et al*., 2005; Oishi *et al*., 2006; Kudo *et al*., 2007; Kudo *et al*., 2008; Kaneko *et al*., 2009; Sans-Fuentes *et al*., 2010; Ando *et al*., 2011; Delezie and Challet, 2011). In addition, dietary changes inducing obesity (e.g. high-fat diets) have an impact on the circadian axis (Hill *et al*., 1992; Havel *et al*., 1999; Cha *et al*., 2000; Kaneko *et al*., 2009). In particular, high-fat diets in nocturnal rodents can induce transcriptional changes in *Rev-erba*, *Bmal1* and *Clock* while lengthening the free-running period, disrupting light-induced SCN synchronisation and altering phase shifts (Wells *et al*, 1997; Kohsaka *et al*., 2007; Jenkins *et al*., 2006; Yanagihara *et al*., 2006; Kennaway *et al*., 2007; Mendoza *et al*., 2008; Barnea *et al*., 2009; Hsieh *et al*., 2010; Doi *et al*., 2010; Garaulet *et al*., 2011; Otway *et al*., 2011; Delezie and Challet, 2011). LSD models mimic some of the impact high-fat diets have on the circadian axis due to the inherent lipid pathology involved.

Core metabolic deficits in LSDs include a build-up of cholesterol, glycosphingolipids and an altered calcium homeostasis (Lloyd-Evans *et al*., 2008; Platt *et al*., 2012). Importantly, altered calcium homeostasis has been previously linked to circadian rhythm abnormalities (van Ooesterhout *et al*., 2008). Additionally, impaired insulin (circadian-regulated) signalling has been recently documented in the brain of another NPC mouse model (Kalsbeek and Strubbe, 1998; Ong *et al*., 2012). Circadian rhythm alterations such as unstable periodicity and activity fragmentation have previously been documented in the LSD mucopolysaccharidosis VII mouse (Ross *et al*., 2000; Yan *et al*., 2008; Parente *et al*., 2012). Several transcriptomic alterations were identified in the brainstem (Parente *et al*., 2012). Specifically, urotensin II was up-regulated which is known to have an effect on cholinergic neurons during REM sleep (Huitron-Resendiz *et al*., 2005; de Lecea and Bourgin, 2008; Ono *et al*., 2008; Parente *et al*., 2012). Moreover, arginine vasproressin (AVP), a vital circadian rhythm hormone, was also up-regulated in the striatum (Parente *et al*., 2012). These findings recapitulate the significance of the cross-talk between metabolic homeostasis and circadian rhythms.

Finally, rodent sleep restriction studies have indicated altered glucose metabolism, confirming the association between sleep debt and obesity in humans (Spiegel *et al*., 2009; Nedeltcheva *et al*., 2009; Barf *et al*., 2010; Delezie and Challet, 2011). Daytime feeding/activity in nocturnal rodents de-couples circadian rhythms from the master SCN oscillator and may lead to altered body mass, particularly when high-fat diets are prescribed (Mistlberger *et al*., 1998; Damiola *et al*., 2000; Stokkan *et al*., 2001; Feillet *et al*., 2006; Salgado-Delgado *et al*., 2008; Arble *et al*., 2009; Salgado-Delgado *et al*., 2010; Delezie and Challet, 2011). These findings further demonstrate the association between circadian and metabolic homeostasis.

Hexb$^{-/-}$ mice exhibit widespread GM2 gangliosidosis that has an impact on cognition, lifespan and motor function, mimicking the human Sandhoff disease (Tay, 1881; Sachs, 1887; Svennerholm, 1962; Schneck, 1964; Makita and Yamakawa, 1963; Ledeen and Salsman, 1965; Sandhoff *et al*., 1968; Sango *et al*., 1995; Bley *et al*., 2011; Smith *et al*., 2012; Sargeant *et al*., 2012). Interestingly, we identified a prodromal wheel-running phenotype in the *Hexb*$^{-/-}$ that includes shorter free-running periods in DD (Livieratos *et al*., 2014; unpublished data). Importantly, preliminary qPCR data on clock genes show differential expression in mutant animals in line with a core clock deficit (Richardson *et al*., 2014; unpublished data).

In contrast, *Npc1*$^{-/-}$ neurodegenerative phenotype, glycosphingolipid accumulation, and de-regulated calcium homeostasis did not generate any overt non-motor circadian phenotype (Butler *et al*., 1993; Patterson *et al*., 1993; Liscum *et al*., 2000; Davies *et al*., 2000; Ko *et al*., 2001; Vanier and Millat, 2003; te Vruchte *et al*., 2004; Patterson and Platt, 2004; Lloyd-Evans *et al*., 2008). Re-entrainment deficits in the *Npc1*$^{-/-}$ line could be attributed to extensive end-stage CNS neuropathology. However, locomotion deficits via the running-wheel were detected in both models, consistent with published reports (Weintraub *et al*., 1987; Akaboshi *et al*., 1997; MacQueen *et al*., 1998; Andersson *et al*., 2004; Denny *et al*., 2006; Reddy *et al*., 2006; De Windt *et al*., 2007; Denny *et al*., 2007; Voikar *et al*., 2002; Stanley *et al*., 2005; Gullinelo *et al*., 2008; Vanier *et al*., 2010; Vazquez *et al*., 2011).

Recent analysis of two distinct metabolic neurodegenerative disorders from a mouse model of mucopolysaccharidosis [MPS] IIA, another lysosomal storage disorder, and multiple sulphatase deficiency (MSD) revealed unexpected fusion defects in up-regulated cholesterol lysosomes with autophagosomes (Fraldi *et al*., 2010). This pioneering work elegantly demonstrated attenuation of soluble N-ethylmaleimide sensitive factor attachment protein (SNAP) receptors (SNARES) in cholesterol perturbed lysosomal organelles (Fraldi *et al*., 2010).

Abnormal cholesterol accumulation spatially locks SNAREs in an inactive state, thereby restricting synaptic vesicle recycling (Figure 6.1) (Fraldi *et al*., 2010). Moreover, decreasing cholesterol levels restores SNARE function in the endocytic pathway of cells (Fraldi *et al*., 2010). Therefore, it is suggested that during LSD lipidosis, cholesterol-induced synaptic dysfunction occurs via impairments of the fusion machinery (Fraldi *et al*., 2010). These findings demonstrate an interesting role of the SNARE complex in LSDs.

Figure 6.1: Synaptic trafficking defects in LSDs

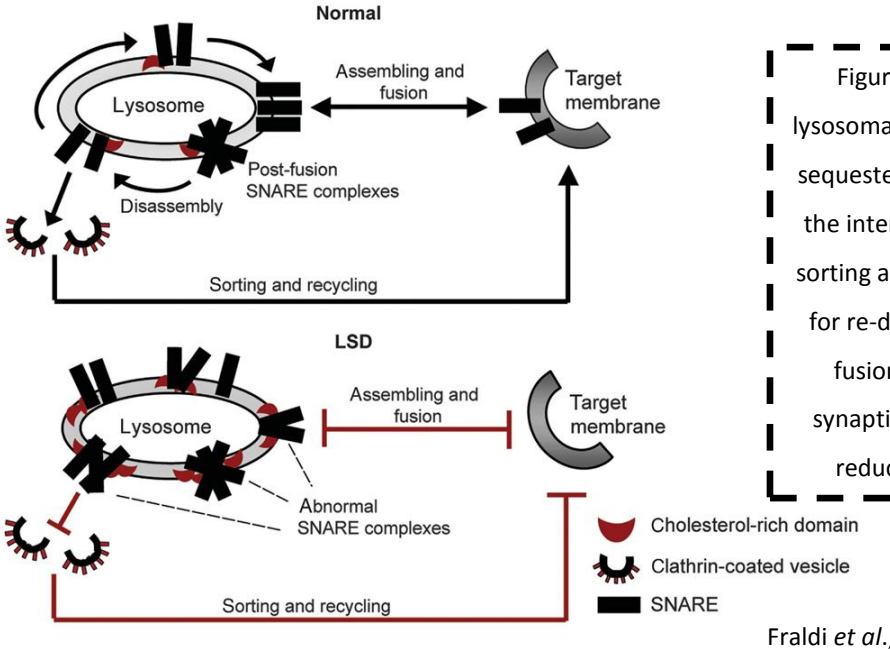

Figure 6.1: Cholesterol-rich lysosomal membrane domains lock sequestered SNAREs. This reduces the interaction between synaptic sorting and recycling partners vital for re-distribution of membrane fusion factors. Eventually, a synaptic vesicle-trafficking drag reduces new fusion events.

Fraldi *et al*., 2010

Collectively, our longitudinal circadian running-wheel data identified circadian disruption in LSDs, and the significance of the genetic lesion (HEXB) to the mechanics of the core clock rather than systemic pathology (NPC1). Despite extensive neurodegenerative disruption in the *Npc1*$^{-/-}$ mice, core clock deficits were not detected. The functionality of each gene with *Hexb* involved in enzymatic sphingolipid catabolic processes, while *Npc1* involved in cholesterol trafficking, could potentially address the discrepancy of circadian disruption in metabolic pathology (Schulze and Sandhoff, 2011).

6.4 BAC models of PD and Circadian Disruption

There has been a long-standing association between circadian disruption and PD (Factor *et al*., 1990; Tandberg *et al*., 1998; Scaravilli *et al*., 2003; Rahman *et al*., 2008; Qin *et al*., 2009; Louter *et al*., 2012). PD and FTDP-17 are part of a spectrum of neuropsychiatric disorders that include both motor and non-motor manifestations depending on disease stage (Braak *et al*., 2004; Ponsen *et al*., 2004; Stiasny-Kolster *et al*., 2005; Chaudhuri *et al*., 2006; Brooks, 2010). Major molecular players participating in the familial and sporadic heterogeneity of PD pathology includes a-synuclein, Parkin and Tau (Jakes *et al*., 1994; Bayer *et al*., 1999; Klein *et al*., 2000; Farrer *et al*., 2001; Vekrellis *et al*., 2004; Kozikowski *et al*., 2006;; Saiki *et al*., 2012).

All PD mutant lines investigated in this thesis displayed hyperactivity compared to controls. Importantly, BAC SNCA OVX mice display evoked dopaminergic release deficits from an early age (3 months old) that persist throughout their lifespan (Janezic *et al*., 2013). BAC SNCA A30P mice also display early regional dopamine-specific deficits in the dorsal striatum (Taylor *et al*., 2014). Studies of *Parkin*$^{-/-}$ mice recorded elevated extracellular dopamine levels, although they did not present any dopaminergic neurodegeneration in the substantia nigra (Goldberg *et al*., 2003). There have been studies linking dopamine dysfunction to restless leg syndrome (Allen, 2004; Wulff *et al*., 2009). Additionally, dopamine dysfunction has been associated with wakefulness, and in fact, mice lacking dopamine transporters exhibit hyperactive phenotypes and decreased sleep epochs (Wisor *et al*., 2001).

Collectively, our longitudinal circadian running-wheel data on BAC MAPT/SNCA and *Parkin*$^{-/-}$ mice illustrated scotophase hyperactivity, as well as alterations in activity fragmentation patterns. Importantly, NASA analysis in BAC SNCA OVX demonstrated significant differences in IV and IS factors compared to controls. The hyperactive phenotype

shared across PD models could be a common response to wheel exposure. Indeed, wheel-running exercises motivational reinforcement on mouse behavioural activity patterns (Careau *et al*., 2012). However, some of these mouse models report variable activity responses in other behavioural tests (Taylor *et al*., 2014; Wobst *et al*., 2014; unpublished data). Interestingly, dopamine deficits in PD have been implicated in reward-related impulsivity, and increased wheel-running in the BAC PD models could potentially reflect that phenotype (Aarts *et al*., 2012). Rhythm fragmentation differences in the BAC SNCA OVX and A30P models represent a potentially interesting circadian finding reminiscent of PD pathology in patients. Therefore, this body of work identified potential involvement of rest/activity mechanisms in mouse models of PD via scotophase fragmentation patterns (Adler and Thorpy, 2005; Iranzo *et al*., 2009; Claassen *et al*., 2010; Kudo *et al*., 2012). However, further behavioural testing is essential to confirm this association.

6.5 Summary

This project attempts to characterise circadian disruption in numerous mouse models of PD and LSDs. We have associated particular genetic lesions (SNCA, MAPT, *Parkin*, *Hexb*, *Npc1*) with characteristic circadian endophenotypes. The impact of circadian disruption has been evaluated in each mouse model and further molecular investigations are currently being pursued. It is hoped that the translational potential of the identified circadian pathology will be directly compared to findings from patient cohorts with the corresponding genetic defect. This project has identified a range of circadian disruption parameters in mouse models and addressed the longitudinal impact of ageing in metabolic and neuropsychiatric conditions.

This body of work examined the mechanistic association between circadian disruption and synaptic dysfunction in the *Bdr* mouse model of schizophrenia. The circadian axis was investigated and input and core clock defects were excluded. Instead our work focused on addressing the underlying synaptic trafficking events regulating critical output neuropeptide signalling. Utilising next-generation MS-seq instruments we were able to identify temporally de-regulated candidate proteins during synaptic pathology. Novel targets involved in mood-related disorders appear to regulate SCN critical output signalling events. This constitutes an attempt to link circadian disruption and post-transcriptional pathways involved in neuropsychiatric disorders.

6.6 Future Efforts

6.6.1 LSDs (Sandhoff and NPC)

Hexb$^{-/-}$ and *Npc1*$^{-/-}$ mice display different pathologies; however, a comparative circadian molecular study between the two can provide valuable insight into circadian core clock pathology in LSDs. *Hexb*$^{-/-}$ have demonstrated prodromal core clock defects as well as mild hypoactivity. *Npc1*$^{-/-}$ report no core clock pathology, although severe hypoactivity is present and end-stage circadian pathology cannot be completely excluded. Therefore, potential future efforts in LSDs include:

Assessing core clock expression in the SCN in both *Hexb*$^{-/-}$ and *Npc1*$^{-/-}$ mice

Based on circadian data on *Hexb*$^{-/-}$ and *Npc1*$^{-/-}$ data we expect to see de-regulation of core clock genes in the *Hexb*$^{-/-}$ mouse model. However, no core clock de-regulation would be observed in the *Npc1*$^{-/-}$ mice despite extensive CNS neurodegeneration and limited lifespan.

Prodromal sleep analyses in SD would be particularly useful for early screening and monitoring of disease onset and progression in genetically predisposed individuals (Vanier *et al*., 2010; Platt *et al*., 2012). Currently, misdiagnosis of SD due to the complicated disease manifestation prevents rapid onset of symptomatic and experimental treatment (Platt *et al*., 2012). However, core clock defects could represent a unique tool for a SD endophenotype.

Enzyme replacement/Substrate reduction therapy in *Hexb*$^{-/-}$ and core clock pathology

SD patients undergoing experimental treatment should have endogenous core clock genes monitored as a marker of disease progression. Therapies alleviating the gangliosidosis debt might rescue core clock pathology. However, given the prodromal nature of the core clock defects encountered in the *Hexb*$^{-/-}$ mice prior to extensive CNS neuropathology, that may not be the case without actual gene therapy.

Inducible *Hexb*$^{-/-}$ and core clock genes

Recently, inducible mouse models of *Hexb*$^{-/-}$ under the mouse *Hexb* promoter illustrated that *Hexb* silencing after 5 weeks induced progressive neurodegeneration reminiscent of a GM2 gangliosidosis (Sargeant *et al*., 2012). Importantly, recovery of *Hexb*$^{-/-}$ activity occurred following re-activation of the transgene as well as neurodegenerative rescue in the inducible *Hexb*$^{-/-}$ mice.

Understanding the dose-dependent response between the *Hexb* gene and circadian disruption might allow the identification of a minimum threshold of HEXB expression in SD patients. That could be particularly useful in future gene therapy studies for SD patients. Additionally, a similar approach could be undertaken for *Hexa*$^{-/-}$ (Tay-Sachs mouse models) that exhibit milder phenotypes, but biochemically overlapping defects with SD mice (Phaneuf *et al*., 1996). Therefore, if similar circadian phenotypes were observed, this would suggest that the *Hexa/b* genes have an impact on core clock functionality independent of disease stage or progression.

6.6.2 PD mouse models

BAC SNCA, MAPT and *Parkin*$^{-/-}$ mice exhibited scotophase hyperactivity. Particularly, BAC SNCA OVX mice exhibited variable fragmentation patterns and differences in interdaily stability and intradaily variability. Interestingly, motor function is enhanced and IS and IV improved in the mutant lines, possibly due to regional-specific dopaminergic alterations (Janezic *et al*., 2013; Taylor *et al*., 2014). This is in contrast to previous findings from the ASO line that records progressive motor deterioration and increased fragmentation (Kudo *et al*., 2012). Therefore, potential future efforts in PD models include:

Video tracking to assess sleep/wake behaviour in PD mice

Video tracking could be utilised to study sleep in PD mice in their home cage (Fisher *et al*., 2012). Indeed, this EEG-validated alternative allows for evaluation of sleep latency and duration as well as fragmentation patterns (Fisher *et al*., 2012). BAC SNCA OVX and A30P mice displayed variable fragmentation levels and video tracking would validate these preliminary findings. Indeed, sleep fragmentation, daytime somnolence and RBD are estimated to affect up to 90% of PD patients (Swick, 2012). Therefore, rest/activity fragmentation of activity profiles in the BAC SNCA OVX and A30P mice could reflect some of the sleep/wake disturbances identified in patients. Additionally, in the absence of a running-wheel, home cage activity could be assessed by analysing the total distance travelled (Fisher *et al*., 2012). That would be particularly relevant as exposure to a running-wheel may generate differences in activity data; as illustrated in the BAC SNCA A30P mice (Taylor *et al*.,

2014). Finally, home cage activity monitoring could be correlated to 24h wrist actigraphy data from PD patients in order to assess sleep quality (Stavitsky *et al*., 2010).

Whole-cell SCN patch clamp of BAC mice to record 24hr electrical firing rate

Aged BAC OVX SNCA display reduced SNc dopaminergic electrical firing (Janezic *et al*., 2013). Importantly, given the prodromal phenotype in BAC OVX mice, similar neurotransmitter defects might be identified in the SCN. The ASO line displays reduced firing rate of daytime SCN neurons (Kudo *et al*., 2012). Given the fragmented rest/activity patterns as well as the scotophase activity changes in both the OVX and ASO lines, we would expect some changes in neurotransmission to occur in the SCN of BAC SNCA OVX mice.

This finding would be particularly relevant as BAC mice represent high construct and face validity models. Understanding fragmentation differences in the BAC OVX mice will further our understanding of the impact of dopaminergic de-regulation on the circadian axis and increase the translatable potential of new therapeutics.

L-DOPA administration and circadian screening of PD models

L-DOPA administration has been utilised for the symptomatic relief of PD pathology (Lu, 2009). Similarly, it can used to assess the predictive validity of BAC PD models (Lu, 2009). L-DOPA administration in BAC SNCA OVX mice could reverse the wheel-running scotophase hyperactivity recorded by our screen. This finding would further validate the mechanism of circadian dysfunction in the malfunctioning dopaminergic neuro-circuitry in PD.

6.6.3 The schizophrenic *Bdr* model

Post-transcriptional screening of the *Bdr* mouse confirmed MARCKS/pMARCKs de-synchrony alongside a potential PKC-dependent de-regulated mechanism (Livieratos *et al*., 2014; unpublished data). Therefore, potential future efforts in the *Bdr* model include:

In vivo selective PKC inhibition of the *Bdr* circadian axis

PKC inhibition of the *Bdr* should down-regulate pMARCKS and halt the de-synchronous pro-active neurotransmitter release form of MARCKS (Fitzgerald *et al*., 2010). In turn, suppression of AVP/NT release at de-synchronous epochs should occur (Abou-Samra *et al*., 1986; Liu *et al*., 1994) in the *Bdr* and potentially rescue the phase advance exhibited by the model. This would address the cause and effect relationship regarding circadian disruption and schizophrenia. PKC inhibition has specific behavioural effects in WT mice (Abrial *et al*., 2013; Bonsall and Lall, 2013). These include a range of WT circadian responses to light that are temporally regulated (Bonsall and Lall, 2013) If indeed PKC inhibition restores circadian rhythms in the *Bdr*, PPI assessment would then follow. Depending on the findings it might establish a cause/effect condition whereby circadian rhythms are restored in the absence of alleviated PPI or the reverse. That would be particularly useful in understanding circadian disruption in context of schizophrenic endophenotypes.

This finding will be particularly relevant in schizophrenic cohorts with potential post-transcriptional SCN disruption. Alleviation of schizophrenic endophenotypes via targeted modulators on the circadian axis would be particularly useful and would complement existing antipsychotic treatments.

RNA-seq of the *Bdr* SCN transcriptome

RNA-seq work on the *Bdr* across an entire LD cycle would be complementary to the current proteomic screen conducted in this project. Importantly, due to the complexity of MS-seq and RNA-seq datasets, a global representation of the dynamics of transcriptional/translational rhythmic oscillations could be constructed. Additionally, long non-coding RNA transcripts and their functional relevance in the WT SCN clock as well as in the synaptic *Bdr* mutant could also be addressed.

PNS enhances circadian disruption and MARCKS/pMARCKS de-regulation?

Environmental x genetic interplay has been demonstrated during PNS-stimulated PPI aggravation in the *Bdr* model (Oliver and Davies, 2009). Similarly, circadian disruption could also be aggravated in PNS *Bdr* mice. Moreover, factors participating in the *Bdr* dysfunctional clock such as AVP and MARCKS could also be further de-synchronised and de-regulated.

This finding will be particularly relevant in the understanding of the aetiology of schizophrenia and the complex cross-talk between environmental and genetic mechanisms. An understanding of the environmental impact on circadian disruption would address the plasticity of the clock during synaptic dysfunction.

6.7 Beyond this Project

This project has suggested an association between circadian disruption and a variety of neuropsychiatric and metabolic disorders. Indeed the Royal College of Psychiatrists formally recognises sleep/wake deficits as a significant clinical manifestation in a variety of mood-related disorders.

However, a greater emphasis needs to be placed on personalised medicine of neuropsychiatric conditions like schizophrenia and bipolar disorder. With the future rise of neurological disorders due to demographics, one cannot ignore the urgency in addressing this healthcare challenge. High-resolution, high-throughput molecular and behavioural screening will be critical in unlocking the mechanisms driving the pathogenesis of complex disorders.

The principal conclusion from this work is that genetic predisposition to particular neuropsychiatric or metabolic disorders might have an impact on the functionality of the circadian axis. Possible therapeutic intervention along that axis could potentially be investigated in clinical studies for neuropsychiatric and metabolic disorders.

7 Acknowledgements

I would like to thank the Medical Research Council, Wolfson College and Oxford University for their funding and support. I would like to acknowledge Prof. Dame Kay Davies for her input into this project and support during these years of the D.Phil. I would also like to recognise Dr Benjamin Thomas for his contribution to this project. Special thanks goes to Dr Peter Oliver for the wonderful tutoring he provided and the opportunity to explore what science is all about. I would also like to acknowledge Dr Katharina Wulff for her help regarding analysis of circadian data as well as Benjamin Edwards for his aid regarding tissue collection and genotype screening. Finally, I would like to thank my family and friends including my partner, Steluta Raduica, for her continuing belief in me.

8 Appendix

Word count: 43,314 (excluding Figure Legends, Acknowledgements, Appendix, References).

8.1 Abbreviations

12:12	12 hour: 12 hour
2D PAGE	Two-dimensional polyacrylamide gel-electrophoresis
3V	Third Ventricle
5-HT	5-hydroxytryptamine
AAV	Adeno-Associated Virus
ABC	Avidin-biotin complex
ACTH	Adrenocorticotropin
AD	Alzheimer's disease
ADHD	Attention deficit hyperactivity disorder
Alpha	Active phase
AMPA	α-amino-3-hydroxyl-5-methyl-4-isoxazole-propionate
ANOVA	Analysis of variance

AP	Action Potential
ARC	Arcuate nuclei
ASD	Autism spectrum disorders
ASO	Alpha-synuclein over-expressing
AVP	Arginine Vasopressin
BAC	Bacterial artificial chromosomes
Bdr	Blind-drunk
Bmal1	Brain and muscle ARNTL 1
Bp	Base pairs
cAMP	Cyclic adenosine mono-phosphate
CBD	Corticobasal degeneration
CCGs	Core clock genes
Cckar	Cholecystokinin A receptor
cdk5	Cyclin-dependent kinase 5
cDNA	Complementary DNA
CART	Cocaine-and amphetamine-regulated transcript protein
CLOCK	Circadian locomotor output kaput
CNS	Central nervous system
CRBL	Cerebellum
CREB	cAMP response element binding protein
CRF	Corticotropin-releasing factor
Cry	Cryptochrome
CSF	Cerebrospinal fluid
CT	Circadian time
Ct	Critical threshold
d/vSPVZ	Dorsal/ventral subparaventricular zone of the hypothalamus
DAB	Diaminobenzidine
DAG	Diacylglycerol
Dao	D-amino acid oxidase
$Dbh^{-/-}$	Dopamine β-hydroxylase -/-
DD	Dark-Dark

DISC1	Disrupted-in-schizophrenia-1
DLB	Dementia with Lewy Body
DM	Dorsomedial
DMH	Dorsomedial hypothalamus
DNA	Deoxyribonuleic acid
DSPS	Delayed sleep phase syndrome
ECL	Enhanced chemiluminescence
EDS	Excessive daytime sleepiness
EEG	Electro-encephalongraphy
ELISA	Enzyme-linked immunosorbent assay
ENU	n-ethyl-n-nitrosourea
FASP	Familial advanced sleep phase syndrome
FBXL3	F-box/LRR-repeat protein 3
FCTX	Frontal Cortex
F-DOPA	Fluorodopa
FEO	Food-entrainable oscillator
FTD	Frontal Temporal Dementia
FTDP-17	Frontotemporal dementia with parkinsonism linked to chromosome 17
G_{A2}	Asialo-GM2
GABA	Gamma-amino butyric acid
GalNAc	N-acetylgalactosamine
GAP-43	Growth Associated Protein 43
GAPDH	Glyceraldehyde 3-phosphate dehydrogenase
GFAP	Glial fibrillary acidic protein
Glu	Glutamate
Glut2	Glucose transporter 2
GM2	Ganglioside
GRP	Gastrin-releasing peptide
GSK3β	Glycogen synthase kinase 3β
GWAS	Genome-wide association study
HD	Huntington disease

HEXA	α- hexosaminidase
HEXB	β-hexosaminidase
HPA	Hypothalamic-pituitary-adrenal
HPR	Horse peroxidase reaction
htau	Human tau
I.p.	Intraperitoneal injection
ICAT	Isotope-coded affinity tag
IEG	Immediate early gene
IGL	Intergeniculate Leaflet
IHC	Immunohistochemistry
ipRGC	Intrinsically photosensitive retinal ganglion cells
IS	Intradaily stability
ISH	*In situ* hybridisation
IV	Interdaily variability
KO, -/-	Knockout
LB	Lewy bodies
LC/MS	Liquid Chromatography-Mass spectrometry
LCM	Laser Capture Microdissection
LD	Light-Dark
LDL	Low-density lipoprotein
LED	Light-emitting diode
LH	Lateral hypothalamus
LL	Light-Light
LMA	Locomotor activity
LRRK2	Leucine-rich repeat kinase 2
LSDs	Lysosomal storage disorders
MAPT	Microtubule-associated protein tau
MARCKS	Myristoylated alanine-rich C-kinase substrate
MCBs	Membranous cytoplasmic bodies
MMIF	Macrophage migration inhibitory factor
MPO	Median pre-optic area

MPS	Mucopolysaccharidosis
MR	Median Raphe
mRNA	Messenger ribonucleic acid
MSD	Multiple sulphatase deficiency
MS-seq	Mass Spectrometry-sequencing
MW	Molecular weight
NASA	Nonparametric activity and sleep analysis
NFTs	Neurofibrillary tangles
NMDA	n-methyl D-aspartate
NMDAR	n-methyl D-aspartate receptor
NPC	Niemann-Pick type C
NPY	Neuropeptide Y
NREM	Non-rapid eye movement
Nrg1	Neuregulin 1
NSF	N-ethyl-maleimide-sensitive factor
NT	Neurotensin
NTO	Non-transcriptional oscillation
OVX	Over-expressing
PACAP	Pituitary adenylate cyclase activating polypeptide
PBS	Phosphate buffered saline
PCAP	Pituitary adenylate cyclase activating polypeptide
PCP	Phencyclidine
PCR	Polymerase chain reaction
PD	Parkinson Disease
PDD	Parkinson Disease Dementia
Per	Period
PH	Posterior Hypothalamus
PINK1	PTEN-induced putative kinase 1
PIP_2	Phosphatidylinositol 4, 5-bisphosphate
PK2	Prokineticin 2
PKA	Protein Kinase A

PKC	Protein Kinase C
PLCɣ	Phospholipase Cɣ
pMARCKS	Phosphorylated MARCKS
PNS	Pre-Natal Stress
PPI	Pre-pulse inhibition
PRC	Phase response curve
PSP	Progressive supranuclear pasly
PUTM	Putamen
PVH	Paraventricular nucleus
Q Exactive	Hybrid Quadrupole Obritrap Mass spectrometer
qPCR	Quantitative PCR
qRT-PCR	Quantitative reverse transcriptase polymerase chain reaction
rANOVA	Repeated measures Analysis of variance
REM	Rapid eye movement
REV-ERBa	Nuclear receptor subfamily 1, group D, member 1
Rho	Rest phase
RHT	Retinohypothalamic Tract
RIN	RNA Integrity Number
RNA	Ribonucleic acid
ROR	RAR-related orphan receptors
ROS	Reactive oxygen species
RP	Reserve pool
RRP	Readily releasable pool
RT	Reverse transcription
SC	Spinal cord
SCN	Suprachiasmatic nucleus
SD	Sandhoff disease
SEM	Standard error of mean
SM	Sec1/Munc18-like
SN	Substantia nigra
SNAP-25	Synaptosomal-associated protein 25kDa

SNARE	Soluble NSF Attachment Receptor proteins
SNc	Substantia Nigra pars compacta
SNCA	A-synuclein
SNPs	Single nucleotide polymorphisms
SP	Substance P
STR	Striatum
SWA	Slow-wave activity
Tac1	Tachykinin 1
Tau	Period length
TBST	Tris-buffered Saline Tween-20
Tg	Transgenic
TH	Tyrosine Hydroxylase
TMN	Tuberomamillary nucleus
TTFL	Transcriptional/translational feedback loop
VAMP	Vesicle-associated membrane protein
VIP	Vasoactive intestinal polypeptide
Vipr2	VIP-receptor
VL	Ventrolateral
VLPO	Vetrolateral pre-optic nucleus
VMAT-2	Vesicular monoamine transporter 2
VMH	Ventromedial nuclei
WB	Western blot
WR	Working Reagent
WT, +/+	Wild type control
ZT	Zeitgeber time
β-TrCP1	Beta-transducin repeat containing E3 ubiquitin protein ligase

8.2 Tables

Table 1.1: Human neurological diseases and sleep endophenotypes **(page 22)**

Table 1.2: Disrupted sleep/wake cycles and associated systemic impact **(page 30)**

Table 1.3: Risk genes in familial PD **(page 40)**

Table 1.4: Summary of α-synuclein transgenic mouse models **(page 41)**

Table 1.5: Summary of MAPT transgenic mouse models **(page 42)**

Table 1.6: Circadian deficits in the ASO line **(page 47)**

Table 1.7: LSDs genetic perturbations and phenotype observed **(page 49)**

Table 2.1: Circadian parameters investigated during screening of transgenic mouse models **(page 63)**

Table 2.2: qRT-PCR targets investigated and primers utilized **(page 68)**

Table 2.3: *In situ* genes investigated and corresponding primer sequence **(page 69)**

Table 2.4: SCN proteomic targets investigated by IHC **(page 77)**

Table 3.1: Parkinson's disease motor and non-motor symptoms **(page 81)**

Table 3.2: 12:12hr LD cycle **(page 97)**

Table 3.3: DD period **(page 98)**

Table 3.4: LL period **(page 98)**

Table 3.5: Summary table of screened BAC SNCA mice **(page 102)**

Table 3.6: 12:12hr LD cycle **(page 107)**

Table 3.7: DD period **(page 108)**

Table 3.8: LL period **(page 108)**

Table 3.9: Summary table of screened BAC MAPT mice **(page 114)**

Table 3.10: 12:12hr LD cycle **(page 118)**

Table 3.11: DD period **(page 119)**

Table 3.12: LL period **(page 119)**

Table 3.13: Summary table of screened Parkin mice **(page 124)**

Table 3.14: Behavioural abnormalities in *Parkin*$^{-/-}$ mouse models of PD **(page 134)**

Table 4.1: 12:12hr LD cycle **(page 149)**

Table 4.2: 6hr phase advance **(page 150)**

Table 4.3: DD period **(page 150)**

Table 4.4: Summary table of screened *Npc* mice **(page 155)**

Table 4.5: 12:12hr LD cycle **(page 159)**

Table 4.6: DD period **(page 160)**

Table 4.7: LL period **(page 160)**

Table 4.8: Summary table of screened *Hexb* mice **(page 165)**

Table 5.1: Neuropeptides identified from 1mm WT SCN tissue punch via label-free MS/MS **(page 184)**

Table 5.2: MS data table of proteomic WT spatio-temporal controls **(page 192)**

Table 5.3: WT SCN non-overlapping proteomic targets **(page 196)**

Table 5.4: MS data table of potentially de-regulated endogenous peptidomic targets **(page 198)**

Table 5.5: MS data table of potentially de-regulated SCN proteomic targets **(page 200)**

Table 5.6: MS data table of followed-up de-regulated proteomic targets **(page 203)**

Table 5.7: Summary data of proteomic SCN targets **(page 211)**

Table 5.8: Granin peptides in neurological disorders **(page 215)**

Table 8.1: Mouse models screened via running-wheel **(page 256)**

8.3 Figures

Figure 1.1: The circadian axis **(page 12)**

Figure 1.2: SCN sleep/wake connectivity **(page 13)**

Figure 1.3: Homeostatic and circadian regulation of sleep/wake cycles (**page 16**)

Figure 1.4: Signalling in the circadian axis **(page 20)**

Figure 1.5: Representative control versus schizophrenic actograms (**page 25)**

Figure 1.6: Chromosomal map of genetic anomalies associated with schizophrenia and bipolar disorder **(page 27)**

Figure 1.7: SNAREs facilitate fusion of synaptic vesicles to the membrane **(page 33)**

Figure 1.8: Mouse protein *Snap-25b* sequence versus orthologous and paralogous targets **(page 36)**

Figure 1.9: Circadian wheel-running data on *Bdr* mice **(page 38)**

Figure 1.10: Potential PD impacts on the circadian axis **(page 45)**

Figure 1.11: Circadian and metabolic factors cooperate **(page 53)**

Figure 2.1: Circadian screening protocol illustration of PD mouse models **(page 61)**

Figure 2.2: Circadian screening protocol illustration of LSD mouse models **(page 62)**

Figure 2.3: Representative circadian running-wheel set-up **(page 62)**

Figure 2.4: Anatomical mouse brain areas of SCN, PVH and CTX collected **(page 64)**

Figure 2.5: Abrupt 30 minute photic stimulation experiment investigating retinal input pathways to the SCN **(page 65)**

Figure 2.6: Methodology for quantifying SCN peptidome and proteome **(page 72)**

Figure 2.7: Experimental and data analysis flowchart pursued for the 24hr (6 time points) SCN WT versus *Bdr* proteomic investigation **(page 76)**

Figure 3.1: Representative double-plotted actograms of the screen for each line **(page 91)**

Figure 3.2: Activity Count By Day **(page 93)**

Figure 3.3: LD activity profiles over 7-14 days at different stages of the circadian screen **(page 94)**

Figure 3.5: Total activity bouts over 7-14 days at different stages of the circadian screen **(page 95)**

Figure 3.5: IS and IV values among mouse lines in LD **(page 96)**

Figure 3.6: Negative masking effects of photic stimulation on day of pulse administration on each PD line **(page 100)**

Figure 3.7: Representative A30P double-plotted actograms of the DD paradigm **(page 101)**

Figure 3.8: Representative double-plotted actograms of the screen for each line **(page 103)**

Figure 3.9: Activity Count By Day **(page 105)**

Figure 3.10: LD activity profiles over 7-14 days at different stages of the circadian screen **(page 106)**

Figure 3.11: Negative masking effects of photic stimulation on day of pulse administration on each PD line **(page 110)**

Figure 3.12: Phase advance observed in all lines during the 6hr phase shift **(page 111)**

Figure 3.13: Representative double-plotted actograms of the 6hr phase shift **(page 112)**

Figure 3.14: DD phase onset plots **(page 112)**

Figure 3.15: Type II Phase Delay **(page 113)**

Figure 3.16: Representative BAC MAPT double-plotted actograms of the DD paradigm **(page 113)**

Figure 3.17: LL phase onset plots **(page 114)**

Figure 3.18: Representative double-plotted actograms of the screen for each genotype **(page 115)**

Figure 3.19: Activity Count By Day **(page 116)**

Figure 3.20: LD activity profiles over 7-14 days at different stages of the circadian screen **(page 117)**

Figure 3.21: Negative masking effects of photic stimulation on day of pulse administration on each genotype **(page 120)**

Figure 3.22: Phase advance observed in both lines during the 6hr phase shift **(page 121)**

Figure 3.23: DD phase onset plots **(page 122)**

Figure 3.24: Type II Phase Delay **(page 123)**

Figure 3.25: Representative double-plotted actograms of the DD paradigm **(page 123)**

Figure 3.26: LL phase onset plots **(page 124)**

Figure 4.1: Clinical signs of NPC patients with varying disease onset **(page 137)**

Figure 4.2: Shared biochemistry in Tay-Sachs and Sandhoff diseases **(page 138)**

Figure 4.3: Circadian paradigms employed for *Npc1*$^{-/-}$ mice **(page 145)**

Figure 4.4: Circadian paradigms employed for *Hexb*$^{-/-}$ mice **(page 145)**

Figure 4.5: Representative double-plotted actograms of the screen for each genotype **(page 146)**

Figure 4.6: Activity Count By Day **(page 147)**

Figure 4.7: LD activity profiles over 11 days **(page 148)**

Figure 4.8: Negative masking effects of photic stimulation on day of pulse administration on each genotype **(page 152)**

Figure 4.9: Phase advance observed in both lines during the 6hr phase shift **(page 153)**

Figure 4.10: Representative double-plotted actograms of the 6hr phase shift **(page 154)**

Figure 4.11: DD phase onset plots **(page 154)**

Figure 4.12: Representative double-plotted actograms of the DD paradigm **(page 155)**

Figure 4.13: Representative double-plotted actograms of the screen for each genotype **(page 156)**

Figure 4.14: Activity Count By Day **(page 157)**

Figure 4.15: LD activity profiles over 7 days **(page 158)**

Figure 4.16: Negative masking effects of photic stimulation on day of pulse administration on each genotype **(page 162)**

Figure 4.17: DD phase onset plots **(page 163)**

Figure 4.18: Type II Phase Delay **(page 163)**

Figure 4.19: Representative double-plotted actograms of the DD paradigm **(page 164)**

Figure 4.20: LL phase onset plots **(page 164)**

Figure 4.21: Representative double-plotted actograms of the LL paradigm **(page 165)**

Figure 4.22: Light-dependent retinal input pathways separating the visual from the circadian system **(page 170)**

Figure 5.1: Circadian axis operation in *Bdr* versus WT **(page 173)**

Figure 5.2: qRT-PCR of IEGs, *Per1- 2*, *Six-6* and *VIP* on WT versus *Bdr* SCN **(page 178)**

Figure 5.3: Representative i*n situ* of pre-pulse and post-pulse WT SCN *c-fos* induction **(page 180)**

Figure 5.4: ISH of *c-fos*, *jun-B* and *VIP* targets on WT and *Bdr* SCN **(page 180)**

Figure 5.5: Proteomic yield of alternative buffers and increasing tissue quantity **(page 182)**

Figure 5.6: Representative SCN neuropeptides extracted from different buffers **(page 185)**

Figure 5.7: Representative SCN ion intensity map **(page 186)**

Figure 5.8: Quantification Protocol by Progenesis LC-MS **(page 188)**

Figure 5.9: Dendogram profile of Proteins **(page 190)**

Figure 5.10: WT SCN spatio-temporal controls quantified over 24h **(page 193)**

Figure 5.11: WT SCN non-overlapping targets versus control **(page 195)**

Figure 5.12: SCN WT/*Bdr* spatio-temporal controls quantified over 24hr **(page 197)**

Figure 5.13: Representative Prothyroliberin peptide in ion intensity maps **(page 199)**

Figure 5.14: Temporally de-regulated proteomic targets in *Bdr* SCN versus WT SCN **(page 201)**

Figure 5.15: Representative MARCKS peptide in ion intensity maps **(page 204)**

Figure 5.16: IHC SCN confirmation of proteomic de-regulation over 24h in WT versus *Bdr* **(page 205)**

Figure 5.17: WB SCN confirmation of proteomic de-regulation in WT versus *Bdr* **(page 208)**

Figure 5.18: IHC/ELISA SCN confirmation of pMARCKS/PKC activity de-synchrony **(page 210)**

Figure 5.19: Methodological variations between MS and IHC **(page 214)**

Figure 5.20: CGF scoring of potential biomarkers in suicidality in mental health disorders **(page 222)**

Figure 6.1: Synaptic trafficking defects in LSDs **(page 233)**

8.4 Mouse models

Table 8.1: Mouse models screened via running-wheel

Mouse model	Genetic Design	Background Strain	Sex	Age at onset of circadian screen	Duration of screen	Molecular pathology	Behavioural Pathology
SNCA OVX	BAC transgenic	C57BL/6	M/F	8 months	110 days	3-4 month Dopamine deficits 18 month Nigrostrital neuronal loss	GI dysfunction 18 month Rotarod defictis
SNCA A30P	BAC transgenic	C57BL/6	M/F	8 months	110 days	3-4 month Dopamine deficits	6 month Anxiety phenotype
$SNCA^{-/-}$	Exon knockout	C57BL/6	M/F	8 months	110 days	3 month Altered dopamine release	3 month Reduced amphetamine-stimulated locomotion
SNCA WT	BAC transgenic	C57BL/6	M/F	8 months	110 days	N/A	N/A
MAPT N51	BAC transgenic	C57BL/6	M/F	10 months	87 days	Not Available	6 month Depressive phenotype in tail suspension test
$MAPT^{-/-}$	Exon Knockout	C57BL/6	M/F	10 months	87 days	MIcortube density reduced in cerebellum	4 month Hyperactivity in open field testing Deficits in rod walking tests
MAPT WT	BAC transgenic	C57BL/6	M/F	10 months	87 days	N/A	N/A
Parkin$^{-/-}$	Exon Knockout	C57BL/6	M	10 months	68 days	3 month Enhanced striatal dopamine metabolism	Age independent increased anxiety in open field testing
Hexb$^{-/-}$	Exon Knockout	C57BL/6	M	7 weeks	31 days	3-4 month Ganglioside deposition and neurodegeneration	2.5 month Motor deficits and memory impairment
Npc1$^{-/-}$	Retroposon insertion	BALB/cJ albino mice	M	7 weeks	21 days	40 days Progressive cerebellar and thalamic neuronal atrophy	40 days Retarded growth and weight loss Motor deficits in rotarod

Table 8.1: Mouse models investigated including the genetic design, background strain, sex, age, duration of screen and accompanying molecular and behavioural pathology.

9 References

Aarsland D., *et al*. (1999) Range of neuropsychiatric disturbances in patients with Parkinson's disease. *J. Neurol. Neurosurg. Psychiatry.* **67:** 492–496

Aarsland D., *et al*. (2012) Depression in Parkinson disease-epidemiology, mechanisms and management. *Nature Reviews Neurology.* **8:** 35–47

Aarts E., *et al*. (2012) Aberrant reward processing in Parkinson's disease is associated with dopamine cell loss. *Neuroimage*. **59**: 3339–3346

Abdul-Salam V. B., *et al.* (2010) Proteomic analysis of lung tissues from patients with pulmonary arterial hypertension. *Circulation*. **122**: 2058–2067

Abe M., *et al*. (2000) Lithium lengthens the circadian period of individual suprachiasmatic nucleus neurons. *Neuroreport.* **11:** 3261–3264

Abeliovich A., *et al.* (2000) Mice lacking alpha-synuclein display functional deficits in the nigrostriatal dopamine system. *Neuron*. **25:** 239–352

Abou-Samra A.B., *et al*. (1986) Involvement of protein kinase C in the regulation of adrenocorticotropin release from rat anterior pituitary cells. *Endocrinology.* **118:** 212–217

Abraham U., *et al*. (2010) Coupling governs entrainment range of circadian clocks. *Mol. Syst. Biol*. **6**: 438

Abrahamson E.E., Moore R.Y. (2001) Suprachismatic nucleus in the mouse: retinal innervation, intrinsic organization and efferent projections. *Brain Res*. **916**: 172-191

Abrial E., *et al.* (2013) Protein kinase C regulates mood-related behaviors and adult hippocampal cell proliferation in rats. *Prog Neuropsychopharmacol Biol Psychiatry.* **43:** 40–48

Abrial E., *et al.* (2011) A role for the PKC signaling system in the pathophysiology and treatment of mood disorders: involvement of a functional imbalance? *Mol. Neurobiol.* **44:** 407–419

Acheson A., *et al.* (2007) Effects of sleep deprivation on impulsive behaviors in men and women. *Physiol Behav.* **91:** 579–587

Acosta-Galvan G., *et al*. (2011) Interaction between hypothalamic dorsomedial nucleus and the suprachiasmatic nucleus determines intensity of food anticipatory behavior. *Proc. Natl. Acad. Sci. USA*. **108**: 5813–5818

Adamantidis A., de Lecea L. (2009) The hypocretins as sensors for metabolism and arousal. *J Physiol*. **587:** 33–40

Adler C.M., Thorpy M.J. (2005) Sleep issues in Parkinson's disease. *Neurology.* **64:** 12–20

Agius L. (2008) Glucokinase and molecular aspects of liver glycogen metabolism. *Biochem. J*. **414:** 1–18

Akaboshi S., Ohno K. (1995) Niemann-Pick disease type C. *Nihon Rinsho.* **53:** 3036–3040

Akashi M. *et al.* (2002) Control of intracellular dynamics of mammalian period proteins by casein kindase I epsilon (CKIε) and CKIδ in cultured cells. *Mol. Cell. Biol*. **22**: 1693-1703

Albrecht U., *et al.* (2005) A guideline for analyzing circadian wheel-running behavior in rodents under different lighting conditions. *Biol. Proced. Online.* **7**: 101–116

Albrecht U., *et al*. (2001) MPer1 and mper2 are essential for normal resetting of the circadian clock. *J. Biol. Rhythms.* **16:** 100–104

Albus H., *et al*. (2005) A GABAergic mechanism is necessary for coupling dissociable ventral and dorsal regional oscillators within the circadian clock. *Curr. Biol*. **15**: 886–893

Alim M.A., *et al*. (2002) Tubulin seeds alpha-synuclein fibril formation. *Journal of Biological Chemistry.* **277**: 2112–2117

Alix J.J., *et al*. (2008) Vesicular apparatus, including functional calcium channels, are present in developing rodent optic nerve axons and are required for normal node of Ranvier formation. *J Physiol.* **586:** 4069–4089

Allen R., (2004) Dopamine and iron in the phathophysiology of restless legs syndrome (RLS). *Sleep Med*. **5**: 385–391

Allen N.C., *et al.* (2008) Systematic meta-analyses and field synopsis of genetic association studies in schizophrenia: the SzGene database. *Nat. Genet.* **40:** 827–834

Almond S.L., *et al*. (2006) Behavioral and biochemical characterization of a mutant mouse strain lacking D-amino acid oxidase activity and its implications for schizophrenia. *Mol Cell Neurosci.* **32:** 324–334

Alonso S.J., *et al*. (2000) Behavioral despair in mice after prenatal stress. *J. Physiol. Biochem.* **56:** 77–82

Alonso W.J., Sheldon S.H. (2010) Sleep abnormalities in children and adolescents with endocrine and metabolic disorders. *Pediatr Endocrinol Rev.* **7:** 292**–**299

Alt A., *et al*. (2006) In vitro and in vivo studies in rats with LY293558 suggest AMPA/kainite receptor blockade as a novel potential mechanism for the therapeutic treatment of anxiety disorders. *Psychopharmacology.* **185:** 240–247

Amadio M., *et al*. (2006) The different facets of protein kinases C: old and new players in neuronal signal transduction pathways. *Pharmacol Res.* **54:** 317–325

Amann L.C., *et al*. (2010) Mouse behavioral endophenotypes for schizophrenia. *Brain Res Bull*. **83:** 147–161

Ambelas A. (1979) Psychologically stressful events in the precipitation of manic episodes. B*r. J. Psychiatry.* ***135*:** 15–21

American Psychiatric Association (1994) *Diagnostic and statistical manual ofmental disorders*, 4th ed. American Psychiatric Association. Washington, DC

Amrollahi Z., *et al*. (2010) Double-blind, randomized, placebo-controlled 6-week study on the efficacy and safety of the tamoxifen adjunctive to lithium in acute bipolar mania. *J. Affect Disord.* **129:** 327–331

Andersson U., *et al*. (2004) Improved outcome of *N*-butyldeoxygalactonojirimycin-mediated substrate reduction therapy in a mouse model of Sandhoff disease. *Neurobiol Dis.* **16:** 506–515

Ando H., *et al*. (2011). Impairment of peripheral circadian clocks precedes metabolic abnormalities in ob/ob mice. *Endocrinology.* **152:** 1347–1354

Andorfer C., *et al*. (2005) Cell-cycle reentry and cell death in transgenic mice expressing nonmutant human tau isoforms. *J. Neurosci.* **25:** 5446–5454

Andorfer C., *et al*. (2003) Hyperphosphorylation and aggregation of tau in mice expressing normal human tau isoforms. *J. Neurochem.* **86**: 582–590

Arai Y., *et al*. (2001) *α*-Synuclein-positive structures in cases with sporadic Alzheimer's disease: morphology and its relationship to tau aggregation. *Brain Research*. **888:** 287–296

Arble D.M., *et al*. (2009) Circadian timing of food intake contributes to weight gain. *Obesity.* **17:** 2100–2102

Arinami T., *et al*. (2005) Genomewide high-density SNP linkage analysis of 236 Japanese families supports the existence of schizophrenia susceptibility loci on chromosomes 1p, 14q, and 20p. *Am J Hum Genet.* **77:** 937–944

Arnsten A.F.T., Manji H.K. (2008) Mania: a rational neurobiology. *Future Medicine.* **3:** 125–131

Asher G., Schibler U. (2011) Crosstalk between components of circadian and metabolic cycles in mammals. *Cell Metab.* **13:** 125–137

Askenasy J.J. (2003) Sleep disturbances in Parkinsonism. *J. Neural. Transm*. **110**: 125–150

Aton S.J., *et al.* (2004) Plasticity of circadian behavior and the suprachiasmatic nucleus following exposure to non-24-hour light cycles. *J Biol Rhythms* **19:** 198–207

Aton S.J., *et al*. (2005) Vasoactive intestinal polypeptide mediates circadian rhythmicity and synchrony in mammalian clock neurons. *Nat Neurosci.* **8:** 476–483

Attems J., *et al*. (2007) Tau and *α*-synuclein brainstem pathology in Alzheimer disease: relation with extrapyramidal signs. *Acta Neuropathologica*l. **113:** 53–62

Ayalew M., *et al*. (2012) Convergent functional genomics of schizophrenia: from comprehensive understanding to genetic risk prediction. *Mol Psychiatr.* **17:** 887–905

Ayhan Y., *et al*. (2009) Animal models of gene–environment interactions in schizophrenia. *Behav. Brain Res.* **204:** 274–281

Bachus S.E., *et al*. (1997) Abnormal cholecystokinin mRNA levels in entorhinal cortex of schizophrenics. *J Psychiatr Res*. **31:** 233–256

Badner J.A., Gershon E.S. (2002) Meta-analysis of whole-genome linkage scans of bipolar disorder and schizophrenia. *Mol Psychiatry*. **7:** 405–411

Baggerly K. A., *et al*. (2005) Signal in noise: evaluating reported reproducibility of serum proteomic tests for ovarian cancer. *Journal of the National Cancer Institute*. **97:** 307–309

Baglioni C., *et al*. (2010) Sleep and emotions: a focus on insomnia. *Sleep Medicine Reviews.* **14:** 227–238

Baker M., *et al*. (1999) Association of an extended haplotype in the tau gene with progressive supranuclear palsy. *Hum. Mol. Genet.* **8:** 711–715

Ballabio A., Gieselmann V. (2009) Lysosomal disorders: from storage to cellular damage. *Biochim. Biophys. Acta*. **1793:** 684–696

Balsalobre A., *et al*. (2000) Resetting of circadian time in peripheral tissues by glucocorticoid signalling. *Science*. **289**: 2344–2347

Ban Y., Shigeyoshi Y., Okamura (1997) Development of vasoactive intenstinal peptide mRNA rhythm in the rat suprachiasmatic nucleus. *J. Neuroscience.* **17:** 3920–3931

Banaschewski T. (2005) Towards an understanding of unique and shared pathways in the psychopathophysiology of ADHD. *Developmental science.* **8:** 132

Banks R. E., *et al*. (2005) Influences of blood sample processing on low-molecular-weight proteome identified by surface-enhanced laser desorption/ionization mass spectrometry. *Clinical Chemistry*. **51:** 1637–1649

Banks S., Dinges D.F. (2007) Behavioral and physiological consequences of sleep restriction. *J Clin Sleep Med*. **3:** 519–528

Barakauskas V.E., *et al*. (2010) A novel mechanism and treatment target for presynaptic abnormalities in specific striatal regions in schizophrenia. *Neuropsychopharmacology.* **35:** 1226–1238

Baranski J.V., *et al*. (2007) Effects of sleep loss on team decision making: motivational loss or motivational gain? *Hum Factors*. **49:** 646–660

Barf R.P., *et al*. (2010) Chronic sleep disturbance impairs glucose homeostasis in rats. *Int. J. Endocrinol.* **2010:** 819414

Bark C. (2009) SNAP-25 and gene-targeted mouse mutants. *Ann N Y Acad Sci.* **1152:** 145–153

Barkus C., Feyder M., *et al*. (2012) Do GluA1 knockout mice exhibit behavioral abnormalities relevant to the negative or cognitive symptoms of schizophrenia and schizoaffective disorder? *Neuropharmacology.* **62:** 1263–1272

Barnard A.R., Nolan P.M. (2008) When clocks go bad: neurobehavioral consequences of disrupted circadian timing. *PLoS Genetics*. **4:** e100040

Barnea M., *et al*. (2009) High-fat diet delays and fasting advances the circadian expression of adiponectin signaling components in mouse liver. *Endocrinology.* **150:** 161–168

Barnes J., David A. (2001) Visual hallucination in Parkinson's disease: a review and phenomenological survey. *J Neurol Neurosurg Psychiatry*. **70:** 727–733

Barr A.M., *et al*. (2006) In Dityatev, A. and El-Husseini, A. (eds), Molecular Mechanisms of Synaptogenesis. *Springer Verlag.* 391–408

Barros C.S., *et al*. (2009) Impaired maturation of dendritic spines without disorganization of cortical cell layers in mice lacking NRG1/ErbB signaling in the central nervous system. *Proc. Natl. Acad. Sci. USA.* **106**: 4507

Bartolomucci A., *et al*. (2010) Granins as disease-biomarkers: translational potential for psychiatric and neurological disorders. *Neuroscience.* **170:** 289–297

Bassett A.S., *et al*. (1993) Positive and negative symptoms in families with schizophrenia. *Schizophrenia Research.* **11:** 9-19

Basta-Kaim A., *et al*. (2006) Antipsychotic drugs inhibit the human corticotropin-releasing-hormone gene promoter activity in neuro-2A cells-an involvement of protein kinases. *Neuropsychopharmacology*. **31:** 853–865

Bayer T.A., *et al*. (1999) Alpha synuclein accumulates in Lewy bodies in Parkinson's disease and dementia with Lewy bodies but not in Alzheimer's disease betaamyloid plaque cores. *Neurosci. Lett.* **266:** 213–216

Beasley C.L., *et al*. (2006) Proteomic analysis of the anterior cingulate cortex in the major psychiatric disorders: Evidence for disease-associated changes. *Proteomics*. **6**: 3414–3425

Bebchuk J.M., *et al.* (2000) A preliminary investigation of a protein kinase C inhibitor in the treatment of acute mania. *Arch Gen Psychiatry.* **57:** 95–97

Becker K.G. (2004) The common variants/multiple disease hypothesis of common complex genetic disorders. *Medical hypotheses.* **62:** 309

Bekris L.M., *et al*. (2010) The genetics of Parkinson disease. *J. Geriatr. Psychiatry Neurol.* **23:** 228–242

Belenky M.A., *et al*. (2008) Heterogeneous expression of gamma-aminobutyric acid and gamma-aminobutyric acid-associated receptors and transporters in the rat suprachiasmatic nucleus. *J Comp Neurol.* **506:** 708–732

Benson K.L. (2006) Sleep in schizophrenia: impairments, correlates, and treatment. *Psychiatr Clin North Am.* **29:** 1033–1045

Benson M.A., *et al*. (2001) Dysbindin, a novel coiled-coil-containing protein that interacts with the dystrobrevins in muscle and brain. *J Biol Chem.* **276:** 24232–24241

Bernstein H.G., *et al*. (2006) Localization of neuregulin-1alpha (heregulin-alpha) and one of its receptors, ErbB-4 tyrosine kinase, in developing and adult human brain. *Brain Res Bull.* **69:** 546-559

Berrettini W.H.W., Berrettini W.W. (2000) Susceptibility loci for bipolar disorder: Overlap with inherited vulnerability to schizophrenia. *Biological Psychiatry.* **47:** 245–251

Bertoli-Avella A.M., *et al*. (2004) Chasing genes in Alzheimer's and Parkinson's disease. *Hum. Genet.* **114:** 413–438

Bertsch B., *et al*. (2005) Convergent functional genomics: a Bayesian candidate gene identification approach for complex disorders. *Methods*. **37:** 274–279

Betarbet R., *et al*. (2002) Animal model of Parkison's disease. *BioEssays.* **24**: 308–318

Blasi J., *et al*. (1993) Botulinum neurotoxin A selectively cleaves the synaptic protein SNAP-25. *Nature.* **365:** 160–163

Bley A.E., *et al*. (2011) Natural history of infantile G(M2) gangliosidosis. *Pediatrics.* **128:** 1233–1241

Boivin D.B. (2000) Influence of sleep-wake and circadian rhythm disturbances in psychiatric disorders. *J. Psychiatry Neurosci*. **25:** 446–458

Boks M.P., *et al*. (2007) Reviewing the role of the genes G72 and DAAO in glutamate neurotransmission in schizophrenia. *Eur Neuropsychopharmacol.* **17:** 567–572

Bonini N.M., Giasson B.I. (2005) Snaring the function of alpha-synuclein. *Cell.* **123**: 359–61

Bonsall D.R., Lall G.S. (2013) Protein kinase C differentially regulates entrainment of the mammalian circadian clock. *Chronobiol Int.* **30:** 460–469

Bora A., *et al*. (2008) Neuropeptidomics of the supraoptic rat nucleus. *J.of Proteome Research.* **4992:** 4922–5003

Borbely A.A. (1982) A two process model of sleep regulation. *Hum Neurobiol*. **1**: 195–204

Borbely A.A.,*et al*. (1981) Sleep deprivation: effect on sleep stages and EEG power density in man. *Electroencephalogr Clin Neurophysiol*. 51: 483–495

Bordet R., *et al*. (2003) Study of circadian melatonin secretion pattern at different stages of Parkinson's disease. *Clinical Neuropharmacology.* **26:** 65–72

Boucher A.A.,*et al*. (2007) Heterozygous neuregulin 1 mice are more sensitive to the behavioral effects of Delta(9)-tetrahydrocannabinol. *Psychopharmacology.* **192:** 325–336

Braak H., *et al*. (2003) Staging of brain pathology related to sporadic Parkinson's disease. *Neurobiol Aging.* **24:** 197–211

Braak H., *et al*. (2004) Stages in the development of Parkinson's disease-related pathology. *Cell Tissue Res*. **318:** 121–134

Braff D.L. (2008) Advances in endophenotyping schizophrenia. *World psychiatry.* **7:** 11–18

Brandt R., *et al*. (2005) Tau alteration and neuronal degeneration in tauopathies: mechanisms and models. *Biochim. Biophys. Acta.* **1739:** 331–354

Brion J.P., *et al*. (1999) Transgenic expression of the shortest human tau affects its compartmentalization and its phosphorylation as in the pretangle stage of Alzheimer's disease. *Am. J. Pathol.* **154:** 255–270

Brooks D.J. (2010) Examining Braak's Hypothesis by Imaging Parkinson's Disease. *Movement Disorders.* **25:** 83–88

Brown M., Goldstein J. (1986) A receptor-mediated pathway for cholesterol homeostasis. *Science.* **232:** 34–47

Brownstein S., *et al*. (1980) Sandhoff disease (G_{M2} gangliosidosis type 2). Histopathology and ultrastructure of the eye. *Arch Ophthalmol.* **98:** 1089–1097

Bruguerolle B., Simon N. (2002) Biologic rhythms and Parkinson's disease: a chronopharmacologic approach to considering fluctuations in function. *Clinical Neuropharmacology.* **25:** 194–201

Bult A., Smale L., (1999) Distribution of Ca2+-dependent protein kinase C isoforms in the suprachiasmatic nucleus of the diurnal murid rodent, Arvicanthis niloticus. *Brain Res.* **816:** 190–199

Burns J.M., *et al*. (2005) The pathology of the substantia nigra in Alzheimer disease with extrapyramidal signs. *Neurology.* **64:** 1397–1403

Burre J., *et al*. (2010) Alpha-synuclein promotes SNARE-complex assembly in vivo and in vitro. *Science.* **329**: 1663–1667

Butcher G.Q., *et al*. (2002) The p42/44 mitogen-activated protein kinase pathway couples photic input to circadian clock entrainment. *J. Biol. Chem.* **277:** 29519–29525

Butler J.D., *et al*. (1993) Niemann-Pick C disease: cystine and lipids accumulate in the murine model of this lysosomal cholesterol lipidosis. *Biochem. Biophys. Res. Commun.* **196:** 154–159

Cabin D.E. (2002) Synaptic vesicle depletion correlates with attenuated synaptic responses to prolonged repetitive stimulation in mice lacking alpha-synuclein. *J. Neurosci.* **22**: 8797–8807

Cáceda R., *et al*. (2006) Neurotensin: role in psychiatric and neurological diseases. *Peptides.* **27:** 2385–2404

Cachon-Gonzalez M.B., *et al*. (2006) Effective gene therapy in an authentic model of Tay-Sachsrelated diseases. *Proc. Natl. Acad. Sci. USA.* **103:** 10373–10378

Caffrey T.M., *et al*. (2006) Haplotype-specific expression of exon 10 at the human MAPT locus. *Hum. Mol. Genet.* **15:** 3529–3537

Caffrey T.M., *et al*. (2008) Haplotype-specific expression of the N-terminal exons 2 and 3 at the human MAPT locus. *Neurobiol. Aging.* **29:** 1923–1929

Caffrey T.M., Wade-Martins R. (2012) The role of MAPT sequence variation in mechanisms of disease susceptibility. *Biochem. Soc. Trans.* **40:** 687–692

Cannon T.D., *et al*. (1998) The genetic epidemiology of schizophrenia in a Finnish twin cohort. A population-based modeling study. *Arch. Gen. Psychiatry.* **55:** 67–74

Cardno A.G., Gottesman I.I. (2000) Twin studies of schizophrenia: from bow-and-arrow concordance to star wars Mx and functional genomics. *Am.J.Genet.* **97:** 12–17

Cardno A.G., *et al*. (1999) Heritability estimates for psychotic disorders: the Maudsley twin psychosis series. *Arch. Gen. Psychiatry*. **56:** 162-168

Cardno A.G., *et al*. (2002) Heritability of Schneider's first-rank symptoms. *Br. J. Psychiatry.* **180:** 35–38

Careau V., *et al*. (2012) Are voluntary wheel running and open-field behavior correlated in mice? Different answers from comparative and artificial selection approaches. *Behav Genet.* **42:** 830–844

Carrette O., *et al*. (2003) A panel of cerebrospinal fluid potential biomarkers for the diagnosis of Alzheimer's disease. *Proteomics.* **3:** 1486–1494

Carskadon M.A. (2004) Sleep deprivation: health consequences and societal impact. *Med Clin North Am.* **88:** 767–776

Carstea E.D., *et al*. (1997) Niemann-Pick C1 disease gene: homology to mediators of cholesterol homeostasis. *Science*. **277:** 228–231

Carter C.J. (2006) Schizophrenia susceptibility genes converge on interlinked pathways related to glutamatergic transmission and long-term potentiation, oxidative stress and oligodendrocyte viability. *Schizophr Res.* **86:** 1–14

Carter C.J. (2007) Multiple genes and factors associated with bipolar disorder converge on growth factor and stress activated kinase pathways controlling translation initiation: implications for oligodendrocyte viability. *Neurochem Int.* **50:** 461–490

Caspi A., Moffitt T.E. (2006) Gene–environment interactions in psychiatry: joining forces with neuroscience. *Nat. Rev. Neurosci.* **7:** 583–590

Castillo C., *et al*. (2011) Restricted wheel access following a light cycle inversion slows re-entrainment without internal desynchrony as measured in *PER2Luc* mice. *Neurosci*. **182:** 169–176

Castrén E. (2005) Is mood chemistry? *Nat Rev Neurosci.* **6:** 241– 246

Caudle W.M., *et al*. (2007) Reduced vesicular storage of dopamine causes progressive nigrostriatal neurodegeneration. *J Neurosci.* **27:** 8138–8148

Cayetanot F., *et al*. (2005) Arginine-vasopressin and vasointestinal polypeptide rhythms in the suprachiasmatic nucleus of the mouse lemur reveal aging-related alterations of circadian pacemaker neurons in a non-human primate. *Eur. J. Neurosci*. **22**: 902–910

Cersosimo M.G., Benarroch E.E. (2008) Neural control of the gastrointestinal tract: implications for Parkinson disease. *Mov Disord.* ***2*3**: 1065–1075

Cha M.C., *et al*. (2000) High-fat diet feeding reduces the diurnal variation of plasma leptin concentration in rats. *Metabolism.* **49:** 503–507

Challet E., Pevet P. (2003) Interactions between photic and nonpphotic stimuli to synchronize the master circadian clock in mammmals. *Front. Biosci*. **8**: 246–257

Chanock S.J., Manolio T., et al (2007) Replicating genotype-phenotype associations. *Nature.* **447:** 655–660

Chaudhuri K.R., *et al*. (2006) Non-motor symptoms of Parkinson's disease: diagnosis and management. *Lancet Neurol.* **5:** 235–245

Chee M.W., Chuah L.Y. (2008) Functional neuroimaging insights into how sleep and sleep deprivation affect memory and cognition. *Curr Opin Neurol.* **21:** 417–423

Chelius D., Bondarenko P. V. (2002) Quantitative Profiling of Proteins in Complex Mixtures Using Liquid Chromatography and Mass Spectrometry. *J Proteome Res.* **1:** 317–323

Chemelli R. M., *et al*. (1999) Narcolepsy in orexin knockout mice: molecular genetics of sleep regulation. *Cell*. **98**: 437–451

Chen D., *et al*. (1999) Pituitary adenylyl cyclase-activating peptide: a pivotal modulator of glutamatergic regulation of the suprachiasmatic circadian clock. *Proc. Natl. Acad. Sci. USA*. **96**: 13468–13473

Chen J., *et al.* (2010) Switching to hypomania and mania: differential neurochemical, neuropsychological, and pharmacologic triggers and their mechanisms. *Curr Psychiatry Rep.* **12:** 512–521

Chen J., *et al*. (2006) Genetic mouse models of schizophrenia: from hypothesis-based to susceptibility gene-based models. *Biol Psychiatry.* **59:** 1180–1188

Chen W.J., Faraone S.V. (2000) Sustained attention deficits as markers of genetic susceptibility to schizophrenia. *Am J Med Genet.* **97:** 52–57

Cheng M.Y., *et al*. (2002) Prokineticin 2 trasnmits the behavioral circadian rhythm of the suprachiasmatic nucleus. *Nature*. **417**: 405–410

Chesselet M.F. (2008) In vivo alpha-synuclein overexpression in rodents: a useful model of Parkinson's disease? *Exp. Neurol.* **209:** 22–27

Chevalier F. (2010). Highlights on the capacities of "Gel-based" Proteomics. *Proteome Sci*. **8:** 23

Chou T.C., *et al*. Afferents to the ventrolateral preoptic nucleus. *J Neurosci*. **22**: 977–990

Chouinard S., *et al*. (2004) Sleep in untreated patients with schizophrenia: a meta-analysis. *Schizophr Bull.* **30:** 957–967

Chung S., *et al*. (2005) Differential adaptive responses to chronic stress of maternally stressed male mice offspring. *Endocrinology.* **146:** 3202–3210

Church S.M., *et al*. (2002) Does schizophrenia result from developmental or degenerative processes? *J Neural Transm*. **63**: 129–147

Ciarleglio C. M., *et al*. (2011) Perinatal photoperiod imprints the circadian clock. *Nat. Neurosci.* **14**: 25-27

Cichon S., *et al*. (2009) Genomewide association studies: history, rationale, and prospects for psychiatric disorders. *Am. J. Psychiatry.* **166:** 540–556

Cilia J., *et al*. (2010) Further neurochemical and behavioral investigation of Brattleboro rats as a putative model of schizophrenia. *J Psychopharmacol*. **24:** 407-419

Claassen D.O., *et al*. (2010) REM sleep behavior disorder preceding other aspects of synucleino-pathies by up to half a century. *Neurology.* **75:** 494–499

Clarimon J., *et al*. (2009) Early-Onset familial lew body dementia with extensive tauopathy: a clinical, genetic, and neuropathological study. *J Neuropathol Exp Neurol*. **68**: 73–82

Clark D., *et al*. (2006) A proteome analysis of the anterior cingulate cortex gray matter in schizophrenia. *Mol Psychiatry*. **11**: 459–470

Clinton S.M., *et al*. (2004) Abnormalities of the NMDA receptor and associated intracellular molecules in the thalamus in schizophrenia and bipolar disorder. *Neuropsychopharmacology*. **29**: 1353–1362

Cloues R.K., Sather W.A. (2003) Afterhyperpolarization regulates firing rate in neyrons of the suprachiasmatic nucles. *J Neurosci*. **23**: 1593–1604

Cohrs S. (2008) Sleep disturbances in patients with schizophrenia: impact and effect of antipsychotics. *CNS Drugs.* **22:** 939–962

Collins F.S., *et al*. (2007) A mouse for all reasons. *Cell*. **128:** 9–13

Colwell C.S. (2011). Linking neural activity and molecular oscillations in the SCN. *Nat. Rev. Neurosci.* **12:** 553–569

Comella C.L. (2007) Sleep disorders in Parkinson's disease: An overview. *Movement Disorders*. **17**: 367–373

Conzelmann E., Sandhoff K. (1978) Deficiency of a factor necessary for stimulation of hexosaminidase A–catalyzed degradation of ganglioside GM2 and glycolipid GA2. *Proc. Natl. Acad. Sci. USA.* **75:** 3979–3983

Cornblatt B.A., Malhotra A.K. (2001) Impaired attention as an endophenotype for molecular genetic studies of schizophrenia. *Am J Med Genet.* **105:** 11–15

Corradini I., *et al*. (2009) SNAP-25 in neuropsychiatric disorders. *Annals of the New York Academy of Sciences.* **1152:** 93–99

Costas J., *et al*. (2013) Role of DISC1 interacting proteins in sczhizophrenia risk from genome-wide analysis of missense SNPs. *Ann. Hum. Genet*. **77**: 504–512

Cox T.M., Cachon-Gonzalez M.B. (2012) The cellular pathology of lysosomal diseases. *J Pathol.* **226:** 241–254

Coyle J.T. (2006) Glutamate and schizophrenia: beyond the dopamine hypothesis. *Cell. Mol. Neurobiol*. **26:** 365–384

Craddock N., *et al*. (2005) The genetics of schizophrenia and bipolar disorder:dissecting psychosis. *J Med Genet*. **42:** 193–204

Craft G.E., *et al*. (2013) Recent advances in quantitative neuroproteomics. *Methods*. **61:** 186–218

Crespo-Facorro B., *et al*. (2007) Reduced thalamic volume in first-episode non-affective 281 psychosis: correlations with clinical variables, symptomatology and cognitive functioning. *Neuroimage.* **35:** 1613–1623

Crosio C., *et al*. (2000) Light induces chromatin modification in cells of the mammalian circadian clock. *Nat. Neurosci.* **3:** 1241–1247

Cryan J.F., Slattery D.A. (2007) Animal models of mood disorders: Recent developments. *Curr Opin Psychiatry.* **20:** 1–7

Cuesta M., *et al*. (2012) The methamphetamine-sensitive circadian oscillator is dysfunctional in a transgenic mouse model ofHuntington's disease. *Neurobiol. Dis.* **45:** 145–155

Czeisler C.A. (1995) The effect of light on the human circadian pacemaker. *Ciba Found Symp.* **183:** 254–290

Czeisler C.A., *et al*. (1980) Timing of REM sleep is coupled to the circadian rhythm of body temperature in man. *Sleep*. **2**: 329–346

Daan S., *et al*. (1984) Timing of human sleep: recovery process gated by a circadian pacemaker. *Am J Physiol.* **246:** 161–183

Dahl R.E., Lewin D.S. (2002) Pathways to adolescent health sleep regulation and behavior. *J Adolesc Health*. **31:** 175–184

Damiola F., *et al*. (2000) Restricted feeding uncouples circadian oscillators in peripheral tissues from the central pacemaker in the suprachiasmatic nucleus. *Genes Dev*. **14:** 2950–2961

Dardente H., Cermakian N. (2007). Molecular circadian rhythms in central and peripheral clocks in mammals. *Chronobiol. Int.* **24:** 195–213

Darios F., *et al*. (2003) Parkin prevents mitochondrial swelling and cytochrome C release in mitochondria-dependent cell death. *Hum. Mol.Genet.* **12:** 517–526

Dauer W., Ho C.C. (2010) The biology and pathology of the familial Parkinson's disease protein LRRK2. *Mov. Disord.* **25:** 40–43

Dauer W., Przedborski S. (2003) Parkinson's disease: mechanisms and models. *Neuron*. **39:** 889–909

Dauvilliers Y. (2007) Insomnia in patients with neurodegenerative conditions. *SleepMedicine.* **8:** 27–34

David D.C., *et al*. (2005) Proteomic and functional analyses reveal a mitochondrial dysfunction in P301L tau transgenic mice. *J. Biol. Chem.* **280:** 23802–23814

Davies J.P., *et al*. (2000) Transmembrane molecular pump activity of Niemann-Pick C1 protein. *Science*. **290:** 2295–2298

Davis S., Mirick D.K. (2006) Circadian disruption, shift work and the risk of cancer: a summary of the evidence and studies in Seattle. *Cancer Causes Control.* **17:** 539–545

Dawson H.N., *et al*. (2001) Inhibition of neuronal maturation in primary hippocampal neurons from tau deficient mice. *J. Cell Sci.* **114:** 1179–1187

Dawson T.M., *et al*. (2010) Genetic animal models of Parkinson's disease. *Neuron*. **66:** 646–661

Dayon L., *et al*. (2008) Relative quantification of proteins in human cerebrospinal fluids by MS/MS using 6-plex isobaric tags. *Anal Chem.* **80:** 2921–2931

De Bacquer D., *et al*. (2009) Rotating shift work and the metabolic syndrome: a prospective study. *Int J Epidemiol.* **38:** 848–854

De Gennaro L., *et al*. (2001) The boundary between wakefulness and sleep: quantitative electroencephalographic changes during the sleep onset period. *Neurosci*. **107:** 1–11

de Lecea L., Bourgin P. (2008) Neuropeptide interactions and REM sleep: a role for Urotensin II? *Peptides.* **29:** 845–851

De Wied D., Sigling H.O. (2002) Neuropeptides involved in the pathophysiology of schizophrenia and major depression. *Neurotox. Res.* **4:** 453–468

De Windt A., *et al*. (2007) Gene set enrichment analyses revealed several affected pathways in Niemann-pick disease type C fibroblasts. *DNA Cell Biol.* **26:** 665–671

Deakin I.H., *et al*. (2009) Behavioral characterization of neuregulin 1 type I overexpressing transgenic mice. *Neuroreport*. **20:** 1523–1528

Deery M.J., *et al*. (2009) Proteomic Analysis Reveals the Role of Synaptic Vesicle Cycling in Sustaining the Suprachiasmatic Circadian Clock. *Curr Biol.* **19:** 2031–2036

Delezie J., Challet E. (2011) Interactions between metabolism and circadian clocks: reciprocal disturbances. *Ann. N.Y. Acad. Sci.* **1243:** 30–46

Denk F., Wade-Martins R. (2009) Knock-out and transgenic mouse models of tauopathies. *Neurobiology of Aging.* **30:** 1–13

Denny C.A., *et al*. (2007) Neurochemical,morphological, and neurophysiological abnormalities in retina of Sandhoff and GM1 gangliosidosis mice. *J. Neurochem.* **101:** 1294–1302

Denny C.A., *et al*. (2006) Influence of caloric restriction on motor behavior, longevity and brain lipid composition in Sandhoff Disease mice. *Journal of Neuroscience Research.* **83:** 1028–1038

Deschenes C.L., McCurry S.M. (2009) Current treatments for sleep disturbances in individuals with dementia. *Current Psychiatry Reports.* **11**: 20–26

Devos D., *et al*. (2003) Heart rate variability and Parkinson's disease severity. *Journal of Neural Transmission.* **110:** 997–1011

Diaz C.M., *et al*. (2007) EAAT1 and D-serine expression are early features of human retinal development. *Exp Eye Res.* **84:** 876–885

Dickerson P.A., *et al*. (2005) Early emergence of increased fearful behavior in prenatally stressed rats. *Physiol. Behav.* **86:** 586–593

Dickmeis T. (2009) Glucocorticoids and the circadian clock. *J*. *Endocrinol.* **200:** 3–22

Dijk D.J., Duffy J.F. (1999) Circadian regulation of human sleep and age-related changes in its timing, consolidation and EEG characteristics. *Ann Med.* **31:** 130–140

Dijk D.J., *et al*. (2000) Contribution of circadian physiology and sleep homeostasis to age-related changes in human sleep. *Chronobiol Int.* **17:** 285–311

Djik D.J., Edgar D.M. (1999) ''Circadian and homeostatic control of wakefulness and sleep,''in *Regulation of Sleep and Wakefulness*, Turker F.W and Zee P.C.., Eds., pp. 111–147. Marcel Dekker, New York, NY, USA

Ding H., *et al*. (2011) Decreased expression of Bmal2 in patients with Parkinson's disease. *Neuroscience Letters*. **499**: 186–188

Dinges D.F., *et al*. (1997) Cumulative sleepiness, mood disturbance, and psychomotor vigilance performance decrements during a week of sleep restricted to 4–5 hours per night. *Sleep.* **20:** 267–270

Doi R., *et al*. (2010) CLOCK regulates circadian rhythms of hepatic glycogen synthesis through transcriptional activation of Gys2. *J. Biol. Chem.* **285:** 22114– 22121

Donaldson J.A., Stephan F.K. (1982) Entrainment of circadian rhythms: retinofugal pathways and unilateral suprachiasmatic nucleus lesions. *Physiol Behav.* **29:** 1161–1169

Dong G., *et al*. (2010) Elevated ATPase activity of KaiC applies a circadian checkpoint on cell division in Synechococcus elongatus. *Cell*. **140**: 529–539

Dubocovich M.L., *et al*. (2003) Molecular pharmacology, regulation and function of mammalian melatonin receptors. *Front Biosci*. **8**: 1093–1108

Duff K., *et al*. (2000) Characterization of pathology in transgenic mice over-expressing human genomic and cDNA tau transgenes. *Neurobiol. Dis.* **7**: 87–98

Dun Y., *et al*. (2007) Functional and molecular analysis of D-serine transport in retinal Muller cells. *Exp Eye Res.* **84:** 191–199

Dwivedi Y., *et al*. (2005) Single and repeated stress-induced modulation of phospholipase C catalytic activity and expression: role in LH behavior. *Neuropsychopharmacology*. **30:** 473–483

Dworak M., *et al.* (2007) Impact of singular excessive computer game and television exposure on sleep patterns and memory performance of school-aged children. *Pediatrics.* **120:** 978–985

Easton A., *et al*. (2003) The circadian Clock mutation increases exploratory activity and escape-seeking behavior. *Genes Brain Behav.* **2:** 11–19

Ebisawa T. (2007) Circadian rhythms in the CNS and peripheral clock disorders: human sleep disorders and clock genes*. J Pharmacol Sci.* **103:** 150–154

Edwards L.L., *et al*. (1992) Gastrointestinal dysfunction in Parkinson's disease: frequency and pathophysiology. *Neurology*. **42:** 726–732

Egashira N., *et al*. (2005) Altered depression-related behavior and neurochemical changes in serotonergic neurons in mutant R406W human tau transgenic mice. *Brain Res.* **1059:** 7–12

Ehlen J.C., *et al*. (2001) In vivo resetting of the hamster circadian clock by 5-HT7 receptors in the suprachiasmatic nucleus. *J. Neurosci*. **21**: 5351–5357

Eide E.J., *et al*. (2002) The circadian regulatory protein BMAL1 and cryptochromes are substrates of casein kinase 1ε (CKIε). *J. Biol. Chem*. **277**: 17248–17254

Einat H., *et al*. (2007) Protein kinase C inhibition by tamoxifen antagonizes manic-like behavior in rats: implications for the development of novel therapeutics for bipolar disorder. *Neuropsychobiology.* **55:** 123–131

Eisener-Dorman A.F., *et al*. (2009) Cautionary insights on knockout mouse studies: The gene or not the gene? *Brain Behav Immun.* **23:** 318–324

Ellison-Wright I., Bullmore E. (2009) Meta-analysis of diffusion tensor imaging studies in schizophrenia. *Schizophr. Res.* **108:** 3–10

Elrick M.J., *et al*. (2010) Conditional Niemann–Pick C mice demonstrate cell autonomous Purkinje cell neurodegeneration. *Hum. Mol. Genet.* **19:** 837–847

Engelhardt J.K., *et al*. (1989) Cable properties of spinalcord motoneu- ronsin adult and aged cats. *J. Neurophysiol.* **61:** 194–201

English J.A., *et al*. (2011) The neuroproteomics of schizophrenia. *Biol Psychiatry.* **69:** 163–172

Enomoto T., *et al*. (2007) Phencyclidine and genetic animal models of schizophrenia developed in relation to the glutamate hypothesis. *Methods Find Exp Clin Pharmacol.* **29:** 291–301

Erickson R.P., *et al*. (2000) Pharmacological and genetic modifications of somatic cholesterol do not substantially alter the course of CNS disease in Niemann-Pick C mice. *J. Inherit. Metab. Dis.* **23:** 54–62

Estanislau C., Morato S. (2006) Behavior ontogeny in the elevated plus-maze: prenatal stress effects. *Int. J. Dev. Neurosci*. **24:** 255–262

Ewen J. (1934) Sleep and its Relationship to Schizophrenia. *J Neurol Psychopathol.* **14:** 247–251

Ezaki J., *et al*. (1996) Specific delay in the degradation of mitochondrial ATP synthase subunit c in late infantile neuronal ceroid lipofuscinosis is derived from cellular proteolytic dysfunction rather than structural alteration of subunit c. *J. Neurochem.* **67:** 1677–1687

Factor S.A., *et al*. (1990) Sleep disorders and sleep effect in Parkinson's disease. *Mov Disord.* **5:** 280–285

Fanous A.H., *et al*. (2010) Association study of SNAP25 and schizophrenia in Irish family and case-control samples. *Am. J. Med. Genet. B Neuropsychiatr. Genet.* **153B:** 663–674

Faranjnia S., Deboer T., Rohling J.H.T., Meijer J.H., Michelr S. (2013) Aging of the suprachiasmatic clock. *Neurosci*. **XX:** 1–12

Farfel-Becker T., *et al*. (2011) Spatial and temporal correlation between neuron loss and neuroinflammation in a mouse model of neuronopathic Gaucher disease. *Hum. Mol. Genet.* **20:** 1375–1386

Farrer M., *et al*. (2001) Lewy bodies and parkinsonism in families with parkin mutations. *Ann Neurol.* **50:** 293–300

Fatemi S.H., *et al*. (2000) Reduction in reelin immunoreactivity in hippocampus of subjects with schizophrenia, bipolar disorder and major depression. *Molecular Psychiatry.* **5**: 654–663

Feillet C.A., *et al*. (2006) Lack of food anticipation in Per2 mutant mice. *Curr. Biol.* **16:** 2016–2022

Feinberg I., Campbell I.G. (2010) Sleep EEG changes during adolescence: an index of a fundamental brain reorganization. *Brain Cogn.* **72:** 56–65

Fenelon G., *et al*. (2000) Hallucination in Parkinson's disease: prevalence, phenomenology, and risk factor. *Brain*. **123:** 733–745

Fernagut P.O., Chesselet M.F. (2004) Alpha-synuclein and transgenic mouse models. *Neurobiology of Disease.* **17**: 123–130

Fernandez H.H., *et al*. (2012) Nonmotor Manifestations in Parkinson Disease. *The Neurologist.* **18**: 1–16

Ferrarelli F., *et al*. (2007) Reduced sleep spindle activity in schizophrenia patients. *Am J Psychiatry.* **164:** 483–492

Ferreira A., *et al*. (2000) Synapsin III: developmental expression, subcellular localisation, and role in axon formation. *J Neurosci.* **20***:* 3736–3744

Ferreira J.J., *et al*. (2006) Sleep disruption, daytime somnolence, and sleep attacks in Parkinson disease: A clinical survey in PD patients and age-matched healthy volunteers. *Eur J Neurol.* **13:** 209–214

Fertl E., *et al*. (1991) Circadian secretion pattern of melatonin in Parkinson's disease. *Journal of Neural Transmission.* **3:** 41–47

Fertl E., *et al*. (1991) Circadian secretion pattern of melatonin in de novo Parkinsonian patients: evidence for phase-shifting properties of l-dopa. *Journal of Neural Transmission.* **5:** 227–234

Figeys D. (2005) Proteomics: The Basic Overview. *Methods Biochem. Anal.* **45:** 1–62

Fink A.L., *et al*. (2002) Conformational Behavior of Human a-Synuclein is Modulated by Familial Parkinson's Disease Point Mutations A30P and A53T. *NeuroToxicology.* **23**: 553–567

Fischer-Colbrie R., *et al*. (2005) Secretoneurin: a new player in angiogenesis and chemotaxia linking nerves, bloos vessels and the immune system. *Curr.Protein Pept. Sci.* **6:** 373–385

Fisher S. P., *et al*. (2012) Rapid Assessment of Sleep-Wake Behavior in Mice. *J Biol Rhythms.* **27**: 48–60

Fitzgerald P.J., *et al*. (2010) Does gene deletion of AMPA GluA1 phenocopy features of schizoaffective disorder? *Neurobiology of Disease*. **40:** 608–621

Fleming S.M., Chesselet M.F. (2009) Modeling non-motor symptoms of Parkinson's disease in genetic mouse models. *Basal Ganglia. Springer.* 483–492

Fleming S.M., *et al*. (2005) Genetic mouse models of Parkinsonism: strengths and limitations. *The J. of the American Society for Exp. NeuroTherapeutics.* **2:** 495–503

Fleming S.M., *et al*. (2004) Early and progressive sensorimotor anomalies in mice overexpressing wild-type human alpha-synuclein. *J. Neurosci.* **24:** 9434–9440

Fleming S.M., *et al*. (2006) Behavioral effects of dopaminergic agonists in transgenic mice overexpressing human wildtype alpha-synuclein. *Neuroscience.* **142:** 1245–1253

Fonken L.K., *et al*. (2010) Light at night increases body mass by shifting the time of food intake. *Proc. Natl. Acad. Sci. USA.* **107:** 18664–18669

Fontaine C., *et al*. (2003) The orphan nuclear receptor Rev-Erbalpha is a peroxisome proliferator-activated receptor (PPAR) gamma target gene and promotes PPARgamma-induced adipocyte differentiation. *J Biol Chem*. **278:** 37672–37680

Forest G., *et al*. (2007) Attention and non-REM sleep in neuroleptic-naive persons with schizophrenia and control participants. *Psychiatry Res.* **149:** 33–40

Fraldi A., *et al*. (2010) Lysosomal fusion and SNARE function are impaired by cholesterol accumulation in lysosomal storage disorders. *The EMBO Journal.* **29:** 3607–3620

Freedman M.S., *et al*. (1999) Regulation of mammalian circadian behavior by non-rod, non-cone, ocular photoreceptors. *Science.* **284:** 502–504

Frey B.N., *et al*. (2006) Effects of lithium and valproate on amphetamine-induced oxidative stress generation in an animal model of mania. *J Psychiatry Neurosci.* **31:** 326–332

Fujimaki Y., *et al*. (2009) The effects of age, gender, and body mass index on amplitude of sensory nerve action potentials: multivariate analyses. *Clinc Neurophysiol*. **120**: 1683–1686

Fujishiro H., *et al*. (2008) Co-localization of tau and α-synuclein in the olfactory bulb in Alzheimer's disease with amygdala Lewy bodies. *Acta Neuropathologica*. **116**: 17–24

Fujiwara T., *et al*. (2006) Analysis of knock-out mice to determine the role of HPC-1/syntaxin 1A in expressing synaptic plasticity. *J Neurosci.* **26**: 5767–5776

Fuller P.M., *et al*. (2006) Neurobiology of the sleep-wake cycle: sleep architecture, circadian regulation, and regulatory feedback. *J Biol Rhythms.* **21:** 482–493

Fuller P.M., *et al*. (2007) The pontine REM switch: past and present. *J Physiol*. **584:** 735–741

Gachon F., *et al*. (2004) The mammalian circadian system: from gene expression to physiology. *Chromosoma*. **114**: 103–112

Gaig C., Tolosa E. (2009) When does Parkinson's disease begin? *Mov Disord*. **24:** 656–664

Galeotti N., Ghelardini C. (2011) Antidepressant phenotype by inhibiting the phospholipase Cβ(1)–protein kinase Cγ pathway in the forced swim test. *Neuropharmacology*. **60:** 937–943

Gallopin T., *et al*. (2000) Identification of sleep-promoting neurons in vitro. *Nature*. **404**: 992–995

Gangwisch J.E., *et al*. (2005) Inadequate sleep as a risk factor for obesity: analyses of the NHANES I. *Sleep*. **28:** 1289–1296

Garaulet M., *et al*. (2011) An approximation to the temporal order in endogenous circadian rhythms of genes implicated in human adipose tissue metabolism. *J. Cell Physiol.* **226:** 2075–2080

Garbelli R., *et al*. (2008) Heterogeneous expression of SNAP-25 in rat and human brain. *J Comp Neurol*. **506:** 373–386

Garcia R.A., *et al*. (The neuregulin receptor ErbB-4 interacts with PDZ-containing proteins at neuronal synapses. *Proc. Natl. Acad. Sci. USA.* **97:** 3596–3601

Gattaz W.F., *et al*. (1990) Increased serum phospholipase A2 activity in schizophrenia: a replication study. *Biological Psychiatry.* **28:** 495–501

Gekakis N., *et al*. (1998) Role of the CLOCK protein in the mammalian circadian mechanism. *Science*. **280**: 1564–1569

Gerlai R. (1996) Gene-targeting studies of mammalian behavior: is it the mutation or the background genotype?. *Trends Neurosci.* **19:** 177–181

German D.C., *et al.* (1992) Disease-specific patterns of locus coeruleus cell loss. *Ann Neurol.* **32:** 667– 676

German D.C., *et al*. (2001) Selective neurodegeneration, without neurofibrillary tangles, in a mouse model of Niemann-Pick C disease. *J Comp Neurol.* **433:** 415–25

Gerstner J.R., Yin J.C. (2010) Circadian rhythms and memory formation. *Nat. Rev. Neurosci*. **11**: 577–588

Geschwind D.H. (2003) Tau phosphorylation, tangles, and neurodegeneration: the chicken or the egg? *Neuron.* **40:** 457–460

Ghiani C.A., *et al*. (2009) The dysbindin-containing complex (BLOC-1) in brain: developmental regulation, interaction with SNARE proteins and role in neurite outgrowth. *Mol Psychiatry.***115:** 204–15

Giasson B.I., *et al*. (2002) Neuronal alpha-synucleinopathy with severe movement disorder in mice expressing A53T human alpha-synuclein. *Neuron.* **34**: 521–533

Giasson B.I., *et al*. (2003) Initiation and synergistic fibrillization of tau and alphasynuctein. *Science.* **300:** 636–640

Gisnberg S. D., *et al*. (2012) Expression profiling in neuropsychiatric disorders: emphasis on glutamate receptors in bipolar disorder. *Pharmacol. Biochem. Behav*. **100**: 705–711

Glass J.D., *et al*. (2003) Midbrain raphe modulation of nonphotic circadian clock resetting and 5-HT release in the mammalian suprachiasmatic nucleus. *J. Neurosci*. **23**: 7451–7460

Gleason S.D., Shannon H.E. (1997) Blockade of phencyclidine-induced hyperlocomotion by olanzapine, clozapine and serotonin receptor subtype selective antagonists in mice. *Psychopharmacology*. **129:** 79–84

Goder R., *et al*. (2007) Visual declarative memory is associated with non-rapid eye movement sleep and sleep cycles in patients with chronic non-restorative sleep. *Sleep Med.* **8:** 503–508

Godinho S.I., Nolan P.M. (2006) The role of mutagenesis in defining genes in behavior. *Eur. J. Hum. Genet.* **14:** 651–659

Godinho S.I.H., *et al*. (2012) Disrupted Circadian Rhythms in a Mouse Model of Schizophrenia. *Current Biology.* **22**: 1–6

Goedert M., Jakes R. (2005) Mutations causing neurodegenerative tauopathies. *Biochim. Biophys. Acta*. **1739:** 240–250

Gogos J.A., Gerber D.H. (2006) Schizophrenia susceptibility genes: emergence of positional candidates and future directions. *Trends Pharmacol Sci.* **27**: 226–233

Goldberg M.S., *et al*. (2003) Parkin-deficient mice exhibit nigrostriatal deficits but not loss of dopaminergic neurons. *J Biol Chem.* **278:** 43628–43635

Goldstein J.M., *et al*. (2007) Hypothalamic abnormalities in schizophrenia: sex effects and genetic vulnerability. *Biol Psychiatry.* **61:** 935–945

Gong H., *et al*. (2004) Activation of c-fos in GABAergic neurones in the preoptic area during sleep and in response to sleep deprivation. *J Physiol*. **556**: 935–946

Gosso M.F., *et al*. (2008) Common variants underlying cognitive ability: further evidence for association between the SNAP-25 gene and cognition using a family-based study in two independent Dutch cohorts. *Genes Brain Behav.* **7:** 355–364

Gottesman I.I. (1973) Genetic theorizing and schizophrenia. *The British journal of psychiatry*. **122:** 15–30

Gottesmann C., Gottesman I. (2007) The neurobiological characteristics of rapid eye movement (REM) sleep are candidate endophenotypes of depression, schizophrenia, mental retardation and dementia. *Prog Neurobiol.* **81:** 237–250

Götz J., *et al*. (2001) Tau filament formation in transgenic mice expressing P301L tau. *J Biol Chem*. **276:** 529–534

Gould T.D. (2006) Psychiatric endophenotypes and the development of valid animal models. *Genes, brain, and behavior.* **5:** 113–119

Grant N.J., *et al*. (1999) Differential expression of SNAP-25 isoforms and SNAP-23 in the adrenal gland. *J Neurochem*. **72**: 363–372

Gravel R.A., *et al*. (2001) The G_{M2} gangliosidoses; in Scriver C.R., *et al*. (eds): The Metabolic Basis of Inherited Disease. *McGraw-Hill.* 3827–3876

Green C.B., *et al*. (2008) The meter of metabolism. *Cell*. **134**: 728–742

Green D.R., *et al*. (2011) Mitochondria and the autophagy- inflammation-cell death axis in organismal aging. *Science*. **333:** 1109–1112

Green D.J., Gillete R. (1982) Circadian rhythm of firing rate recorded from single cells in the rat suprachiasmatic brain slice. *Brain Res*. **5**: 198–200

Greenamyre J.T. (1993) Glutamate-dopamine interactions in the basal ganglia; relationship to Parkinson's disease. *J Neural Transm Gen Sect*. **91**: 255–269

Gros-Louis F., *et al*. (2009) Chromogranin B P413L variant as risk factor and modifier of disease onset for amyotrophic lateral sclerosis. *Proc. Natl. Acad. Sci. USA.* **106:** 21777–21782

Gu Z., *et al*. (2005) Regulation of NMDA receptors by neuregulin signaling in prefrontal cortex. *J Neurosci*. **25:** 4974–4984

Güler A.D., *et al*. (2008) Melanopsin cells are the principal conduits for rod-cone input to non-image-forming vision. *Nature.* **453:** 102–105

Gullinello M., *et al*. (2008) Early deficits in motor coordination and cognitive dysfunction in a mouse model of the neurodegenerative lysosomal storage disorder, Sandhoff disease. *Behavioural Brain Research*. **193:** 315–319

Gygi S. P., *et al*. (1999) Quantitative Analysis of Complex Protein Mixtures Using Isotope-Coded Affinity Tags. *Nat Biotechnol.* **17:** 994–999

Hahn C.-G., *et al*. (2005) Lithium and valproic acid treatments reduce PKC activation and receptor-G protein coupling in platelets of bipolar manic patients. *J Psychiatr Res.* **39:** 355–63

Hajek T., *et al*. (2012) Smaller hippocampal volumes in patients with bipolar disorder are masked by exposure to lithium: a meta-analysis. *J Psychiatry Neurosci*. **37:** 333–43

Hamada T., *et al*. (1999) Involvement of glutamate release in substance P-induced phase delays of suprachiasmatic neuron activity rhythm in vitro. *Brain Res*. **836**: 190–193

Hamet P., Tremblay J. (2006) Genetics of the sleep-wake cycle and its disorders. *Metabolism.* **55:** 7–12

Hampp G., *et al*. (2008) Regulation of monoamine oxidase A by circadian-clock components implies clock influence on mood. *Current Biology.* **18:** 678–683

Hansen J. (2006) Risk of breast cancer after night- and shift work: current evidence and ongoing studies in Denmark. *Cancer Causes Control.* **17:** 531–537

Hansen K. C., *et al*. (2003) Mass spectrometric analysis of protein mixtures at low levels using cleavable 13C-isotope-coded affinity tag and multidimensional chromatography. *Mol Cell Proteomics.* **2:** 299–314

Harada A., *et al*. (1994) Altered microtubule organization in small-calibre axons of mice lacking tau protein. *Nature*. **369:** 488–491

Harms M.P., *et al*. (2007) Thalamic shape abnormalities in individuals with schizophrenia and their nonpsychotic siblings. *J Neurosci.* **27:** 13835–13842

Harrison P.J., Law A.J. (2006) Neuregulin 1 and schizophrenia: genetics, gene expression, and neurobiology. *Biol Psychiatry.* **60:** 132–140

Harrison P.J., Weinberger D.R. (2005) Schizophrenia genes, gene expression, and neuropathology: on the matter of their convergence. *Mol. Psychiatry* **10:** 40–68

Harrison Y., Horne J.A. (2000) The impact of sleep deprivation on decision making: a review. *J Exp Psychol Appl.* **6:** 236–249

Hashimoto M., *et al*. (2003) Transgenic models of alpha-synuclein pathology: past, present, and future. *Ann. N. Y. Acad. Sci.* **991:** 171–188

Hastings M.H., Herzog E.D. (2004) Clock genes, oscillators, and cellular networks in the suprachiasmatic nuclei. *J.Biol. Rhythms.* **19:** 400–413

Hastings M.H., *et al*. (2003) A clockwork web: Circadian timing in brain and periphery, in health and disease. Nat. Rev. *Neurosci.* **4:** 649–661

Hatcher N. G., *et al*. (2008) Mass spectrometry-based discovery of circadian peptides. *Proc. Natl. Acad. Sci. USA.* **105:** 12527–32

Hattar S., *et al*. (2003) Melanopsin and rod-cone photoreceptive systems account for all major accessory visual functions in mice. *Nature.* **424:** 76–81

Hattori N., *et al*. (1998) Molecular genetic analysis of a novel Parkin gene in Japanese families with autosomal recessive juvenile parkinsonism: evidence for variable homozygous deletions in the Parkin gene in affected ndividuals. *Ann. Neurol*. **44:** 935–941

Hattori N., Mizuno Y. (2004) Pathogenetic mechanisms of parkin in Parkinson's disease. *Lancet.* **364:** 722–724

Hauck S. M., *et al*. (2010) Deciphering membrane-associated molecular processes in target tissue of autoimmune uveitis by label-free quantitative mass spectrometry. *Mol. Cell. Proteomics*, **9**: 2292–2305

Havel P.J., *et al*. (1999) High-fat meals reduce 24-h circulating leptin concentrations in women. *Diabetes.* **48:** 334– 341

Hechtman P., *et al*. (1982) Deficiency of the hexosaminidase A activator protein in a case of GM2 gangliosidosis; variant AB. *Pediatr. Res.* **16:** 217–222

Hermes M.L., *et al*. (1996) GABA and glutamate mediate rapid neurotransmission from suprachiasmatic nucleus to hypothalamic paraventricular nucleus in rat. *J Physiol*. **496:** 749–757

Hernández F., *et al*., Avila J. (2010) GSK3: a possible link between beta amyloid peptide and tau protein. *Experimental Neurology.* **223:** 322–325

Hers H.G. (1963) alpha-Glucosidase deficiency in generalized glycogenstorage disease (Pompe's disease). *Biochem. J.* **86:** 11–16

Herzog E.D., *et al*. (2004) Temporal precision in the mammalian circadian system: a reliable clock from less reliable neurons. *J. Biol. Rhythms*. **19**: 35–46

Herzog E.D., *et al*. (1998) Clock controls circadian period in isolated suprachiasmatic nucleus neurons. *Nat. Neurosci.* **1:** 708–713

Higashi S., *et al*. (2007) Concurrence of TDP-43, tau and α-synuclein pathology in brains of Alzheimer's disease and dementia with Lewy bodies. *Brain Research*. **1184:** 284–294

Higashi Y., *et al*. (1993) Cerebellar degeneration in the Niemann-Pick type C mouse. *Acta Neuropathol.* **85:** 175–184

Higashi Y., *et al*. (1991) Pathology of Niemannn-Pick type C studies of murine mutants. *Neuropathology in Brain Research*. **Elsevier Science:** 85–102

Higuchi M., *et al*. (2002) Transgenic mouse model of tauopathies with glial pathology and nervous system degeneration. *Neuron.* **35:** 433–446

Higuchi M., *et al*. (2005) Axonal degeneration induced by targeted expression of mutant human tau in oligodendrocytes of transgenic mice that model glial tauopathies. *J. Neurosci.* **25:** 9434–9443

Hilker R., *et al*. (2001) Positron emission tomographic analysis of the nigrostriatal dopaminergic system in familial parkinsonism associated with mutations in the parkin gene. *Ann Neurol*. **49:** 367–376

Hill J.O., *et al*. (1992) Development of dietary obesity in rats: influence of amount and composition of dietary fat. *Int. J. Obes. Relat. Metab. Disord.* **16:** 321–333

Hirota T., Fukada Y. (2004) Resetting mechanism of central and peripheral circadian clocks in mammals. *Zoolog. Sci.* **21:** 359–368

Hoglinger G.U., *et al*. (2011) Identification of common variants influencing risk of the tauopathy progressive supranuclear palsy. *Nat. Genet*. **43:** 699–705

Hon-Chiu Eastwood Leung. (2012) INTEGRATIVE PROTEOMICS

Honer W.G., *et al*. (2002) Abnormalities of SNARE mechanism proteins in anterior frontal cortex in severe mental illness. *Cereb Cortex.* **12**: 349–356

Honma S., *et al*. (1998) Circadian rhythms of arginine-vasopressin and vasoactive intestinal polypeptide do not depend on cytoarchitecutre of dispersed cell culture rat suprachiasmatic nucleus. *Neuroscience*. **86**: 967–976

Hood S., *et al*. (2010) Endogenous dopamine regulates the rhythm of expression of the clock protein PER2 in the rat dorsal striatum via daily activation of D2 dopamine receptors. *Journal of Neuroscience.* **30:** 14046–14058

Hooper C., *et al*. (2008) The GSK3 hypothesis of Alzheimer's disease. *Journal of Neurochemistry*. **104:** 1433–1439

Horrobin D.F., *et al*. (1994) The membrane hypothesis of schizophrenia. *Schizophrenia Research*. **13:** 195–207

Hosokawa N., *et al*. (2011) Circadian transcriptional regulation by the posttranslational oscillator without de novo clock gene expression in Synechococcus*. Proc. Natl. Acad. Sci. USA*. **108**: 15396–15401

Houlden H., Singleton A.B., (2012) The genetics and neuropathology of Parkinson's disease. *Acta Neuropathol.* **124:** 325–338

Hsieh M.C., *et al*. (2010) Abnormal expressions of circadianclock and circadian clock-controlled genes in the livers and kidneys of long-term, high-fat-diet-treated mice. *Int. J. Obes.* **34:** 227–239

Hsu S.J., *et al*. (2000) Fine linkage and physical mapping suggests cross-over suppression with a retroposon insertion at the npc1 mutation. *Mamm. Genome.* **11:** 774–778

Huang J.T., *et al*. (2006) Disease biomarkers in cerebrospinal fluid of patients with first-onset psychosis. *PLoS Med* **3:** e428

Huang J.T., *et al*. (2007) CSF metabolic and proteomic profiles in patients prodromal for psychosis. *PLoS One.* **2:** e756

Hudson J.I., *et al*. (1993) Polysomnographic characteristics of schizophrenia in comparison with mania and depression. *Biol Psychiatry.* **34:** 191–193

Hughes A.T., *et al*. (2004) Aberrant gating of photic input to the suprachiasmatic circadian pacemaker of mice lacking the VPAC2 receptor. *J Neurosci*. **24**: 3522–3526

Hughes A.T., Piggins H.D. (2008) Behavioral responses of Vipr2-/- mice to light. *J Biol Rhythms.* **23:** 211–219

Huitron-Resendiz S., *et al*. (2005) Urotensin II modulates rapid eye movement sleep through activation of brainstem cholinergic neurons. *J Neurosci.* **25:** 5465–5474

Hunsley M.S., Palmiter R.D. (2003) Norepinephrine-deficient mice exhibit normal sleep–wake states but have shorter sleep latency after mild stress and low doses of amphetamine. *Sleep.* **26:** 521–526

Hussain R.J., *et al*. (2006) Myristoylated AlanineRich C Kinase Substrate (MARCKS) Heterozygous Mutant Mice Exhibit Deficits in Hippocampal Mossy Fiber-CA3 Long-Term Potentiation. *Hipppocampus*. **16:** 495–503

Hutton M., *et al*. (1998) Association of missense and 5'-splicesite mutations in tau with the inherited dementia FTDP-17. *Nature.* **393:** 702–705

Iitaka C., *et al*. (2005) A role for glycogen synthase kinase-3beta in the mammalian circadian clock. *J Biol Chem.* **280:** 29397–29402

Ikeda M., *et al*. (2003) Developmental and circadian changes in Ca2+ mobilization mediated by GABAA and NMDA receptors in the suprachiasmatic nucleus. Eur. *J. Neurosci.* **17:** 58–70

Ikegami S., *et al*. (2000) Muscle weakness, hyperactivity, and impairment in fear conditioning in tau-deficient mice. *Neurosci. Lett.* **279:** 129–132

Ikonen E. (2008) Cellular cholesterol trafficking and compartmentalization. *Nat Rev Mol Cell Biol.* **9:** 125–138

Imai A., *et al*. (2004) Roles of Munc18-3 in amylase release from rat parotid acinar cells. *Arch. Biochem. Biophys.* **422:** 175–182

Imbesi M., *et al*. (2009) Dopamine receptor-mediated regulation of neuronal "clock" gene expression. *Neuroscience.* **158:** 537–544

Infante R.E., *et al*. (2008) NPC2 facilitates bidirectional transfer of cholesterol between NPC1 and lipid bilayers, a step in cholesterol egress from lysosomes. *Proc. Natl. Acad. Sci. USA*. **105:** 15287–15292

Inoue S., *et al*. (2007) Synaptotagmin XI as a candidate gene for susceptibility to schizophrenia. *Am. J. Med. Genet.* **144B**: 332–340

Iqbal K., *et al*. (2009) Mechanisms of tau-induced neurodegeneration. *Acta Neuropathol*. **118:** 53–69

Iranzo A., *et al*. (2009) The clinical and pathophysiological relevance of REM sleep behavior disorder in neurodegenerative diseases. *Sleep Med. Rev.* **13:** 385–401

Irwin M. (2002) Effects of sleep and sleep loss on immunity and cytokines. *Brain Behav Immun.* **16:** 503–512

Irwin R.P., Allen C.N. (2007) Calcium response to retinohypothalamic tract synaptic transmission in suprachiasmatic nucleus neurons. *J Neurosci.* **27:** 11748–11757

Ishizawa T., *et al*. (2003) Colocalization of tau and alpha-synuclein epitopes in Lewy bodies. *J. of Neuropathology and Exp. Neurology*. **62:** 389–397

Itier J.M., *et al*. (2003) Parkin gene inactivation alters behavior and dopamine eurotransmission in the mouse. *Hum Mol Genet.* **12:** 2277–2291

Jahn R., Fasshauer D. (2012) Molecular machines governing exocytosis of synaptic vesicles. *Nature.* **490:** 201–7

Jahn R., *et al*. (2003) Membrane fusion. *Cell.* **112:** 519–533

Jahn R., Scheller R.H. (2006) SNAREs-engines for membrane fusion. *Nat. Rev. Mol. Cell Biol.* **7:** 631–643

Jakes R., *et al*. (1994) Identification of two distinct synucleins from human brain. *FEBS Lett.* **345:** 27–32

Jan J.E., *et al*. (2009) The role of the thalamus in sleep, pineal melatonin production, and circadian rhythm sleep disorders. *J. Pineal. Res*. **46**: 1–7

Janezic S., *et al*. (2013) Deficits in dopaminergic transmission precede neuron loss and dysfunction in a new Parkinson model. *Proc. Natl. Acad. Sci. USA*. **110**: E4016-E4025

Jankovic J. (2007) Parkinson's disease: clinical features and diagnosis. *J. Neurol Neurosurg Psychiatry.* **79**: 368–376

Javitt D.C., Zukin S.R. (1991) Recent advances in the phencyclidine model of schizophrenia. *Am J Psychiatry.* **148:** 1301–1308

Jeans A.F., *et al*. (2007) A dominant mutation in Snap25 causes impaired vesicle trafficking, sensorimotor gating, and ataxia in the blind-drunk mouse. *Proc. Natl. Acad. Sci. USA***. 104:** 2431–2436

Jellinger K. A. (2010) Basic mechanisms of neurodegeneration: a critical update. *Journal of Cellular and Molecular Medicine*. **14:** 457–487

Jellinger K.A. (2011) Interaction between α-Synuclein and other proteins in neurodegenerative disorders. *TheScientificWorldJOURNAL.* **11:** 1893–1907

Jenkins J.B., *et al*. (2006) Sleep is increased in mice with obesity induced by high-fat food. *Physiol. Behav.* **87:** 255– 262

Jennings J.J. Jr., *et al*. (2006) Mitochondrial aberrations in mucolipidosis Type IV. *J. Biol. Chem.* **281:** 39041–39050

Jesionek-Kupnicka D., *et al*. (1997) Krabbe disease: an ultrastructural study of globoid cells and reactive astrocytes at the brain and optic nerves. *Folia Neuropathol.* **35:** 155–162

Ji L., *et al*. (2012) Reduced activity of protein kinase C in the frontal cortex of subjects with regressive autism: relationship with developmental abnormalities. *Int. J. Biol. Sci.* **8:** 1075–1084

Johnson M.A., *et al*. (2002) The cysteine-rich domain of the neuregulin-1 gene (crd-NRG-1) is required for survival of a subset of neurons in the suprachiasmatic nucleus (SCN). Society for Neuroscience, Washington DC (online). 2002 Abstract Viewer/Itinerary Planner, 2002

Johnson E.O., *et al*. (2006) The association of insomnia with anxiety disorders and depression: exploration of the direction of risk. *J Psychiatr Res.* **40:** 700–708

Johnson R.D., *et al*. (2008) SNARE proteins and schizophrenia: linking synaptic and neurodevelopmental hypotheses. *Acta Biochimica Polonica.* **55:** 619–628

Johnson S.J., Wade-Martins R. (2011) A BACwards glance at neurodegeneration: molecular insights into disease from LRRK2, SNCA and MAPT BAC-transgenic mice. *Biochemical Society Transactions.* **39:** 4

Johnston-Wilson N.L. *et al*. (2000) Disease-specific alterations in frontal cortex brain proteins in schizophrenia, bipolar disorder and major depressive disorder. The Stanley Neuropathology Consortium. *Mol Psychiatry*. **5**: 142–149

Jones C.R., *et al*. (1999) Familial advanced sleep-phase syndrome: A short-period circadian rhythm variant in humans. *Nat Med.* **5:** 1062–1065

Jones K., Harrison Y. (2001) Frontal lobe function, sleep loss and fragmented sleep. *Sleep Med. Rev*. **5:** 463–475

Kahle P.J., Haass C. (2004) How does parkin ligate ubiquitin to Parkinson's disease? *EMBO Rep* **5:** 681–685

Kahn-Greene E.T., *et al*. (2007) The effects of sleep deprivation on symptoms of psychopathology in healthy adults. *Sleep Med.* **8:** 215–221

Kahol K., *et al*. (2008) Effect of fatigue on psychomotor and cognitive skills. *Am J Surg.* **195:** 195–204

Kalsbeek A., *et al*. (2006) SCN outputs and the hypothalamic balance of life. *J Biol Rhythms.* **21:** 458–469

Kalsbeek A., Strubbe J.H. (1998) Circadian control of insulin secretion is independent of the temporal distribution of feeding. *Physiol. Behav*. **63**: 553–558

Kaneko K., *et al*. (2009) Obesity alters circadian expressions of molecular clock genes in the brainstem. *Brain Res*. **1263:** 58–68

Kapas L., *et al*. (1988) Effects of nocturnal intraperitoneal administration of cholecystokinin in rats: simultaneous increase in sleep, increase inEEG slowwave activity, reduction of motor activity, suppression of eating, and decrease in brain temperature. *Brain Res.* **438**: 155–164

Karatsoreos I.N., *et al*. (2011) Disruption of circadian clocks has ramifications for metabolism, brain, and behavior. *Proc. Natl. Acad. Sci. USA.* **108**: 1657–1662

Karayiorgou M., *et al*. (1995) Schizophrenia susceptibility associated with interstitial deletions of chromosome 22q11. *Proc. Natl. Acad. Sci. USA.* **95**: 7612–7616

Karl T., *et al*. (2006) Effect of Y1 receptor deficiency on motor activity, exploration, and anxiety. *Behav. Brain Res*. **167:** 87–93

Karlsson B., *et al*. (2001) Is there an association between shift work and having a metabolic syndrome? Results from a population based study of 27,485 people. *Occup Environ Med.* **58:** 747–752

Karson C.N., *et al*. (1999) Alterations in synaptic proteins and their encoding mRNAs in prefrontal cortex in schizophrenia: a possible neurochemical basis for 'hypofrontality'. *Mol. Pshychiatry.* **4:** 39–45

Karten B., *et al*. (2009) Mechanisms and consequences of impaired lipid trafficking in Niemann-Pick type C1-deficient mammalian cells. *Biochim Biophys Acta*. **1791:** 659–670

Kataoka M., *et al*. (2011) A Single Amino Acid Mutation in SNAP-25 Induces Anxiety-Related Behavior in Mouse. *PLoS ONE.* **6:** e25158

Katsuse O., *et al*. (2006) Neurofibrillary tangle-related synaptic alterations of spinal motor neurons of P301L tau transgenic mice. *Neurosci. Lett.* **409:** 95–99

Kawashima K., *et al*. (2008) No association between tagging SNPs of SNARE complex genes (STX1A, VAMP2 and SNAP25) and schizophrenia in a Japanese population. *Am. J. Med. Genet. B Neuropsychiatr Genet.* **147:** 1327–1331

Kay D.M., *et al*. (2007) Heterozygous parkin point mutations are as common in control subjects as in Parkinson's patients. *Ann Neurol*. **61:** 47–54

Kelman B.B. (1999) The sleep needs of adolescents. *J Sch Nurs.* **15:** 14–19

Kennaway D.J., *et al*. (2006) Functional central rhythmicity and light entrainment, but not liver and muscle rhythmicity, are Clock independent. *Am. J. Physiol. Regul. Integr. Comp. Physiol*. **291:** 1172–1180

Keshavan M.S. (1999) Development, disease and degeneration in schizophrenia: a unitary pathophysiological model. *J Psychiatr Res.* **33**: 513–521

Keshavan M.S., *et al*. (1998) Delta sleep deficits in schizophrenia: evidence from automated analyses of sleep data. *Arch Gen Psychiatry*. **55:** 443–448

Khan N.L., *et al*. (2002) Progression of nigrostriatal dysfunction in a parkin kindred: an [18F] dopa PET and clinical study. *Brain.* **125:** 2248–2256

Killgore W.D., *et al*. (2008) Sleep deprivation reduces perceived emotional intelligence and constructive thinking skills. *Sleep Med*. **9:** 517–526

Killgore W.D., *et al*. (2007) The effects of 53 hours of sleep deprivation on moral judgment. *Sleep*. **30:** 345–352

Kim J.S., *et al*. (1980) Low cerebrospinal fluid glutamate in schizophrenic patients and a new hypothesis on schizophrenia. *Neurosci Lett*. **20:** 379–382

Kim J.W., *et al*. (2007) Investigation of variation in SNAP-25 and ADHD and relationship to co-morbid major depressive disorder. *Am J Med Genet B Neuropsychiatr Genet* **144:** 781–790

Kirov G., *et al*. (2005) Finding schizophrenia genes. *J. Clin. Invest.* **115:** 1440–1448

Kitada T., *et al*. (1998) Mutations in the parkin gene cause autosomal recessive juvenile parkinsonism. *Nature.* **392:** 605–608

Klein C., *et al*. (2000) Parkin deletions in a family with adult-onset, tremor-dominant parkinsonism: expanding the phenotype. *Ann Neurol.* **48** :65–71

Klemfuss H. (1992) Rhythms and the pharmacology of lithium. *Pharmacol. Ther*. **56:** 53–78

Knable M.B., *et al*. (2004) Molecular abnormalities of the hippocampus in severe psychiatric illness: postemortem finding from the Stanley Neuropathology Consortium. *Mol.Psychiatry.* **9:** 609–620

Knutson K.L., *et al*. (2007) The metabolic consequences of sleep deprivation. *Sleep Med Rev.* **11:** 163–178

Knutson K.M., *et al*. (2008) Neural correlates of caregiver burden in cortical basal syndrome and frontotemporal dementia. *Dement Geriatr Cogn Disord.* **26:** 467–474

Ko D.C., *et al*. (2001) Dynamic movements of organelles containing Niemann-Pick C1 protein: NPC1 involvement in late endocytic events. *Mol. Biol. Cell.* **12:** 601–614

Koefoed P., *et al*. (2009) An intron 1 polymorphism in the cholecystokinin-A receptor gene associated with schizophrenia in males. *Acta Psychiatr Scand.* **120:** 281–287

Koenig J.I., *et al*. (2005) Prenatal exposure to a repeated variable stress paradigm elicits behavioral and neuroendocrinological changes in the adult offspring: potential relevance to schizophrenia. *Behav. Brain Res.* **156:** 251–261

Kofman O. (2002) The role of prenatal stress in the etiology of developmental behavioral disorders. *Neurosci. Biobehav. Rev.* **26:** 457–470

Kohsaka A., Bass J. (2007) A sense of time: how molecular clocks organize metabolism. *Trends Endocrinol Metab.* **18:** 4–11

Kohsaka A., *et al*. (2007) High-fat diet disrupts behavioral and molecular circadian rhythms in mice. *Cell Metab.* **6:** 414–421

Kolter T., Sandhoff K. (2010) Lysosomal degradation of membrane lipids. *FEBS Letters*. **584:** 1700–1712

Kong J., *et al*. (2002) Brain glycogen decreases with increased periods of wakefulness: implication for homeostatic drive to sleep. *J Neurosci*. **22**: 5581–5587

Koolschijn P.C., *et al*. (2008) Hypothalamus volume in twin pairs discordant for schizophrenia. *Eur Neuropsychopharmacol*. **18:** 312–315

Kopp C., *et al*. (2002) Homeostatic sleep regulation is preserved in mPer1 and mPer2 mutant mice. *Eur J Neurosci.* **16:** 1099–1106

Kornhauser J.M., *et al*. (1990) Photic and circadian regulation of *c-fos* gene expression in the hamster suprachiasmatic nucleus. *Neuron*. **5**: 127–134

Kornhuber J. (1992) Phencyclidine and schizophrenia. *Am. J. Psychiatry.* **149:** 848–9

Kozikowski A. P., *et al*. (2006) Highly potent and specific GSK-3β inhibitors that block tau phosphorylation and decrease α-synuclein protein expression in a cellular model of Parkinson's disease. *ChemMedChem.* **1:** 256–266

Kracun I., *et al*. (1984) Topographical atlas of the gangliosides of the adult human brain. *J. eurochem.* **43:** 979–989

Kramer A., Merrow M. (2013) Circadian clocks. *Handbook of Experimental Pharmacology*. **217**

Kruger M., *et al*. (2008) Silac Mouse for Quantitative Proteomics Uncovers Kindlin-3 as an Essential Factor for Red Blood Cell Function. *Cell.* **134:** 353–364

Kruger R., *et al*. (2001) Familial parkinsonism with synuclein pathology: clinical and PET studies of A30P mutation carriers. *Neurology*. **56**: 1355–1362

Krüger R., *et al*. (1998) Ala30Pro mutation in the gene encoding alphasynuclein in Parkinson's disease. *Nat. Genet*. **18:** 106–108

Krystal A.D., *et al*. (2008) Sleep disturbance in psychiatric disorders: effects on function and quality of life in mood disorders, alcoholism, and schizophrenia. *Ann Clin Psychiatry*. **20:** 39–46

Kudo T., *et al*. (2011) Circadian dysfunction in a mouse model of Parkinson's disease. *Experimental Neurology*. **YEXNR-10863:**4C

Kumamoto N., *et al*. (2006) Hyperactivation of midbrain dopaminergic system in schizophrenia could be attributed to the downregulation of dysbindin. *Biochem Biophys Res Commun.* **345**: 904–909

Kume K., *et al*. (1999) mCRY1 and mCRY2 are essential components of the negative limb of the circadian clock feedback loop. *Cell*. **98**: 193–205

Kuo Y.M., *et al*. (2010) Extensive enteric nervous system abnormalities in mice transgenic for artificial chromosomes containing Parkinson disease-associated *α*-synuclein gene mutations precede central nervous system changes. *Hum. Mol. Genet*. **19**: 1633–1650

Kurian S.M., *et al*. (2011) Identification of blood biomarkers for psychosis using convergent functional genomics. *Mol Psychiatr.* **16:** 37–58

Kuroda Y., *et al*. (2006) Parkin affects mitochondrial function and apoptosis in neuronal and myogenic cells. *Biochem. Biophys. Res.Commun.* **348:** 787–793

Kytzia H.J. and Sandhoff K. (1985) Evidence for two different active sites on human beta–hexosaminidase A. Interaction of GM2 activator protein with beta–hexosaminidase A. *J. Biol. Chem.* **260:** 7568–7572

Lachman H.M., *et al*. (2005) Association of schizophrenia in African Americans to polymorphisms in synapsin III gene. *Psychiatr. Genet.* **15**: 127–132

Lam C.K., *et al*. (2009) CNS regulation of glucose homeostasis. *Physiology.* **24:** 159–170

Lam R.W., Levitan R.D. (2000) Pathophysiology of seasonal affective disorder: A review. *J Psychiatry Neurosci.* **25:** 469–480

Lambe E.K., *et al*. (2007) Schizophrenia, hypocretin (orexin), and the thalamocortical activating system. *Schizophr Bull*. **33:** 1284–1290

Lamond N., *et al*. (2007) The dynamics of neurobehavioral recovery following sleep loss. *J Sleep Res.* **16:** 33–41

Lancel M., *et al*. (1991) Effects of circadian phase and duration of sleep deprivation on sleep and EEG power spectra in the cat. *Brain Res*. **548**: 206–214

Landolt H.P., *et al*. (1996) Effect of age on the sleep EEG: slow-wave activity and spindle frequency activity in young and middle-aged men. *Brain Res.* **738:** 205–212

Lang U.E., *et al*. (2007) Molecular mechanisms of schizophrenia. *Cell. Physiol. Biochem.* **20:** 687–702

Langston J.W. (2006) The Parkinson's complex: parkinsonism is just the tip of the iceberg. *Ann Neurol*. **59:** 591–596

Laposky A.D., *et al*. (2008) Sleep and circadian rhythms: key components in the regulation of energy metabolism. *FEBS Lett.* **582:** 142–151

Larsen J.P. (2003) Sleep disorders in Parkinson's disease. *Adv Neurol*. **91:** 329–334

Larsen J.P., Tandberg E. (2001) Sleep disorders in patients with Parkinson's disease: epidemiology and management. *CNS Drugs.* **15:** 267–275

Lau C.G., *et al*. (2010) SNAP-25 Is a Target of Protein Kinase C Phosphorylation Critical to NMDA Receptor Trafficking. *The J. of Neurosci.* **30:** 242–254

Lebel M., *et al*. (2009) Dopamine D1 receptor activation induces tau phosphorylation via cdk5 and GSK3 signaling pathways. *Neuropharmacology*. **57:** 392–402

Ledeen R., Salsman K. (1965) Structure of the Tay-Sachs' ganglioside. *Biochemistry.* **4:** 2225–2233

Lee B., *et al*. (2007b) Protein kinase C modulates the phase-delaying effects of light in the mammalian circadian clock. *Eur. J. Neurosci.* **26:** 451–462

Lee C., *et al*. (2001) Posttranslational mechanisms regulate the mammalian circadian clock. *Cell*. **107**: 855–867

Lee H.J., *et al*. (2005) Association study of polymorphisms in synaptic vesicle-associated genes, SYN2 and CPLX2, with schizophrenia. *Behav. Brain Funct.* **1**: 15–23

Lee J.E., *et al*. (2010) Endogenous peptide discovery of the rat circadian clock: a focused study of the suprachiasmatic nucleus by ultrahigh performance tandem mass spectrometry. *Mol Cell Proteomics.* **9:** 285–297

Lee J.E., *et al*. (2013) Quantitative Peptidomics for Discovery of Circadian-Related Peptides from the Rat Suprachiasmatic Nucleus. *J. Proteome Res.* **12:** 585−593

Lee J.P., *et al*. (2007a) Stem cells act through multiple mechanisms to benefit mice with neurodegenerative metabolic disease. *Nat Med*. **13:** 439–447

Lee M.K., *et al*. (2002) Human alpha-synuclein-harboring familial Parkinson's disease-linked Ala-53→ Thr mutation causes neurodegenerative disease with alpha-synuclein aggregation in transgenic mice. *Proc. Natl. Acad. Sci.USA.* **99:** 8968–8973

Lee V. M. Y., *et al*. (2004) More than just two peas in a pod: common amyloidogenic properties of tau and *α*-synuclein in neurodegenerative diseases. *Trends in Neurosciences*. **27:** 129–134

LeGates T.A., Altimus C.M. (2011) Measuring circadian and acute light responses in mice using wheel running activity. *J Vis Exp*. **48:** 2463

Leger D., *et al*. (1999) Prevalence of sleep/wake disorders in persons with blindness. *Clin Sci (Lond)*. **97**: 193-199

Lehmann, J., *et al*. (2000) Long-term effects of prenatal stress experiences and postnatal maternal separation on emotionality and attentional processes. *Behav. Brain Res.* **107:** 133–144

Lei P., *et al*. (2010) Tau protein: relevance to Parkinson's disease. *International Journal of Biochemistry and Cell Biology*. **42:** 1775–1778

Lemaire V., *et al*. (2000) Prenatal stress produces learning deficits associated with an inhibition of neurogenesis in the hippocampus. *Proc. Natl. Acad. Sci. USA.* **97:** 11032–11037

Le-Niculescu H., *et al*. (2013) Discovery and validation of blood biomarkers for suicidality. *Molecular Psychiatry.* 18: 1249–1264

Levi F., Schibler U. (2007) Circadian rhythms: mechanisms and therapeutic implications. *Annu Rev Pharmacol Toxicol.* **47:** 593–628

Levitan R.D. (2007) The chronobiology and neurobiology of winter seasonal affective disorder. *Dialogues Clin Neurosci*. **9:** 315–324

Lewis C.M., *et al*. (2003) Genome scan meta-analysis of schizophrenia and bipolar disorder, part II: Schizophrenia. *Am J Hum Genet.* **73**: 34–48

Lewis J., *et al*. (2001) Enhanced neurofibrillary degeneration in transgenic mice expressing mutant tau and APP. *Science*. **293:** 1487–1491

Lewis J., *et al*. (2000) Neurofibrillary tangles, amyotrophy and progressive motor disturbance in mice expressing mutant (P301L) tau protein. *Nat. Genet.* **25:** 402–405

Li D., *et al*. (2006) Meta-analysis shows strong positive association of the neuregulin 1 (NRG1) gene with schizophrenia. *Hum. Mol. Genet.* **15:** 1995–2002

Li J., *et al*. (2001) Stabilization of partially-folded conformation during a-synuclein oligomerization in both purified and cytosolic preparations. *Journal Biological Chemistry.* **276**: 43495–43498

Li J., *et al*. (2012) Lithium Impacts on the Amplitude and Period of the Molecular Circadian Clockwork. *PLos One.* **7:** e33292

Lieberman J., *et al*. (2001) Longitudinal study of brain morphology in first episode schizophrenia. *Biological Psychiatry.* **49:** 487–499

Lieberman J.A. (1999) Is schizophrenia a neurodegenerative disorder? A clinical and neurobiological perspective. *Biological Psychiatry.* **46:** 729–739

Lim F., *et al*. (2001) FTDP-17 mutations in tau transgenic mice provoke lysosomal abnormalities and Tau filaments in forebrain. *Mol. Cell. Neurosci.* **18:** 702–714

Lin W.L., *et al*. (2003) Filamentous tau in oligodendrocytes and astrocytes of transgenic mice expressing the human tau isoform with the P301L mutation. *Am. J. Pathol.* **162:** 213–218

Lin W.L., *et al*. (2005) Progressive white matter pathology in the spinal cord of transgenic mice expressing mutant (P301L) human tau. *J. Neurocytol.* **34:** 397–410

Liscum L. (2000) Niemann-Pick type C mutations cause lipid traffic jam. *Traffic*. **1:** 218–225

Liu A.C., *et al*. (2007) Mammalian circadian signalling networks and therapeutic targets. *Nat. Chem. Biol*. **3**: 630–639

Liu A.C. *et al*. (2007b) Intercellular coupling confers robustness against mutations in the SCN circadian clock network. *Cell*. **129**: 605–616

Liu H., *et al*. (2004) A Model for Random Sampling and Estimation of Relative Protein Abundance in Shotgun Proteomics. *Anal Chem.* **76:** 4193–4201

Liu J.P., *et al*. (1992) Evidence that the stimulation by arginine vasopressin of the release of adrenocorticotropin from the ovine anterior pituitary involves the activation of protein kinase C. *Molecular and Cellular Endocrinology.* **87:** 35–47

Liu J.P., *et al*. (1994) Arginine vasopressin (AVP) causes the reversible phosphorylation of the myristoylated alanine-rich C kinase substrate (MARCKS) protein in the ovine anterior pituitary: evidence that MARCKS phosphorylation is associated with adrenocorticotropin (ACTH) secretion. *Mol. Cell Endocrinol.* **105:** 217–226

Liu J.P., *et al*. (1990) The Biosynthesis and Secretion of Adrenocorticotropin by the Ovine Anterior Pituitary Is Predominantly Regulated by Arginine Vasopressin (AVP). *The Journal of Biological Chemistry.* **265:** 14136–14142

Liu Y., *et al*. (1997) Pathological correlates of extrapyramidal signs in Alzheimer's disease. *Annals of Neurology*. **41:** 368–374

Lloyd-Evans E., *et al*. (2008) Niemann-Pick disease type C1 is a sphingosine storage disease that causes deregulation of lysosomal calcium. *Nat. Med.* **14:** 1247–1255

Loftus S.K., *et al*. (2002) Rescue of neurodegeneration in Niemann-Pick-C mice by a prion-promoter Npc1 cDNA transgene. *Hum. Mol. Genet*. **11:** 3107– 3114

Loftus S.K., *et al*. (1997) Murine model of Niemann–Pick C disease: mutation in a cholesterol homeostasis gene. *Science*. **277:** 232–235

Lohmann E., *et al*. (2003) How much phenotypic variation can be attributed to parkin genotype? *Ann Neurol.* **54:** 176–185

Lorton D., *et al*. (2006) Bidirectional communication between the brain and the immune system: implications for physiological sleep and disorders with disrupted sleep. *Neuroimmunomodulation.* **13:** 357–374

Louris J. N., *et al*. (1987) Instrumentation, applications, and energy deposition in quadrupole ion-trap tandem mass-spectrometry. *Anal. Chem.* **59:** 1677–1685

Louter M., *et al*. (2012) Recognition and diagnosis of sleep disorders in Parkinson's disease. *J Neurol.* **259:** 2031–2040

Low-Zeddies S.S., Takahashi J.S. (2001) Chimera analysis of the Clock mutation in mice shows that complex cellular integration determines circadian behavior. *Cell*. **105**: 25–42

Lu J., *et al*. (2002) Selective activation of the extended ventrolateral preoptic nucleus during rapid eye movement sleep. *J Neurosci*. **22**: 4568–4576

Lu J., *et al*. (2000) Effect of lesions on the ventrolateral preoptic nucleus on NREM and REM sleep. *J Neurosci*, **20**: 3830–3842

Lu J., *et al*. (2006) A putative flip-flop switch for control of REM sleep. *Nature*. **441:** 589–594

Lu X.H. (2009) BAC to degeneration bacterial artificial chromosome (BAC)-mediated transgenesis for modelling basal ganglia neurodegenerative disorders. *Int. Rev. Neurobiol*. **89**: 37–56

Lucas R.J., *et al*. (2001) Identifying the photoreceptive inputs to the mammalian circadian system using transgenic and retinally degenerate mice. *Behav. Brain. Res*. **125**: 97–102

Lucidi F., *et al*. (2006) Sleep-related car crashes: risk perception and decisionmaking processes in young drivers. *Accid Anal Prev.* **38:** 302–309

Lucking C. B., *et al*. (2000) Association between early-onset Parkinson's disease and mutations in the parkin gene. *N. Engl. J. Med.* **342:** 1560–1567

Lundgren D. H., *et al*. (2010) Role of Spectral Counting in Quantitative Proteomics. *Expert Rev Proteomics*. **7:** 39–53

Macek, B., Waanders, *et al*. (2006) Top-down protein sequencing and MS3 on a hybrid linear quadrupole ion traporbitrap mass spectrometer. *Mol. Cell Proteomics* .**5:** 949–958

Mackiewicz M., Pack A.I. (2003) Functional genomics of sleep. *Respir Physiol Neurobiol.* **135:** 207–220

MacQueen G.M., *et al*. (1998) Neuropsychiatric aspects of the adult variant of Tay-Sachs disease. *J. Neuropsychiatry Clin. Neurosci.* **10:** 10–19

Maemura K., *et al*. (2007) Circadian rhythms in the CNS and peripheral clock disorders: role of the biological clock in cardiovascular diseases. *J Pharmacol Sci.* **103:** 134–138

Magnusson A., Boivin D. (2003) Seasonal affective disorder: An overview. *Chronobiol Int*. **20:** 189–207

Makita A., Yamakawa T. (1963) The glycolipids of the brain of Tay-Sachs' disease. The chemical structures of globoside and main ganglioside. *Jpn J Exp. Med*. **33:** 361–368

Malisch J.L., *et al*. (2009) Behavioral despair and home-cage activity in mice with chronically elevated basleine corticosterone concentrations. *Beha Genet*. **39**: 192–201

Mandal P.K., *et al*. (2006) Interaction between A*β* peptide and *α* synuclein: molecular mechanisms in overlapping pathology of Alzheimer's and Parkinson's in dementia with Lewy body disease. *Neurochemical Research*. **31:** 1153–1162

Mandelkow E.M., *et al*. (1995) Tau domains, phosphorylation, and interactions with microtubules. *Neurobiol. Aging.* **16:** 355–362

Manfredsson F.P., *et al*. (2009) Tight Long-term dynamic doxycycline responsive nigrostriatal GDNF using a single rAAV vector. *Mol Ther.* **17:** 1857–1867

Mann M. (2006) Functional and quantitative proteomics using SILAC. *Nat. Rev. Mol. Cell Biol*. **7:** 952–958

Mansour H.A., *et al*. (2006) Association study of eight circadian genes with bipolar I disorder, schizoaffective disorder and schizophrenia. *Genes Brain Behav.* **5:** 150–157

Marcheva B., *et al*. (2010) Disruption of the clock components CLOCK and BMAL1 leads to hypoinsulinaemia and diabetes. *Nature*. **466:** 627–631

Marcheva B., *et al*. (2013) Circadian clocks and metabolism. *Handb. Exp. Pharmacol.* **217:** 127–155

Martens S., *et al*. (2007) How synaptotagmin promotes membrane fusion. *Science.* **316**: 1205–1008

Martin J., *et al*. (2001) Actigraphic estimates of circadian rhythms and sleep/wake in older schizophrenia patients. *Schizophr Res*. **47:** 77–86

Martin J.L., *et al*. (2005) Older schizophrenia patients have more disrupted sleep and circadian rhythms than age-matched comparison subjects. *J Psychiatr. Res*. **39:** 251–259

Martins-de-Souza D. (2012) Proteomics Tackling Schizophrenia as a Pathway Disorder. *Schizophrenia Bulletin*. **38**: 1107–1108

Martins-de-Souza D., *et al*. (2009) Proteomic analysis of dorsolateral prefrontal cortex indicates the involvement of cytoskeleton, oligodendrocyte, energy metabolism and new potential markers in schizophrenia. *Journal of Psychiatric Research.* **43:** 978–986

Martins-de-Souza D., *et al*. (2010c) Proteome analysis of the thalamus and cerebrospinal fluid reveals glycolysis dysfunction and potential biomarkers candidates for schizophrenia. *J. of Psychiatric Research.* **44:** 1176–1189

Masliah E., *et al*. (2000) Dopaminergic loss and inclusion body formation in alpha-synuclein mice: implications for neurodegenerative disorders. *Science.* **287:** 1265–1269

Masson M., *et al*. (1992) Calmodulin antagonists chlorpromazine and W-7 inhibit exogenous cholesterol esterification and sphingomyelinase activity in human skin fibroblast cultures. Similarities between drug-induced and Niemann-Pick type C lipidoses. *J Neurosci Res*. **21**: 84–88

Mattai A.A., *et al*. (2006) Sleep disturbances in childhood-onset schizophrenia. *Schizophr Res.* **86:** 123–129

Matteoli M., *et al*. (2008) The synaptic split of SNAP-25: Different roles in glutamatergic and GABAERGIC neurons? *Neuroscience.* **158:** 223–230

Maue R.A., *et al*. (2012) A novel mouse model of Niemann-Pick type C disease carrying a D1005G-Npc1 mutation comparable to commonly observed human mutations. *Hum. Mol. Genet*. **21:** 730–750

Mauvoisin D., *et al*. (2014) Circadian clock-dependent and –independent rhythmic proteomes implement distrinct diurnal functions in mouse liver. *Proc. Natl. Acad. Sci. USA.* **111**: 167–172

Maywood E.S., *et al*. (2010) Disruption of Peripheral Circadian Timekeeping in a Mouse Model of Huntington's Disease and Its Restoration by Temporally Scheduled Feeding. *The J of Neuroscience.* **30:** 10199–10204

Maywood E.S., *et al*. (2003) Expression of mCLOCK and other circadian clock-relevant proteins in the mouse suprachiasmatic nuclei. *J Neuroendocrinol*. **15:** 329–334

Maywood E.S., *et al*. (2006) Synchronization and maintenance of timekeeping in suprachiasmatic circadian clock cells by neuropeptidergic signaling. *Curr Biol.* **16:** 599–605

Maywood E.S., *et al*. (1997) A thalamic contribution to arousal-induced, non-photic entrainment of the circadian clock of the Syrian hamster. *Eur J Neurosci.* **9:** 1739–1747

Maziade M. (2001) A search for specific and common susceptibility loci for schizophrenia and bipolar disorder: a linkage study in 13 target chromosomes. *Molecular Psychiatry*. **6:** 684

McAlister, G. C., *et al*. (2008) A proteomics grade electron transfer dissociationenabled hybrid linear ion trap-orbitrap mass spectrometer. *J. Proteome Res.* **7,** 3127–3136

McArthur A.J., *et al*. (1997) Melatonin Action and Signal Transduction in the Rat Suprachiasmatic Circadian Clock: Activation of Protein Kinase C at Dusk and Dawn. *Endocrinology*. **138:** 627–634

McCarter S.J., *et al*. (2013) Is rapid eye movement sleep behavior disorder in Parkinson disease a specific disease subtype? *Sleep Med*. **14**: 931–933

McClatchy D. B., *et al*. (2007) 15n Metabolic Labeling of Mammalian Tissue with Slow Protein Turnover. *J Proteome Res.* **6:** 2005–2010

McClatchy D.B., Yates J.R. (2008) Stable Isotope Labeling of Mammals (SILAM). *CSH Protoc.* **3**

McClung C.A. (2007) Circadian genes, rhythms, and the biology of mood disorders. *Pharmacol. Ther.* **114:** 222–232

McCormack P.L. (2010) Olanzapine: in adolescents with schizophrenia or bipolar I disorder. *CNS Drugs.* **24:** 443–452

McCormick D.A., Bal T. (1997) Sleep and arousal: thalamocortical mechanisms. *Annu Rev Neurosci.* **20:** 185–215

McGinty D., Szymusiak R. (2000) The sleep-wake switch: A neuronal alarm clock. *Nat. Med.* **6:** 510–511

McGinty D., Szymusiak R. (2003) Hypothalamic regulation of sleep and arousal. *Front Biosci.* **8:** 1074–1083

McGlincy N., *et al*. (2012) Regulation of alternative splicing by the circadian clock and food related cues. *Genome Biology.* **12:** R54

McKenna B.S., *et al*. (2007) The effects of one night of sleep deprivation on known-risk and ambiguous-risk decisions. *J Sleep Res.* **16:** 245–252

McNamara R.K., *et al*. (2005) Effect of myristoylated alanine-rich C kinase substrate (MARCKS) overexpression on hippocampus-dependent learning and hippocampal synaptic plasticity in MARCKS transgenic mice. *Hippocampus.* **15:** 675–683

Meador-Woodruff J.H., *et al*. (2003) Molecular abnormalities of the glutamate synapse in the thalamus in schizophrenia. *Ann N Y Acad Sci*. **1003:** 75–93

Meerlo P., *et al*. (2008) Restricted and disrupted sleep: effects on autonomic function, neuroendocrine stress systems and stress responsivity. *Sleep Med Rev.* **12:** 197–210

Mei L., Xiong W.C. (2008) Neuregulin 1 in neural development, synaptic plasticity and schizophrenia. *Nat Rev Neurosci.* **9:** 437–452

Meltzer H.Y., Stahl S.M. (1976) The dopamine hypothesis of schizophrenia: a review. *Schizophr Bull.* **2**: 19–76

Mendoza J., *et al*. (2008) High-fat feeding alters the clock synchronization to light. *J. Physiol.* **586:** 5901–5910

Menza M., *et al*. (2010) Sleep disturbances in Parkinson's disease. *Movement Disorders*. **25:** 117–122

Michalski A., *et al*. (2011) Mass spectrometry-based proteomics using Q Exactive, a high-performance benchtop quadrupole Orbitrap mass spectrometer. *Mol. Cell Proteomics*. **10:** 111.011015

Middleton F.A., Strick P.L. (1998) Cerebellar output: motor and cognitive channels. *Trends Cogn Sci*. **2:** 348–354

Miklyaeva E.I., *et al*. (2004) Late onset Tay-Sachs disease in mice with targeted disruption of the *Hexa* gene: behavioral changes and pathology of the central nervous system. *Brain Res.* **1001:** 37–50

Mill J., *et al*. (2004) Haplotype analysis of SNAP-25 suggests a role in the aetiology of ADHD. *Mol. Psychiatry.* **9:** 801–810

Mill J., *et al*. (2005) Quantitative trait locus analysis of candidate gene alleles associated with attention deficit hyperactivity disorder (ADHD) in five genes: DRD4, DAT1, DRD5, SNAP-25, and 5HT1B. *Am J Med Genet B Neuropsychiatr Genet.* **133:** 68–73

Miller D.D. (2004) Atypical antipsychotics: sleep, sedation, and efficacy. *Prim Care Companion J Clin Psychiatry*. **6:** 3–7

Mirsky A.F., Duncan C.C. (1986) Etiology and expression of schizophrenia: neurobiological and psychosocial factors. *Annu.Rev.Psychol.* **37:** 291–319

Mistlberger R.E., *et al*. (1998) Circadian rhythms in the Zucker obese rat: assessment and intervention. *Appetite.* **30:** 255–267

Mitchell J.W., *et al*. (2011) Direct cellular peptidomics of hypothalamic neurons. *Frontiers in Neuroendocrinology.* **32:** 377–386

Miyoshi Y., *et al*. (2009) Determination of D-serine and D-alanine in the tissues and physiological fluids of mice with various D-amino-acid oxidase activities using two-dimensional high-performance liquid chromatography with fluorescence detection. *J Chromatogr B Analyt Technol Biomed Life Sci.* **877:** 2506–2512

Mohandas E., Rajmohan V. (2009) Frontotemporal dementia: an updated overview. *Indian J Psychiatry* . **51:** 65–69

Mohawk J.A., *et al*. (2012) Central and peripheral circadian clocks in mammals. *Annu. Rev. Neurosci*. **35**: 445–462

Moises H.W., *et al*. (1995) An international two-stage genome-wide search for schizophrenia susceptibility genes. *Nat Genet*. **11:** 321–324

Moldavan M.G., Allen C.N. (2010) Retinohypothalamic tract synapses in the rat suprachiasmatic nucleus demonstrate short-term synaptic plasticity. *J.Neurophysiol.* **103:** 2390–2399

Molnár Z., *et al*. (2002) Normal development of embryonic thalamocortical connectivity in the absence of evoked synaptic activity. *J Neurosci.* **22**: 10313–10323

Monteleone P., *et al*. (1997) Decreased nocturnal secretion of melatonin in drug-free schizophrenics: no change after subchronic treatment with antipsychotics. *Neuropsychobiology*. **36:** 159–163

Monti J.M., Monti D. (2005) Sleep disturbance in schizophrenia. *Int Rev Psychiatry.* **17:** 247–253

Moore R.Y. (1983) Organiziation and function of a central nervous system circadian oscillator: the suprachiasmatic hypothalamic nucleus. *Fed. Proc*. **42**: 2783–2789

Morikawa A., *et al*. (2008) Circadian changes of D-alanine and related compounds in rats and the effect of restricted feeding on their amounts. *J Chromatogr B Analyt Technol Biomed Life Sci.* **875:** 168–173

Moron J.A., *et al*. (2007) Morphine administration alters the profile of hippocampal postsynaptic density-associated proteins: a proteomics study focusing on endocytic proteins. *Mol. Cell. Proteomics*. **6:** 29–42

Morris M.D., *et al*. (1982) Lysosome lipid storage disorder in NCTR-BALB/c mice. I. Description of the disease and genetics. *Am J Pathol.* **108:** 140–149

Morris M.E., *et al*. (1998) A screen for genes induced in the suprachiasmatic nucleus by light. *Science.* **279:** 1544–1547

Morton A.J., *et al*. (2005) Disintegration of the sleep-wake cycle and circadian timing in Huntington disease. *J Neurosci*. **25:** 157–163

Mouri A., *et al*. (2007) Phencyclidine animal models of schizophrenia: approaches from abnormality of glutamatergic neurotransmission and neurodevelopment. *Neurochem Int.* **51:** 173–184

Mrosovsky N. (2003) Contribution of classic photoreceptors to entrainment. *J. Comp. Physiol. A. Neuroethol. Sens. Neural. Behav. Physiol.* **189:** 69–73

Muecke S. (2005) Effects of rotating night shifts: literature review. *J Adv Nurs.* **50:** 433–439

Muench J., Hamer A.M. (2010) Adverse effects of antipsychotic medications. *Am Fam Physician*. **81:** 617–622

Mueser K.T., McGurk S.R. (2004) Schizophrenia. *Lancet.* **363:** 2063–2072

Mukaetova-Ladinska E., *et al*. (2002) Loss of synaptic but not cytoskeletal proteins in the cerebellum of chronic schizophrenics. *Neurosci. Lett.* **317:** 161–165

Muller D.J., *et al*. (2005) The SNAP-25 gene may be associated with clinical response and weight gain in antipsychotic treatment of schizophrenia. *Neurosci Lett.* **379**: 81–89

Munch M., *et al*. (2004) The frontal predominance in human EEG delta activity after sleep loss decreases with age. *Eur J Neurosci.* **20:** 1402–1410

Muntané G., *et al*. (2008) Phosphorylation of tau and α-synuclein in synapticenriched fractions of the frontal cortex in Alzheimer's disease, and in Parkinson's disease and related α- synucleinopathies. *Neuroscience.* **152:** 913–923

Murakami N., *et al*. (1991) Long term cultured neurons from rat supraciasmatic nucleus retain the capacity for circadian oscillation of vasopressing release. *Brain Res*. **545**: 347–350

Murakami T., *et al*. (2006) Cortical neuronal and glial pathology in TgTauP301L transgenic mice: neuronal degeneration, memory disturbance, and phenotypic variation. Am. *J. Pathol*. **169:** 1365–1375

Murphy D.D., *et al*. (2000) Synucleins are developmentally expressed, and alpha-synuclein regulates the size of the presynaptic vesicular pool in primary hippocampal neurons. *J. Neurosci.* **20:** 3214–3220

Musiek E.S., *et al*. (2013) Circadian clock proteins regulate neuronal redox homeostasis and neurodegeneration. *J. Clin. Invest*. **123**: 5389–5400

Nagashima K., *et al*. (1981) Retinal amacrine cell involvement in Tay- Sachs disease. *Acta Neuropathol.* **53:** 333–336

Nahnsen S., *et al*. (2013) Tools for label-free peptide quantification. *Mol. Cell. Proteomics.* **12:** 549–556

Nakahira K., *et al*. (2011) Autophagy proteins regulate innate immune responses by inhibiting the release of mitochondrial DNA mediated by the NALP3 inflammasome. *Nat. Immunol.* **12:** 222–230

Nakajima M., *et al*. (2005) Reconstituion of circadian oscillation of cyanobacterial KaiC phosphorylation. *Science*. **307**: 251–254

Nakamura T.J., *et al*. (2011) Age-related decline in circadian output. *J Neurosci.* **31:** 10201–10205

Nakamura W., *et al* (2002) *Clock* mutation lengthens the circadian period without damping rhythms in individual SCN neurons. *Nat. Neurosci*. **5**: 399–400

Naureckiene S., *et al*. (2000) Identification of HE1 as the second gene of Niemann-Pick C disease. *Science.* **290:** 2298–2301

Nedeltcheva A.V., *et al*. (2009) Exposure to recurrent sleep restriction in the setting of high caloric intake and physical inactivity results in increased insulin resistance and reduced glucose tolerance. *J. Clin. Endocrinol. Metab.* **94:** 3242–3250

Nelson D.E., Takahashi J.S. (1991) Sensitivity and integration in a visual pathway for circadian entrainment in the hamster (Mesocricetus auratus). *J Physiol*. **439:** 115–145

Nelson R.J., Zucker I. (1981) Photoperiodic control of reproduction in olfactory-bulbectomized rats. *Neuroendocrinology.* **32:** 266–271

Nemani V.M. (2010) Increased expression of α-synuclein reduces neurotransmitter release by inhibiting synaptic vesicle reclustering after endocytosis. *Neuron.* **65**: 66–79

Niculescu A., *et al*. (2000) Identifying a series of candidate genes for mania and psychosis: a convergent functional genomics approach. *Physiol Genomics*. **4:** 83–91

Nieto M.A., *et al*. (1996) Chapter 11 In Situ Hybridization Analysis of Chick Embryos in Whole Mount and Tissue Sections. *Cell Biology.* **51:** 219–235

Nieuwenstein M.R., *et al*. (2001) Relationship between symptom dimensions and neurocognitive functioning in schizophrenia: a meta-analysis of WCST and CPT studies. Wisconsin Card Sorting Test. Continuous Performance *Test. J Psychiatr Res.* **35:** 119–125

Nilsson M., *et al*. (2006) Differential effects of classical neuroleptics and a newer generation antipsychotics on the MK-801 induced behavioral primitivization in mouse. *Prog Neuropsychopharmacol Biol Psychiatry*. **30:** 521–530

Nishino S. (2007) The hypothalamic peptidergic system, hypocretin/orexin and vigilance control. *Neuropeptides*. **41:** 117–133

Nishio H., *et al*. (2006) Effects of perinatal stress on the anxiety-related behavior of the adolescence mouse. *Int. J. Dev. Neurosci.* **24:** 263–268

Niwa J., *et al*. (2001) A novel centrosomal ring-finger protein, dorfin, mediates ubiquitin ligase activity. *Biochemical and Biophysical Research Communications.* **281**: 706–713

Nixon R.A., *et al*. (2008) Neurodegenerative lysosomal disorders: a continuum from development to late age. *Autophagy*. **4:** 590–599

Nobili L., *et al*. Local aspects of sleep: observations from intracerebral recordings in humans. *Prog Brain Res*. **199**: 219–232

Noble F., *et al*. (1999) International Union of Pharmacology. XXI. Structure, distribution, and functions of cholecystokinin receptors. *Pharmacol. Rev.* **51:** 745–781

Nock M.K., *et al*. (2008) Suicide and suicidal behavior. *Epidemiol Rev.* **30:** 133–154

Nonaka T., *et al*. (2010) Seeded aggregation and toxicity of α-synuclein and tau: cellular models of neurodegenerative diseases. *J.Biol.Chem.* **285:** 34885–98

Nygard M., *et al*. (2005) Age-related changes in electrophysiological properties of the mouse suprachiasmatic nucleus in vitro. *Brain Res. Bull.* **65:** 149–154

O'Brien E.M., Mindell J.A. (2005) Sleep and risk-taking behavior in adolescents. *Behav Sleep Med.* **3:** 113–133

Obi K., *et al*. (2008) Relationship of phosphorylated *α*-synuclein and tau accumulation to A*β* deposition in the cerebral cortex of dementia with Lewy bodies. *Experimental Neurology*. **210:** 409–420

O'Farrell P. H. (1975) High resolution two-dimensional electrophoresis of proteins. *J Biol Chem.* **250**: 4007–4021

Ogden C.A., *et al*. (2004) Candidate genes, pathways and mechanisms for bipolar (manic-depressive) and related disorders: an expanded convergent functional genomics approach. *Mol Psychiatr.* **9:** 1007–1029

Oginska H., Pokorski J. (2006) Fatigue and mood correlates of sleep length in three age-social groups: school children, students, and employees. *Chronobiol Int.* **23:** 1317–1328

O'Hara B.F., *et al*. (1995) GABAA, GABAC, and NMDA receptor subunit expression in the suprachiasmatic nucleus and other brain regions. *Brain Res Mol Brain Res*. **28:** 239–250

Ohta H., *et al*. (2005) Constant light desynchronizes mammalian clock neurons. *Nat Neurosci*. **8:** 267–269

Ohta T., Endo S. (1985) Chronobiological comparison of sleep-wake rhythm between chronic schizophrenia and normal control. *Folia Psychiatr Neurol Jpn.* **39:** 489–497

Oishi K., *et al*. (2006) Disrupted fat absorption attenuates obesity induced by a high-fat diet in Clock mutant mice. *FEBS Lett*. **580:** 127–130

Okamura H., *et al*. (1989) Demonstration of GABAergic cell bodies in the suprachiasmatic nucleus: in situ hybridization of glutamic acid decarboxylase (GAD) mRNA and immunocytochemistry of GAD and GABA. *Neurosci. Lett*. **102**: 131–136

Okawa M., Uchiyama M. (2007) Circadian rhythm sleep disorders: Characteristics and entrainment pathology in delayed sleep phase and non-24-h sleepwake syndrome. *Sleep Med Rev*. **11:** 485–496

Oken B.S., *et al*. (2006) Vigilance, alertness, or sustained attention: physiological basis and measurement. *Clin Neurophysiol.* **117:** 1885–1901

Okuda H., *et al*. (2010) Dysbindin Regulates the Transcriptional Level of Myristoylated Alanine-Rich Protein Kinase C Substrate via the Interaction with NF-YB in Mice Brain. *PLoS One.* **5:** e8773

Olanow C.W., Tatton W.G. (1999) Etiology and pathogenesis of Parkinson's disease. *Annu Rev Neurosci.* **22:** 123–144

Oliver P.L. (2011) Challenges of analysing gene-environment interactions in mouse models of Schizophrenia. *The Scientific World J.* **11:** 1411–1420

Oliver P.L., Davies K.E. (2009) Interaction between environmental and genetic factors modulates schizophrenic endophenotypes in the Snap-25 mouse mutant blind-drunk. *Human Molecular Genetics.* **18:** 4576–4589

Oliver P.L., *et al*. (2012) Disrupted Circadian Rhythms in a Mouse Model of Schizophrenia. *Current Biology.* **22**: 1–6

Olney J.W., *et al*. (1999)NMDA receptor hypofunction model of schizophrenia. *J. Psychiatr. Res.* **33:** 523–533

O'Neil J.S., Reddy A. B. (2011) Circadian clocks in human red blood cells. *Nature*. **469**: 498–503

Ong Q.R., *et al*. (2012) Impaired insuling signalling in an animal model of Niemann-Pick Type C disease. *Biochem. Biophys. Res. Commun*. **424**: 482–487

Ong S.E., *et al*. (2002) Mol. Cell. *Proteomics.* **1:** 376–384

Ono T., *et al*. (2008) Urotensin II evokes neurotransmitter release from rat cerebrocortical slices. *Neurosci Lett*. **440:** 275–279

Ono Y., *et al*. (1988) The structure, expression, and properties of additional members of the protein kinase C family. *J. Biol. Chem.* **263:** 6927–6932

Ono Y., *et al*. (1989) Protein kinase C zeta subspecies from rat brain: its structure, expression, and properties. *Proc. Natl. Acad. Sci. USA.* **86:** 3099–3103

Oster H., *et al*. (2003) cGMP-dependent protein kinase II modulates mPer1 and mPer2 gene induction and influences phase shifts of the circadian clock. *Curr Biol.* **13:** 725–733

O'Tuathaigh C.M., *et al*. (2007) Susceptibility genes for schizophrenia: characterisation of mutant mouse models at the level of phenotypic behavior. *Neurosci Biobehav Rev.* **31:** 60–78

Otway D.T., *et al*. (2011) Rhythmic diurnal gene expression in human adipose tissue from individuals who are lean, overweight, and type 2 diabetic. *Diabetes.* **60:** 1577–1581

Owen E.H., *et al*. (1997) Assessment of learning by the Morris water task and fear conditioning in inbred mouse strains and F1 hybrids: implications of genetic background for single gene mutations and quantitative trait loci analyses. *Neuroscience.* **80:** 1087–1099

Owen M.J., *et al*. (2005) Schizphrenia: a genetic disorder of the synpase. *British Med J.* **330**: 158–159

Pace-Schott E.F., Hobson J.A. (2002) The neurobiology of sleep: genetics, cellular physiology and subcortical networks. *Nat. Rev. Neurosci.* **3:** 591–605

Pakkenberg B., *et al*. (2009) Schizophrenia; from structure to function with special focus on the mediodorsal thalamic prefrontal loop. *Acta. Psychiatr. Scand.* **120:** 345–354

Palacino J.J., *et al*. (2004) Mitochondrial dysfunction and oxidative damage in parkin-deficient mice. *J. Biol.Chem.* **279:** 18614–18622

Pallier P.N., *et al*. (2007) Pharmacological imposition of sleep slows cognitive decline and reverses dysregulation of circadian gene expression in a transgenic mouse model of Huntington's disease. *J Neurosci.* **27:** 7869–7878

Panchaud A. (2008) Experimental and computational approaches to quantitative proteomics: Status quo and outlook. *J. Proteomics* **71:** 19–33

Panda S., *et al*. (2002) Coordinated transcription of key pathways in the mouse by the circadian clock. *Cell*. **109:** 307–320

Panda S., Hogenesch J.B. (2004) It's all in the timing: many clocks, many outputs. *J Biol Rhythms.* **19:** 374–387

Pandey G.N., *et al*. (2003) Altered expression and phosphorylation of myristoylated alanine-rich C kinase substrate (MARCKS) in postmortem brain of suicide victims with or without depression. *J Psychiatr Res.* **37:** 421–432

Pandi-Perumal S. R., Trakht I., (2008) The roles of melatonin and light in the pathophysiology and treatment of circadian rhythm sleep disorders. *Nat. Clin. Pract. Neurol*. **4**: 436–447

Pando M.P., *et al*. (2002) Phenotypic rescue of a peripheral clock genetic defect via SCN hierarchical dominance. *Cell*. **110**: 107–117

Parente M.K., *et al*. (2012) Dysregulation of gene expression in a Lysosomal storage disease varies between brain regions implicating unexpected mechanisms of neuropathology. *PLOS ONE.* **7:** e32419

Park A., Stacy M. (2009) Non-motor symptoms in Parkinson's disease. *Journal of Neurology*. **256:** 293–298

Pasinetti G.M., *et al*. (2006) Identification of potential CSF biomarkers in ALS. *Neurology*. **66:** 1218–1222

Patel S.D., *et al*. (2010) Coming to grips with complex disorders: genetic risk prediction in bipolar disorder using panels of genes identified through convergent functional genomics. *Am J Med Genet B Neuropsychiatr Genet.* **153:** 850–877

Patel V.J., *et al*. (2009) A comparison of labeling and label-free mass spectrometry-based proteomics approaches. *J. Proteome Res.* **8:** 3752–3759

Patel V.R., *et al*. (2012) CircadiOmics: integrating circadian genomics, transcriptomics, proteomics and metabolomics. *Nat. Methods.* **9:** 772–773

Paterlini M., *et al*. (2005) Transcriptional and behavioral interaction between 22q11.2 orthologs modulates schizophrenia-related phenotypes in mice. *Nat Neurosci.* **8:** 1586–1594

Patterson M.C., *et al*. (1993) The effect of cholesterol-lowering agents on hepatic and plasma cholesterol in Niemann-Pick disease type C. *Neurology.* **43:** 61–64

Patterson M.C., Platt F. (2004) Therapy of Niemann-Pick disease, type C. *Biochim. Biophys. Acta.* **1685:** 77–82

Patterson M.C., *et al*, (2001) Niemann-Pick disease type C. A lipid trafficking disorder. In The metabolic and molecular basis of inherited disease. **II:** 3611–3633

Patton W.F. (2002) Detection technologies in proteome analysis. *Journal of Chromatography BAnalytical Technologies in the Biomedical and Life Sci.* **771:** 3–31

Peirson S.N., *et al*. (2007) Microarray analysis and functional genomics identify novel components of melanopsin signalling. *Curr Biol*. **17**: 1363–1372

Peng M.T., Kang M. (1984) Circadian Rhythms and Patterns of Running- Wheel Activity, Feeding and Drinking Behaviors of Old Male Rats. *Physiology & Behavior.* **33:** 615–620

Peng Z.W., *et al*. (2007) Cryptochrome1 maybe a candidate gene of schizophrenia. *Med Hypotheses*. **69:** 849–851

Pennanen L., *et al*. (2004). Accelerated extinction of conditioned taste aversion in P301L tau transgenic mice. *Neurobiol. Dis.* **15:** 500–509

Pennanen L., *et al*. (2006) Impaired spatial reference memory and increased exploratory behavior in P301L tau transgenic mice*. Genes Brain Behav.* **5:** 369–379

Pennington K., *et al*. (2007) Prominent synaptic and metabolic abnormalities revealed by proteomic analysis of the dorsolateral prefrontal cortex in schizophrenia and bipolar disorder. *Mol Psychiatry*. **13**: 1102–1117

Perez F.A., Palmiter R.D. (2005) Parkin-deficient mice are not a robust model of parkinsonism. *Proc. Natl. Acad. Sci. USA.* **102:** 2174 –2179

Peruzzi P. P., *et al*. (2009) Physiological transgene regulation and functional complementation of a nuerological disease gene deficiency in neurons. *Mol. Ther*. **17**: 1517–1526

Peyron C., *et al*. (2000) A mutation in a case of early onset narcolepsy and a generalized absence of hypocretin peptides in human narcoleptic brains. *Nature Med*. **6**: 991–997

Phaneuf D., *et al*. (1996) Dramatically different phenotypes in mouse models of human Tay-Sachs and Sandhoff diseases. *Hum Mol Genet.* **5:** 1–14

Philip P., Akerstedt T. (2006) Transport and industrial safety, how are they affected by sleepiness and sleep restriction? *Sleep Med Rev.* **10:** 347–356

Pierce A., *et al*. (2008) Eight-Channel Itraq Enables Comparison of the Activity of Six Leukemogenic Tyrosine Kinases. Mol *Cell Proteomics.* **7:** 853–863

Pierpaoli W. (2013) Aging-reversing properties of thyrotropin-releasing hormone. *Curr Aging Sci.* **6:** 92–98

Pilcher J.J., Huffcutt A.I. (1996) Effects of sleep deprivation on performance: a meta-analysis. *Sleep.* **19:** 318–326

Pilcher J.J., *et al*. (2000) Differential effects of permanent and rotating shifts on self-report sleep length: a metaanalytic review. *Sleep*. **23:** 155–163

Pilny R., *et al*. (2006) Surface-enhanced laser desorption ionization/time-of-flight mass spectrometry reveals significant artifacts in serum obtained from clot activatorcontaining collection devices. *Clinical Chemistry.* **52:** 2115–2116

Pinner A.L., *et al*. (2014) Alterations of the myristoylated, alanine-rich C kinase substrate (MARCKS) in prefrontal cortex in schizophrenia. *Schizophrenia Res.* **154**: 36–41

Pittenger C., Duman R.S. (2008) Stress, depression, and neuroplasticity: a convergence of mechanisms. *Neuropsychopharmacology*. **33:** 88–109

Pittman A.M., *et al*. (2005) Linkage disequilibrium fine mapping and haplotype association analysis of the tau gene in progressive supranuclear palsy and corticobasal degeneration. *J. Med. Genet.* **42:** 837–846

Platt F.M., *et al*. (2012) The cell biology of disease: lysosomal storage disorders: the cellular impact of lysosomal dysfunction. *J. Cell Biol.* **199:** 723–34

Platt F.M., Walkley S.U. (2004) Lysosomal defects and storage. *In Lysosomal Disorders of the Brain*. 32–49

Pletnikov M.V., *et al*. (2008) Inducible expression of mutant human Dros. Inf. Serv.C1 in mice is associated with brain and behavioral abnormalities reminiscent of schizophrenia. *Mol Psychiatry.* **13:** 173–186

Polymeropoulos M.H., *et al*. (1997) Mutation in the alpha-synuclein gene identified in families with Parkinson's disease. *Science*. **276:** 2045–2047

Ponsen M.M., *et al*. (2004) Idiopathic hyposmia as a preclinical sign of Parkinson's disease. *Ann Neurol.* **56:** 173–181

Portas C.M., *et al*. (1998) A specific role for the thalamus in mediating the interaction of attention and arousal in humans. *J Neurosci*. **18:** 8979–8989

Porton B., *et al*. (2004) A rare polymorphism affects a mitogen-activated protein kinase site in synapsin III: possible relationship to schizophrenia. *Biol. Psychiatry.* **55**: 118–125

Poulin J., *et al*. (2003) Sleep architecture and its clinical correlates in first episode and neuroleptic-naive patients with schizophrenia. *Schizophr Res.* **62:** 147–153

Pozzi D., *et al*. (2008) Activity-dependent phosphorylation of Ser187 is required for SNAP-25-negative modulation of neuronal voltage-gated calcium channels. *Proc. Natl. Acad. Sci. USA.* **105:** 323–328

Prabakaran S., *et al*. (2004) Mitochondrial dysfnction in schizophrenia: Evidence for compromised brain metabolism and oxidative stress. *Mol Psychiatry*. **9**: 684–697

Preitner N., *et al*. (2002) The orphan nuclear receptor REV-ERBa controls circadian transcription within the positive limb of the mammalian circadian oscillator. *Cell*. **110**: 251–260

Pressey S.N., *et al*. (2012) Early glial activation, synaptic changes and axonal pathology in the thalamocortical system of Niemann-Pick type C1 mice. *Neurobiol. Dis.* **45:** 1086– 1100

Price J.C., *et al*. (2010) Analysis of proteome dynamics in the mouse brain. *Proc. Natl. Acad. Sci. USA.* **107:** 14508–14513

Pritchard J.K. (2001) Are rare variants responsible for susceptibility to complex diseases? *Am. J. Hum. Genet.* **69:** 124–137

Pritchett D., *et al*. (2012) Evaluating the link between schizophrenia and sleep and circadian rhythm disruption. *J. Neural. Transm.* **119:** 1061–1075

Qin Z., *et al*. (2009) Health related quality of life in early Parkinson's disease: impact of motor and non-motor symptoms, results from Chinese levodopa exposed cohort. Parkinsonism *Relat Disord.* **15:** 767–771

Rademakers R., *et al*. (2005) High-density SNP haplotyping suggests altered regulation of tau gene expression in progressive supranuclear palsy. *Hum. Mol. Genet.* **14**: 3281–3292

Rahman S., *et al*. (2008) Quality of life in Parkinson's disease: the relative importance of the symptoms. *Mov Disord*. **23:** 1428–1434

Ralph M.R., *et al*. (1990) Transplanted suprachiasmatic nucleus determines circadian period. *Science*. **247**: 975–978

Ramsden M., *et al*. (2005) Age-dependent neurofibrillary tangle formation, neuron loss, and memory impairment in a mouse model of human tauopathy (P301L). *J. Neurosci.* **25:** 10637–10647

Ran Y., Fanucci G.E. (2009) Ligand extraction properties of the GM2 activator protein and its interaction with lipid vesicles. *Biophys J.* **97:** 257–266

Randazzo A.C., *et al*. (1998) Cognitive function following acute sleep restriction in children ages 10–14. *Sleep*. **21:** 861–868

Rao M.L., *et al*. (1994) Circadian rhythm of tryptophan, serotonin, melatonin, and pituitary hormones in schizophrenia. *Biological Psychiatry*. **35:** 151–163

Rao M.L., *et al*. (1995) Circadian rhythm of vital signs, norepinephrine, epinephrine, thyroid hormones, and cortisol in schizophrenia. *Psychiatry Research*. **57:** 21–39

Reddy A.B., *et al*. (2006) Circadian orchestration of the hepatic proteome. *Curr Biol.* **16:** 1107–1115

Rehn A.E., Rees S.M. (2005) Investigating the neurodevelopmental hypothesis of schizophrenia. *Clin. Exp. Pharmacol. Physiol.* **32:** 687–696

Reischl S., *et al*. (2007) Beta-TrCP1-mediated degradation of PERIOD2 is essential for circadian dynamics. *J. Biol. Rhythms*. **22**: 375–386

Renner T.J., *et al*. (2008) Allelic variants of SNAP25 in a family-based sample of ADHD. *J. Neural Transm*. **115:** 317–321

Reppert S.M., Weaver D.R. (2002) Coordination of circadian timing in mammals. *Nature.* **418:** 935–941

Ribeiro C.S., *et al*. (2002) Synphilin-1 is developmentally localized to synaptic terminals, and its association with synaptic vesicles is modulated by alphasynuclein. *Journal of Biological Chemistry.* **277**: 23927–23933

Richardson H.N., *et al*. (2006) Exposure to repetitive versus varied stress during prenatal development generates two distinct anxiogenic and neuroendocrine profiles in adulthood. *Endocrinology.* **147:** 2506–2517

Richfield E.K., *et al*. (2002) Behavioral and neurochemical effects of wild-type and mutated human alpha-synuclein in transgenic mice. *Exp. Neurol.* **175:** 35–48

Riemann D., Voderholzer U. (2003) Primary insomnia: a risk factor to develop depression? *J Affect Disord.* **76:** 255–259

Rijsdijk F.V., *et al*. (2005) Brain MRI abnormalities in schizophrenia: same genes or same environment? *Psychol. Med.* **35:** 1399–1409

Robertson I.H.G. (2004) Vigilant Attention In: The Cognitive Neurosciences vol. III. *Cambridge, MA: The MIT Press*

Robinson B.G. *et al*. (1988) Vasopressin mRNA in the suprachiasmatic nuclei: daily regulation of polyadenylate tail length. *Science*. **241**: 342–344

Robles M.S., *et al*. (2010) Identification of RACK1 and protein kinase Calpha as integral components of the mammalian circadian clock. *Science.* **327:** 463–466

Robles M.S., *et al*. (2014) In-vivo quantitative proteomics reveals a key contribution of post-transcriptional mechanisms to the circadian regulation of liver metabolism. *PLoS Geenet*. **10**: e1004047

Robles M.S., Mann M. (2013) Proteomic approaches in circadian biology. *Handb.Exp.Pharmacol.* **217:** 389–407

Rockstroh B.S., *et al*. (2007) Abnormal oscillatory brain dynamics in schizophrenia: a sign of deviant communication in neural network? *BMC Psychiatry.* **7:** 44

Rodriguez-Lafrasse C., *et al*. (1994) Free sphingoid bases in tissues from patients with type C Niemann-Pick disease and other lysosomal storage disorders. *Biochim Biophys Acta.* **1226:** 138–144

Rodriguez-Oroz M.C., *et al*. (2009) Initial clinical manifestations of Parkinson's disease: features and pathophysiological mechanisms. *The Lancet Neurology.* **8:** 1128–1139

Rogers D.C., *et al*. (1999) Use of SHIRPA and discriminant analysis to characterise marked differences in the behavioral phenotype of six inbred mouse strains. *Behav Brain Res.* **105:** 207–217

Rothman S., Mattson M.P. (2012) Sleep disturbances in Alzheirmer's and Parkinson's diseases. *Neurmolecular Med*. **14**: 194–204

Rorick-Kehn L.M., *et al*. (2007) In vivo pharmacological characterization of the structurally novel, potent, selective mGlu2/3 receptor agonist LY404039 in animal models of psychiatric disorders. *Psychopharmacology*. **193:** 121–136

Ross C.J., *et al*. (2000) Somatic gene therapy for a neurodegenerative disease using microencapsulated recombinant cells. *Exp Neurol.* **166:** 276–286

Roth R.M., *et al*. (2008) Apathy and the processing of novelty in schizophrenia. *Schizophr Res*. **98:** 232–238

Roybal K., *et al*. (2007) Mania-like behavior induced by disruption of CLOCK. *Proc. Natl. Acad. Sci. USA*. **104:** 6406–6411

Rudic R.D., *et al*. (2004) BMAL1 and CLOCK, two essential components of the circadian clock, are involved in glucose homeostasis. *PLoS Biol.* **2:** e377

Rüetschi U., *et al*. (2005) Identification of CSF biomarkers for frontotemporal dementia using SELDI-TOF. *Exp Neurol.* **196:** 273–281

Ruhrmann S., *et al*. (2010) Prediction of psychosis in adolescents and young adults at high risk: results from the prospective European prediction of psychosis study. *Arch Gen Psychiatry.* **67:** 241–251

Rusak B., *et al*. (1990) Light pulses that shift rhythms induce gene expression in the suprachiasmatic nucleus. *Science*. **248**: 1237–1240

Rutten S., *et al*. (2012) Bright Light Therapy in Parkinson's Disease: An Overview of the Background and Evidence. *Parkinsons Dis.* **2012:** 767105

Sachs B. (1887) On arrested cerebral development with special reference to cortical pathology. J *Nerv Ment Dis.* **14:** 541–554

Sachs G.S. (2000) Comorbidity of attention deficit hyperactivity disorder with early-and late-onset bipolar disorder. *The American journal of psychiatry.* **157:** 466

Sadacca L.A., *et al*. (2011) An intrinsic circadian clock of the pancreas is required for normal insulin release and glucose homeostasis in mice. *Diabetologia*. **54:** 120–124

Saffen D.W., *et al*. (1988) Convulsant-induced increase in transcription factor messenger RNAs in rat brain. *Proc. Natl. Acad. Sci. USA*. **85**: 7795–7799

Saftig P., Klumperman J. (2009) Lysosome biogenesis and lysosomal membrane proteins: trafficking meets function. *Nat. Rev. Mol. Cell Biol.* **10:** 623–635

Sahar S., Sassone-Corsi P. (2012) Regulation of metabolism: the circadian clock dictates the time. *Trends Endocrinol Metab*. **23:** 1–8

Saiki S., *et al*. (2012) Molecular pathogenesis of Parkinson's disease: update. *J.Neurol.Neurosurg.Psychiatry*. **83:** 460–466

Sakai T., *et al*. (2004) A clock gene, period, plays a key role in long-term memory formation in Drosophila. *Proc. Natl. Acad. Sci.USA.* **101:** 16058–16063

Sakamoto K., *et al*. (2005) Dopamine regulates melanopsin mRNA expression in intrinsically photosensitive retinal ganglion cells. *European Journal of Neuroscience.* **22:** 3129–3136

Sakurai T., *et al*. (2005) Input of orexin/hypocretin neurons revealed by a genetically encoded tracer in mice. *Neuron*. **46**: 297–308

Salgado-Delgado R., *et al*. (2008) Internal desynchronization in a model of night-work by forced activity in rats. *Neuroscience.* **154:** 922–931

Salgado-Delgado R., *et al*. (2010) Food intake during the normal activity phase prevents obesity and circadian desynchrony in a rat model of night work. *Endocrinology.* **151:** 1019–1029

Samson W.K., *et al*. (1979) Radioimmunologic localization of vasoactive intestinal polypeptide in hypothalamic and extrahypothalamic sites in the rat brain. *Neurosci. Lett*. **12**: 265–269

Sandhoff K. (2001) The G_{M2} gangliosidoses and the elucidation of the β-hexosaminidase system; in Desnick R.J., Kaback M.M. (eds): Tay-Sachs Disease. *Advances in Genetics.* **44:** 67–91

Sandhoff K., *et al*. (1968) Deficient hexosaminidase activity in an exceptional case of Tay-Sachs disease with additional storage of kidney globoside in visceral organs. *Life Sci.* **7:** 283–288

Sango K., *et al*. (2008) Involvement of Retinal Neuron and Pigment Epithelial Cells in a Murine Model of Sandhoff Disease. *Ophthalmic Res.* **40:** 241–248

Sango K., *et al*. (2005) Impaired neurite outgrowth in the retina of a murine model of Sandhoff diease. *Invest Ophthalmol Vis Sci*. **46**: 3420–3425

Sango K., *et al*. (1995) Mouse models of Tay-Sachs and Sandhoff diseases differ in neurologic phenotype and ganglioside metabolism. *Nat Genet 1995*. **11:** 170–176

Sans-Fuentes M.A., *et al*. (2010) Light responses of the circadian system in leptin deficient mice. *Physiol. Behav.* **99:** 487–494

SantaCruz K., *et al*. (2005) Tau suppression in a neurodegenerative mouse model improves memory function. *Science.* **309:** 476– 481

Saper C.B. (2006) Staying awake for dinner: hypothalamic integration of sleep, feeding, and circadian rhythms. *Prog Brain Res.* **153:** 243–252

Saper C.B. (2013) The central circadian timing system. *Curr Opin Neurobiol*. **23:** 747–751

Saper C.B., *et al*. (2002) The need to feed: homeostatic and hedonic control of eating. *Neuron*. **36:** 199–211

Saper C.B., *et al*. (2001) The sleep switch: hypothalamic control of sleep and wakefulness. *Trends Neurosci*. **24**: 726–731

Saper C.B., *et al*. (2005) Hypothalamic regulation of sleep and circadian rhythms. *Nature*. **437:** 1257–1263

Sargeant T.J., *et al*. (2012) Characterization of inducible models of Tay-Sachs and related disease. *PLOS Genetics.* **8:** e1002943

Sato T.K., *et al*. (2006) Feedback repression is required for mammalian circadian clock function. *Nat. Genet*. **38**: 312–359

Savas J.N., *et al*. (2012) Extremely long-lived nuclear pore proteins in the rat brain. *Science.* **335:** 942

Saviouk V., *et al*. (2007) Association of synapsin 2 with schizophrenia in families of Northern European ancestory. *Schizophrenia Res.* **96**: 100–111

Scammell T.E., *et al*. (2001) An adenosine A2A agonist increases sleep and induces FOS in ventrolateral preoptic preoptic neurons. *Neuroscience*. **107**: 653–663

Scaravilli T., *et al*. (2003) Health-related quality of life and sleep disorders in Parkinson's disease. *Neurol Sci.* **24:** 209–210

Schalkwyk L.C., *et al*. (2007) Interpretation of knockout experiments: the congenic footprint. *Genes, Brain and Behavior.* **6:** 299–303

Scheer F.A., *et al*. (2005) Envionrmental light and supracchiasmatic nucleus interact in the regulation of body temperature. *Neuroscience*. **132**: 465–477

Schengrund C.L. (1990) The role(s) of gangliosides in neural differentiation and repair, a perspective. *Brain Res. Bull.* **24:** 131–141

Schenck C. H., *et al*. (2013) Delayed emergence of a parkinsonian disorder or dementia in 81% of older men initially diagnosed with idiopathic rapid eye movement sleep behaviour disorder: a 16-year update on a previously reported series. *Sleep* Med. **14**: 744–748

Schiavo G., *et al*. (2000) Neurotoxins affecting neuroexocytosis. *Physiol. Rev.* **80:** 717–766

Schlösser R.G., *et al*. (2007) White matter abnormalities and brain activation in schizophrenia: a combined DTI and fMRI study. *Schizophr. Res.* **89:** 1–11

Schneck L. (1964) The clinical aspects of Tay-Sachs disease. *Tay-Sachs' Disease*. 16–35

Schoch S., *et al.* (2001) SNARE function analysed in synaptobrevin/VAMP knockout mice. *Science.* **294**: 1117–1122

Schröder B.A., *et al*. (2010) The proteome of lysosomes. *Proteomics*. **10:** 4053–4076

Schrott-Fischer A., *et al*. (2009) Chromogranin peptides in amyotrophic lateral sclerosis. *Regul Pept* **152:** 13–21

Schulze H., Sandhoff K. (2011) Lysosomal Lipid Storage Diseases. *Cold Spring Harb Perspect Biol.* **3:** a004804

Schurov I.L., *et al*. (1999) Glutamatergic induction of CREB phosphorylation and Fos expression in primary cultures of the suprachiasmatic hypothalamus in vitro is mediated by co-ordinate activity of NMDA and non-NMDA receptors. *J. Neuroendocrinol*. **11:** 43–51

Schwab S.G., *et al*. (2003) Support for association of schizophrenia with genetic variation in the 6p22.3 gene, disbindin, in sub-pair families with linkage and in an additional sample of triad families. *Am. J. Hum. Genet.* **72**: 185–190

Schwartz W.J., Zimmerman P. (1990) Circadian timekeeping in BALB/c and C57BL/6 inbred mouse strains. *J Neurosci*. **10**: 3685–3694

Scolnick E.M., *et al*. (2006) Schizophrenia: do the genetics and neurobiology of neuregulin provide a pathogenesis model? *Harv Rev Psychiatry.* **14:** 64–77

Scott J.P., *et al*. (2006) Effects of sleep deprivation and exercise on cognitive, motor performance and mood. *Physiol Behav.* **87:** 396–408

Scott L.D., *et al*. (2007) The relationship between nurse work schedules, sleep duration, and drowsy driving. *Sleep*. **30:** 1801–1807

Sebat J., *et al*. (2009) Rare structural variants in schizophrenia: one disorder, multiple mutations; one mutation, multiple disorders. *Trends Genet.* **25:** 528–535

Seidel K., *et al*. (2010) First appraisal of brain pathology owing to A30P mutant alpha-synuclein. *Ann. Neurol.* **67:** 684–689

Sellix M.T., *et al*. (2012) Aging differentially affects tyhe re-entrainment response of central and peripheral circadian oscillators. *J Neurosci.* **32:** 16193–16202

Selvi Y., Gulec M., Agargun M.Y., Besiroglu L. (2007) Mood changes after sleep deprivation in morningness–eveningness chronotypes in healthy individuals. *J Sleep Res.* **16:** 241–244

Settembre C., *et al*. (2008) A block of autophagy in lysosomal storage disorders. *Hum. Mol. Genet.* **17:** 119–129

Shapiro B.E., *et al*. (2008) Late-onset Tay-Sachs disease: the spectrum of peripheral neuropathy in 30 affected patients. *Muscle Nerve*. **38:** 1012–1015

Sharif A., *et al*. (2009) Differential erbB signaling in astrocytes from the cerebral cortex and the hypothalamus of the human brain. *Glia.* **57:** 362–379

Sharma V., Mazmanian D. (2003) Sleep loss and postpartum psychosis. *Bipolar Disord.* **5:** 98–105

Shearman L.P., *et al*. (2000) Interacting molecular loops in the mammalian circadian clock. *Science*. **288**: 1013–1019

Sherin J.E., *et al*. (1996) Activation of ventrolateral preoptic neurons during sleep. *Science*. **271**: 216–219

Shi J., *Gershon E. S., Liu C*. (2008) Genetic associations with schizophrenia: meta-analyses of 12 candidate genes. *Schizophr. Res*. **104**: 96–107

Shifman S., *et al*. (2004) COMT: a common susceptibility gene in bipolar disorder and schizophrenia. *Am. J. Med. Genet. B. (Neuropsychiatr Genet).* **128**: 61–64

Shigeyoshi Y., *et al*. (1997) Light-induced resetting of a mammalian circadian clock is associated with rapid induction of the mPer1 transcript. *Cell.* **91:** 1043–1053

Shim H.S., *et al*. (2007) Rapid activation of CLOCK by Ca2+-dependent protein kinase C mediates resetting of the mammalian circadian clock. *EMBO Rep*. **8:** 366–371

Shimazoe T., *et al*. (2008) Cholecystokinin-A receptors regulate photic input pathways to the circadian clock. *FASEB J.* **22:** 1479–1490

Shimura H., *et al*. (2000) Familial Parkinson disease gene product, parkin, isaubiquitin-protein ligase. *Nat. Genet.* **25:** 302–305

Shirakawa T., *et al*. (2004) Neuronal expression of catechol O-methyltransferase mRNA in neonatal rat suprachiasmatic nucleus. *Neuroreport*. **15:** 1239–1243

Shiromani P.J., *et al*. (2004) Sleep rhythmicity and homeostasis in mice with targeted disruption of mPeriod genes. *Am J Physiol Regul Integr Comp Physiol.* **287:** 47–57

Siepka S.M., *et al*. (2007) Genetics and neurobiology of circadian clocks in mammalians. *Cold Spring Harbor Symp. Quant. Biol*. **72**:251–259

Silva J. C., *et al*. (2006) Simultaneous Qualitative and Quantitative Analysis of the Escherichia Coli Proteome: A Sweet Tale. Mol Cell Proteomics. **5:** 589–607

Simons K., Gruenberg J. (2000) Jamming the endosomal system: lipid rafts and lysosomal storage diseases. *Trends Cell Biol.* **10:** 459–462

Simón-Sánchez J., *et al*. (2009) Genome-wide association study reveals genetic risk underlying Parkinson's disease. *Nat. Genet.* **41:** 1308–1312

Simonsen A.H., *et al*. (2007) A novel panel of cerebrospinal fluid biomarkers for the differential diagnosis of Alzheimer's disease versus normal aging and frontotemporal dementia. *Dement Geriatr Cogn Disord* **24:** 434–440

Singletary K.G., Naidoo N. (2011) Disease and degeneration of aging neural systems that integrate sleep drive and circadian oscillations. *Frontiers in Neurology*. **2**: 1–8

Sládek M., *et al*. (2007)Postnatal ontogenesis of the circadian clock within the rat liver. *Am J Physiol Regul Integr Comp Physiol.* **292:** 1224–1229

Sleat D.E., *et al*. (2004) Genetic evidence for nonredundant functional cooperativity between NPC1 and NPC2 in lipid transport**.** *Proc. Natl. Acad. Sci. USA.* **101:** 5886–5891

Sleiman P., Wang D., *et al*. (2013) GWAS meta analysis identifies TSNARE1 as a novel schizophrenia/bipolar suscpitibility locus. *Sci. Rep*. **3**: 3075

Smejkal G.B. (2004) The Coomassie chronicles: past, present and future perspectives in polyacrylamide gel staining. *Expert Review of Proteomics.* **1:** 381–387

Smith N.J., *et al*. (2012) GM2 gangliosidosis in a UK study of children with progressive neurodegeneration: 73 cases reviewed. *Dev Med Child Neurol.* **54:** 176–182

Snodgrass-Belt P., *et al*. (2005) Central administration of transforming growth factor-alpha and neuregulin-1 suppress active behaviors and cause weight loss in hamsters. *Brain Res*. **1038:** 171–182

Snyder D.A., *et al*. (2006) SNARE Complex Regulation by Phosphorylation. *Cell Biochemistry and Biophysics.* **45:** 111–123

Solano R.M., *et al*. (2008) Glial dysfunction in parkin null mice: effects of aging. *J. Neurosci.* **3:** 598–611

Sollner T., *et al*. (1993) SNAP receptors implicated in vesicle targeting and fusion. *Nature.* **362**: 318–214

Son G.H., *et al*. (2006) Maternal stress produces learning deficits associated with impairment of NMDA receptor-mediated synaptic plasticity. *J. Neurosci.* **26:** 3309–3318

Sorge S., *et al*. (2004) Clozapine alters sleep-wake behavior in rats. *Neuropsychopharmacology*. **29:** 1462–1469

Spada M., *et al*. (2006) High incidence of later-onset fabry disease revealed by newborn screening. *Am. J. Hum. Genet.* **79:** 31–40

Spellmann I., *et al*. (2008) Associations of SNAP-25 polymorphisms with cognitive dysfunctions in Caucasian patients with schizophrenia during a brief trail of treatment with atypical antipsychotics. *Eur. Arch. Psychiatry Clin. Neurosci.* **258:** 335–344

Spiegel K., *et al*. (2009) Effects of poor and short sleep on glucose metabolism and obesity risk. *Nat. Rev. Endocrinol.* **5:** 253–261

Spires T.L., Orne J.D., SantaCruz K., Pitstick R., Carlson G.A., Ashe K.H., Hyman B.T. (2006) Region-specific dissociation of neuronal loss and neurofibrillary pathology in a mouse model of tauopathy. *Am. J. Pathol.* **168:** 1598–1607

Strecker R.E., *et al*. (2000) Adenosinergic modulation of basal forebrain and preoptic/anterior hypothalamic neuronal activity in the control of behavioural state. *Behav. Brain Res*. **115**: 183–204

Stadler F., *et al*. (2010) Lack of calbindin-D28K alters response of the murine circadian clock to light. *Chronobiol. Int*. **27:** 68–82

Stanford S.C. (2007) The open field test: reinventing the wheel. *J Pscyhopharm*. **21**: 134–135

Stavitsky K., *et al*. (2010) Sleep in Parkinson's disease: a comprasion of actigraphy and subjective meaures. *Parkinsonism Relat Disord*. **16**: 280–283

Stefansson H., *et al*. (2002) Neuregulin 1 and susceptibility to schizophrenia. *Am. J. Hum. Genet.* **71**: 877–892

Stephan K.E., *et al*. (2006) Synaptic plasticity and dysconnection in schizophrenia. *Biol Psychiatry.* **59:** 929–939

Stephan F.K., Zucker I. (1972) Circadian rhythms in drinking behavior and locomotor activity of rats are eliminated by hypothalamic lesions. *Proc. Natl. Acad. Sci. USA*. **69**: 1583–1586

Steriade M., *et al*. (1993) Thalamocortical oscillations in the sleeping and aroused brain. *Science*. **262:** 679–685

Sterniczuk R., *et al*. (2010) Investigating the role of substance P in photic responses of the circadian system: individual and combined actions with gastrin-releasing peptide. *Neuropharmacology*. **58**: 277–285

Stiasny-Kolster K., *et al*. (2005) Combination of 'idiopathic' REM sleep behavior disorder and olfactory dysfunction as possible indicator for alpha-synucleinopathy demonstrated by dopamine transporter FP-CIT-SPECT. *Brain*. **128:** 126–137

Stichel C.C., *et al*. (2007) Mono- and double-mutant mouse models of Parkinson's disease display severe mitochondrial damage. *Hum. Mol. Genet.* **16:** 1–17

Stokkan K.A., *et al*. (2001) Entrainment of the circadian clock in the liver by feeding. *Science.* **291:** 490–493

Storch J., Xu Z. (2009) Niemann-Pick C2 (NPC2) and intracellular cholesterol trafficking. *Biochim Biophys Acta*. **1791:** 671–678

Straub R.E., *et al*. (2002) Genetic variation in the 6p22.3 gene *DTNBP1*, the human ortholog of the mouse dysbindin gene, is associated with schizophrenia. *Am J Hum Genet.* **71:** 337–348

Su Y.A., *et al*. (2007) Risperidone attenuates MK-801-induced hyperlocomotion in mice via the blockade of serotonin 5-HT 2A/2C receptors. *Eur J Pharmacol.* **564:** 123–130

Sudhof T.C. (1995) The synaptic vesicle cycle: a cascade of protein-protein interactions. *Nature.* **375**: 645–653

Sudhof T.C. (2004) The synaptic vesicle cycle. *Annu Rev Neurosci.* **27**: 509–547

Sudhof T.C., Rizo J. (2011) Synaptic vesicle exocytosis. *Cold Spring Harb Perspect Biol*. **3**: a005637

Sujino M., *et al*. (2003) Suprachiasmatic nucleus grafts restore circadian behavioral rhythms of genetically arrhythmic mice. *Curr Biol.* **13:** 664–668

Sullivan P.F. (2007) Spurious genetic associations. *Biol Psychiatry.* **61:** 1121–1126

Suzuki K., *et al*. (2007) Neuronal and glial accumulation of alpha- and beta-synucleins in human lipidoses. *Acta Neuropathol.* **114:** 481–489

Svennerholm L. (1962) The chemical structure of normal human brain and Tay- Sachs gangliosides. *Biochem Biophys Res Commun.* **9:** 436–441

Svennerholm L. (1980) Gangliosides and synaptic transmission. *Adv. Exp. Med. Biol*. **125:** 533–544

Swick T.J. (2012) Parkinson's disease and sleep/wake disturbances. *Parkinsons Dis*. **2012**: 205471

Szabo S.T., *et al*. (2009) Glutamate receptors as targets of protein kinase C in the pathophysiology and treatment of animal models of Mania. *Neuropharmacology.* **56:** 47–55

Tabandeh H., *et al*. (1998) Disturbance of sleep in blindness. *Am J Ophthalmol*. **126**: 707-712

Tachikawa H., *et al*. (2000) Novel polymorphisms of the human cholecystokinin A receptor gene: an association analysis with schizophrenia. *Am J Med Genet*. **96:** 141–145

Tachikawa H., *et al*. (2001) Polymorphism of the 5'-upstream region of the human SNAP-25 gene: an association analysis with schizophrenia. *Neuropsychobiology.* **43:** 131–3

Tada M., *et al*. (2004) Combined treatment of quetiapine with haloperidol in animal models of antipsychotic effect and extrapyramidal side effects: comparison with risperidone and chlorpromazine. *Psychopharmacology*. **176:** 94–100

Taffe M.A., *et al*. (2002) Ketamine impairs multiple cognitive domains in rhesus monkeys. *Drug Alcohol Depend.* **68:** 175–187

Tafoya L.C., *et al*. (2006) Expression and function of SNAP-25 as a universal SNARE component in GABAergic neurons. *J Neurosci.* **26:** 7826–38

Tafoya L.C., *et al*. (2008) The role of the t-SNARE SNAP-25 in action potential-dependent calcium signaling and expression in GABAergic and glutamatergic neurons. *BMC Neurosci*. **9:** 105

Takai Y., *et al*. (1979) Calcium-dependent activation of a multifunctional protein kinase by membrane phospholipids. *J. Biol. Chem.* **254:** 3692–3695

Takao T., *et al*. (2007) CLOCK gene T3111C polymorphism is associated with Japanese schizophrenics: a preliminary study. *Eur Neuropsychopharmacol.* **17:** 273–276

Talbot K., *et al*. (2006) Dysbindin-1 is a synaptic and microtubular protein that binds brain snapin. *Hum Mol Genet.* **15**: 3041–3054

Tamaru T., *et al*. (2000) Light and glutamate-induced degradation of the circadian oscillating protein BMAL1 during the mammalian clock resetting. *J Neurosci.* **20:** 7525–7530

Tan H.Y., Ang Y.G. (2001) First-episode psychosis in the military: a comparative study of prodromal symptoms. *Aust N Z J Psychiatry.* **35:** 512–519

Tanaka J., *et al*. (1988) Cerebellar involvement in mouse sphingomyelinosis: a new model of Niemann–Pick disease, *J. Neuropathol. Exp. Neurol.* **47 :** 291– 300

Tandberg E., *et al*. (1999) Excessive daytime sleepiness and sleep benefit in Parkinson's disease: a community-based study. *Movement Disorders.* **14:** 922–927

Taniguchi T., *et al*. (2005) Transgenic mice expressing mutant (N279K) human tau show mutation dependent cognitive deficits without neurofibrillary tangle formation. *FEBS Lett.* **579:** 5704–5712

Tanis K.Q., Duman R.S. (2007) Intracellular signaling pathways pave roads to recovery for mood disorders. *Ann Med.* **39:** 531–544

Tay W. (1881) Symmetrical changes in the region of the yellow spot in each eye of an infant. *Trans Ophthalmol Soc.* **1:** 55–57

Taylor T.N., *et al*. (2011) VMAT2-Deficient mice display nigral and extranigral pathology and motor and nonmotor symptoms of Parkinson's disease. *Parkinsons Dis*. **2011**: 124165

Taylor T.N. *et al*. (2009) Nonmotor symtpoms of parkinson's disease revealed in an animal model with reduced monoamine storage capacity. *J Neurosci*. **29**: 8103–8113

Taylor T.N., *et al*. (2014) Region-specific deficits in dopamine, but not norepinephrine, signaling in a novel A30P α-synuclein BAC transgenic mouse. *Neurobiology of Disease*. **62**: 193–207

Taylor T., *et al*. (1990) The paraventricular nucleus of the hypothalamus has a major role in thyroid hormone feedback regulation of thyrotropin synthesis and secretion. *Endocrinology.* **126:** 317–324

Taylor T.N., *et al*. (2010) Behavioral phenotyping of mouse models of Parkinson's disease. *Behavioural Brain Research*. **211**: 1–10

Tazumi T., *et al*. (2005) Effects of prenatal maternal stress by repeated cold environment on behavioral and emotional development in the rat offspring. *Behav. Brain Res.* **162:** 153–160

te Vruchte D., *et al*. (2004) Accumulation of glycosphingolipids in Niemann-Pick C disease disrupts endosomal transport. *J Biol Chem.* **279:** 26167–26175

Terman A., *et al*. (2010) Mitochondrial turnover and aging of long-lived postmitotic cells: the mitochondrial-lysosomal axis theory of aging. *Antioxid. Redox Signal.* **12:** 503–535

Terwel D., *et al*. (2005) Changed conformation of mutant Tau-P301L underlies the moribund tauopathy, absent in progressive, nonlethal axonopathy of Tau-4R/2N transgenic mice. *J. Biol. Chem.* **280:** 3963–3973

Tessitore A., *et al*. (2009) Abnormal autophagy, ubiquitination, inflammation and apoptosis are dependent upon lysosomal storage and are useful biomarkers of mucopolysaccharidosis VI. *Pathogenetics*. **2:** 4

Thakur D., *et al*. (2010) Nerve conduction study in healthy inviduals: a preliminary age based study. *Kathmandu Univ Med J*. **8**: 311–316

Thompson A., *et al*. (2003) Tandem Mass Tags: A Novel Quantification Strategy for Comparative Analysis of Complex Protein Mixtures by Ms/Ms. *Anal Chem.* **75:** 1895–1904.

Thompson P.M., *et al*. (2003) SNAP-25 reduction in the hippocampus of patients with schizophrenia. *Prog. Neuropsychopharmacol. Biol. Psychiatry.* **27:** 411–417

Tian R., *et al*. (2011) Uncovering the proteome response of the master circadian clock to light using an AutoProteome system. *Mol Cell Proteomics*. **10:** 007252

Tischkau S.A., *et al*. (2000) Differential cAMP gating of glutamatergic signaling regulates long-term state changes in the suprachiasmatic circadian clock. *J Neurosci*. **20:** 7830–7837

Tischkau S.A., *et al*. (2003) Ca2+/cAMP response element-binding protein (CREB)-dependent activation of Per1 is required for light-induced signaling in the suprachiasmatic nucleus circadian clock. *J. Biol. Chem.* **278:** 718–723

Tobler I., *et al*. (1983) The effect of sleep deprivation on sleep in rats with suprachiasmatic lesions. *Neurosci Lett*. **42**: 49–54

Toh K.L., *et al*. (2001) An hPer2 phosphorylation site mutation in familial advanced sleep phase syndrome. *Science.* **291:** 1040–1043

Toirac I., *et al*. (2007) Association between CCK-AR gene and schizophrenia with auditory hallucinations. *Psychiatr Genet.* **17:** 47–53

Tomita J., *et al*. (2005) No transcription-translation feedback in circadian rhythm of KaiC phosphorylation. *Science*. **307**: 251–254

Toshinai K., *et al*. (2010) Neuroendocrine regulatory peptide-2 regulates feeding behavior via the orexin system in the hypothalamus. *Am. J. Physiol. Endocrinol. Metab*. **299:** 394–401

Tousson E., Meissl H. (2004) Suprachiasmatic nuclei grafts restore the circadian rhythm in the paraventricular nucleus of the hypothalamus. *J. Neurosci*. **24:** 2983–8

Trabzuni D., *et al*. (2012) MAPT expression and splicing is differentially regulated by brain region: relation to genotype and implication for tauopathies. *Human Molecular Genetics.* **21:** 4094–4103

Travnickova-Bendova Z., *et al*. (2002) Bimodal regulation of mPeriod promoters by CREB-dependent signaling and CLOCK/BMAL1 activity. *Proc. Natl. Acad. Sci. USA.* **99:** 7728–7733

Tretter L., *et al*. (2004) Initiation of neuronal damage by complex I deficiency and oxidative stress in Parkinson's disease. *Neurochem. Res.* **29:** 569–577

Trovò L., *et al*. (2013) Low hippocampla $PI(4.5)P_2$ contributes to reduced cognition in old mice as a result of loo of MARKS. *Nature Neuroscience.* **16:** 449–455

Tsujino N., *et al*. (2005) Cholecystokinin activates orexin/hypocretin neurons through the cholecystokinin A receptor. *J Neurosci.* **25:** 7459–7469

Turek F.W., *et al*. (2005) Obesity and metabolic syndrome in circadian Clock mutant mice. *Science*. **308:** 1043–1045

Turner P.L., Mainster M.A. (2008) Circadian photoreception: ageing and the eye's important role in systemic health. *Br J Ophthalmol.* **92:** 1439–1444

Tzamaloukas A.H., *et al*. (2008) Pathophysiology and management of fluid and electrolyte disturbances in patients on chronic dialysis with severe hyperglycemia. *Semin. Dial.* **21:** 431–439

Ueda H.R., *et al*. (2002) A transcription factor response element for gene expression during circadian night. *Nature.* **418:** 534–539

Uversky V.N. (2007) Neuropathology, biochemistry, and biophysics of *α*-synuclein aggregation. *Journal of Neurochemistry*. **103:** 17–37

Vacic V., McCarthy S., *et al*. (2011) Duplications of the neuropeptide receptor gene VIPR2 confer significant risk for schizophrenia. *Nature*. **471:** 499–503

Valentinuzzi V.S., *et al*. (1997) Effects of aging on the circadian rhythm of wheel-running activity in C57BL/6 mice. *Am J Physiol.* **273:** R1957–R1964

Van der Maagdenberg A.M., *et al*. (2004) A cacnala knockin migraine mouse model with increased susceptibility to cortical spreading depression. *Neuron*. **41**: 701–710

van den Pol A.N. (1993) Glutamate and GABA presence and action in the suprachiasmatic nucleus. *J Biol Rhythms.* **8:** 11–15

van der Putten H., *et al*. (2000) Neuropathology in mice expressing human alpha-synuclein. *J. Neurosci.* **20**: 6021–6029

van Ooijen G., Millar A. J. (2012) Non-transcriptonal oscillators in circadian timekeeping. *Trends Biochem. Sci*. **37**: 484–492

van Oosterhout F., *et al*. (2008) Enhanced circadian phase resetting in R192Q $Ca_v2.1$ calcium channel migraine mice. *Ann Neurol*. **64**: 315–324

van Os J., *et al*. (2008) Gene–environment interactions in schizophrenia: review of epidemiological findings and future directions. *Schizophr. Bull.* **34:** 1066–1082

van Someren E.J. (2000) Circadian rhythms and sleep in human aging. *Chronobiol Int.* **17:** 233–243

van Someren E.J., *et al*. (1999) Bright light therapy: improved sensitivity to its effects on rest-activity rhythms in Alzheimer patients by application of nonparametric methods. *Chronobiol Int.* **16**: 505–518

Vanier M.T. (2010) Niemann-Pick disease type C. *Orphanet Journal of Rare Diseases.* **5**:16

Vanier M.T., Millat G. (2003) Niemann-Pick disease type C. *Clin. Genet*. **64:** 269–281

Varrone A., *et al*. (2004) Imaging of dopaminergic dysfunction with [123I]FP-CIT SPECT in early-onset parkin disease. *Neurology.* **63:** 2097–103

Vásquez M.C., *et al*. (2011) Alteration of Gene Expression Profile in Niemann-Pick Type C Mice Correlates with Tissue Damage and Oxidative Stress. *PLoS ONE.* **12:** e28777

Vekrellis K., *et al*. (2004) Neurobiology of α-synuclein. *Mol Neurobiol.* **30:** 1–21

Venda L.L., *et al*. (2010) α-Synuclein and dopamine at the crossroads of Parkinson's disease. *Trends in Neurosciences*. **33**: 559–568

Venkatraman V., *et al*. (2007) Sleep deprivation elevates expectation of gains and attenuates response to losses following risky decisions. *Sleep*. **30:** 603–609

Vitaterna M.H., *et al*. (1999) Differential regulation of mammalian period genes and circadian rhythmicity by cryptochromes 1 and 2. *Proc. Natl. Acad. Sci. USA*. **96**: 12113–12119

Vitaterna M.H., *et al*. (2006) Large-scale mutagenesis and phenotypic screens for the nervous system and behavior in mice. *Trends Neurosci.* **29:** 233–240

Vitner E.B., *et al*. (2010) Common and uncommon pathogenic cascades in lysosomal storage diseases. *J. Biol. Chem.* **285:** 20423–20427

Voikar V., *et al*. (2002) Cognitive deficit and development of motor impairment in a mouse model of Niemann-Pick type C disease. *Behavioural Brain Research*. **132:** 1–10

Volicer L., *et al*. (2001) Sundowning and circadian rhythms in Alzheimer disease. *Am J Psychiatry*. **158:** 704–711

Volk B.W., *et al*. (1975) The gangliosidoses. *Hum Pathol .* **6**: 555–569

Von Coelln R., *et al*. (2004) Loss of locus coeruleus neurons and reduced startle in parkin null mice. *Proc. Natl. Acad. Sci. USA.***101:** 10744–10749

von Gall C., *et al*. (1998) CREB in the mouse SCN: a molecular interface coding the phase-adjusting stimuli light, glutamate, PACAP, and melatonin for clockwork access. *J Neurosci.* **18:** 10389–10397

Vyazovskiy V.V., *et al*. (2011) Electrophysiological correlates of sleep homeostatis in freely behaving rats. *Prog Brain Res*. **193**: 17–38

Wada R., *et al*. (2000) Microglial activation precedes acute neurodegeneration in Sandhoff disease and is uppressed by bone marrow transplantation. *Proc. Natl. Acad. Sci. USA*. **97:** 10954–10959

Wade-Martins R. (2012) The MAPT locus – a genetic paradigm in disease susceptibility. *R. Nat. Rev. Neurol.* **8:** 477–478

Wade-Martins R., Johnson S.J. (2011) A BACwards glance into neurodegeneration: molecular insights into disease from LRRK2, SNCA and MAPT BAC-transgenic mice. *Biochem Soc Trans*. **39**: 862–867

Wakabayashi K., *et al*. (1998) Accumulation of alpha-synuclein/NACP is a cytopathological feature common to Lewy body disease and multiple system atrophy. *Acta Neuropathol.* **96**: 445–452

Walkley S., Suzuki K. (2004) Consequences of NPC1 and NPC2 loss of function in mammalian neurons. *Biochimica et Biophysica Acta.* **1685:** 48– 62

Walsh T., *et al*. (2008) Rare structural variants disrupt multiple genes in neurodevelopmental pathways in schizophrenia *Science* **320:** 539–543

Wang H.Y., Friedman E. (1996) Enhanced protein kinase C activity and translocation in bipolar affective disorder brains. *Biol.Psychiatry.* **40:** 568–75

Wang L., *et al*. (2008) Abnormal colonic motility in mice overexpressing human wildtype α-synuclein. *Neuroreport.* **19**: 873–876

Washbourne P., *et al*. (2002) Genetic ablation of the t-SNARE SNAP-25 distinguishes mechanisms of neuroexocytosis. *Nat Neurosci.* **5**: 19–26

Watis L., *et al*. (2008) Glutamatergic abnormalities of the thalamus in schizophrenia: a systematic review. *J Neural Transm.* **115:** 493–511

Waxman E.A., Giasson B.I. (2011) Induction of intracellular tau aggregation is promoted by *α*-synuclein seeds and provides novel insights into the hyperphosphorylation of tau. *Journal of Neuroscience.* **31:** 7604–7618

Weaver D.R. (1998) The suprachiamsatic nucleus: a 25-year retrospective. *J Biol Rhythms*. **12**: 100–112

Webb A.B., *et al*. (2009) Intrinsic, nondeterministic circadian rhythm generation in identified mammalian neurons. *Proc. Natl. Acad. Sci. USA.* **106:** 16493–16498

Webb I.C., *et al*. (2010) Circadian clock resetting by behavioral arousal: neural correlates in the midbrain raphe nuclei and locus coeruleus. *Neuroscience*. **166:** 739–751

Weder N.D., *et al*. (2007) Frontotemporal dementias: a review. *Ann Gen Psychiatry.* **6:** 15–25

Weinberger D.R., (1987) Implications of normal brain development for the pathogenesis of schizophrenia. *Arch Gen Psychiatry.* **44**: 660–669

Weintraub H., *et al*. (1987) Dysmyelination in NCTR-Balb/C mouse mutant with a lysosomal storage disorder. Morphological survey. *Acta Neuropathol.* **74:** 374–381

Welckert C.S., *et al*. (2001) Reduced gap-34 mRNA in dorsolateral prefrontal cortex of patients with sczhiophrenia. *Cereb Cortex*. **11**: 136–147

Wells A.S., *et al*. (1997) Influences of fat and carbohydrate on postprandial sleepiness, mood, and hormones. *Physiol. Behav.* **61:** 679–686

Welsh D.K., *et al*. (1995) Individual neurons dissociated from rat suprachiasmatic nucleus express independently phased circadian firing rhythms. *Neuron*. **14:** 697–706

Welsh D.K., *et al*. (2010) Suprachiasmatic nucleus: cell autonomy and network properties. *Annu Rev Physiol.* **72:** 551–577

Wendeler M., *et al*. (2004) Expression of the GM2 – activator protein in the methylotrophic yeast Pichia pastoris, purification, isotopic, labelling and biophysical characterization. *Protein Expr.Purif.* **34:** 147–157

Wersinger S.R., *et al*. (2007) Disruption of the vasopressin 1b receptor gene impairs the attack component of aggressive behavior in mice. *Genes Brain Behav.* **6:** 653–660

West A.E. *et al*. (2001) Calcium regulation of neuronal gene expression. *Proc. Natl. Acad. Sci. USA*. **98**: 11024–11031

Wieczorek S., *et al*. (2004) Screening for candidate gene regions in narcolepsy using a microsatellite based approach and pooled DNA. *J Mol Med.* **82:** 696–705

Wilhelmus M.M.M., *et al*. (2012) Involvement and interplay of Parkin, PINK1, and DJ1 in neurodegenerative and neuroinflammatory disorders. *Free Radical Biology and Medicine.* **53:** 983–992

Williams-Gray C.H., *et al*. (2009) The distinct cognitive syndromes of Parkinson's disease: 5 year follow-up of the CamPaIGN cohort. *Brain*. **132:** 2958–2969

Williamson P. (2007) Are anticorrelated networks in the brain relevant to schizophrenia? *Schizophr. Bull*. **33:** 994–1003

Willis G.L., *et al*. (2012) A historical justification for and retrospective analysis of the systematic application of light therapy in Parkinson's disease. *Reviews in the Neurosciences.* **23:** 199–226

Willison L.D., *et al*. (2013) Circadian dysfunction may be a key component of the non-motor symptoms of Parkinson's disease: Insights from a transgenic mouse model. *Exp. Neurol.* **243:** 57–66

Wills J., *et al*. (2011) Tauopathic changes in the striatum of A53T *α*-synuclein mutant mouse model of Parkinson's disease. *PLoS One*. **6:** e17953

Wills J., *et al*. (2010) Elevated tauopathy and alpha-synuclein pathology in postmortem Parkinson's disease brains with and without dementia. *Experimental Neurology*. **225:** 210–218

Winchester B. (2004) Primary defects in lysosomal enzymes. *In Lysosomal Disorders of the Brain*. 81–130

Wine J.N., *et al*. (2009) Effects of quetiapine on sleep in nonpsychiatric and psychiatric conditions. *Ann Pharmacother.* **43:** 707–713

Winslow A.R., *et al*. (2010) α-Synuclein impairs macroautophagy: implications for Parkinson's disease. *J. Cell Biol.* **190:** 1023–1037

Wirz-Justice A. (2006) Biological rhythm disturbances in mood disorders. *Int Clin Psychopharmacol.* **21:** 11–15

Wisor J.P., Nishino S., *et al*. (2001) Dopaminergic role in stimulant-induced wakefulness. *J. Neurosci*. **21**: 1787–1794

Witte M.E., *et al*. (2009) Parkinson's disease-associated parkin colocalizes with Alzheimer's disease and multiple sclerosis brain lesions. *Neurobiol Dis*. **36**: 445–452

Wong A.H., *et al*. (2003) Identification of candidate genes for psychosis in rat models, and possible association between schizophrenia and the 14-3-3eta gene. *Mol Psychiatry.* **8:** 156–166

Wong A.H., *et al*. (2004) Association between schizophrenia and the syntaxin 1A gene. *Biol. Psychiatry.* **56**: 24–29

Wong C.C., Wallhangen M.I. (2012) Frontotemporal Dementia: The impact of patient behavioral symptoms on the physical and mental health of family caregivers. *Dement Geriatr Cogn Disord Extra.* **2:** 516–528

Wong E., Cuervo A.M. (2010) Autophagy gone awry in neurodegenerative diseases. *Nat. Neurosci.* **13:** 805–811

Wraith J.E. (2002) Lysosomal disorders. *Semin. Neonatol.* **7:** 75–83

Wraith J.E. (2004) Clinical aspects and diagnosis. *In Lysosomal disorders of the brain.* 50–77

Wray S., Lewis P.A. (2010) A tangled web—tau and sporadic Parkinson's disease. *Front Psychiatry*. **1:** 150

Wright K.P.Jr. Czeisler C.A. (2002) Absence of circadian phase resetting in response to bright light behind the knee. Science. **297**: 571

Wright, C.S., *et al*. (2003) Structural analysis of lipid complexes of GM2-activator protein. *J. Mol. Biol.* **331:** 951–964

Wu C.C., *et al*. (2004) Metabolic labeling of mammalian organisms with stable isotopes for quantitative proteomic analysis. *Anal. Chem*. **76:** 4951–4959

Wulff K., *et al*. (2012) Sleep and circadian rhythm disruption in schizophrenia. *Br J Psychiatry.* **200:** 308–316

Wulff K., *et al*. (2010) Sleep and circadian rhythm disruption in psychiatric and neurodegenerative disease. *Nat Rev Neurosci.* **11**: 589–599

Wulff K., *et al*. (2006) The suitability of actigraphy, diary data, and urinary melatonin profiles for quantitative assessment of sleep disturbances in schizophrenia: a case report. *Chronobiol Int.* **23:** 485–495

Wulff K., *et al*. (2009) Sleep and circadian rhythm disturbances: multiple genes and multiple phenotypes. *Curr Opin Genet Dev.* **19:** 237–246

Yagita K., *et al*. (2002) Nucleocytoplasmic shuttling and mCRY-dependent inhibition of ubiquitylation of the mPER2 protein. *EMBO J*. **21**: 1301–1314

Yamada A., *et al*. (2001) Progressive neuronal loss in the ventral posterior lateral and medial nuclei of thalamus in Niemann–Pick disease type C mouse brain. *Brain Dev.* **5:** 288– 297

Yamaguchi A., *et al*. (2004) Possible role of autoantibodies in the pathophysiology of G_{M2} gangliosidosis. *J Clin Invest.* **113:** 200–208

Yamaguchi S., *et al*. (2003) Synchronization of cellular clocks in the suprachiasmatic nucleus. *Science.* **302:** 1408–1412

Yamamoto H., *et al*. (1987) Role of SCN in daily rhythms of plasma glucose, FFA, insulin and glucagon. *Chronobiol. Int.* **4:** 483–491

Yamanaka S., *et al*. (1994) Targeted disruption of the *Hexa* gene results in mice with biochemical and pathologic features of Tay-Sachs disease. *Proc. Natl. Acad. Sci. USA.* **91:** 9975–9979

Yamazaki S., *et al*. (1998) Rhythmic properties of the hamster suprachiasmatic nucleus in vivo. *J. Neurosci*. **18**: 10709–10723

Yan J., *et al*. (2008) Analysis of gene regulatory networks in the mammalian circadian rhythm. *PLoS Comput Biol*. **4:** e1000193

Yan L., Silver R. (2002) Differential induction and localization of mPer1 and mPer2 during advancing and delaying phase shifts. *Eur. J. Neurosci.* **16:** 1531–1540

Yanagihara H., *et al*. (2006) High-fat feeding exerts minimal effects on rhythmic mRNA expression of clock genes in mouse peripheral tissues. *Chronobiol. Int.* **23:** 905–914

Yang C., Winkelman J.W. (2006) Clinical significance of sleep EEG abnormalities in chronic schizophrenia. *Schizophr Res.* **82:** 251–260

Yavich L. (2004) Role of alpha-synuclein in presynaptic dopamine recruitment. *J. Neurosci*. **24**: 11165–11170

Yildiz A., *et al*. (2008) Protein kinase C inhibition in the treatment of mania: a double-blind, placebocontrolled trial of tamoxifen. *Arch Gen Psychiatry.* **65:** 255–263

Yin L., *et al*. (2006) Nuclear receptor Rev-erbalpha is a critical lithium-sensitive component of the circadian clock. *Science*. **311:** 1002–1005

Young C.E., *et al*. (1998) SNAP-25 deficit and hippocampal connectivity in schizophrenia. *Cereb Cortex.* **8**: 261–268

Young M.E., Bray M.S. (2007) Potential role for peripheral circadian clock dyssynchrony in the pathogenesis of cardiovascular dysfunction. *Sleep Med.* **8:** 656–667

Zachrisson O., de Belleroche J., Wendt K.R., Hirsch S., Lindefors N. (1999) Cholecystokinin CCK(B) receptor mRNA isoforms: expression in schizophrenic brains. *Neuroreport.* **10:** 3265–3268

Zanivan S., *et al*. (2012) In vivo Quantitative Proteomics: The SILAC mouse. *Methods in Molecular Biology.* **757:** 435–450

Zantke J., *et al*. (2013) Circadian and circalunar clock interactions in a marine annelid. *Cell Rep*. **17**: 99–113

Zarate C.A. Jr., *et al*. (2007) Efficacy of a protein kinase C inhibitor (tamoxifen) in the treatment of acute mania: a pilot study. Bipolar Disord. **9:** 561–70

Zarranz J.J., *et al*. (2004)The new mutation, E46K, of alpha-synuclein causes Parkinson and Lewy body dementia. *Ann. Neurol.* **55:** 164–73

Zehr C., *et al*. (2004) Apoptosis in oligodendrocytes is associated with axonal degeneration in P301L tau mice. *Neurobiol. Dis.* **15:** 553–562

Zeitzer J.M., *et al*. (2000) Sensitivity of the human circadian pacemaker to nocturnal light: melatonon phase resetting and suppression. *J Physiol.* **526:** 695–702

Zervas M., *et al*. (2001) Critical role for glycosphingolipids in Niemann–Pick disease type C. *Curr Biol.* **11:** 1283–1287

Zhao Z., *et al*. (2008) Vgf is a novel biomarker associated with muscle weakness in amyotrophic lateral sclerosis (ALS), with a potential role in disease pathogenesis. *Int J Med Sci.* **5:** 92–99

Zhong Q., *et al*. (2012) Tau isoform composition influences the rate and extent of filament formation. *J Biol Chem.* **287:** 20711–20719

Zhou R., *et al*. (2011) A role for mitochondria in NLRP3 inflammasome activation. *Nature*. **469:** 221–225

Zhu X. R., *et al*. (2007) Non-motor behavioral impairments in parkin-deficient mice. *European J. of Neuroscience.* **26:** 1902–1911

Zhu W., *et al*. (2010) Mass spectrometry-based label-free quantitative proteomics. *J Biomed Biotechnol*. **2010**: 840518

Zombeck J.A., *et al*. (2011) Selective breeding for increased home cage physical activity in collaborative cross and Hsd:ICR mice. *Behav Genet.* **41:** 571–582

Zuber A.M., *et al*. (2009) Molecular clock is involved in predictive circadian adjustment of renal function. *Proc. Natl. Acad. Sci. USA.* **106:** 16523–16528

Zueger M., *et al*. (2006) mPer1 and mPer2 mutant mice show regular spatial and contextual learning in standardized tests for hippocampus-dependent learning. *J. Neural. Transm*. **113:** 347–356